Synthesis, Characterization and Investigation on Water-Soluble, Aquated Gd(III) and Mn(II) Complexes as MRI Contrast Agents

A Dissertation Submitted in Partial Fulfilment of the Requirement for the Degree of Doctor of Philosophy at IIT Guwahati

by

Mahmuda Khannam

Roll no. 136122016

Department of Chemistry

Indian Institute of Technology Guwahati

Guwahati–781039, Assam

India

July 2018

To my loving family

Failure will never overtake me if my definition to succeed is strong enough

Dr. A. P. J. Abdul Kalam

Indian Institute of Technology Guwahati

Department of Chemistry

Declaration

I do hereby declare that the research work embodied in this thesis entitled "***Synthesis, Characterization and Investigation on Water-Soluble, Aquated Gd(III) and Mn(II) Complexes as MRI Contrast Agents***" has been carried out by me under the supervision of **Dr. Chandan Mukherjee**, Department of Chemistry, Indian Institute of Technology Guwahati, Guwahati–781039, Assam, India. The research works have been carried out in the period of August, 2013 to July, 2018.

In keeping with general practice of reporting scientific observations, due acknowledgements have been made wherever the work described is based on the findings of other investigations.

IIT Guwahati — Mahmuda Khannam

July, 2018 — Roll no. 136122016

Dr. Chandan Mukherjee

Associate Professor
Department of Chemistry
Indian Institute of Technology Guwahati
Guwahati, 781039, Assam, India

Phone no. +91-361-258-2357(O)
Fax no. +91-361-258-2349
Email: cmukherjee@iitg.ac.in

CERTIFICATE

This is to certify that the research work presented in this thesis entitled "***Synthesis, Characterization and Investigation on Water-Soluble, Aquated Gd(III) and Mn(II) Complexes as MRI Contrast Agents***" is an authentic record of the results obtained from the research work carried out by **Miss Mahmuda Khannam** (**Roll No. 136122016**) under my supervision in Department of Chemistry, Indian Institute of Technology Guwahati, India. This work is original and has not been submitted elsewhere for a degree or award.

Place: IIT Guwahati

Date:

Dr. Chandan Mukherjee

(Thesis Supervisor)

Acknowledgements

Immeasurable appreciation and deepest gratitude for the help and support are extended to the following persons who in one way or other have contributed during completion of my thesis work.

I would like to express my sincere gratitude to my supervisor **Dr. Chandan Mukherjee** for his constant support and motivation throughout my thesis work. My work would not be completed within this period of time without his guidance and valuable suggestions.

I will be always thankful to **Indian Institute of Technology, Guwahati** for giving me the opportunity to pursue my research work, and encouraging me with doctoral fellowship.

I would like to express deepest thanks and gratitude to **Dr. Ankona Dutta**, TIFR Mumbai; for allowing me to work in her laboratory, and also with instrumental facility.

I want to acknowledge **Dr. P. K. Dev**, Tezpur University; for giving me the opportunity to work in his laboratory, and allowing me to use the instrumental facility.

I want to offer special thanks to **Dr. Thomas Weyhermüller**, Max-Planck-Institut für Chemische Energiekonversion, Germany; for helping me in solving crystal structure.

I am also grateful to my doctoral committee members, **Prof. Anil Kumar Saikia**, **Dr. Bhubaneswar Mandal**, and **Dr. Shyam Prosad Biswas**; for their valuable suggestions during my research work.

I am highly thankful to the whole team of radiology and imaging department from **GNRC Hospital**, and **Primus Diagnosis**, Guwahati for helping me during MRI imaging at clinical imager.

I am thankful to **Dr. Babulal Das**, **Mr. Imdadul Islam**, **Mr. Aniruddha Gogoi**, **Mr. Diganta Kumar Hira** and **Mr. Kh Kesho Singh** for their help in instrumental laboratory.

I will be always indebted to my labmates; **Dr. Samir Ghorai, Dr. Manas Kumar Mondal, Dr. Bedika Phukan, Richa Rakshit, Ujjal Ghosh**, **Ganesh Chandra Paul** and **Prasenjit Sarkar**. Without their help, suggestions and mental support; this journey would not be possible for me.

I want to offer my deepest thanks to some of my friends; **Gaurangi**, **Dhriti**, **Hironya**, **Ravindra**, **Subhra**, **Nilotpal**, **Anju**, **Ahalya**, **Sumana**, **Soumita**, **Titli**, **Avishek** and **Shaad**; for always being supportive and making my journey beautiful in IIT Guwahati.

I cannot even imagine where I would be today without my family. Thanks to **Abba** and **Amma**, for being my biggest support system. Thank you for never giving up on me. I want to say a heartfelt thanks my elder sister **Dr. Momina Khannam**, who always being there for me, whenever I fell down; and constantly motivating me. I also want to thank my brother in law **Dr. Iftikar Hussain** for motivating me and helping me whenever I need.

Last but not the least, I would like to thank **Almighty Allah** for giving me the strength, knowledge, ability and opportunity to undertake this research study and to persevere and complete it satisfactorily. Without his blessings, this achievement would not have been possible.

Mahmuda Khannam

Thesis Title:

'Synthesis, Characterization and Investigation on Water-Soluble, Aquated Gd(III) and Mn(II) Complexes as MRI Contrast Agents"

List of Publications:

1. "A highly stable L-alanine-based mono(aquated) Mn(II) complex as a T_1-weighted MRI contrast agent", Mahmuda Khannam, Thomas Weyhermüller, Upashi Goswami and Chandan Mukherjee, *Dalton Trans*., 2017, **46**, 10426–10432.
2. "Hexadentate Chelate-Based Contrast Agent and A Method for Producing the Same", Patent application no. **201831020332**.
3. "Pentadentate Chelate-Based Contrast Agent and A Method for Producing the Same", Patent application no. **201831020333**.

List of Conferences/Symposiums:

1. "**Frontiers in Chemical Science, FICS-2016**", Department of Chemistry, Indian Institute of Technology Guwahati.
2. "**20th CRSI National Symposium in Chemistry, 2017**", Gauhati University.
3. "**Modern Trends in Inorganic Chemistry, MTIC-XVII, 2017**", CSIR-NCL, Pune and IISER, Pune.
4. "**9th Asian Biological Inorganic Chemistry Conference, ASBIC9, 2018**," UTown, Stephen Ready centre, Singapore.

Doctoral Committee:

Prof. Anil Kumar Saikia (Chairman)

Dr. Bhubaneswar Mandal (Member)

Dr. Shyam Prosad Biswas (Member)

Dr. Chandan Mukherjee (Supervisor)

Abstract

Chapter I

General Introduction

Magnetic resonance imaging (MRI) is an effective diagnostic imaging modality. Without using any harmful radiation it can penetrate deep inside soft tissues from 1 mm to 1 m. The images are developed from ^{1}H-NMR signals of *in vivo* water molecule protons. The intensity of the developed image depends upon nuclear relaxation times; T_1 = longitudinal, and T_2 = transverse relaxation time. The water molecule protons have different relaxation times depending upon tissue environments and generate contrast in MR images. The contrast in images can provide anatomical information of examined tissues. However, low sensitivity is the prime limitation of this diagnostic technique. To overcome this constraint, a class of substance is injected prior imaging. The substance can enhance the signal intensity by catalytically shortening the relaxation times and known as MRI contrast agent (CA). Contrast agents are paramagnetic, superparamagnetic, and ferromagnetic species with high electron spin relaxation time.

Gd(III) ion bears seven unpaired electrons and has a spherical arrangement of the electrons. Thus, complexes of Gd(III) ion have attained special attention as contrast agents. Nephrogenic Systemic Fibrosis (NSF), a disease was discovered after injecting Gd(III)-based contrast agents to the patients with renal problem. Thus, the use of Gd(III)-based contrast agents is limited. In this regard, Mn(II) ion has gained interests due to its favourable electronic configurations with five unpaired electrons and high water exchange ability. Furthermore, the advantage with Mn(II) ion is that it is biogenic in nature and also present in various enzymes. However, excess level of Mn(II) ion deposition in brain can cause “Manganism”, a neurological disorder. Therefore, it is also necessary to chelate Mn(II) ion strongly with suitable ligand framework to ensure no free metal ion deposition inside living systems.

Chapter II

Motivation, Designing and Syntheses of Ligands

The current commercially available MRI contrast agents are mostly nine-coordinate Gd(III) complexes of polycarboxylates of either macrocyclic 1,4,7,10-tetraazacyclododecane, or acyclic diethylenetriamine and/or their derivatives. With one coordinated-water molecule these Gd(III) complexes afford relaxivity value in between 4-5 $mM^{-1}s^{-1}$at 20 MHz, 298 K, which is relatively low. The relaxivity value could be improved by increasing the number of coordinated-water molecules to the metal centre, irrespective of applied magnetic field. However, judicious ligand designing is required to provide high thermodynamic stability to the metal complexes with more than one coordinated-water molecules as the coordination number by chelates decreases.

Ligands with picolinate moiety were showing impressive properties in its corresponding Gd(III) and Mn(II) complexes. Due to flexible coordination sphere, Gd(III) complexes with picolinate arms possess high water exchange rate. While pyridine moiety in the ligand framework can increase the stability of Mn(II) complexes by metal to ligand back donation. Moreover, functionalization of pyridine ring could provide binding sites for biological macromolecules, which is necessary for the organ selectivity and for decreasing overall tumbling rate of small coordination complexes.

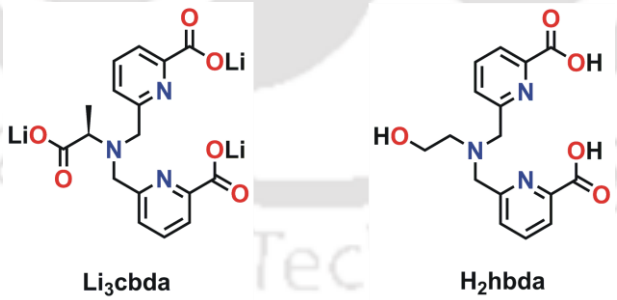

Scheme 1. *Ligands designed with picolinate moieties.*

In this context, two hexadentate ligands with picolinate arms have been synthesized (**Scheme 1**). The ligands are supposed to provide Gd(III) complexes with more than one

coordinated-water molecules as Gd(III) ions in general, acquire coordination number either eight or nine.

Mn(II) complexes are generally six- or seven-coordinate. Thus, employing the hexadentate ligands, Mn(II) complexes with maximum one water molecule could be achieved. Ligand **Li_3cbda** was based on L-alanine backbone, whereas ligand **H_2hbda** had alcoholic side chain. The incorporation of chiral backbone is known for providing structural rigidity. While ligands with alcoholic donor group has been known for providing stability to its corresponding Gd(III) complexes. Therefore, Gd(III) and Mn(II) complexes with the ligands would attain very high thermodynamic stability.

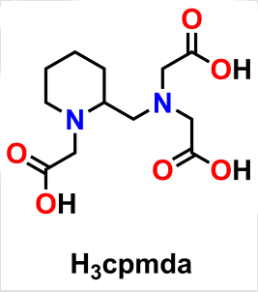

H_3cpmda

Scheme 2. *Ligand designed with piperidine ring.*

MRI contrast agents are usually membrane impermeable due to hydrophilic nature of the complexes. However, some amount of lipophilicity is necessary for their biliary excretion from living systems. To work on the strategy, pentadentate ligand **H_3cpmda** has been designed (**Scheme 2**). The ligand contains a lipophilic piperidine ring with two amine N atoms and three acetate arms, which could provide high thermodynamic stability to the corresponding Mn(II) complex *via* five strong σ-bonds. The complex could have maximum two coordinated-water molecules.

Chapter III

Tris(aquated) Gd(III) Complexes with Picolinate-Based Ligands as MRI Contrast Agents: Effect of Tether-Ligand Donor Groups on Thermodynamic Stability of Complexes

To overcome the low relaxivity issue of commercially available mono(aquated) Gd(III)-based contrast agents, Gd(III) complexes with two hexadentate, picolinate-based ligands **Li_3cbda** and **H_2hbda** have been synthesized (**Scheme 3**).

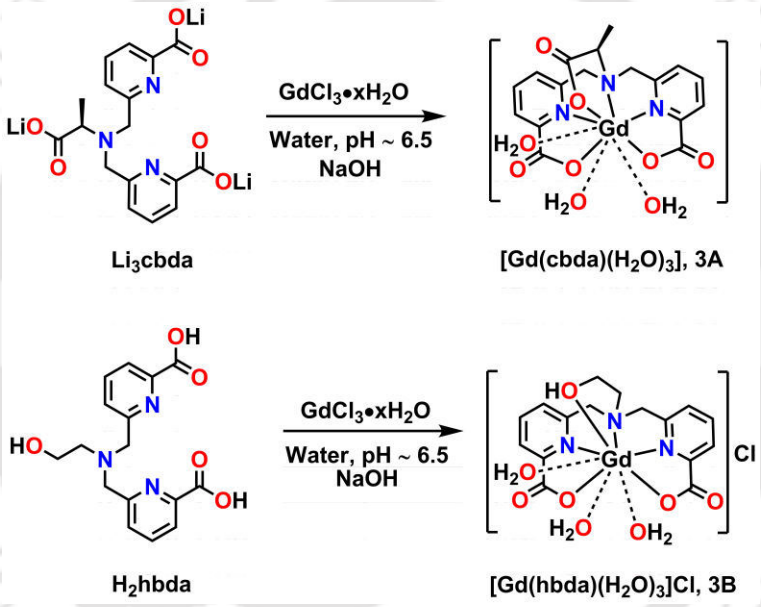

Scheme 3. *Syntheses of complexes **3A** and **3B**.*

Both ligands provided nine-coordinate Gd(III) complexes. While, complex **3A** was neutral in charge, in complex **3B** the coordination complex was monopositive in charge. The luminescence lifetime measurements of Tb(III) congeners of the respective complexes in H_2O *vs* D_2O systems implied number of coordinated water molecules (q) to be 3.0 ± 0.1 for complex **3A**, and 2.8 ± 0.1 for complex **3B** respectively.

pH-potentiometric titrations of the ligands in 0.15 M NaCl, provided ligand protonation constants as 8.10, 2.97, 2.35 (**Li_3cbda**); and 7.68, 4.63, 2.88 (**H_2hbda**) respectively. The

potentiometric titrations of 1:1 molar equivalents of Gd(III) ion and ligands provided stability constants as 12.72 (complex **3A**); and 16.12 (complex **3B**). At pH ~ 7.4, and 25 °C, calculated pGd values were 12.90 and 16.61 respectively. Complex **3A** was more stable than reported analogous tris(aquated) Gd(III) picolinate-based complexes due to its rigid coordination environment. Complex **3B** was found to be more stable than complex **3A**. Akin to the previous reports, the presence of alcoholic donor group was attributed as the stabilizing factor in complex **3B**.

At 1.41T, pH ~ 7.4, and 25 °C, the longitudinal relaxivity values offered by the complexes were 10.96 $mM^{-1}s^{-1}$(complex **3A**), and 9.82 $mM^{-1}s^{-1}$ (complex **3B**). Thus, with three coordinated-water molecules both of the complexes achieved high relaxivity values relative to clinically used mono(aquated) Gd(III) complexes.

Neutral complex **3A** showed less affinity for physiological anions (HCO_3^-, HPO_4^{2-}, F^-) relative to cationic complex **3B**. In both of the cases, one of the coordinated-water molecules was being substituted by these physiological anions. For complex **3A**, even in the presence of 100 equivalents (50 mM) of anions, only one of the three coordinated-water molecules was being substituted. However, the anionic effect on complex **3B** was found higher and upon increasing of concentrations of the anions from 50 equivalents (25 mM) to 100 equivalents (50 mM), the removal of coordinated-water molecules increased from one to two.

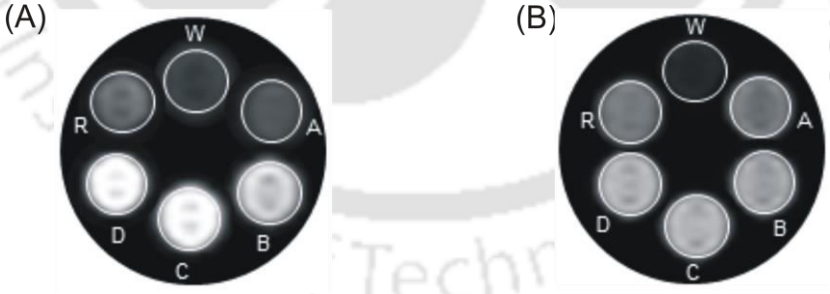

Figure 1. *T_1-weighted phantom MR images of (A) complex **3A**, and (B) complex **3B;** under clinical scanner at 1.5 T; (W= water, A = 0.25, B= 0.50, C= 0.70, and D = 1.00 mM solution of complexes; R = 1.00 mM solution of MultiHance® in HEPES buffer).*

To investigate the efficiency of the synthesized Gd(III) complexes as positive contrast agents, T_1-weighted phantom MR images of aqueous solutions of the complexes were recorded

(**Figure 1**). The increase in brightness with increase in concentration of the complexes (0.25 mM to 1.00 mM) confirmed their contrast efficiency. Thus, with more than one coordinated-water molecules with better relaxivity and better thermodynamic stability have been reported and the effect of rigidity *versus* oxophilicity has been studied.

Chapter IV

A Mono(aquated) Mn(II) Complex with Lipophilic Piperidine Ligand Backbone as T_1-weighted MRI Contrast Agent

Thermodynamically stable Mn(II) complexes with coordinated-water molecule can be synthesized by designing ligand framework wisely. Mn(II) complex with pentadentate lignad **H_3cpmda** [**Scheme 4(A)**] has been synthesized.

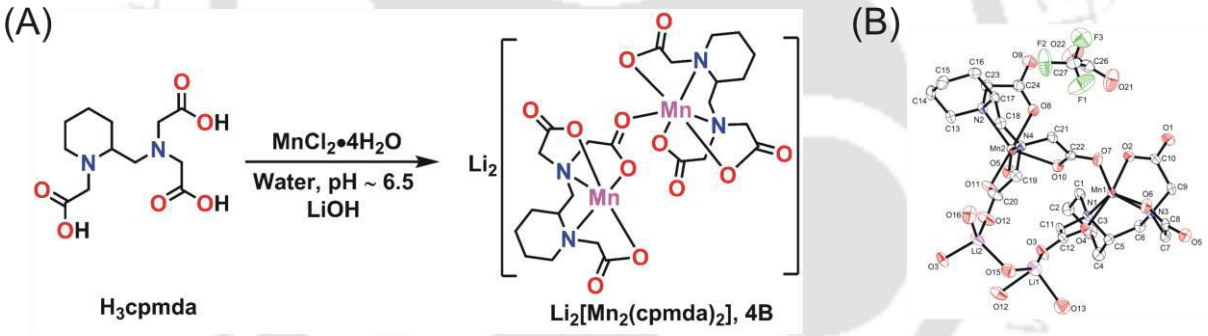

Scheme 4. *(A) Synthesis of complex* ***4B****, and (B) ORTEP view of complex* ***4B•CF$_3$COOH•5H$_2$O****.*

The single crystal X-ray diffraction measurement revealed dimeric nature of complex **4B**; each unit was connected through carbonyl O-atom [**Scheme 4(B)**]. However, two units got separated in solution state, and form hexacoordinate Mn(II) units with one coordinated-water molecule. The potentiometric titrations of ligand **H_3cpmda** in 0.15 M NaCl solution at 25 °C provided protonation constants of the ligand: 9.70, 6.04, 2.88, and 1.18. The stability constant of the complex was found to be 12.72, and pMn value was 7.70 (at pH ~ 7.4, 25 °C, and [M] = $[L]_{total}$ = 10 μM). The stability of the complex was better than similar Mn(II) complexes with five-coordinate ligands with one coordinated-water molecule.

The mono(aquated) six-coordinate complex; $[Mn(cpmda)(H_2O)]^-$ offered longitudinal relaxivity value of 2.90 $mM^{-1}s^{-1}$ at 1.41 T, 25 °C, and pH ~ 7.4 which was better than clinically used Mn(II)-based contrast agent, Teslascan®; and comparable to similar mono(aquated) Mn(II) complexes. The relaxivity value remained consistent in the pH range of 5-9, changes were observed only at higher pH due to formation of hydroxyl species. In the presence of 200 equivalents of physiological anions (HCO_3^-, HPO_4^{2-}, F^-), the complex stability was neither challenged nor its coordinated-water molecule was getting substituted. It was assured by measuring longitudinal relaxivity of complex **4B** at 1.41 T, 25 °C. However, increase in relaxivity value in the presence of HPO_4^{2-} anion was due to formation of slowly rotating species as a result of intermolecular interactions between the species.

Finally, phantom MR imaging under clinical imager at 1.5 T established the efficiency of complex **4B** as T_1-weighted contrast agent (**Figure 2**). Herein, with one coordinated-water molecule, impressive thermodynamic stability, six-coordinate Mn(II) complex **4B** has been reported and its contrast efficiency has been studied.

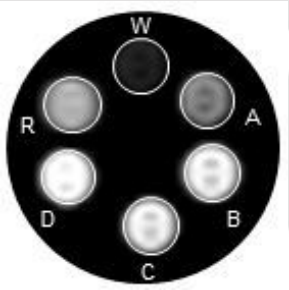

Figure 2*. T_1-weighted phantom MR images of complex **4B** under clinical scanner at 1.5 T; [W= water, A = 0.25, B= 0.50, C= 0.70, and D = 1.00 mM solution of complex (considering molecular weight as a whole); R = 1.00 mM solution of MultiHance® in HEPES buffer].*

Chapter V

A Stable Mono(aquated) Mn(II) Complex as T_1-weighted MRI Contrast Agent

In this chapter, Mn(II) complex of hexadentate picolinate-based ligand **Li_3cbda** has been synthesized [**Scheme 5(A)**].

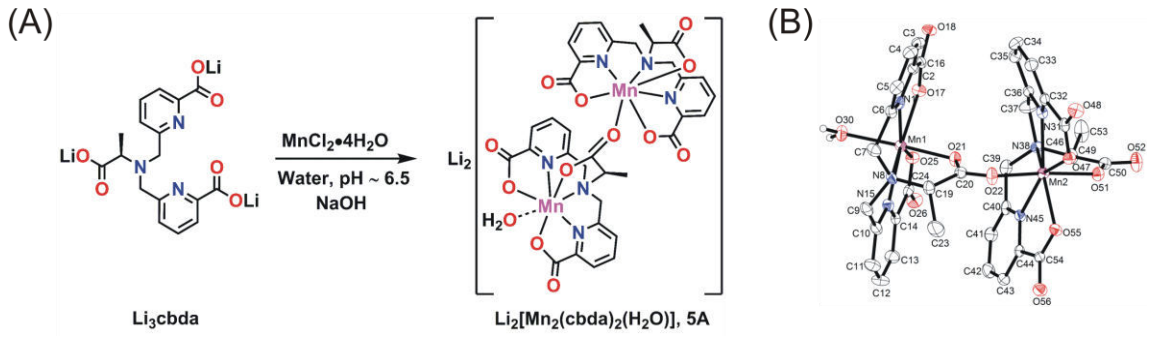

Scheme 5. *(A) Synthesis of complex* ***5A****, and (B) ORTEP view of dianionic form of complex* ***5A****.*

The single crystal XRD analysis revealed that complex **5A** consisted of two seven-coordinate pentagonal bipyramidal Mn(II)units [**Scheme 5(B)**], which in solution separated into two mononegative, mononuclear, Mn(II) coordination units with one coordinated-water molecule ($[Mn(cbda)(H_2O)]^-$).

The thermodynamic stability of the complex was assessed by pH-potoentiometric titration of 1:1 molar equivalents of Mn(II) and ligand **Li_3cbda** in 0.15 M NaCl, 25 °C. The stability constant for the complex was found to be 11.90, and calculated pMn value was 8.06 (at pH ~ 7.4, 25 °C, and $[M] = [L]_{total} = 10\ \mu M$). Notably, the stability of the complex was found to be comparatively higher than analogous mono(aquated) Mn(II) complexes. Two pyridine moieties stabilized the complex *via* metal-to-ligand back donation, while three carboxylate O-atoms, one amine N-atom, and two pyridine N-atoms contributed through six strong σ-bonds.

$[Mn(cbda)(H_2O)]^-$ exhibited longitudinal relaxivity value of 3.02 $mM^{-1}s^{-1}$ at 1.41 T, 25 °C, and pH ~ 7.4. The pH of the medium exerted small effect on the overall stability of the complex; slight decrease in relaxivity was observed at high pH due to replacement of coordinated-water molecule by hydroxyl group. The complex stability was remained unaffected in the presence of 200 equivalents of physiological anions (HCO_3^-, HPO_4^{2-}, F^-); verified by constant relaxivity value in the presence of these physiological anions.

Furthermore, T_1-weighted phantom MR imaging under clinical scanner at 1.5 T confirmed its efficiency as brightening agent. The brightness of the acquired images increased with increase in complex concentration (**Figure 3**). Thus, a seven-coordinate highly stable Mn(II) complex with one coordinated-water molecule has been synthesized, and its efficiency as T_1-weighted MRI contrast agent has been studied.

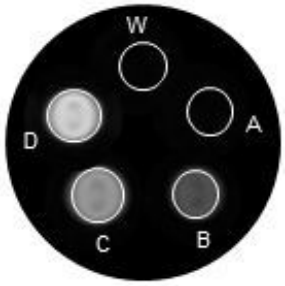

***Figure 3**. T_1-weighted phantom MR images of complex **5A** under clinical scanner at 1.5 T (W= water, A = 0.25, B= 0.50, C= 0.70, and D = 1.00 mM solution of the complex in HEPES buffer).*

Chapter VI

A High Relaxivity, Stable Mn(II) Complex of Picolinate-Based Ligand as MRI Contrast Agent

To the search of thermodynamically stable Mn(II)-based MRI contrast agents, complexation of picolinate-based hexadentate ligand **H_2hbda** has been carried out with Mn(II) ion [**Scheme 6(A)**]. Ligand with alcoholic donor group has been known for stabilizing Gd(III) complexes. Herein, the same strategy has been tried to implement to stabilize Mn(II) complex without imposing rigidity, driven by chirality of ligand backbone.

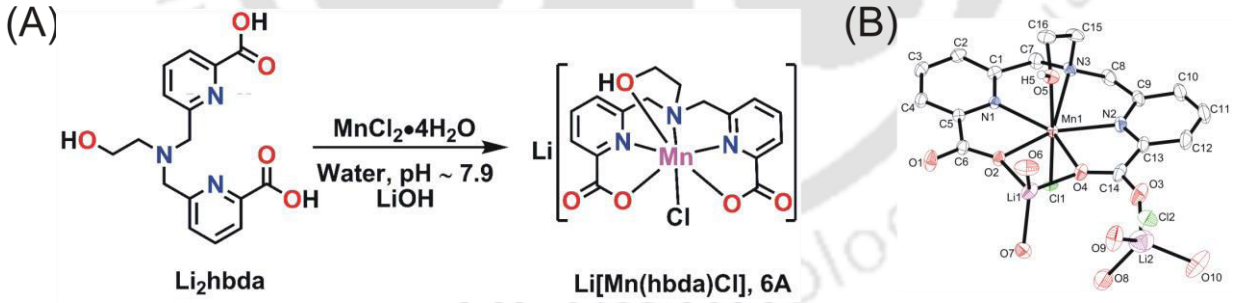

***Scheme 6.** (A) Synthesis of complex **6A**, and (B) ORTEP view of complex **6A•LiCl•5H_2O**.*

Single crystal XRD analysis revealed seven-coordinate Mn(II) complex in pentagonal bipyramidal geometry [**Figure 6(B)**]. Structural analysis implied the presence of one Cl-atom coordinated to Mn(II) ion, which in solution state was substituted by one water molecule forming neutral [Mn(hbda)(H_2O)] complex.

The potentiometric titration was carried out with 1:1 molar equivalents of Mn(II) ion and ligand **H_2hbda** in 0.15 M NaCl solution, at 25 °C to assess the thermodynamic stability constant for complex **6A**. The stability constant of the complex was observed to be 13.46; which was found to be significantly higher compared to seven-coordinate Mn(II) complexes with one coordinated-water molecule. pMn value was calculated to be 9.00 at the particular condition of pH ~ 7.4, 25 °C, and M] = $[L]_{total}$ = 10 μM.

Besides high thermodynamic stability, [Mn(hbda)(H_2O)] owned impressive water proton relaxation properties. At 1.41 T, and 25 °C; the complex depicted longitudinal relaxivity value of 3.74 $mM^{-1}s^{-1}$ in HEPES buffer maintaining pH ~ 7.4. pH-effect was not observable in the range of 4-8. The coordination environment of the complex remained intact in the presence of physiological anions (HCO_3^-, HPO_4^{2-}, F^-), which was confirmed by r_1 relaxivity measurements of the complex in the presence of 200 equivalents (100 mM) of these anions at 1.41 T in pH ~ 7.4, 25 °C. In the presence of HPO_4^{2-} anion, intermolecular interactions might be occurred resulting into decrease in overall tumbling rate of the complex.

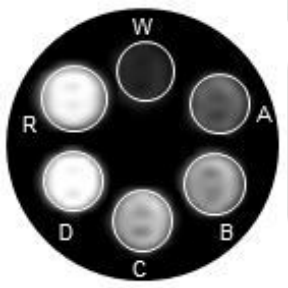

***Figure 4**. T_1-weighted phantom MR images of complex **6A** under clinical scanner at 1.5 T; (W= water, A = 0.25, B= 0.50, C= 0.70, and D = 1.00 mM solution of complex; R = 1.00 mM solution of MultiHance® in HEPES buffer).*

The acquired T_1-weighted phantom images under clinical imager at 1.5 T unveiled the positive contrast efficiency of the complex (**Figure 4**). Herein, mono(aquated) Mn(II) complex of ligand **H_2hbda** with better relaxivity value has been reported and its thermodynamic stability with alcoholic donor group has been studied.

Contents

Chapter IV

A Mono(aquated) Mn(II) Complex with Lipophilic Piperidine Ligand Backbone as T_1-weighted MRI Contrast Agent

Chapter V

A Stable Mono(aquated) Mn(II) Complex as T_1-weighted MRI Contrast Agent

Chapter VI

A High Relaxivity, Stable Mn(II) Complex of Picolinate-Based Ligand as MRI Contrast Agent

Symbols

m/z: mass per charge
λ: wavelength (nm)
δ: isomer shift
B: magnetic field
k_{ex}: water exchange rate
T_1: longitudinal relaxation time
R_1: longitudinal relaxation rate
r_1: longitudinal relaxivity
T_2: transverse relaxation time
R_2: transverse relaxation rate
×: multiplication
E: total energy
q: number of coordinated-water molecules attached to metal ion
J: coupling constant
S: electron spin
s: singlet
d: doublet
t: triplet
q: quartet
τ: phosphorescence lifetime
ΔHpp: peak-to-peak EPR line width
TR: repetition time
TE: echo time
Exp: experimental
Sim: simulated

Unit

Å: angstrom
cm: centimeter
h: hour
K: kelvin
M: molar
N: normal
min: minute
mL: milliliter
mM: milimolar
μM: micromolar
s: second
T: tesla
°C: degree centigrade
Hz: hertz
mm: millimeter
μL: microliter

Solvents and Reagents

CH_2Cl_2: dichloromethane
$CHCl_3$: chloroform
Et_2O: diethyl ether
Et_3N: triethylamine
KBr: potassium bromide
MeOH: methanol
CH_3CN: acetonitrile
$MnCl_2 \bullet 4H_2O$: manganese chloride tetrahydrate
$GdCl_3 \bullet xH_2O$: gadolinium chloride hydrate
TFA: trifluoroacetic acid
DMF: dimethylformamide
KCl: potassium chloride
XO: xylenol orange
H_2SO_4: sulphuric acid
$SOCl_2$: thionyl chloride
NaOH: sodium hydroxide
LiOH: lithium hydroxide
HCl: hydrochloric acid

$TbCl_3 \bullet 6H_2O$: terbium chloride hexahydrate
HEPES: 2-[4-(2-hydroxyethyl)-1-piperazinyl]ethanesulfonic acid)
THF: tetrahydrofuran

Techniques

NMR: nuclear magnetic resonance
IR: infrared
UV-Vis: ultraviolet-visible
ICP-AES: inductively coupled plasma atomic emission spectroscopy
MS: mass spectrometry
EPR: electron paramagnetic resonance
ESI: electrospray ionization

Latin expressions

et al.: and co-workers
e.g.: for example
vs.: versus
viz.: namely
tert-: tertiary
via.: through
i.e.: that is

Chapter I

General Introduction

1.1 Magnetic Resonance Imaging (MRI):

Magnetic resonance imaging is a powerful non-invasive diagnostic imaging modality.[1] It can penetrate inside the soft tissues from 1 mm to 1 m depth level, and captures three dimensional images with exquisite resolution.[2] In contrast to other diagnostic techniques such as X-Ray Computer Tomography (CT), Single-photon Emission Computed Tomography (SPECT) or Positron Emission Tomography (PET), MRI does not involve any harmful high-energy radiation.[3]

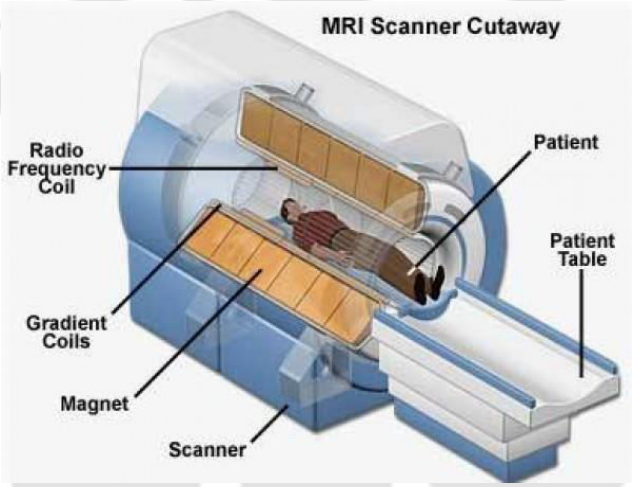

Figure 1.1. *Basic components present in a MRI scanner.*[4]

An MRI machine, as shown in **Figure 1.1**, consists of following components: (*a*) a large magnet, (*b*) gradient coils, (*c*) radio frequency coil, (*d*) patient table, and (*e*) antenna along with computer system. In the presence of static magnet, the gradient coils spatially encode the subjected nuclei with different resonance frequencies. After application of radio frequency pulse, free induction decay signal is Fourier transformed to construct the images based on NMR signal intensity.

Fundamentally, MRI measures ^{1}H-NMR signals of endogenous water molecules (~ 70% of body weight).[5] Tissues present in different parts of our body have different levels of water contents, and these water molecules possess discrete physical and magnetic properties. MRI machine involves water molecule protons present in human body (sample) to generate NMR signals.[6] The signals analyze the local environments of examined tissues, and images are acquired from the variation of longitudinal ($R_1 = 1/T_1$), and transverse ($R_2 = 1/T_2$) relaxation rates of these water molecules.[7] Eventually, the difference in relaxation rates within the tissues depicts anatomy and pathology of examined tissues *via* image contrast.

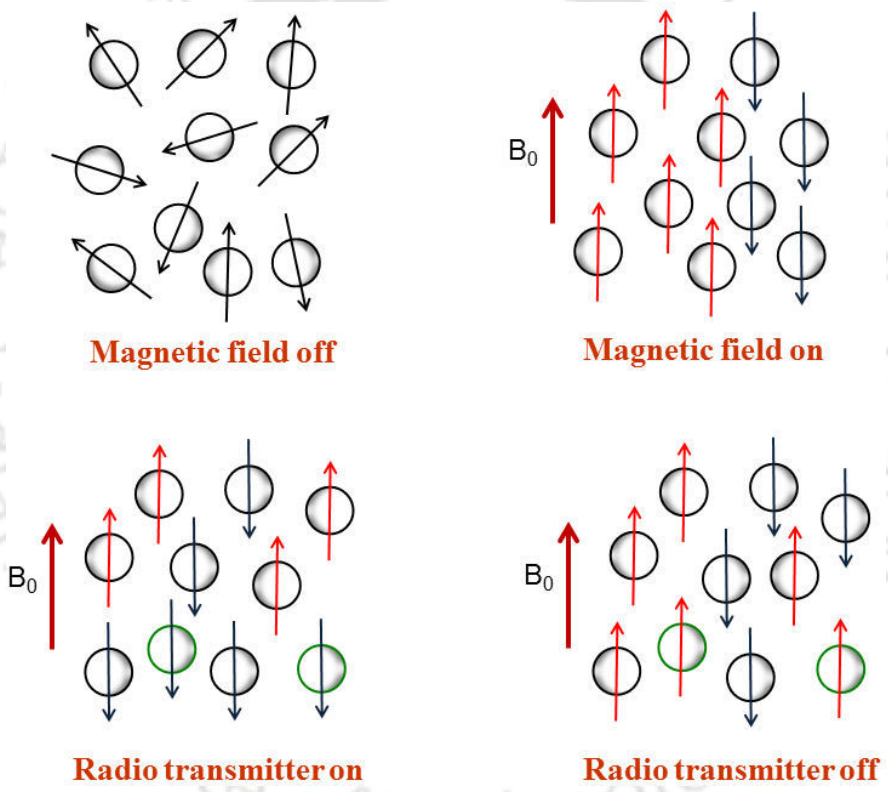

Figure 1.2. *Arrangement of protons during MRI experiment.*

The physical principle of MRI lies on magnetic moment associated with positively charged spinning proton. These charged spheres in spinning motion behave like small magnets which are found randomly oriented in the absence of any external field. After applying a

magnetic field in the MRI machine, these spinning charged spheres get aligned themselves in either parallel (low in energy) or antiparallel (high in energy) directions of the applied magnetic field and precess (Larmor precession). The lower energy state has higher population than that of the higher energy state, and the population-difference differs according to the measurement-temperature and measurement-magnetic field. On application of a radio frequency pulse equal to Larmor frequency, some of charged spheres pick up the energy and jump to higher energy level by flipping its orientation and all start to precess in phase. It produces decrease in net longitudinal magnetization and establishes transverse magnetization. At the end of radio frequency pulse, the whole system returns back to its equilibrium position by a process termed as relaxation (**Figure 1.2**). Depending upon the process of coming back to the equilibrium position, relaxation process is classified into two types.

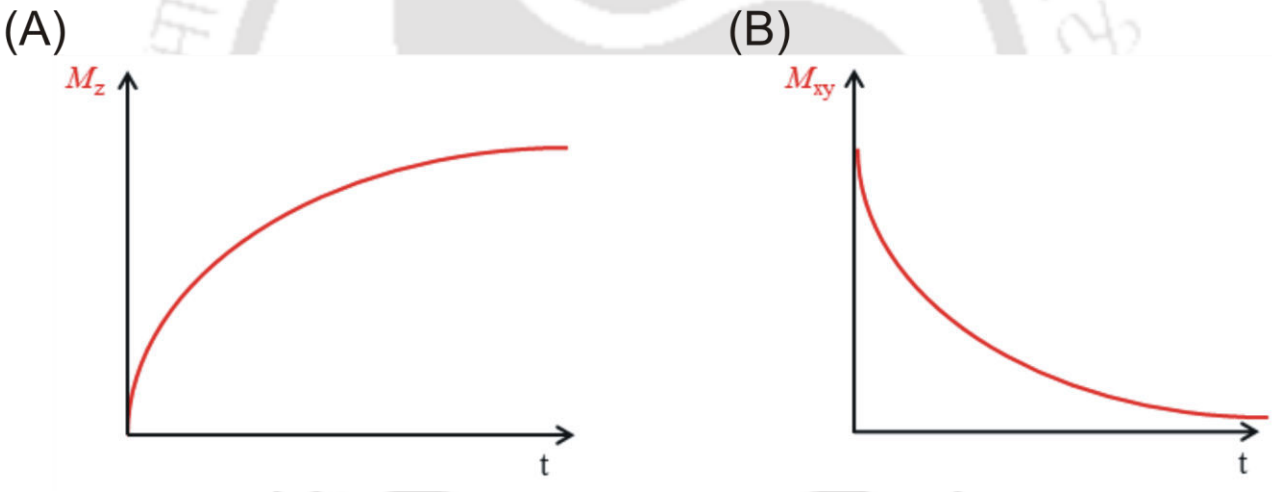

Figure 1.3. *Variation of magnetization in returning back to equilibrium position, (A) on z-axis in longitudinal relaxation, and (B) on xy-plane in transverse relaxation.*

Longitudinal relaxation (T_1 relaxation):

It is the process of relaxation in which magnetization increases exponentially along z-direction to initial maximum value (M_0) by transferring energy to its surrounding lattice [**Figure 1.3(A)**].

This is also known as thermal relaxation or spin-lattice relaxation. T_1 is the time required to recover 63% of its original magnetization along z-direction,

$$M_z = M_0 (1 - e^{-t/T1})$$

Transverse relaxation (T_2 relaxation):

In this relaxation process, net magnetization in xy-plane decreases because of loss of spin coherence. This is called spin-spin relaxation [**Figure 1.3(B)**]. In T_2-time transverse magnetization decreases to 37% of its original magnetization value which is given by the equation,

$$M_{xy} = M_0 e^{-t/T2}$$

T_1 and T_2 relaxation times are highly sensitive to biochemical conditions (such as water concentration, pH, temperature, salt, or fat concentration *etc.*) of examined tissues. T_1 and T_2 relaxation times of malignant tissues are significantly longer than normal tissues. Thus, an MRI experiment can diagnose any abnormalities present in the examined tissues. **Table 1.1** shows difference of T_1 relaxation times between normal and malignant tissues from different parts of human body.

Table 1.1. *T_1 relaxation times in normal and malignant human tissues.*[8]

Tissue	T_1 tumor (s)	T_1 normal (s)
Liver	0.832	0.570
Lung	1.110	0.788
Breast	1.080	0.367
Bone	1.027	0.554
Skin	1.047	0.616

Based on two types of relaxation times, images can be differentiated into either T_1-weighted or T_2-weighted images. The area with high signal intensity appears brighter than the

area with low signal intensity in an MRI image. In T_1-weighted imaging, tissues with short T_1 appear brighter due to regain of most of its longitudinal magnetizations producing strong MR signal. Whereas, tissues with long T_1 appear dark as they are unable to regain much of their longitudinal magnetization, hence producing weak signal. Therefore, tissue with high fat content appears brighter (e.g. white matter), and compartments filled with more water [*e.g.* Cerebrospinal fluid (CSF)] appear dark [**Figure 1.4(A)**].

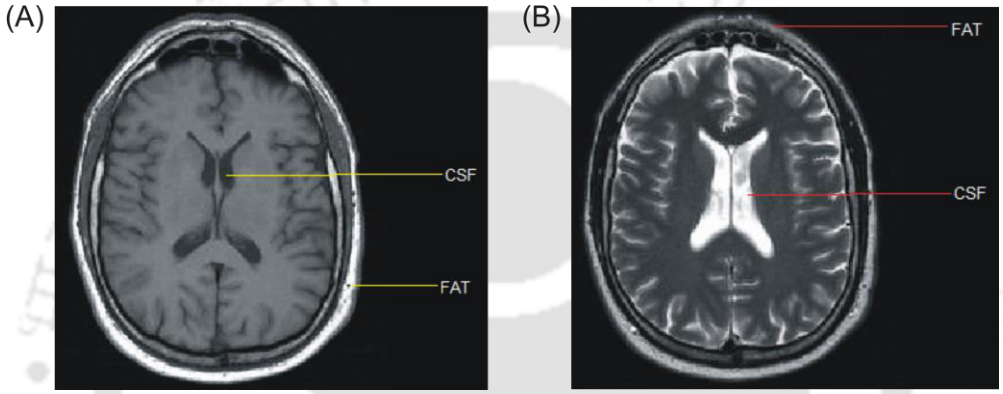

Figure 1.4. *Image contrast between fat and CSF in; (A) T_1-weighted, and (B) T_2-weighted MR imaging.*[9]

In case of T_2-weighted imaging, tissues with short T_2 appear dark due to loss of complete signal. While tissues having long T_2 generate stronger signal and thus appear bright. Therefore, CSF with long T_2 appears brighter on T_2-weighted images compared to fat with short T_2 value [**Figure 1.4(B)**].

1.2 MRI Contrast Agents:

Despite inherent contrast ability, certain diagnostic queries cannot be completely answered from a simple MRI scan. When it is unachievable to attain inherent contrast during any experiment, it becomes necessary to manipulate the image contrast by applying some external agents known as contrast agents.[10] These external agents are normally paramagnetic, superparamagnetic, or

ferromagnetic compounds that can catalytically shorten the relaxation times of bulk water molecules (**Figure 1.5**).[11] Although all contrast agents can decrease both T_1 and T_2 relaxation times, they are mainly classified into two broad groups depending upon their dominant effect.

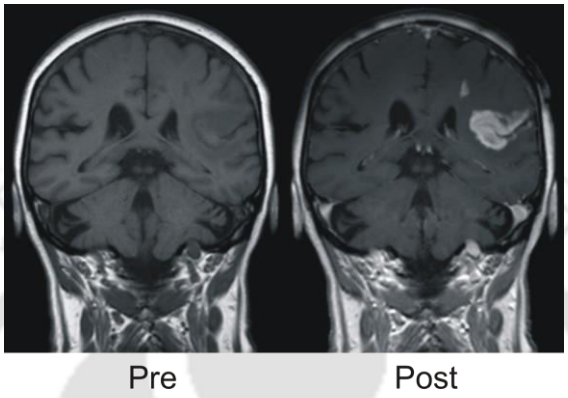

Figure 1.5. *Effect of contrast agent on the images detecting blood-brain barrier after stroke.*

T_1-Contrast Agents:

A number of paramagnetic metal ions with large number of unpaired electrons including Gd(III), Mn(II), Mn(III), Fe(III) *etc*.[12] can provide more image contrast. The unpaired electrons can produce strong fluctuating magnetic field and efficiently relax nearby nuclei. They are predominant in lowering T_1 relaxation times resulting in enhancement of signal intensity. These are known as positive contrast agents.

T_2-Contrast Agents:

These are super paramagnetic and ferromagnetic substances which effect predominantly in lowering T_2 relaxation times. Reduction in T_2 relaxation times decreases MRI signal intensity. These contrast agents are known as negative contrast agents. Iron oxide nanoparticles are mostly

used as T_2 contrast agent. These particles are behaving as small movable magnets, which finally create a strong magnetic field. They are again classified according to their sizes,[13]

(*a*) Super paramagnetic iron oxides (SPIO), average diameter > 50 nm, and

(*b*) Ultra-small super paramagnetic iron oxides (USPIO), average diameter < 50 nm.

1.3 Relaxivity and Solomon-Bloembergen Equations:

The contrast agents influence the relaxation properties of water molecule protons which generate contrast in MRI images. Since, the concentration of water molecules is much higher compared to applied contrast agent; the action of contrast agents on the relaxation rates of water molecules is catalytic. The paramagnetic species can increase the longitudinal ($1/T_1$), and transverse relaxation ($1/T_2$) rates of solvent nuclei. The observed relaxation rate $(1/T_i)_{obsd}$ in the presence of contrast agent is expressed by the following equation,

$$(1/T_i)_{obsd} = (1/T_i)_d + (1/T_i)_p \quad i = 1, 2 \qquad \textbf{(1)}$$

Where, $(1/T_i)_d$ is the diamagnetic solvent relaxation rate in the absence of any paramagnetic species and $(1/T_i)_p$ is the paramagnetic contribution in the presence of paramagnetic species.

The relaxation rates of water protons directly depend upon the concentration of paramagnetic species. Relaxivity (r_i) can be determined from the slope of the linear plot of relaxation rate *vs* concentration of the paramagnetic species. The linear dependence of relaxation rate is given by the following equation:

$$(1/T_i)_{obsd} = (1/T_i)_d + r_i[M] \quad i = 1, 2 \qquad \textbf{(2)}$$

The overall relaxivity value of a contrast agent depends upon the interaction of water molecules present in both inner coordination sphere of the metal ion and also the hydrogen bonded water molecules present in the second coordination sphere. Thus, the total relaxivity value is the summation of relaxation rates of water molecules present in both inner and outer-sphere of the paramagnetic metal ion which is given by the following equation:

$$(1/T_i)_p = (1/T_i)_{inner\text{-}sphere} + (1/T_i)_{outer\text{-}sphere} \quad \textbf{(3)}$$

The inner-sphere longitudinal relaxation process is due to the exchange of water molecules within first coordination sphere of the metal ion and the bulk solvent molecules. The inner-sphere contribution to the relaxation process is expressed by the following equation:

$$(1/T_1)_{inner\text{-}sphere} = P_M q/(T_{1M} + \tau_M) \quad \textbf{(4)}$$

Here, P_M refers to the mole fraction of the paramagnetic metal ion, q is the number of coordinated water molecule per metal ion, T_{1M} and τ_M represent relaxation time and residence lifetime of bound water molecule in the metal ion respectively.

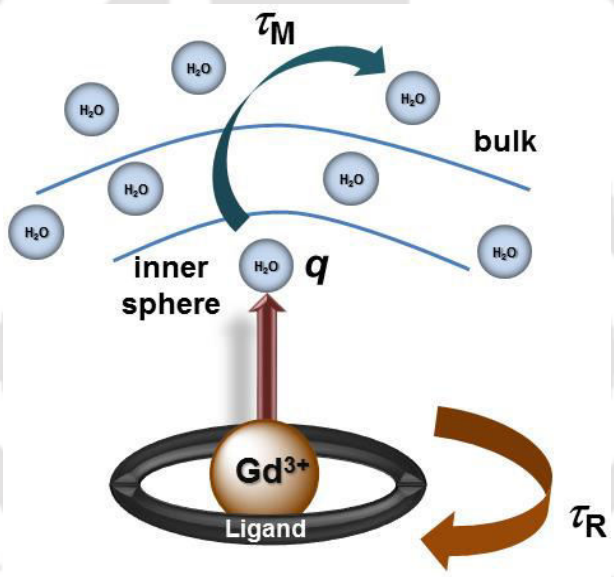

Figure 1.6. *Schematic representation of various parameters affecting relaxivity.*

The relaxation process of bound water molecule is controlled by both dipole-dipole (through-space interaction), and scalar (through contact) mechanisms. The relaxation time of bound water molecule (T_{1M}) is explained by Solomon-Bloembergen-Morgan (SBM) theory with a set of analytical equations as given below,[14]

$$1/T_{1M} = 2/15\ [\gamma_I^2 g^2 S(S+1)\beta^2]/r^6 \left[7\tau_c/(1+\omega_S^2\tau_c^2) + 3\tau_c/(1+\omega_I^2\tau_c^2)\right] +$$

$$2/3S(S+1)\left(A/\hbar\right)^2 \left[\tau_e/(1+\omega_S^2\tau_c^2)\right] \quad \textbf{(5)}$$

$$1/\tau_c = 1/T_{1e} + 1/\tau_M + 1/\tau_R \quad \textbf{(6)}$$

$$1/\tau_e = 1/T_{1e} + 1/\tau_M \quad \textbf{(7)}$$

In the equations (5)–(7), γ_I is the proton gyromagnetic ratio, g is the electronic g-factor, S is the total electron spin of the metal ion, β is the Bohr magneton, r is the distance of proton from the metal ion, ω_S and ω_I are electronic and Larmor precession frequencies respectively, $A/\hbar$ is electron-nuclear hyperfine coupling constant, T_{1e} is the longitudinal electron spin relaxation time, τ_M is the residence time of water molecule, and τ_R is the rotational tumbling time of the whole molecule.

According to this theory, high relaxivity value can be achieved by judicious ligand designing which will enable the complex to have,

(*i*) greater number of inner-sphere water molecules (***q***),

(*ii*) short water residence time ($\boldsymbol{\tau_M}$), and

(*iii*) slow tumbling rate ($\boldsymbol{1/\tau_R}$).

However, Solomon-Bloembergen-Morgan theory has some limitations and not suitable at very low magnetic field and large slowly rotating molecules.

1.4 Contrast Agents with Gd(III) and Mn(II) ions:

The use of Gd(III) ion as prominent T_1-weighted contrast agent relies on high magnetic moment (7.9 BM) due to seven unpaired *f*-electrons, totally symmetric electronic configuration ($^8S_{7/2}$, ground state) which makes long electronic relaxation time (10^{-8}-10^{-9} s).[15] The high magnetic moment of electrons triggers the return of water protons to equilibrium positions. The magnetic

moment of an electron is 658 times stronger than a proton. Thus, the presence of unpaired electrons is more effective in relaxation process and can provide excellent image contrast. But, high toxicity of Gd(III) ion in aqua form necessitates strong coordination of Gd(III) ion by organic ligand frameworks before *in vivo* use.[16] Lanthanide ions belong to "hard" acid family, hence ligand frameworks have been designed with nitrogen and oxygen donor atoms.[17] From structural point of view, mainly two types of ligand frameworks are designed with polyaminocarboxylate arms for coordination: twelve membered tetraazamacrocyclic cyclen derivatives (cyclen = 1,4,7,10-tetraazacyclododecane) and acyclic triamines (diethylenetriamine derivatives) with several chelating arms, offering an octadentate coordination environment for Gd(III) ion leaving one site available for binding one water molecule.[18] The clinically used Gd(III) complexes based on these two types of ligand backbone is shown in **Scheme 1.1**.[19]

Although, most of paramagnetic contrast agents undergoing clinical practices are composed of Gd(III) chelates, the discovery of the disease Nephrogenic systemic fibrosis (NSF) in 2006, has pointed out some restrictions of using these Gd(III) based contrast agents.[20] NSF is a systemic disorder characterized by fibrosis of skin and connective tissues, and often leading to disability and death. Further evaluation reveals that NSF affects patients having severe renal problems and after administration of Gd(III)-based contrast agents.[21] Risk of NSF introduces new research to develop safer MRI contrast agents. In search of suitable alternative which can efficiently relax water protons and also less toxic for our body, both Mn(II) and Fe(III) ions get special attentions. Both play important biological rules and less toxic than Gd(III) ion. Both Mn(II) and Fe(III) ions possess high magnetic moment due to five unpaired electrons (d^5 electronic configuration) and longer electronic relaxation time.[22] In current medical practice, only one Mn(II)-based contrast agent $[Mn(DPDP)]^{4-}$ (TESLASCAN) (**Scheme 1.2**) is used for liver and cardiac imaging [$DPDP^{6-}$ = N,N′-dipydoxylethylenediamine-N,N′-diacetate-5,5′-bis-(phosphate)]. The complex does not possess any directly coordinated water molecule, it effects the relaxation process by slow release of Mn(II) ion inside our body. The slowly released Mn(II) ion is taken up by hepatocytes resulting in impressive image contrast.[23]

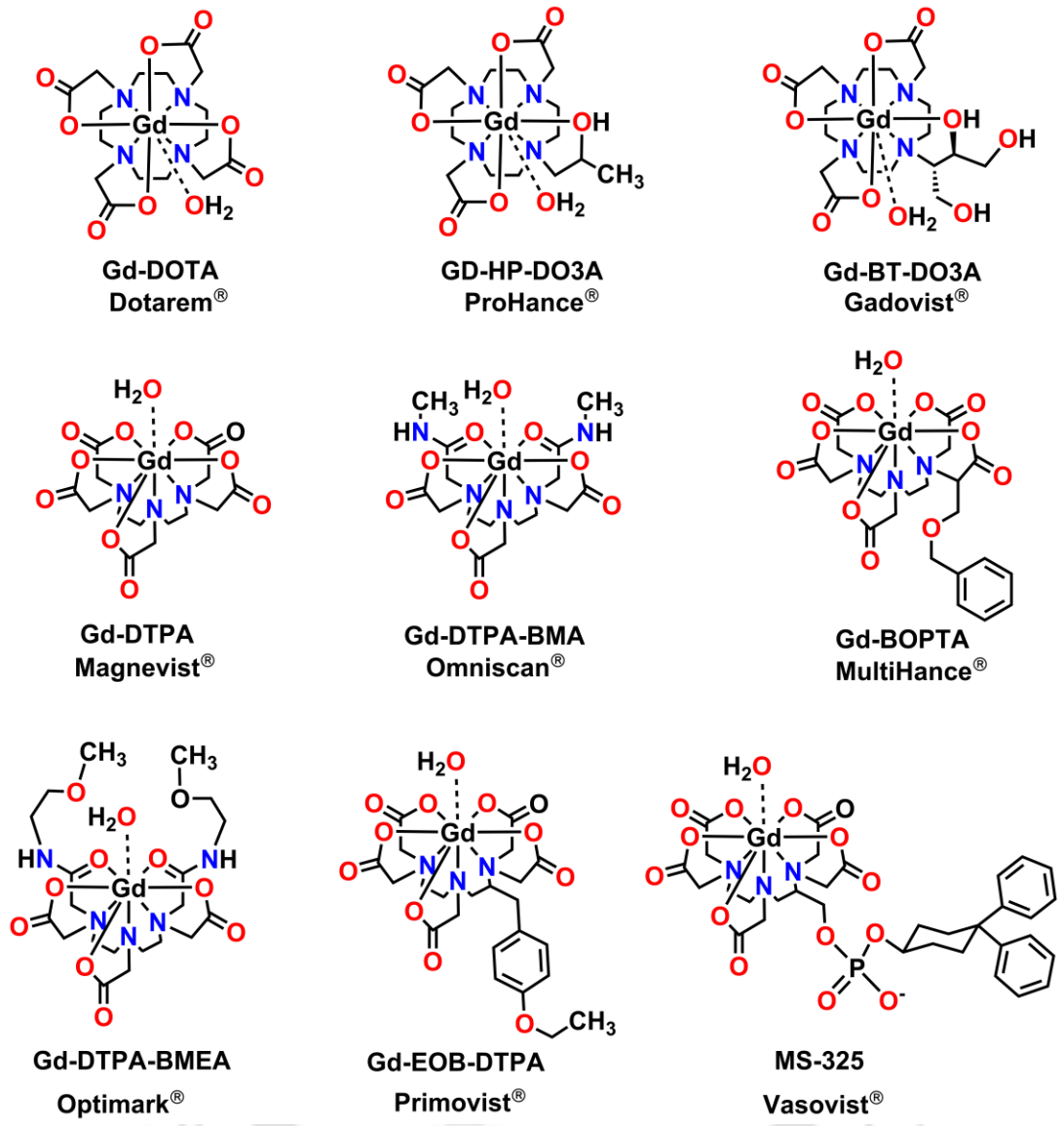

Scheme 1.1. *Commercially available Gd(III)-based MRI contrast agents.*

Recently, another one Mn(II)-based contrast agent that undergoes phase III clinical trials, is CMC-001 (a mixture of $MnCl_2$, alanine, and vitamin D_3).[24] Although Mn(II) ions are biogenic,[25] long term exposure of free Mn(II) ion results in accumulation of free Mn(II) ion in brain and leading to neurotoxicity with symptoms of Parkinson-like disease, known as "Manganism".[26] Thus, designing of suitable ligand framework satisfying stable Mn(II)

complexation along with good MRI efficiency is another challenge. Lack of crystal field stabilization energy due to symmetric d^5 electronic configuration makes Mn(II) complexes as the lowest stable among all high spin divalent first-row transition metal complexes, or Gd(III) analogues. As a consequence, designing of suitable ligand frameworks which can form thermodynamically stable and kinetically inert Mn(II) complexes as potential MRI contrast agents is needed to be evaluated carefully.[27]

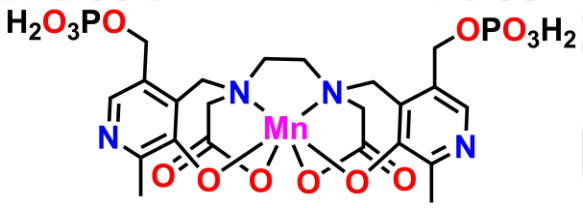

Scheme 1.2. *TESLASCAN®, commercially available Mn(II)-based MRI contrast agent.*

In addition to nuclear relaxation property, contrast agents should possess standard pharmaceutical features like water solubility, *in vivo* stability, less toxicity, and it should be excreted out within hours of administration.[1(*a*)]

Current clinically used contrast agents with polyaminocarboxylate scaffolds have relaxivity values of only 4-5 $mM^{-1}s^{-1}$.[28] The observed relaxivity values are much smaller than theoretically possible values. The main drawback of these kind of complexes is lower number of coordinated water molecule ($q \sim 1$), inability to attain optimum rotational correlation time (in peco second region for small molecules), and optimal water exchange rate (150-1000 ns for commercial contrast agents). Therefore, it is necessary to improve the water exchange rate,[29] slow down the molecular tumbling rate,[2(a),(b)] maintaining long electronic relaxation times with higher number of coordinated-water molecules[30] to achieve maximum possible relaxivity value predicted by the theory.

In this thesis, the following ligands and their corresponding Gd(III) and Mn(II) complexes have been studied to the search of new contrast agents with high q value ($q \geq 1$) and high thermodynamic stability.

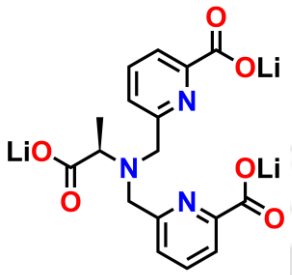

Li_3cbda

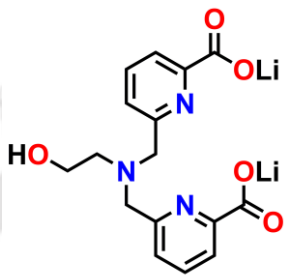

Li_2hbda

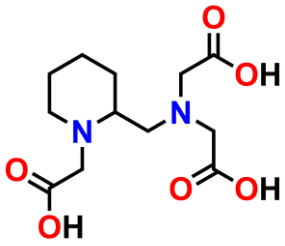

H_3cpmda

References

1. (*a*) R. E**.** Lauffer, *Chem. Rev.*, 1987, **87**, 901; (*b*) K. N. Raymond and V. C. Pierre, *Bioconjugate Chem*., 2005, **16**, 3; (*c*) E. J. Werner, A. Datta, C. J. Jocher and K. N. Raymond, *Angew. Chem. Int. Ed*., 2008, **47**, 8568.

2. (*a*) A. Datta and K. N. Raymond, *Acc. Chem. Res*., 2009, **42**, 938; (*b*) P. Caravan, *Acc. Chem. Res*., 2009, **42**, 851; (*c*) P. Caravan, *Chem. Soc. Rev*., 2006, **35**, 512; (*d*) E. L. Quea and C. J. Chang, *Chem. Soc. Rev*., 2010, **39**, 51; (*e*) P. Caravan, J. J. Ellison, T. J. McMurry and R. B. Lauffer, *Chem. Rev*., 1999, **99**, 2293.

3. R. Salzer, *Biomedical Imaging*: *Principles and applications*, a John Wiley and Sons, Inc., 2012.

4. http://www.maggiephilbin.com/wp-content/uploads/2010/11/mri-scanner.jpg.

5. H. H. Mitchell, T. S. Hamilton, F. R. Steggerda and H. W. Bean, *J. Biol. Chem*., 1945, **158**, 625.

6. (*a*) R. A. Pooly, *RadioGraphics*, 2005, **25**, 1087; (*b*) S. Curie, N. Haggard, I. J. Craven, M. Hadjivassiliou and I. D. Wilkinson, *Postgrad. Med. J*., 2013, **89**, 209; (*c*) K. L. Mcmahon, G. Cowin and G. Galloway, *J. Orthop. Sports Phys. Ther*., 2011, **41**, 806.

7. *The Chemistry of Contrast Agents in Medical Magnetic Resonance Imaging*, ed. A. E. Merbach, and E´. Tóth, John Wiley & Sons, Chichester (England), 2001.

8. R. Damadian, K. Zaner, D. Hor and T. Dimaio, *Proc. Nat. Acad. Sci. USA,* 1974, **71**, 1471.

9. http://casemed.case.edu/clerkships/neurology/NeurLrngObjectives/MRI.htm.

10. (*a*) P. Hermann, J. Kotek, V. Kub˘ícek and I. Lukeš, *Dalton Trans.*, 2008, 3027; (*b*) E. Boros, E. M. Gale and P. Caravan, *Dalton Trans*., 2015, **44**, 4804; (*c*) J. M. Major and T. J. Meade, *Acc. Chem. Res*., 2009, **42**, 893; (*d*) D. Lawson,A. Barge, E. Terreno, D. Parker, S. Aime and M. Botta, *Dalton Trans*., 2015, **44**, 4910.

11. Bluthirnschranke nach Infarkt nativ und KM.png.

12. (*a*) B. Drahoš, I. Lukeš and É. Tóth, *Eur. J. Inorg. Chem*., 2012, 1975; (*b*) S. Aime, M. Botta, M. Fasano and E. Terreno, *Chem. Soc. Rev*., 1998, **27**, 19; (*c*) A. J. L. Villaraja, A. Bumb and M. W. Brechbiel, *Chem. Rev*., 2010, **110**, 2921.

13. R. Qiao, C. Yang and M. Gao, *J. Matter. Chem*., 2009, **19**, 6274.

14. I. Solomon and N. Bloembergen, *J. Chem. Phys*., 1956, **25**, 261.

15. (*a*) M. Bottrill, L. Kwok and N. J. Long, *Chem. Soc. Rev*., 2006, **35**, 557; (*b*) C. F. G. C. Geraldes and S. Laurent, *Contrast Media Mol. Imaging*, 2009, **4**, 1.

16. Zheng-R. Lu, A. M. Mohs, Y. Zong and Y. Feng, *Int. J. Nanomedicine*, 2006, **1**, 31.

17. A. D. Sherry, P. Caravan and R. E. Lenkinski, *J. Magn. Reson. Imaging*, 2009, **30**, 1240.

18. Valtancoli, *Coord. Chem. Rev*., 2000, **204**, 309.

19. (*a*) K. Wai-Y. Chan, S. Barra, M. Botta and Wing-T. Wong, *J. Inorg. Biochem*., 2004, **98**, 677; (*b*) S. Gu, Hee-K. Kim, G. H. Lee, Bong-S. Kang, Y. Chang and Tae-J. Kim, *J. Med. Chem*., 2011, **54**, 143; (*c*) A. Takács, R. Napolitano, M. Purgel, A. C. Bényei, L. Zékány, E. Brücher, I. Tóth, Z. Baranyai and S. Aime, *Inorg. Chem*., 2014, **53**, 1858; (*d*) B. Jebasningh and V. Alexander, *Inorg. Chem*., 2005, **44**, 9434.

20. T. Grobner, *Nephrol. Dial. Transplant*., 2006, **21**, 1104.

21. (*a*) H. S. Thomsen, *Eur. Radiol*., 2007, **17**, 2692; (*b*) N. Nainani and M. Panesar, *Am. J. Nephrol*., 2009, **29**, 1; (*c*) D. R. Martin, *Pediatr. Radiol*., 2008, **38**, S125; (*d*) E. A. Sadowski, L. K. Bennet, M. R. Chan, A. L. Wentland, A. L. Garret, R. W. Garrett and A. Djamali, *Radiology*, 2007, **243**, 148; (*e*) M. Sieber, P. Lengsfeld, J. Walter, H. Schirmer, T. Frenzel, F. Siegmund, H. Weinmann and H. Pietsch, *J. Magn. Reson. Imaging*, 2008, **27**, 955; (*f*) D. J. Todd and J. Kay, *Curr. Rheumatol. Rep*., 2008, **10**, 195; (*g*) S. E. Cowper, *Adv. Dermatol*., 2007, **23**, 131.

22. (*a*) B. Drahoš, M. Pniok, J. Kotek, I. Císařová, P. Hermann, I. Lukeš and É. Tóth, *Dalton. Trans*., 2011, **40**, 10131; (*b*) J. S. Troughton, M. T. Greenfield, J. M. greenwood, S. Dumas, A. J. Wiethoff, J. Wang, M. Spiller, T. J. McCurry and P. Caravan, *Inorg. Chem*., 2004, **43**, 6313; (*c*) E. Molnár, N. Camus, V. Patinec, G. A. Rolla, M. Botta, G. Tircsó, F. K. Kálmán, T. Fodor, R. Tripier and C. Platas-Iglesias, *Inorg. Chem*., 2014, **53**, 5136.

23. S. M. Rocklage, W. P. Cacheris, S. C. Quary, F. E. Hahn and K. N. Raymond, *Inorg. Chem*., 1989, **28**, 477.

24. J. T. Jorgensen, M. Rief, T. B. Brismar, M. Wagner and N. Albeiin, *Acta Radiol*., 2012, **53**, 707.

25. (*a*) J. Crossgrove, W. Zheng, *NMR Biomed.*, 2004, **17**, 544; (*b*) B. Drahoš, J. Kotek, P. Hermann, I. Lukeš and E. Tóth, *Inorg. Chem*., 2010, **49**, 3224.

26. M. G. Cersosimo and W. C. Koller, *Neurotoxicology*, 2006, **27**, 340.

27. (*a*) B. Drahoš, V. Kub´ıcek, C´. S. Bonnet, P. Hermann, I. Lukeš and E´. Tóth, *Dalton Trans.*, 2011, **40**, 1945; (*b*) P. Caravan, C. T. Farrar, L. Frullano, R. Uppal, *Contrast Media Mol. Imaging*, 2009, **4**, 89.

28. A. Merbach, L. Helm and E´. Tóth, *The Chemistry of Contrast Agents in Medical Magnetic Resonance Imaging*, Second Edition. Wiley, New York, 2001.

29. (*a*) M. F. Ferreira, A. F. Martins, J. A. Martins, P. M. Ferreira, E´. Tóth and C. F. G. C. Geraldes, *Chem. Commun*., 2009, 6477; (*b*) M. Woods, S. Aime, M. Botta, J. A. K. Howard, J. M. Moloney, M. Navet, D. Parker, M. Port and O. Rousseaux, *J. Am. Chem. Soc*., 2000, **122**, 9781; (*c*) N. Iki, E. Boros, M. Nakamura, R. Baba and P. Caravan, *Inorg. Chem*., 2016, **55**, 4000.

30. (*a*) E. M. Gale, N. Kenton and P. Caravan, *Chem. Commun*., 2013, **49**, 8060; (*b*) V. C. Pierre, M. Botta, S. Aime and K. N. Raymond, *Inorg. Chem*., 2006, **45**, 8355; (*c*) D. T. Puerta, M. Botta, C. J. Jocher, E. J. Warner, S. Avendano, K. N. Raymond and S. M. Cohen, *J. Am. Chem. Soc*., 2006, **126**, 2222.

Chapter II

Motivation, Designing and Syntheses of Ligands

2.1 Introduction:

Ligands used in currently available commercial Gd(III)-based MRI contrast agents are based on either macrocyclic1,4,7,10-tetraazacyclododecane (**A**), or acyclic diethylenetriamine (**B**) backbones (**Figure 2.1**) with carboxylate and/or their derivatives as chelating arms.[1]

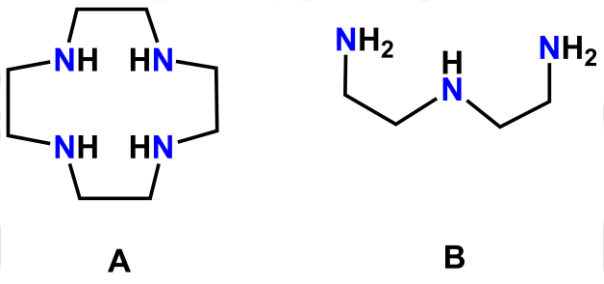

Figure 2.1. *Ligand backbones used in commercially available Gd(III)-based MRI contrast agents.*

The maximum coordination number of central Gd(III) ion in these complexes is nine with one coordinated-water molecule. These complexes exhibit longitudinal relaxivity value of r_1 = 4-5 $mM^{-1}s^{-1}$at 20 MHz, 298 K.[2] The values are relatively low compared to theoretically attainable maximum value of 100 $mM^{-1}s^{-1}$at 20 MHz, 298 K.[3] Therefore, all those parameters influencing relaxivity value are needed to be optimized in coordination complexes to attain high relaxivity.[1(b),4] Among the various parameters (q, τ_M, τ_R), which can influence relaxivity value, the number of inner-sphere water molecule (q) is independent of the applied magnetic field strength. The relaxivity value is directly proportional to the number of inner-sphere water molecules.[5] Hence, to attain higher relaxivity value, the number of inner-sphere water molecules in metal complexes is required to be increased. To obtain more than one inner-sphere water molecules in the complexes the binding sites of ligands should be reduced. However, reduction in ligand denticity decreases the thermodynamic stability of corresponding complexes.[6] Therefore; our main objective is to design suitable ligand frameworks such that their metal complexes could provide high relaxivity value with high thermodynamic stability.

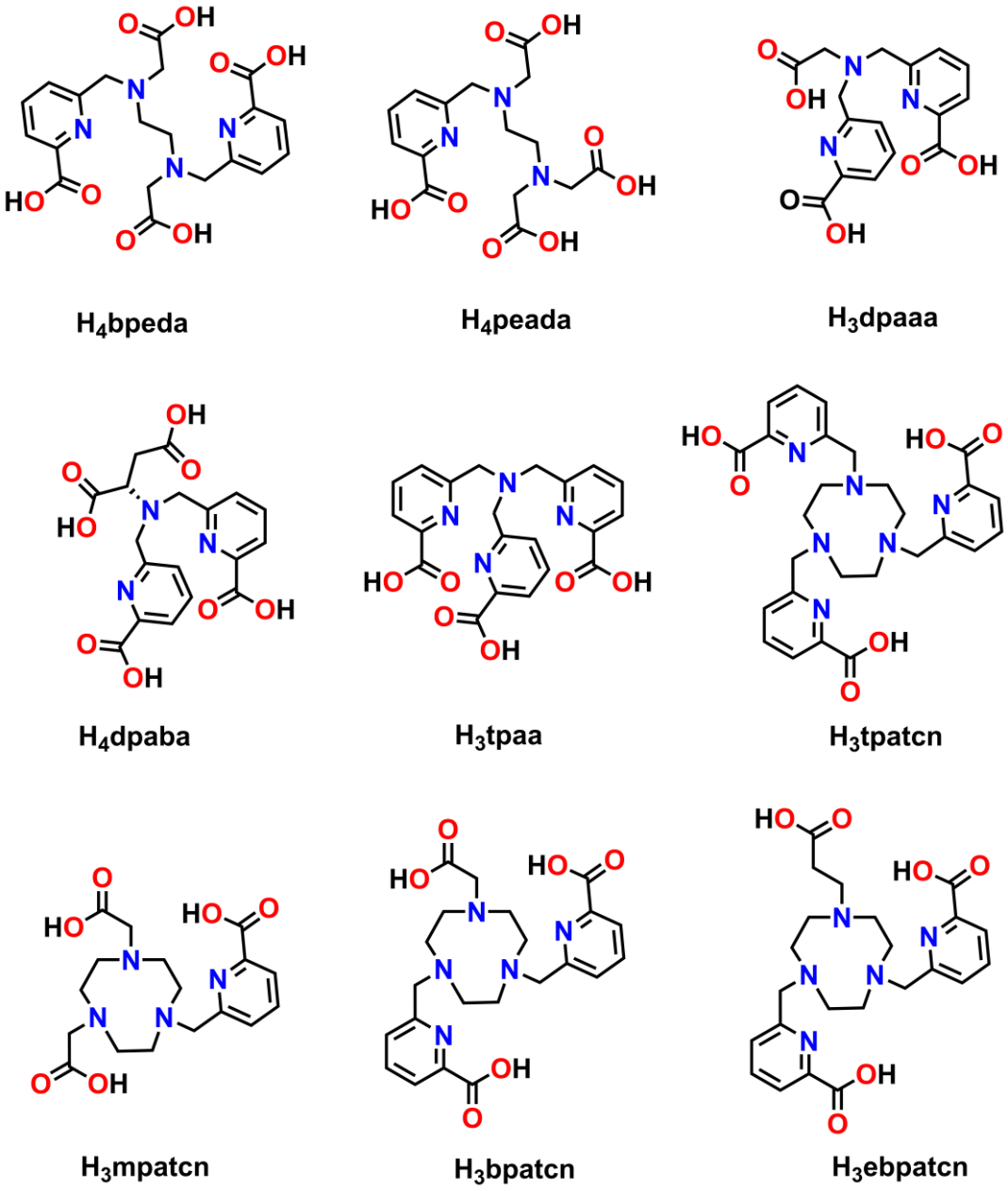

Scheme 2.1. *Picolinate-based ligands used for the synthesis of Gd(III) complexes.*

In last few years, a new series of ligand frameworks with picolinate arms have been introduced (**Scheme 2.1**). These tripodal or tetrapodal ligand systems are showing impressive relaxation properties. It has been observed that Gd(III) complexes of these picolinate-based ligands are associated with very high water exchange rate. The presence of flexible inner

coordination sphere around the metal center might be responsible for high relaxivity value for these Gd(III) complexes.[7] Furthermore, a pyridine moiety can be easily functionalized to bind with biological macromolecules,[8] which can increase the overall correlation time of the molecule to assist in achieving high relaxivity value. Examples of ligands containing picolinate moieties in their frameworks, along with longitudinal relaxivity value, and thermodynamic stability constant of their corresponding Gd(III) complexes are given in **Table 2.1**.

Table 2.1. *Picolinate-based ligands forming Gd(III) complexes, number of inner-sphere water molecules (q), longuitudinal relaxivity value and stability constant.*

Ligand	*q*	r_1 ($mM^{-1}s^{-1}$)	log K_{GdL}
H_4bpeda[7(e)]	2	5.00[a,9(a)]	15.10[7(e)]
H_4peada[8(b)]	2	6.08[b]	17.00
H_3dpaaa[5(b)]	3	9.62[a]	10.60
H_4dpaba[5(a)]	2	7.20[a]	12.50
H_3tpaa[9(b)]	2	13.30[b]	10.20
H_3tpatcn[9(c)]	0	5.30[d,7(a)]	17.40[c]
H_3mpatcn[5(a)]	2	6.60[a]	11.80
H_3bpatcn[7(a)]	1	4.59[e]	15.80
H_3ebpatcn[7(c)]	1	4.68[e]	15.10

[a] 20 MHz, 25 °C; [b] 60 MHz, 25 °C; [c] for TbL; [d] 0.02 MHz, 25 °C; [e] 45 MHz, 25°C.

Similar to Gd(III) complexes, Mn(II) complexes of ligands containing pyridine moieties in their framework have also shown impressive properties in terms of thermodynamic stability. Till now, series of ligands have been reported with pyridine rings as shown in **Scheme 2.2**. Since, Mn(II) ions do not possess crystal-field stabilization energy due to high-spin d^5 electronic configuration; the corresponding complexes are thermodynamically less stable. Therefore, stability of Mn(II) complexes play an important role during designing of ligand frameworks to prevent *in vivo* toxicity. The employment of pyridine ring provides stability to the complex by metal-to-ligand π-back donation. Furthermore, the presence of pyridine moiety rigidifies the ligand backbone and assists increase in longitudinal relaxivity value.

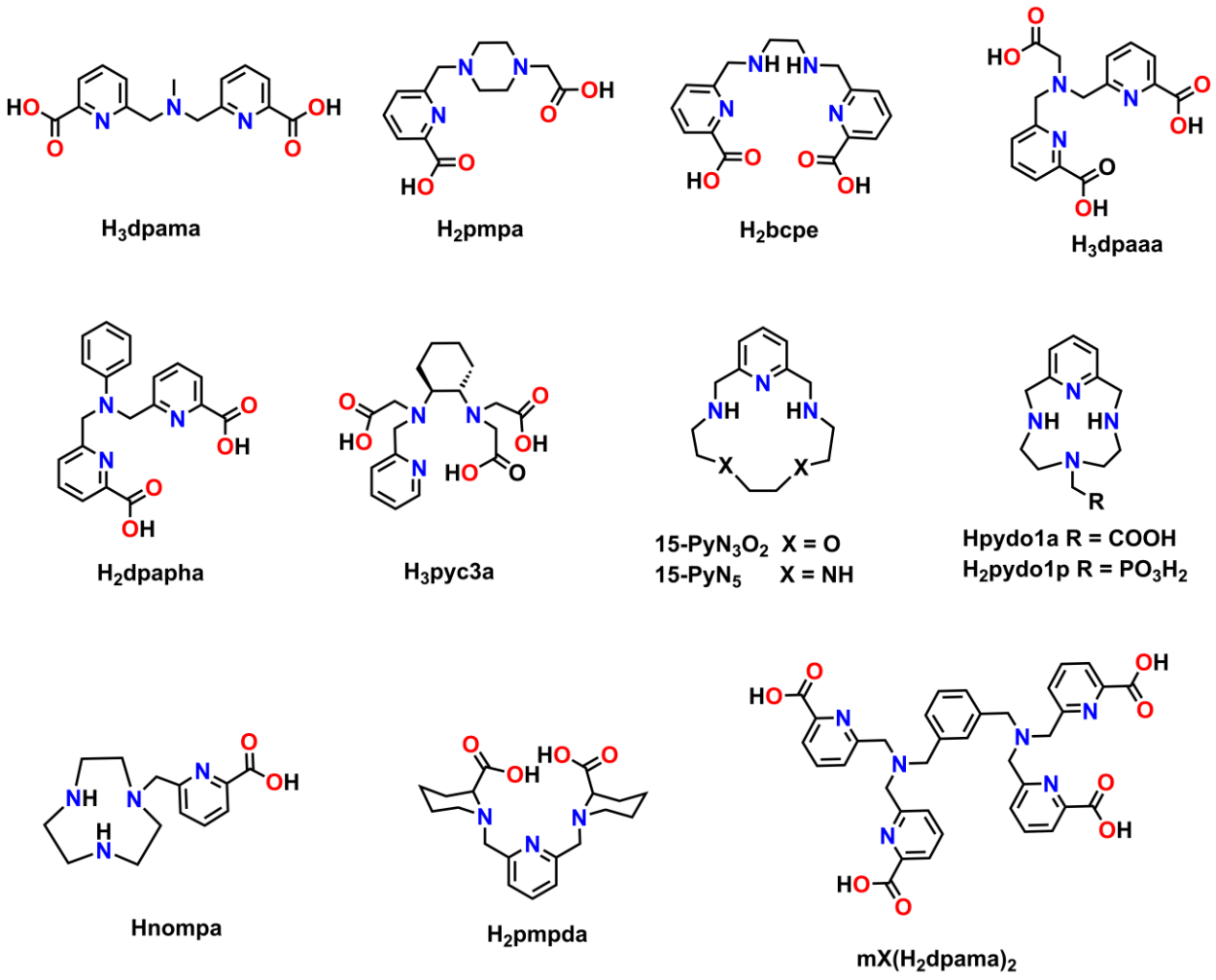

Scheme 2.2. *Examples of ligands containing pyridine ring used for Mn(II) complexation.*

Table 2.2. *Ligands containing pyridine rings forming Mn(II) complexes, number of inner-sphere water molecules (q), longuitudinal relaxivity value and stability constant.*

Ligands	*q*	r_1 ($mM^{-1}s^{-1}$)	log K_{MnL}
H_3dpama[10(a)]	1	5.30[f]	10.13
H_2pmpa[10(b)]	2	5.88[g]	14.29
H_2bcpe[10(a)]	0	1.40[f]	10.63
H_3dpaaa[10(c)]	1	3.60[f]	13.19
H_3dpapha[10(c)]	2	6.70[f]	9.55
H_3pyc3a[10(d)]	1	2.10[h]	14.14
Hnompa[10(e)]	1	3.32[f]	10.28
H_2pmpda[10(f)]	2	3.60[i]	11.37
Hpydo1a[10(g)]	1	2.39[f]	11.54
H_2pydo1p[10(g)]	1	2.84[f]	14.06
mx(H_2dpma)$_2$[10(a)]	2	8.60[f]	11.60
15-PyN_3O_2[10(h)]	2	4.48[f]	7.18
15-PyN_5[10(h)]	2	3.56[f]	10.89

[f] 20 MHz, 25 °C; [g] 60 MHz, 25 °C; [h] 60 MHz, 37 °C; [i] 64 MHz, 20 °C.

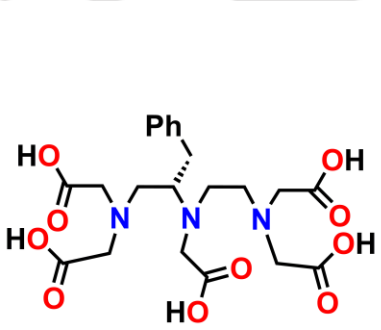

H_5bn-dtpa

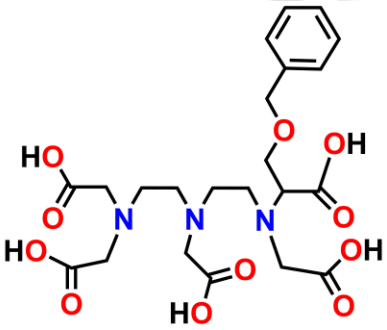

H_5bopta

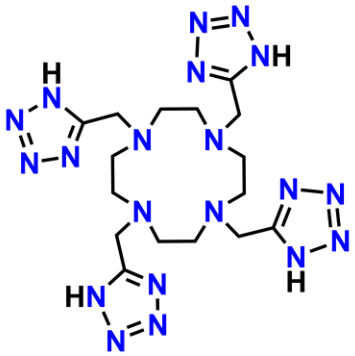

temdo

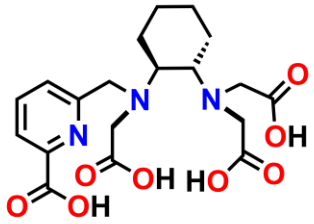

H_4cypic3a

Scheme 2.3. *Examples of some chiral ligands forming Gd(III) complex.*

Literature survey on various ligand frameworks which have been used for Gd(III) complexation; suggests that ligand with chiral backbone are forming thermodynamically stable complexes. Examples of some reported chiral ligands are given in **Scheme 2.3**. Among them **H_5bn-dtpa**[11(a)] and **H_5bopta**[2(c)] are two derivatives of **H_5dtpa**. It has been found that both of them are showing impressive thermodynamic stability. However, ligand **temdo**[11(b)] is derivative of **H_4dota** framework with four tetrazole arms. This chiral ligand is showing high affinity for Gd(III) ion, and found to be kinetically inert compared to Gd(III) complex of ligand **H_4dota**. While, incorporation of chiral moiety; *trans*-1,2-diaminocyclohexane in the ligand framework of **H_4cypic3a**, has increased stability and inertness of its corresponding Gd(III) complex.[6(a)] Although the ligand is lower in denticity, Gd(III) complex of ligand **H_4cypic3a** has shown significant stability and inertness.

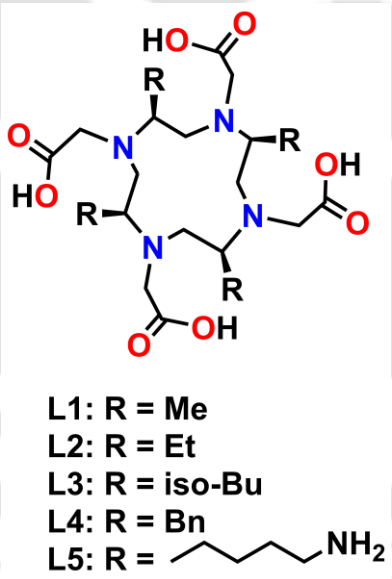

Scheme 2.4. *Examples of derivatives of chiral* ***H_4dota*** *used for Gd(III) complexation.*

Recent report on, a series of chiral derivatives of **H_4dota** (**Scheme 2.4**)[11(c)] reveals that their corresponding Gd(III) complexes are showing impressive thermodynamic stability. Due to substitution by chiral moieties in the ligand framework, rigidity of the system is getting

increased. This favours the thermodynamic stability and kinetic inertness of corresponding Gd(III) complexes.

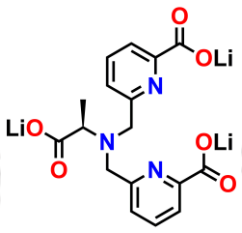

Li_3cbda

Scheme 2.5. *Structure of ligand* ***Li_3cbda****.*

In this context, ligand **Li_3cbda** was designed with chiral L-alanine backbone (**Scheme 2.5**). The ligand was potentially hexadentate and supposed to provide Gd(III) complex with more than one coordinated-water molecule as Gd(III) ions in general acquire coordination number either eight or nine. Mn(II) complexes are generally six- or seven-coordinated. Thus, employing this hexadentate ligand, Mn(II) complex with one metal-coordinated water molecule could be achieved. The ligand framework consisted of two picolinate moieties by substituting two amine H-atoms of L-alanine backbone. These two picolinate moieties would provide stability to its complexes, and also could increase the relaxivity value like previously reported systems. The presence of chiral backbone would provide some amount of rigidity to the complex structure and might enhance the stability of its corresponding complexes.

Studies on various ligand systems with different donor atoms for Ln(III) complexation has shown that the presence of alcoholic group can increase the stability of corresponding Ln(III) complexes. Δ log K value for alcoholic donor group for Ln(III) complexation is found to be ~ 2.9, where Δ log K refers the free energy change after bonding (**Figure 2.2**).[2(c)]

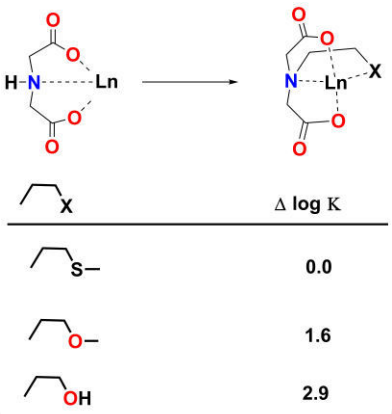

Figure 2.2. *Relative affinity of different donor atoms for Ln(III) ions.*

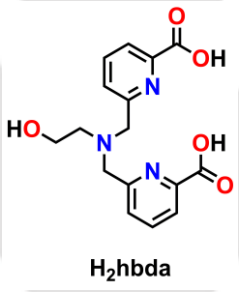

Scheme 2.6. *Structure of ligand* ***H_2hbda****.*

In this respect, ligand **H_2hbda** was designed with ethan-1-ol backbone (**Scheme 2.6**). The hexadentate ligand consisted of two picolinate moieties. Two amine H-atoms present in ethan-1-ol was substituted by two picolinate moieties. Since, ligand has six sites available for coordination with Gd(III) ion, there was possibility of more than one water molecules in its inner-coordination sphere. However, the corresponding Mn(II) complex could have one inner-sphere water molecule. Nevertheless, the thermodynamic stability of both of the complexes has been expected to be high.

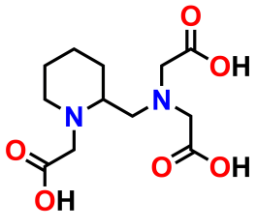

H_3cpmda

Scheme 2.7. *Structure of ligand* ***H_3cpmda****.*

Most of MRI contrast agents are hydrophilic in nature to satisfy the water-soluble property. Therefore, they are unable to penetrate the cell membrane and distributed outside the extracellular matrix.[12] However, some amount of lipophilicity is required for biliary excretion of these contrast agents.[10(d),13] Introduction of lipophilicity can make these contrast agents membrane permeable, providing information regarding cell physiology. To implement this strategy, ligands have been designed with groups, which are lipophilic in nature along with hydrophilic metal coordinating part. To execute this strategy, ligand **H_3cpmda** was designed with piperidine backbone (**Scheme 2.7**). The presence of piperidine ring could provide some amount of lipophilicity and incorporation of three acetate arms could provide suitable binding cavity for the metal ion. Mn(II) complex of this pentadentate ligand could possess more than one metal-coordinated water molecules. The rigid piperidine ring and five strong σ-bonds; two amine N-atoms, and three acetate arms; could provide high thermodynamic stability to its corresponding Mn(II) complex.

2.2 Synthesis and Characterization of Ligand Li_3cbda:

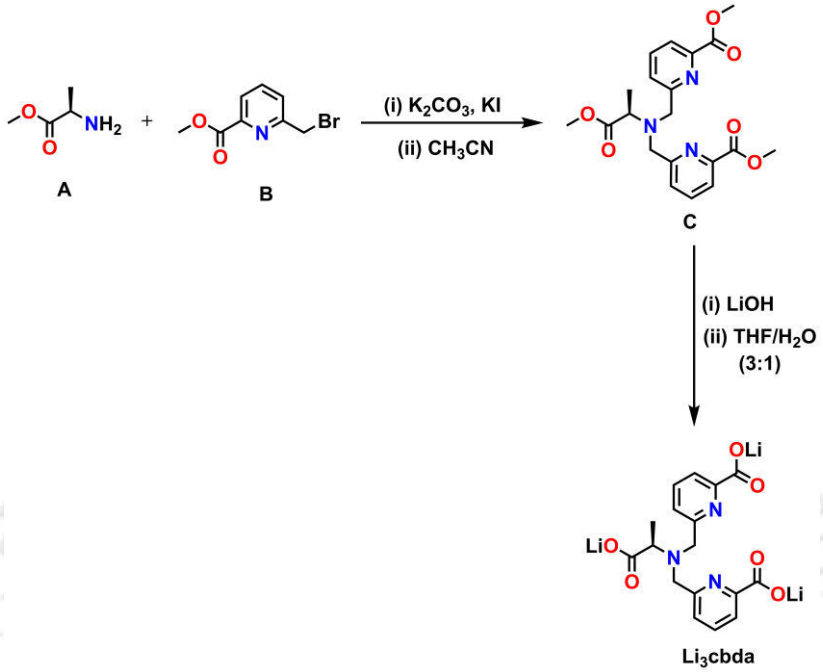

Scheme 2.8. *Synthetic route of ligand* ***Li_3cbda****.*

The chemical reaction of 1:2.2 molar equivalents of (*S*)-methyl 2-aminopropanoate (**A**), and methyl 6-(bromomethyl)picolinate (**B**) in dry acetonitrile in the presence of K_2CO_3, and KI yielded 52% of compound **C**. Treatment of compound **C** with an aqueous LiOH solution in THF provided ligand **Li_3cbda** in 88% yield (**Scheme 2.8**). The ligand was characterized by FTIR spectroscopy, NMR spectroscopy, and mass spectrometric techniques.

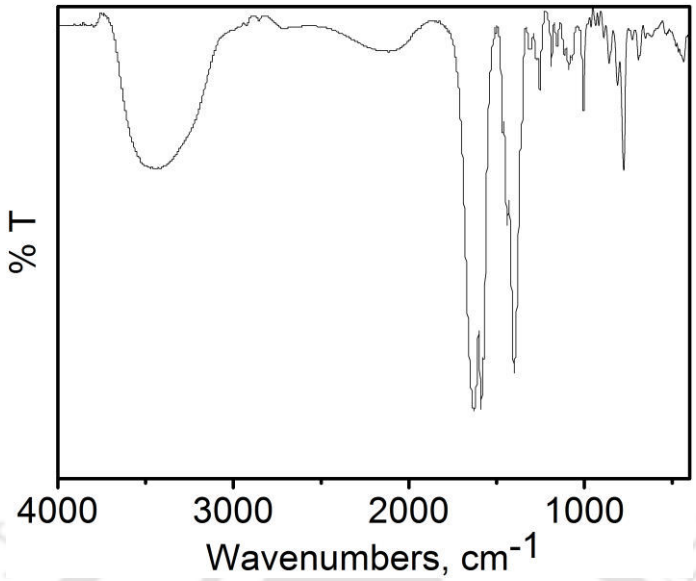

Figure 2.3. *FTIR spectrum of ligand* ***Li$_3$cbda****.*

The FTIR spectrum of ligand **Li$_3$cbda** is presented in **Figure 2.3**. In the spectrum, bands appeared at 1618 cm^{-1} and 1404 cm^{-1} were due to asymmetric and symmetric stretching of ν(C=O) group.[14] The low stretching frequency value compared to ν(C=O) stretching (~ 1720 cm^{-1}) of a free acid group implied that in the ligand the carboxylic acid groups present as its corresponding Li-salt. The band due to ν(C–O) stretching appeared at 1265 cm^{-1}.

The formation of Li-salt of the ligand was further analyzed by mass spectrometry. The electrospray ionization mass spectrum of ligand **Li$_3$cbda** in the positive mode in Mili Q water provided three sets of peaks with *m/z* values of 366.17, 372.16, and 378.16 (**Figure 2.4**). The observed peaks indicated the presence of lithium salt of the ligand as their *m/z* values and isotropic distribution pattern corroborated with $[C_{17}H_{16}N_3O_6Li_1 + H]^+$ (366.13), $[C_{17}H_{15}N_3O_6Li_2 + H]^+$ (372.13), and $[C_{17}H_{14}N_3O_6Li_3 + H]^+$ (378.14) species.

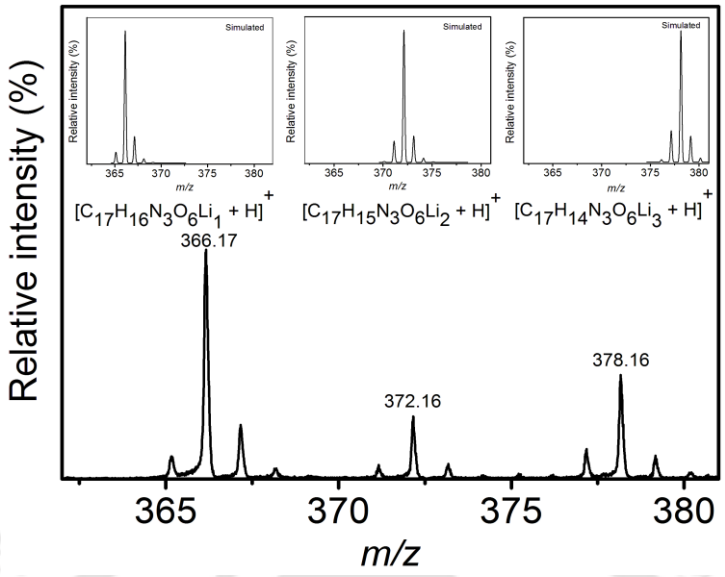

Figure 2.4. *ESI-MS (+ve) mass spectrum of aqueous solution of ligand* ***Li_3cbda****. Simulated spectra have been given as inset.*

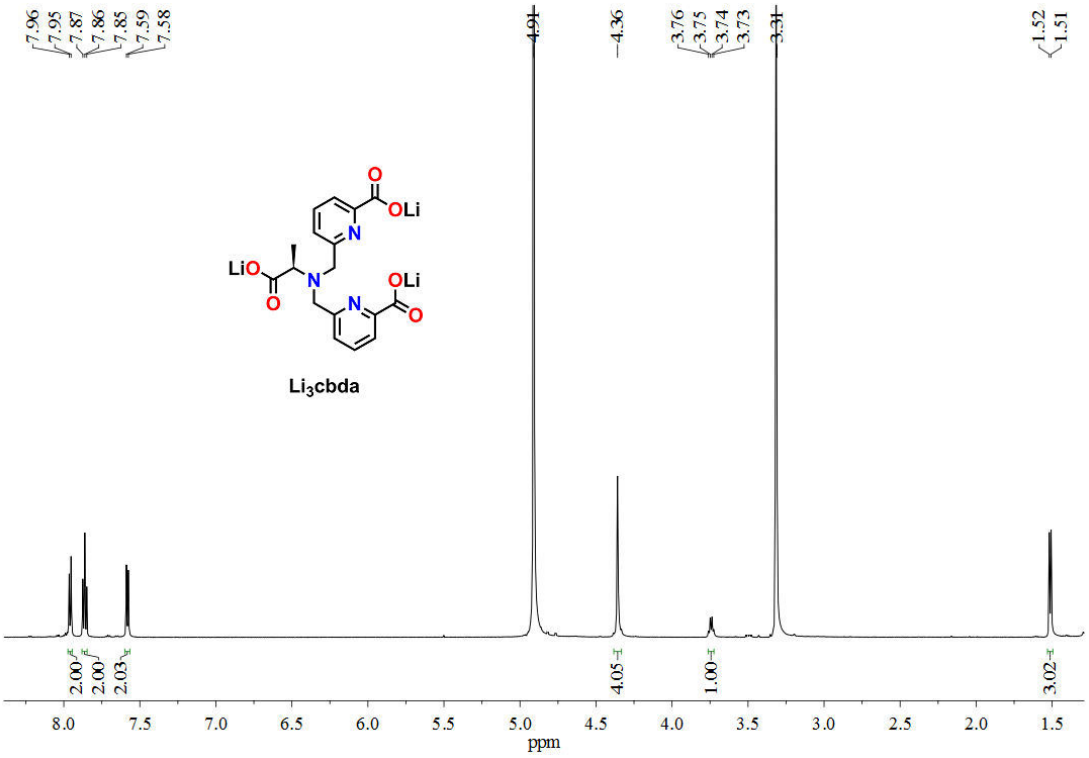

Figure 2.5. *^{1}H-NMR spectrum of ligand* ***Li_3cbda*** *in CD_3OD solvent.*

The ^{1}H-NMR spectrum of ligand **Li_3cbda** in CD_3OD solvent is presented in **Figure 2.5**. The peaks appeared in the region of δ = 7.96-7.58 ppm, were due to three sets of aromatic protons present in pyridine units. The singlet peak at δ = 4.36 ppm was appeared for four hydrogen atoms of two methylene units attached with two pyridine rings. A quartet peak at δ = 3.74 ppm and one doublet peak at δ = 1.52 ppm were appeared for –CH proton, and methyl protons of the acetate arm respectively. The ^{13}C-NMR spectrum of the ligand in CD_3OD solvent is presented in **Figure 2.6**. The spectrum showed 10 characteristic peaks for 10 different kinds of carbon atoms present in the ligand.

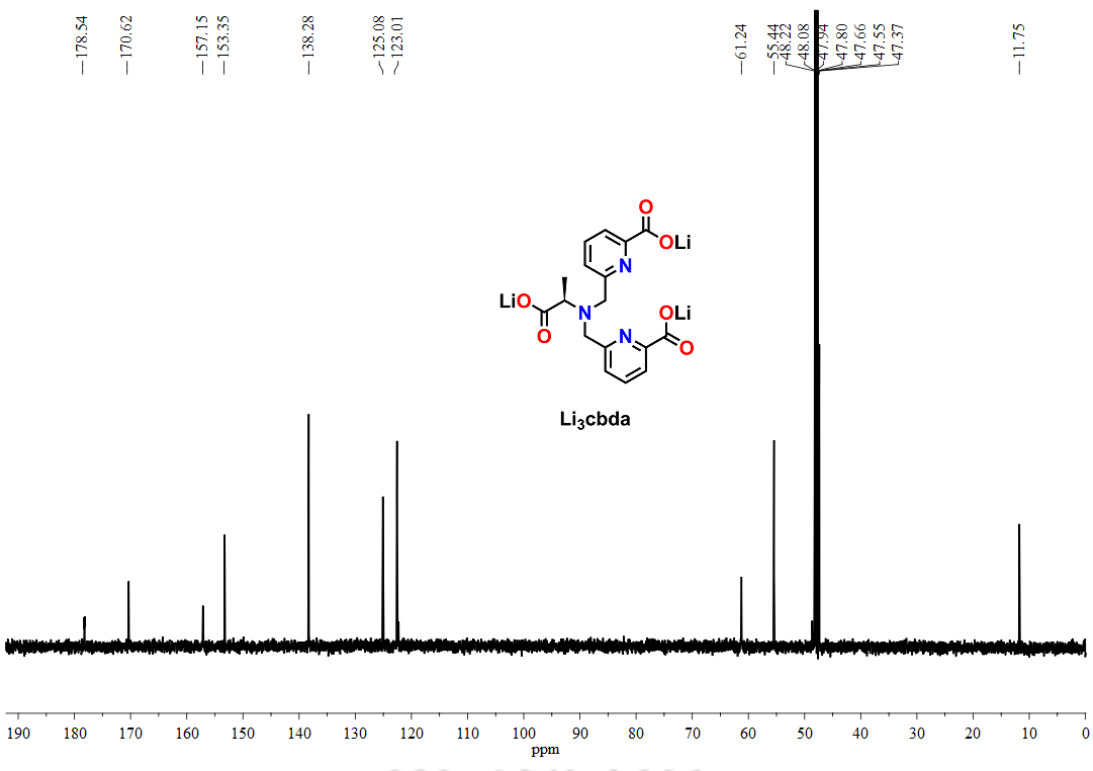

Figure 2.6. *^{13}C-NMR spectrum of ligand **Li_3cbda** in CD_3OD solvent.*

2.3 Synthesis and Characterization of Ligand H_2hbda:

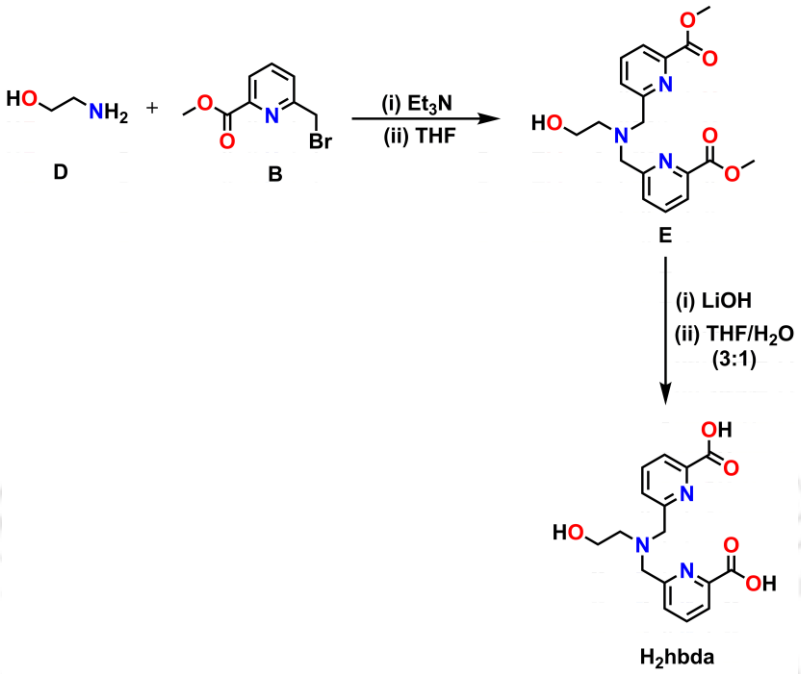

Scheme 2.9. *Synthetic route of ligand* ***H_2hbda****.*

The schematic diagram for the synthesis of ligand **H_2hbda** is presented in **Scheme 2.9**. Compound **E** was obtained in 45% yield by the reaction of 1:2.2 molar equivalents of 2-aminoethan-1-ol (**D**) and 6-(brmomethyl)picolinate (**B**) in THF in the presence of Et_3N. The reaction of compound **E** with aqueous LiOH in THF yielded 83% of ligand **H_2hbda**. The ligand was characterized by various spectroscopic techniques, like FTIR spectroscopy, NMR spectroscopy and mass spectrometry.

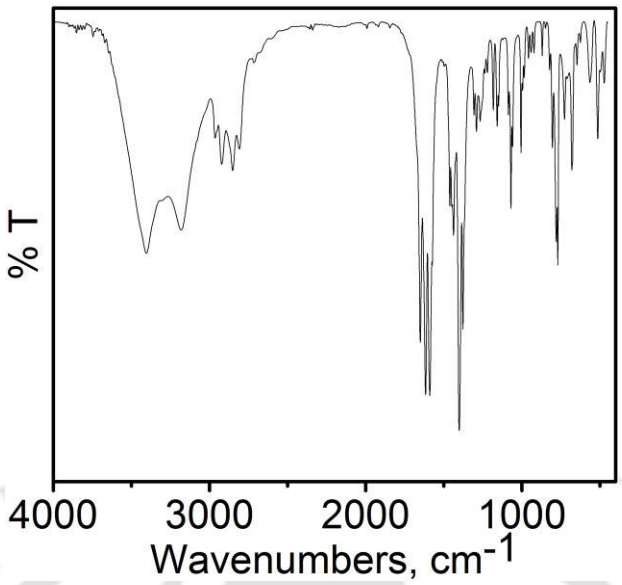

Figure 2.7. *FTIR spectrum of ligand* ***H_2hbda****.*

The FTIR spectrum of ligand **H_2hbda** is presented in **Figure 2.7**. In the spectrum, the band appeared at 3405 cm^{-1} was due to stretching of ν(O–H) group. The bands at 1616 cm^{-1} and 1401 cm^{-1} were due to asymmetric and symmetric stretching of ν(C=O) group respectively.[14] It was found that ligand was obtained as pyridinium salt. The band for ν(C–O) stretching appeared at 1267 cm^{-1}.

The ligand was further characterized by mass spectrometric analysis. The observed mass spectrum of ligand **H_2hbda** is presented in **Figure 2.8**. The simulated spectra for the observed species are given as inset. The electron spray ionization mass spectrum of ligand **H_2hbda** in the positive mode in Mili Q water provided 100% molecular ion peak at *m/z* values of 332.1245. The isotropic distribution pattern examination indicated that the observed peak corresponded to composition (*m/z*) values; $[C_{16}H_{17}N_3O_5 + H]^+$ (332.1241). The simulated spectrum has been given in inset.

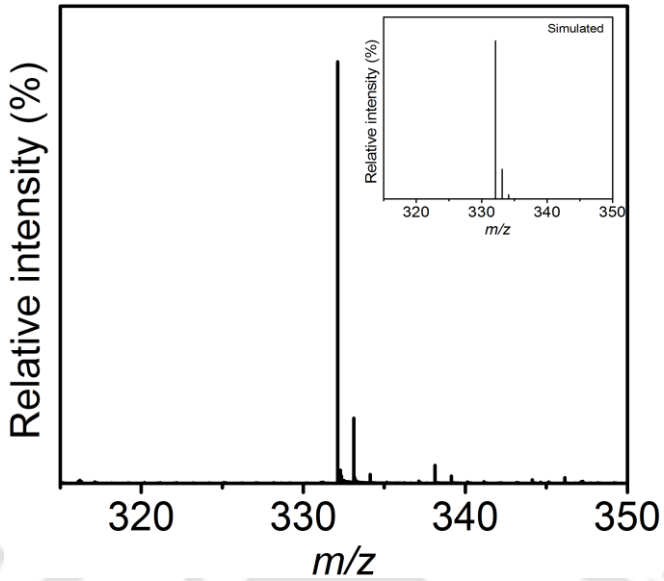

Figure 2.8. *ESI-MS (+ve) mass spectrum of aqueous solution of ligand* ***H_2hbda****. Simulated spectrum has been given as inset.*

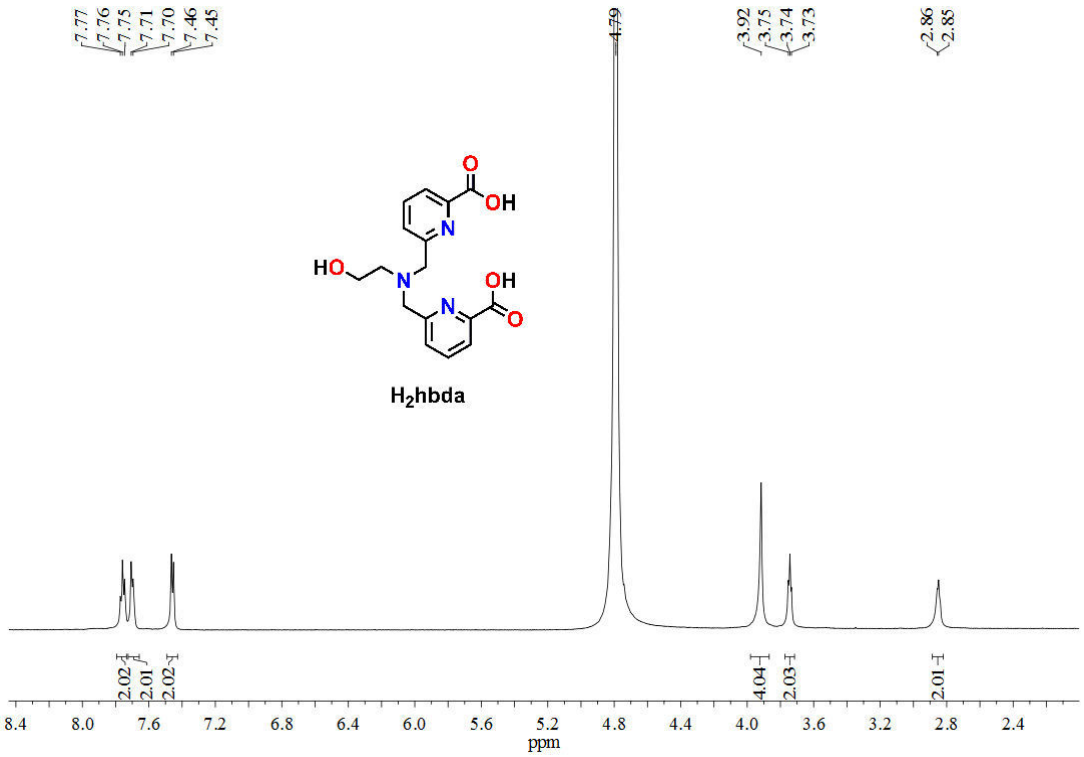

Figure 2.9. *^{1}H-NMR spectrum of ligand* ***H_2hbda*** *in D_2O solvent.*

The ^{1}H-NMR spectrum of ligand **H_2hbda** is shown in **Figure 2.9**. The peaks appeared in the region δ = 7.77-7.45 ppm corresponded to three sets of aromatic protons present in two pyridine units of the ligand. The singlet peak appeared at δ = 3.92 ppm was due to four hydrogen atoms present in two methylene groups attached with two pyridine rings. The appeared peaks at δ = 3.74 and δ = 2.86 ppm were due to two methylene groups present in ethan-1-ol moiety of the ligand. The ^{13}C-NMR spectrum of ligand **H_2hbda** is presented in **Figure 2.10**. In the spectrum, 9-characteristic peaks appeared for 9-different kinds of C-atoms present in ligand **H_2hbda**.

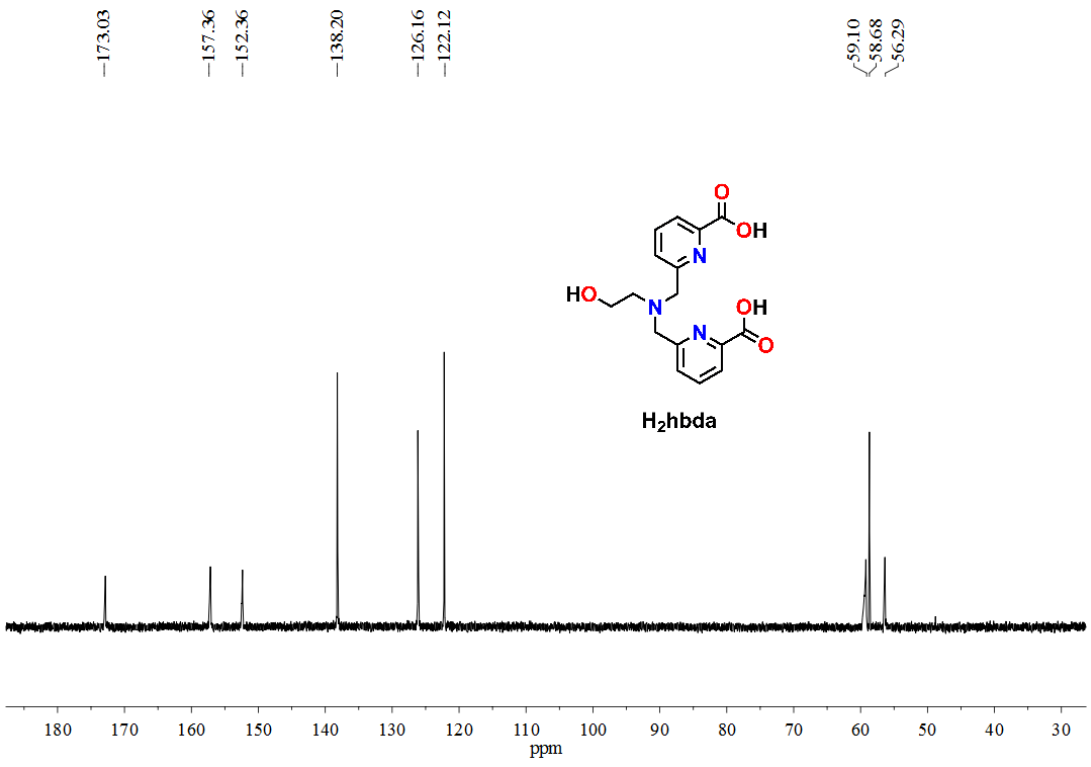

Figure 2.10. *^{13}C-NMR spectrum of ligand **H_2hbda** in D_2O solvent.*

2.4 Synthesis and Characterization of Ligand H_3cpmda:

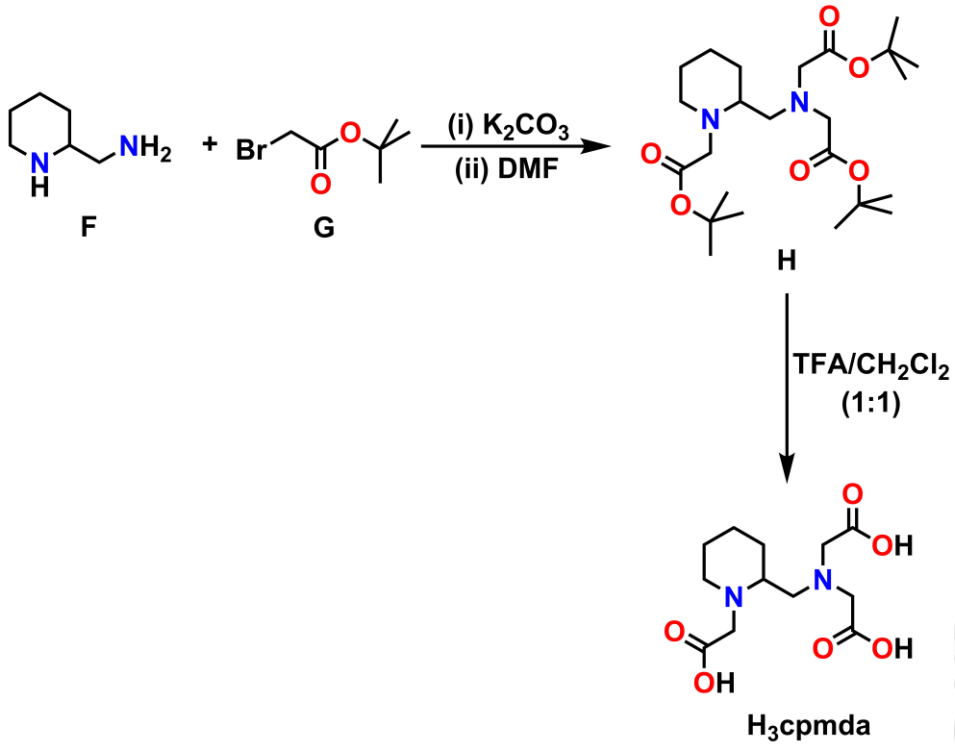

Scheme 2.10. *Synthetic route of ligand* ***H_3cpmda****.*

The reaction of piperidin-2-ylmethanamine (**F**) with five-equivalent amounts of *tert*-butyl bromoacetate (**G**) in the presence of K_2CO_3 in DMF yielded 50% of compound **H**. Ligand **H_3cpmda** was isolated after deprotection of compound **H** using trifluroacetic acid in dichloromethane. The ligand was characterized by various spectroscopic methods like, FTIR spectroscopy, NMR spectroscopy, and mass spectrometry.

The FTIR spectrum of the ligand is presented in **Figure 2.11**. In the spectrum, band appeared at 3433 cm^{-1} was due to ν(O–H) stretching. The bands at ~ 3000 cm^{-1} were due to aliphatic C–H stretching. A broad band was observed near 2500 cm^{-1} indicated the formation of ammonium salt. Sharp band appearing at 1729 cm^{-1} was due to ν(C=O) stretching of carboxylic acid. The peak appeared near 1421 cm^{-1} was due to ν(O–H) bending.

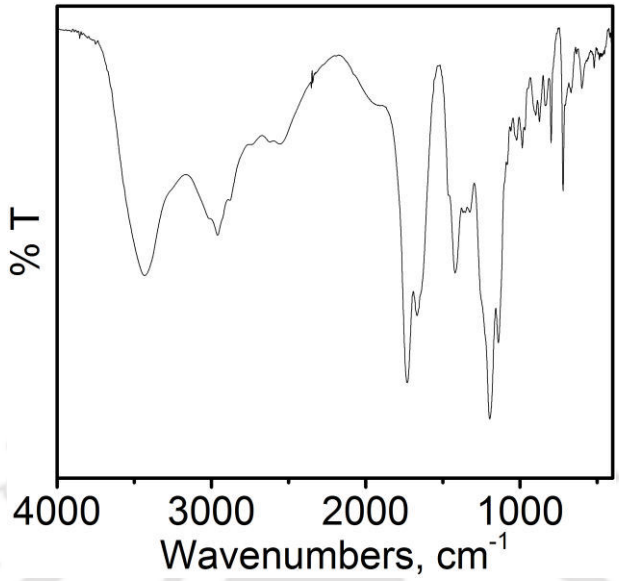

Figure 2.11. *FTIR spectrum of ligand* ***H₃cpmda****.*

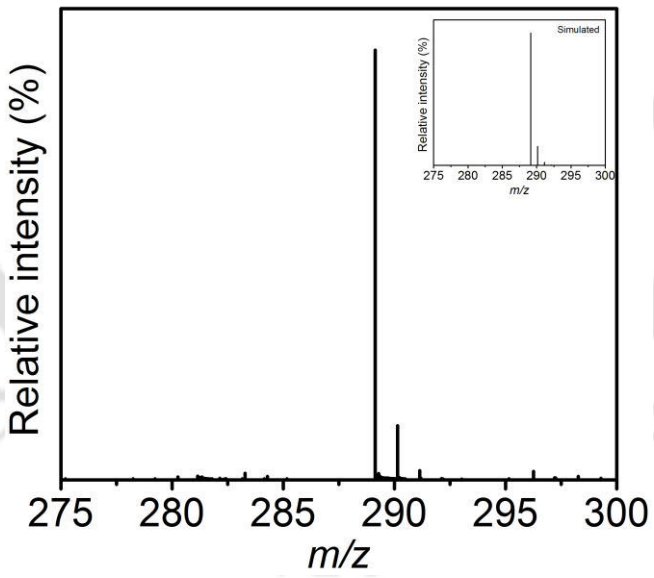

Figure 2.12. *ESI-MS (+ve) mass spectrum of aqueous solution of ligand* ***H₃cpmda****. Simulated spectrum has been given as inset.*

The electrospray ionization mass spectrum of ligand **H₃cpmda** in positive mode in HPLC grade MeOH provided a 100% molecular ion peak at *m*/*z* value 289.1395 (**Figure 2.12**). This

peak corresponded to $[C_{12}H_{20}N_2O_6 + H]^+$ (m/z = 289.1394), and it was evident from isotropic distribution pattern. The simulated spectrum is given as inset.

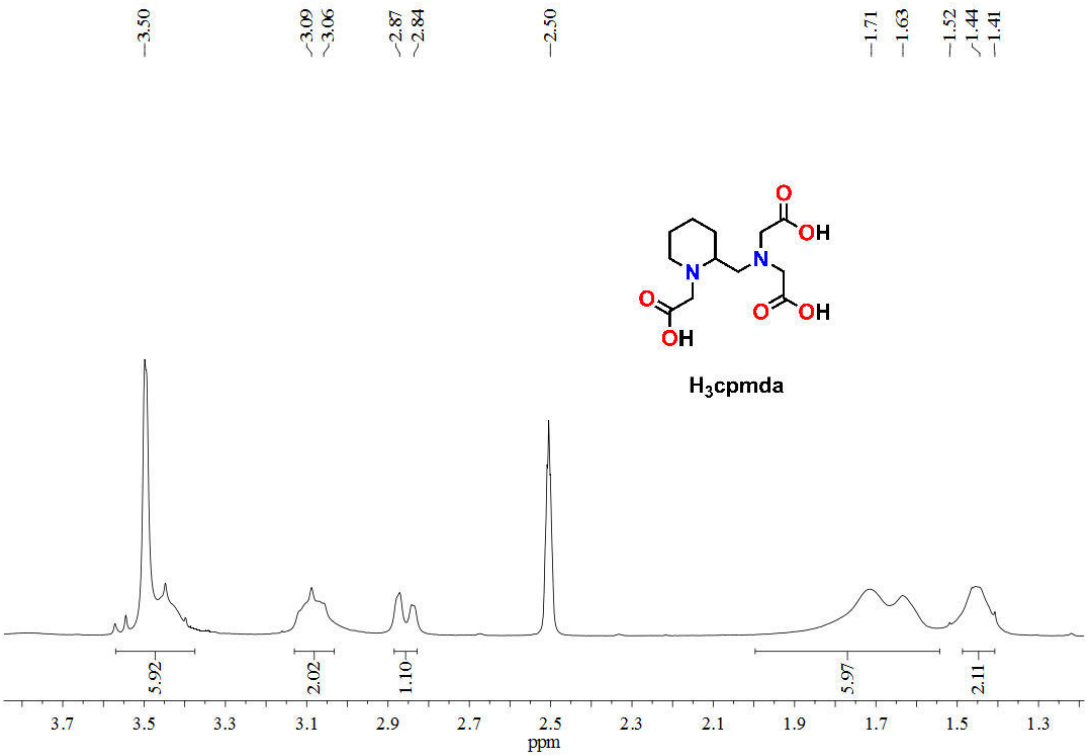

Figure 2.13. *^{1}H-NMR spectrum of ligand* ***H_3cpmda*** *in C_2D_6SO solvent.*

The ^{1}H-NMR spectrum for ligand **H_3cpmda** is presented in **Figure 2.13**. The multiplets appeared in the region δ = 1.41-1.52 ppm and δ = 1.63-1.72 ppm were due to eight hydrogen atoms present in the piperidine ring. The multiplet appeared at δ = 3.06-3.09 ppm was because of methylene hydrogen atoms attached with piperidine ring. The singlet peak corresponded to six hydrogen atoms present in three acetate arms appeared at δ = 3.50 ppm. The multiplet appeared in the region of δ = 2.84-2.87 ppm was due to hydrogen atom present in ring which is attached with methylamine arm. ^{13}C-NMR spectrum of the ligand is presented in **Figure 2.14**. In the spectrum two sets of quartet peaks were observed at δ = 162.84 (J_{C-F} = 35 Hz), and δ = 118.15

(J_{C-F} = 293 Hz) ppm; which were assigned to CF_3COO group of TFA molecule. Thus, the ligand was formed as TFA salt, which was also inferred by IR-spectroscopic analysis. Except these two sets of peaks, seven other peaks were observed for different kinds of C-atoms present in the ligand. However, two peaks coincides at peak position of δ = 23.57 ppm.

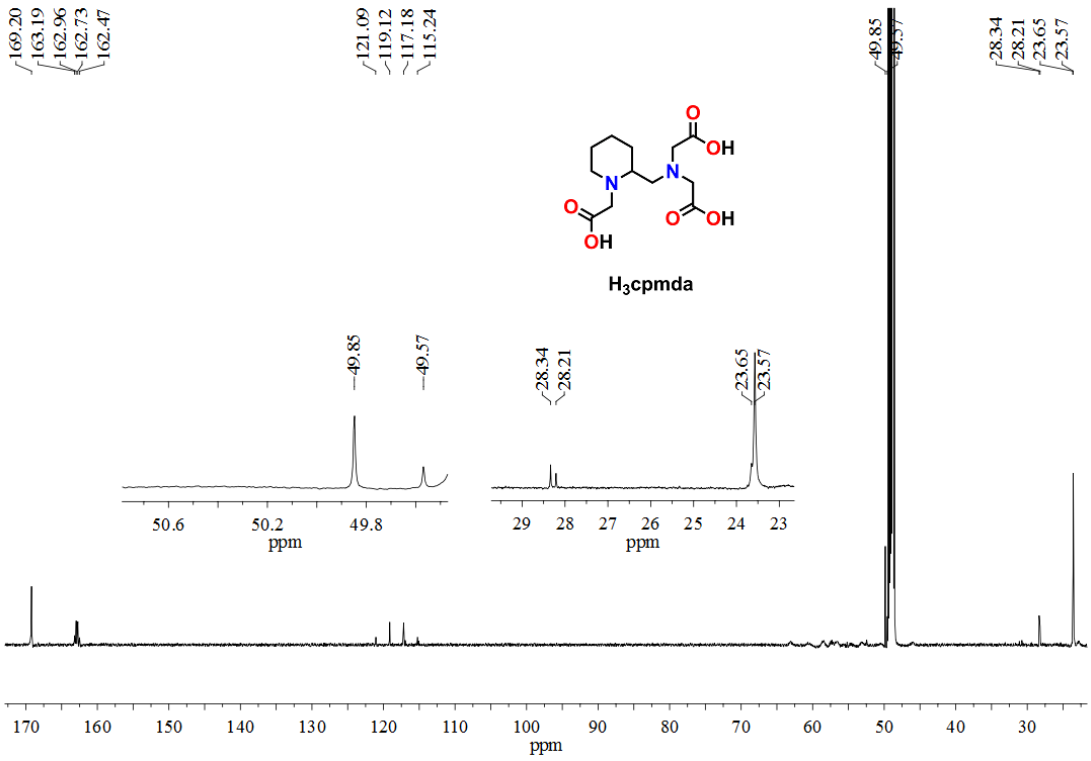

Figure 2.14. *^{13}C-NMR spectrum of ligand **H_3cpmda** in CD_3OD solvent.*

References

1. (*a*) P. Hermann, J. Kotek, V. Kub´ıcek and I. Lukeš, *Dalton Trans*., 2008, 3027; (*b*) *The Chemistry of Contrast Agents in Medical Magnetic Resonance Imaging*, ed. A. E. Merbach and É . Tóth, John Wiley & Sons, Chichester (England), 2001.

2. (*a*) E. J. Werner, S. Avedano, M. Botta, B. P. Hay, E. G. Moore, S. Aime and K. N. Raymond, *J. Am. Chem. Soc*., 2007, **129**, 1870; (*b*) A. Datta and K. Raymond, *Acc. Chem. Res*., 2009, **42**, 938; (*c*) P. Caravan, J. Ellison, T. McMurry and R. Lauffer, *Chem. Rev*., 1999, **99**, 2293; (*d*) S. Aime, M. Botta, M. Fasano, S. Geninatti Crich and E. Terreno, *Coord. Chem. Rev*., 1999, **185**, 321.

3. (*a*) S. Laus, R. Ruloff, É . Tóth and A. Merbach, *Chem. – Eur. J*., 2003, **9**, 3555; (*b*) P. Caravan, C. T. Farrar, L. Frullano and R. Uppal, *Contrast Media Mol. Imaging*, 2009, **4**, 89; (*c*) K. Hanaoka, A. J. Lubag, A. Castillo-Muzquiz, T. Kodadek and A. D. Sherry, *Magn. Reson. Imaging*, 2008, **26**, 608.

4. (*a*) E. J. Werner, A. Datta, C. J. Jocher and K. N. Raymond, *Angew. Chem. Int. Ed*., 2008, **47**, 8568; (*b*) P. Caravan, *Chem. Soc. Rev*., 2006, **35**, 512; (*c*) E. Terreno, D. Delli Castelli, A. Viale and S. Aime, *Chem. Rev*., 2010, **110**, 3019; (*d*) M. C. Heffern, L. M. Matosziuk and T. J. Meade, *Chem. Rev*., 2014, **114**, 4496; (*e*) D. Lawson, A. Barge, E. Terreno, D. Parker, S. Aime and M. Botta, *Dalton Trans*., 2015, **44**, 4910; (*f*) R. E. Lauffer, *Chem. Rev*., 1987, **87**, 901.

5. (*a*) A. M. Nonat, C. Gateau, P. H. Fries, L. Helm and M. Mazzanti, *Eur. J. Inorg. Chem*., 2012, 2049; (*b*) A. Nonat, P. H. Fries, J. Pécaut and M. Mazzanti, *Chem. – Eur. J*., 2007, **13**, 8489; (*c*) E. Toth, L. Helm, A. E. Merbach, J. A. McCleverty and T. J. Meyer, *Comprehensive Coordination Chemistry II*, Pergamon, Oxford, 2003, 841.

6. (*a*) E. M. Gale, N. Kenton and P. Caravan, *Chem. Commun*., 2013, **49**, 8060; (*b*) V. C. Pierre, M. Botta, S. Aime and K. N. Raymond, *Inorg. Chem*., 2006, **45**, 8355; (*c*) S. Aime, L. Calabi, C. Cavallotti, E. Gianolio, G. B. Giovenzana, P. Losi, A. Maiocchi, G.

Palmisano and M. Sisti, *Inorg. Chem*., 2004, **43**, 7588; (*d*) L. Pellagatti, J. Zhang, B. Drahoš, S. Villette, F. Suzenet, G. Gillaument, S. Petoud and É. Tóth, *Chem. Commun*., 2008, 6951; (*e*) Z. Baranyai, L. Tei, G. B. Giovenzana, F. K. Kálmán and M. Botta, *Inorg. Chem*., 2012, **51**, 2597.

7. (*a*) A. Nonat, C. Gateau, P. H. Fries and M. Mazzanti, *Chem. – Eur. J*., 2006, **12**, 7133; (*b*) M. Mato-Iglesias, C. Platas-Iglesias, K. Djanashvili, J. A. Peters, É. Toth, E. Balogh, R. N. Muller, L. V. Elst, A. de Blas and T. Rodríguez-Blas, *Chem. Commun*., 2005, 4729; (*c*) A. Nonat, M. Giraud, C. Gauteau, P. H. Fries, L. Helm and M. Mazzanti, *Dalton Trans*., 2009, 8033; (*d*) C. Platas-Iglesias, M. Mato-Iglesias, K. Djanashvili, R. N. Muller, L. V. Elst, J. A. Peters, A. de Blas and T. Rodríguez-Blas, *Chem. – Eur. J*., 2004, **10**, 3579; (*e*) N. Chatterton, C. Gateau, M. Mazzanti, J. Pècaut, A. Borel, L. Helm and A. Merbach, *Dalton Trans*., 2005, 1129.

8. (*a*) Md. N. Khan, S. Pal, T. Parvinb and L. H. Choudhury, *RSC Adv*., 2012, **2**, 12305; (*b*) B. Phukan, C. Mukherjee and R. Varshney, *Dalton Trans*., 2018, **47**, 135; (*c*) G. Bringmann, Y. Reichert and V. V. Kane, *Tetrahedron*, 2004, **60**, 3539; (*d*) B. B. Fredholm, A. P. Izerman, K. A. Jacobson, K. N. Klotz and J. Linden, *Pharmacol. Rev*., 2001, **53**, 527.

9. (*a*) E. Balogh, M. Mato-Iglesias, C. Plates-Iglesias, É. Tóth, K. Djanashvili, J. A. Peters, A. de Blas and T. Rodríguez-Blas, *Inorg. Chem*., 2006, **45**, 8719; (*b*) Y. Bretonnière, M. Mazzanti, J. Pécaut, F. A. Dunnand and A. E. Merbach, *Chem. Commun*., 2001, 621; (*c*) G. Nocton, A. Nonat, C. Gateau and Marinella Mazzanti, *Helv. Chim. Acta*, 2009, **92**, 2257.

10. (*a*) A. Forgács, M. Regueiro-Figueroa, J. L. Barriada, D. esteban-Gómez, A. de. Blas, T. Rodríguez-Blas, M. Botta and C. Platas-Iglesias, *Inorg. Chem*., 2015, **54**, 9576; (*b*) B. Phukan, C. Mukherjee, U. Goswami, A. Sarmah, S. Mukherjee, S. K. Sahoo and S. C. Moi, *Inorg. Chem*., 2018, **57**, 2631; (*c*) A. Forgács, R. Pujales-Paradela, M. Regueiro-Figueroa, L. Valencia, D. Esteban-Gómez, M. Botta and C. Platas-Iglesias, *Dalton Trans*., 2017, **46**,1546; (*d*) E. M. Gale, I. P. Atanasova, F. Blasi, I. Ay and P. Caravan, *J. Am. Chem. Soc*., 2015, **13**7, 15548; (*e*) E. Molnár, N. Camus, V. Patinec, G. A. Rolla, M.

Botta, G. Tircsó, F. K. Kálmán, T. Fodor, R. Tripier and C. Platas-Iglesias, *Inorg. Chem*., 2014, **53**, 5136; (*f*) H. Su, C. Wu, J. Zhu, T. Miao, D. Wang, C. Xia, X. Zhao, Q. Gong, B. Song and H. Ai, *Dalton Trans*., 2012, **41**, 14480; (*f*) B. Drahoš, J. Kotek, I. Císařová, P. Hermann, L. Helm and I. Lukeš, *Inorg. Chem*., 2011, **50**, 12785; (*h*) B. Drahoš, J. Kotek, P. Hermann, I. Lukeš and É. Tóth, *Inorg. Chem*., 2010, **49**, 3224.

11. (*a*) S. Laurent, F. Botteman, L. V. Elst and R. N. Muller, *Helv. Chim. Acta*, 2004, **87**, 1077; (*b*) A. Boltjes, A. Shrinidhi, K. van de Kolk, E. Herdtweck and A. Dçmling, *Chem. – Eur. J*., 2016, **22**, 7352; (*c*) L. Dai, C. M. Jones, W. T. K. Chan, T. A. Pham, X. Ling, E. M. Gale, N. J. Rotile, W. C. Tai, C. J. Anderson, P. Caravan and G. Law, *Nat. Commun.*, 2018, **9**, 857.

12. (*a*) T. Yamane, K. Hanaoka, Y. Muramatsu, K. Tamura and Y. Adachi, *Bioconjugate Chem*., 2011, **22**, 2227; (*b*) M. J. Allen and T. J. Meade, *J. Biol. Inorg. Chem.,* 2003, **8**, 746; (*c*) M. J. Allen, K. W. MacRenaris, P.N. Venkatasubramanian and T. J. Meade, *Chem. Biol*., 2004, **11**, 301.

13. G. Sechuhmsnn-Giampierri, H. Schitt-Willich and T. Frenzel, *J. Pharm. Sci*., 1993, **82**, 799.

14. (*a*) J. Wang, G. R. Gao, Z. H. Zhang, X. D. Zhang, X. Zh. Liu, Y. M. Kong and Y. Li, *Russ. J. Coord. Chem*., 2007, **33**, 258; (*b*) B. C. Smith, *Infrared Spectral Interpretation: A Systematic Approach*, CRC press, 1998.

Chapter III

Tris(aquated) Gd(III) Complexes with Picolinate-Based Ligands as MRI Contrast Agents: Effect of Tether-Ligand Donor Groups on Thermodynamic Stability of complexes

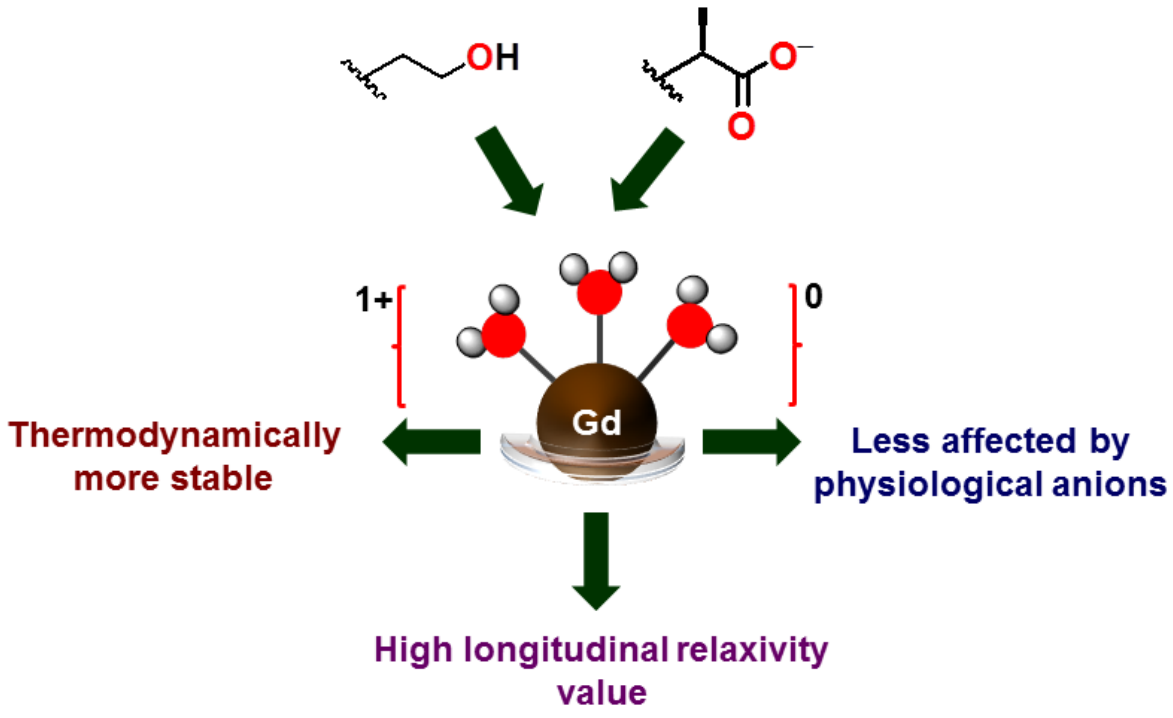

3.1 Introduction:

To fulfill the objective of high-relaxivity MRI contrast agents development, one of the strategies is the synthesis of Gd(III) complexes with more than one inner-sphere water molecules (q), *i.e.* $q > 1$. However, the thermodynamic stability of the complexes diminishes with increasing number of inner-sphere water molecules.[1,2] Therefore, a modification in the coordinating ligand backbone and thereafter, its effect is required to study to achieve Gd(III) complexes with high thermodynamic stability, and $q > 1$. In this context, two Gd(III) complexes were synthesized using two picolinate-based hexadentate ligands **Li_3cbda** and **H_2hbda**. In ligand **Li_3cbda**, a chiral tethered unit was incorporated, while an alcohol group was being included in the backbone of ligand **H_2hbda**. The effect of chirality and the alcohol group to the stability of corresponding Gd(III) complexes have been studied.

3.2 Syntheses and Characterizations of Gd(III) Complexes of Hexadentate Picolinate-Based Ligands:

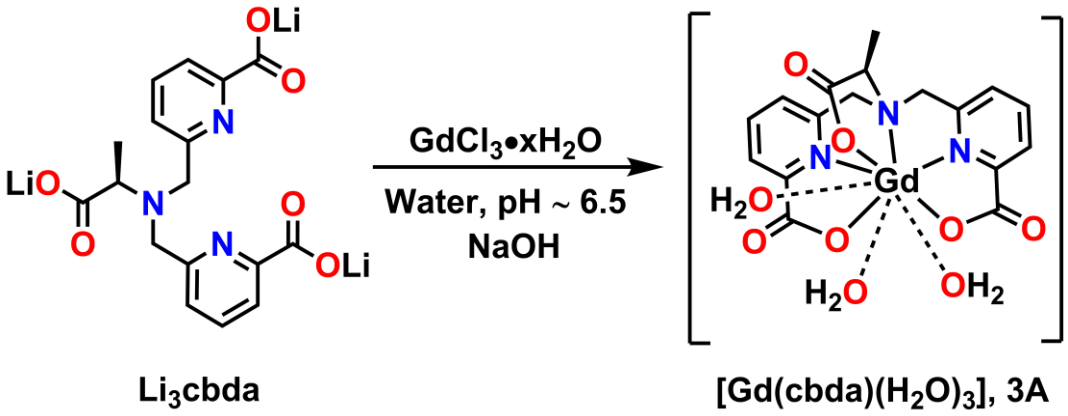

Scheme 3.1. *Synthesis of Gd(III) complex of ligand* ***Li_3cbda****.*

1:1 molar equivalents of ligand **Li_3cbda**, and $GdCl_3 \bullet xH_2O$ were allowed to react in water at pH ~ 6.5 by adding aqueous NaOH solution (**Scheme 3.1**). After 24 h of continuous stirring, filtrate of the reaction mixture provided white solid compound of complex **3A** in 34% yield.

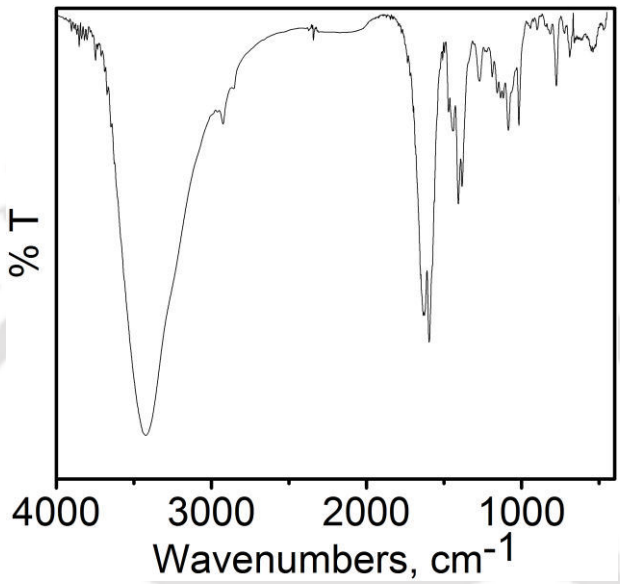

Figure 3.1. *FTIR spectrum of complex **3A**.*

FTIR spectrum of complex **3A** is presented in **Figure 3.1**. The broad band appeared at 3421 cm^{-1} was due to ν(O–H) stretching of coordinated-water molecules present in the complex.[4] The band due to the stretching of ν(C=O) group of the ligand was observed to be shifted from its position at 1618 cm^{-1} to 1626 cm^{-1} in the complex.

The electrospray ionization mass spectrum of complex **3A** in positive mode in Mili Q water provided a 100% molecular ion peak at *m*/*z* value 515.005. This peak corresponded to $[C_{17}H_{14}N_3O_6Gd + H]^+$ (*m*/*z* = 515.0153), and it was evident from the isotropic distribution pattern (**Figure 3.2**). Thus, supported the formation of the complex.

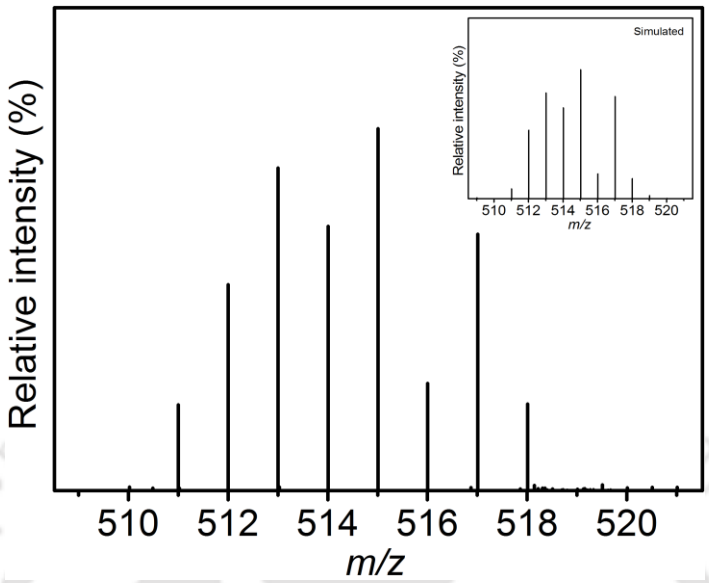

Figure 3.2. *ESI-MS (+ve) mass spectrum of aqueous solution of complex* ***3A****. Simulated spectra has been given as inset.*

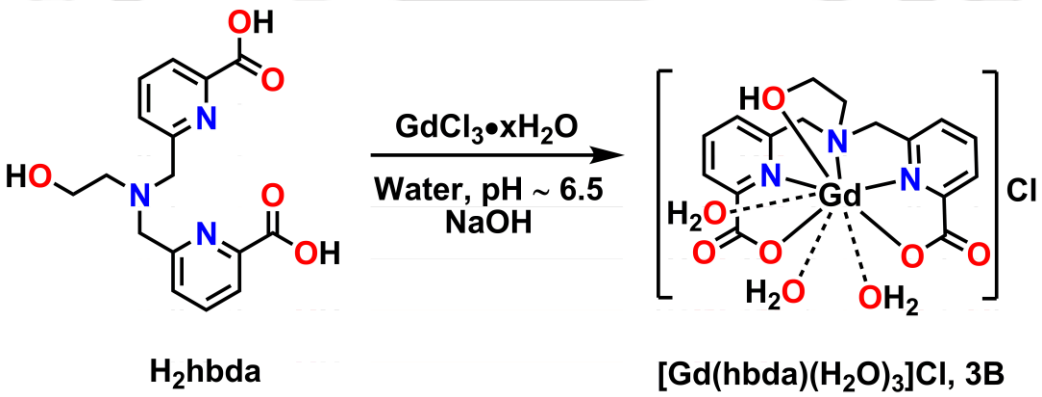

Scheme 3.2. *Synthesis of Gd(III) complex of ligand* ***H₂hbda****.*

Ligand **H_2hbda** was allowed to react with an equivalent amount of $GdCl_3 \bullet xH_2O$ in water at pH ~ 6.5. The pH of the solution was adjusted by adding NaOH (**Scheme 3.2**). Complex **3B** was obtained in 38% yield by continuous stirring of the solution at room temperature for 24 h.

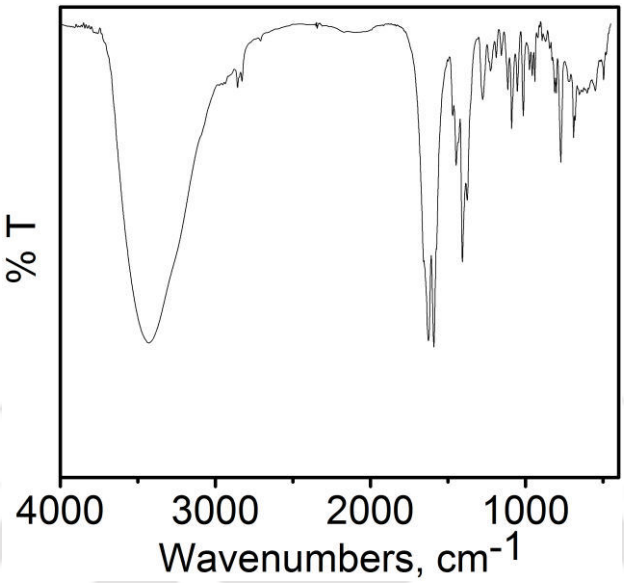

Figure 3.3. *FTIR spectrum of complex* ***3B****.*

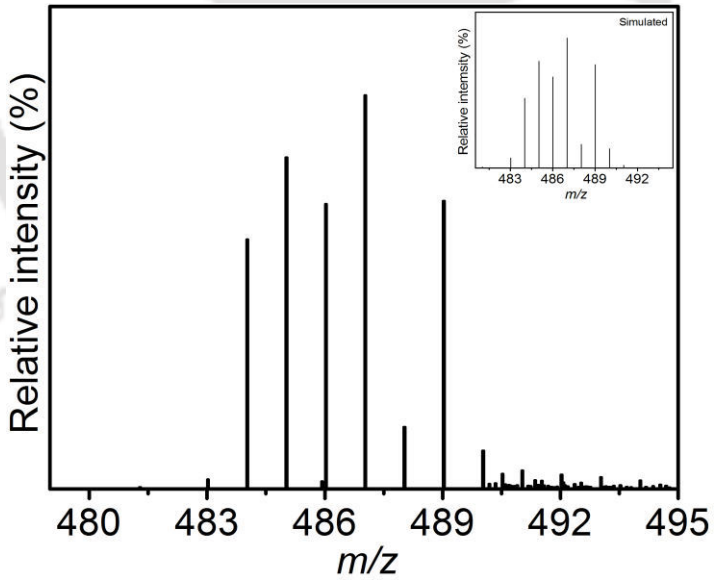

Figure 3.4. *ESI-MS (+ve) mass spectrum of aqueous solution of complex* ***3B****. Simulated spectra has been given as inset.*

The FTIR spectrum of complex **3B** is shown in **Figure 3.3**. The band corresponding to ν(O–H) stretching of coordinated-water molecules was observed at 3431 cm^{-1}.[4] The band for ν(C=O) stretching was observed at 1624 cm^{-1}. The band position was shifted by 8 cm^{-1} compared to the ligand.

The electrospray ionization mass spectrum of complex **3B** in positive mode in Mili Q water provided a 100% molecular ion peak at *m/z* value 487.0291 (**Figure 3.4**). Investigation on the isotropic distribution pattern indicated that the peak corresponded to composition $C_{16}H_{15}N_3O_5Gd$. Thus, the formation of the complex was evident by mass spectrum analysis.

3.3 Xylenol Orange Test to Investigate the Presence of Free Gd(III) ion:

Free Gd(III) ion is highly toxic for living organisms. It is neurotoxic,[5] and also instigates oxidative stress by inhibiting mitochondrial activity.[6] It also interferes cellular uptake processes.[7] Therefore, before using any Gd(III)-based complexes for *in vivo* applications, the absence of free Gd(III) ion should be always ensured. The presence of free Gd(III) ion can be determined by using one complexometric indicator. The most commonly used indicator is xylenol orange (XO). XO shows specific colour depending upon pH of the medium. It shows yellow colour in acidic and neutral pH, whereas the colour changes to violet in basic medium. In the presence of free Gd(III) ion, the colour of XO changes to violet from yellow,[8] due to formation of Gd(III) xylenol orange complex (**Scheme 3.3**). However, slightly acidic or neutral pH (pH ~ 5.8) is needed to be maintained to get precise information about the presence of free Gd(III) ion in the solution.

The thermodynamic stability of Gd(III) xylenol orange complex is comparatively low (log K = 5.8).[9] In the presence of stable Gd(III) complexes, XO cannot able to extract Gd(III) ion from them, and can bind only with free Gd(III) ion present in any complex. The amount of free Gd(III) ion present in any complex can thus be determined from one calibration curve obtained from known concentrations of Gd(III) ion. XO was added to different known concentrations of Gd(III) ion solutions in acetate buffer maintaining pH of the solutions at ~ 5.8.

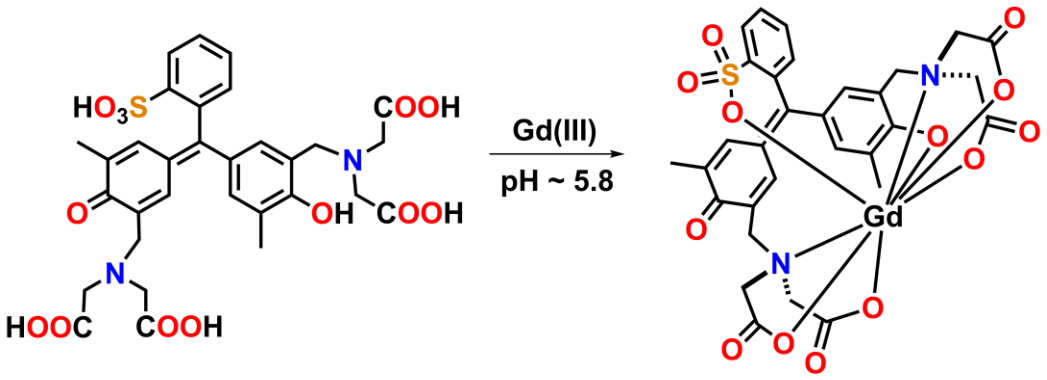

Scheme 3.3. *Formation of Gd(III) complex of xylenol orange.*

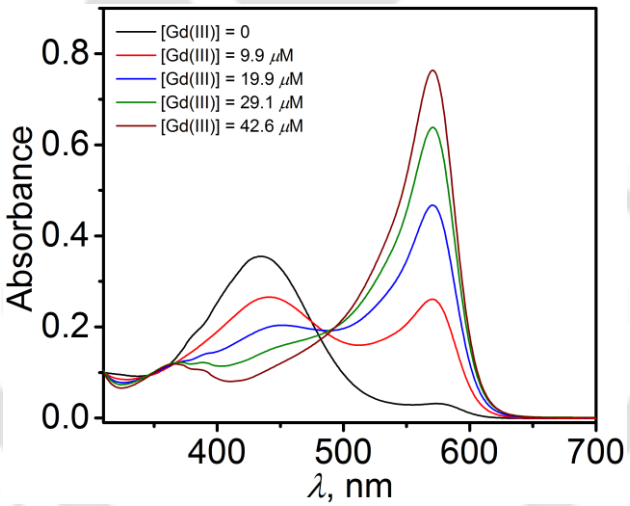

Figure 3.5. *UV-Vis spectral change during addition of various concentrations of Gd(III) ion to xylenol orange in acetate buffer at pH ~5.8.*

The absorbance of these samples showed maxima in the visible region (433 nm and 573 nm) (**Figure 3.5**). In the absence of Gd(III) ion, intensity of absorbance at 433 nm is greater than 573 nm. However, with increasing concentration of Gd(III) ion, the absorbance intensity of these two bands changes. The absorbance at 573 nm increases, while absorbance at 433 nm decreases. The absorbance ratio of these two wavelengths was plotted against Gd(III) ion concentration of

the samples. Since, the absorbance ratio linearly depends upon the concentration of Gd(III) ion, a linear plot was obtained (**Figure 3.6**).

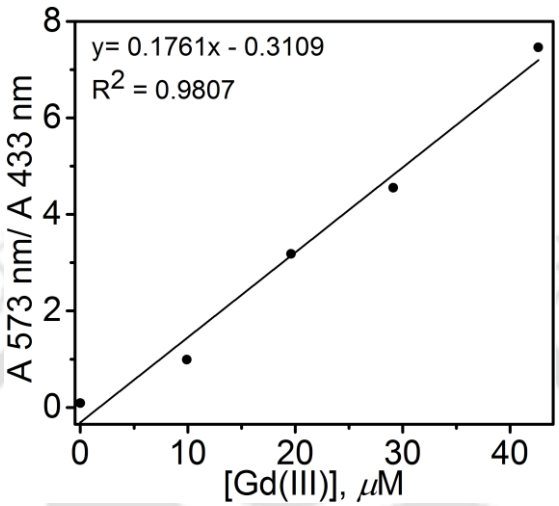

Figure 3.6. *Calibration curve obtained from absorbance ratio of known concentrations of Gd(III) ion in xylenol orange.*

The amount of free Gd(III) ion present in both of the complexes were determined by measuring absorbance of known concentrated samples of the complexes in xylenol orange solution in acetate buffer maintaining pH of the solution at ~ 5.8. The absorbance ratio for complex **3A** (100 μL of 10.67 mM in 2 mL xylenol orange) was found to be 0.15; and complex **3B** (100 μL of 12.45 mM in 2 mL xylenol orange) was found to be 0.23. The inclusion of calculated ratios into the linear calibration curve provided the amount of free Gd(III) ion present in both of the complexes to be almost negligible.

3.4 Determination of Number of Coordinated Water Molecules (q):

Since, lanthanide ions are known to exhibit luminescence both in solid and solution state; luminescence lifetime measurements have been carried out to determine the number of coordinated-water molecules. In case of Gd(III) ion [$^6P_{7/2} \rightarrow {}^7S_{7/2}$], the emission takes place in UV-region (310 nm). However, for Tb(III) ion, the transition from excited $^5D_4$ state to $^7F_6$ state takes place in visible region (543 nm). Due to similar ionic radii and habit of forming similar type of complexes, it is possible to form corresponding Gd(III) and Tb(III) complexes with same hydration number.

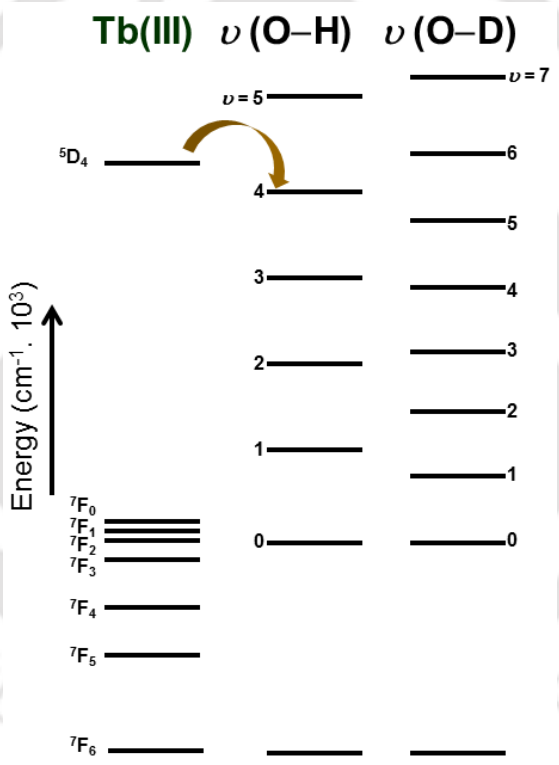

Figure 3.7. *Energy level diagram of Tb(III), vibrational level of O–H, and O–D oscillators. Curved arrow denotes the most likely vibrational transition for the non-radiative decay process.*

The high energy O–H oscillators present in the crystal lattice can provide an efficient pathway for non-radiative deactivation of Tb(III) excited states.[10] The energy gap between the

emissive excited state of Tb(III), $^5D_4$ and vibrational levels of O–H oscillators is less in compared to energy gap with O–D oscillators (**Figure 3.7**). Therefore, energy can be more easily transferred to vibrational energy levels of O–H oscillators than O–D oscillators. Consequently, the deactivation process of excited energy state of Tb(III) ion in H_2O is more efficient than in D_2O. Thus, the luminescence decay life time of Tb(III) excited state in H_2O is less than in D_2O. It is established that the luminescence decay constant is directly proportional to the number of water molecules present in inner-coordination sphere of the metal ion. Based on this linear relationship, the number of water molecules present in inner-coordination sphere (q) can be calculated from the modified Horrock′s equation,[11]

$$q = A\,(1/\tau_{H2O} - 1/\tau_{D2O} - \alpha);$$

where, $A_{Tb} = 5$ ms, and $\alpha_{Tb} = 0.06$ ms^{-1} respectively.

Syntheses and Characterizations of Tb(III) Congeners of Ligands:

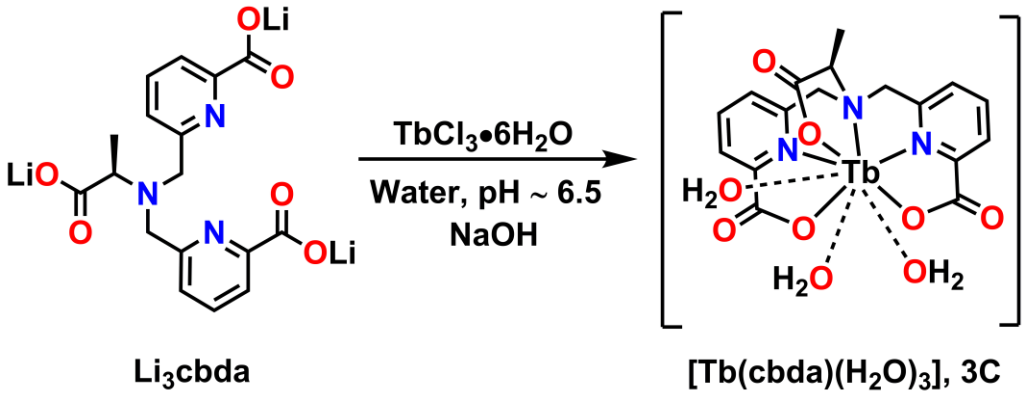

Li_3cbda **[Tb(cbda)$(H_2O)_3$], 3C**

Scheme 3.4. *Synthesis of Tb(III) complex of ligand* ***Li_3cbda****.*

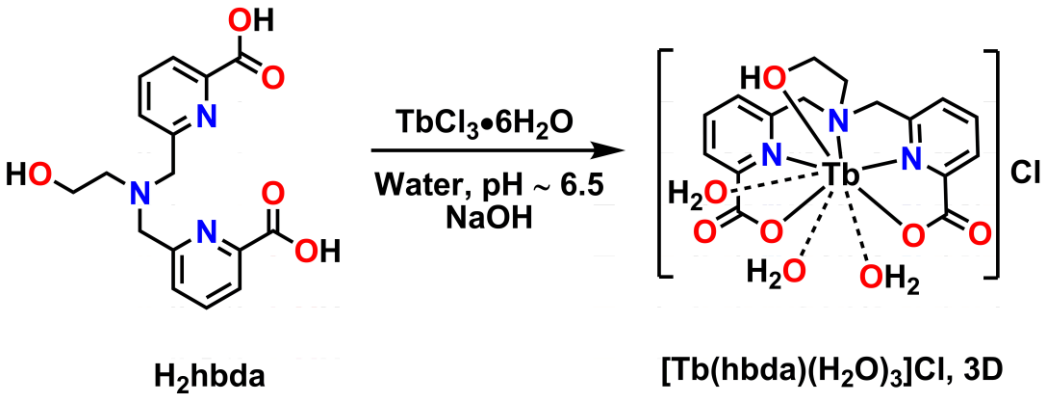

Scheme 3.5. *Synthesis of Tb(III) complex of ligand* ***H₂hbda****.*

By the reaction of 1:1 molar equivalents of ligands (**Li_3cbda** and **H_2hbda**) with $TbCl_3 \bullet 6H_2O$ in water followed by the adjustment of pH of the reaction medium ~ 6.5 by dropwise addition of aqueous NaOH provided complex **3C** (**Scheme 3.4**), and complex **3D** (**Scheme 3.5**) respectively.

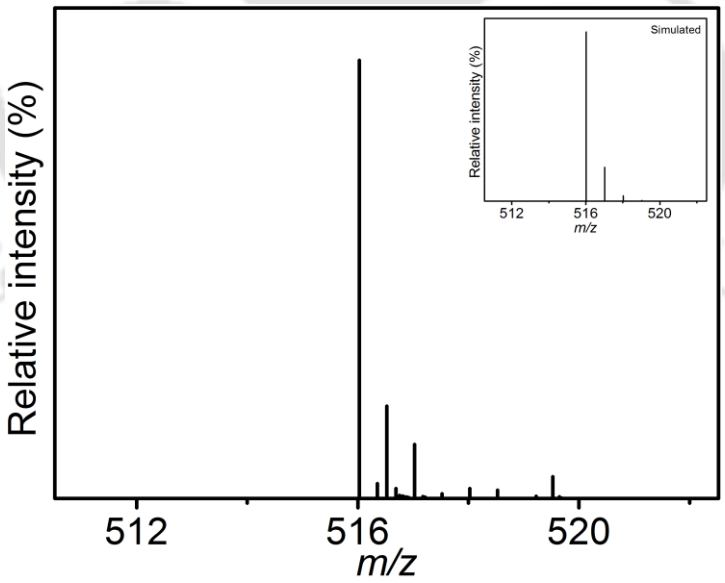

Figure 3.8. *ESI-MS (+ve) mass spectrum of aqueous solution of complex* ***3C****. Simulated spectra has been given as inset.*

The electrospray ionization mass spectrum of aqueous solution of complex **3C** provided a 100% molecular peak at *m/z* value 516.0248 in positive mode. The peak was assigned to $[C_{17}H_{14}N_3O_6Tb + H]^+$ (*m/z* = 516.0209), and it was evident from the isotropic distribution pattern (**Figure 3.8**). The simulated spectrum is given in inset.

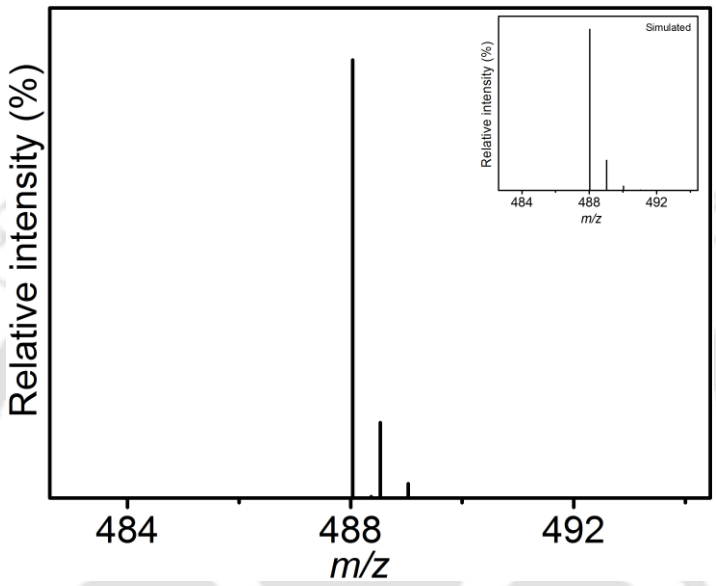

Figure 3.9. *ESI-MS (+ve) mass spectrum of aqueous solution of complex **3D**. Simulated spectra has been given as inset.*

The electrospray ionization mass spectrum of an aqueous solution of complex **3D** in positive mode provided a 100% molecular ion peak at *m/z* value 488.0313. The peak corresponded to $[C_{16}H_{15}N_3O_5Tb]^+$ (*m/z* = 488.0265), and it was evident from its isotropic distribution pattern (**Figure 3.9**). The simulated spectrum is given as inset.

Luminescence Study:

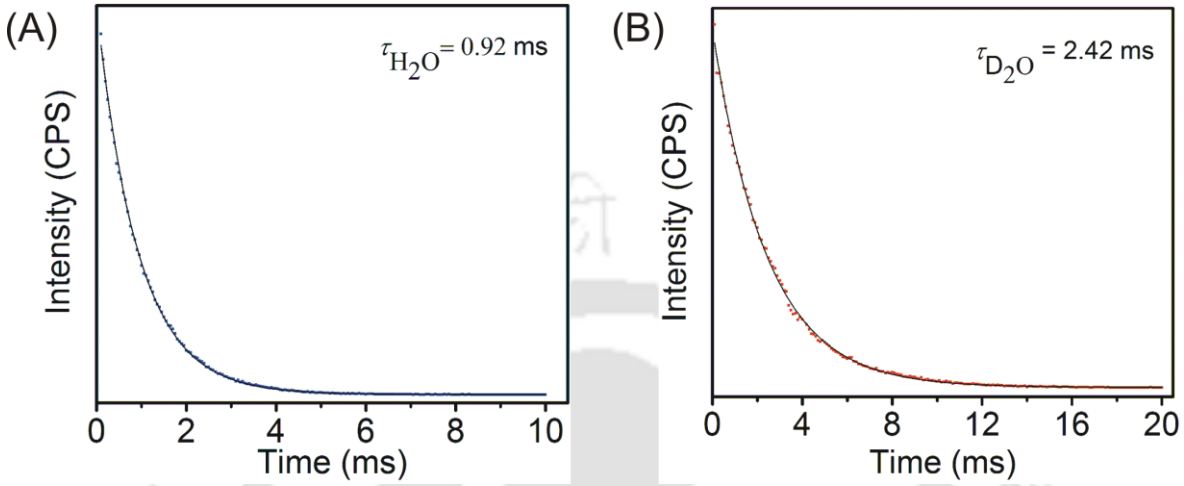

Figure 3.10. *Luminescence lifetime decay curves of complex* ***3C*** *in (A) H_2O, and (B) D_2O.*

50 μM solutions of Tb(III) complexes were prepared in 10 mM HEPES buffer maintaining pH ~ 7.4, 25 °C. The luminescence decay curves were generated by 'decay by delay' method. After completion of lifetime measurements in HEPES buffer, samples were evaporated completely under reduced pressure. Addition of equal volumes of D_2O to the completely dry residues resulted into solutions of same concentration of complex **3C** and **3D** in D_2O-buffer. The excited and emission wavelengths of both of the complexes are given in **Table 3.1**, with measured lifetimes in H_2O and D_2O. The lifetimes (τ) of Tb ($^5D_4$) level were calculated in H_2O and D_2O by single exponential fitting of experimental decay curves using non-linear least square method and goodness of the fittings were determined by minimizing the reduced Chi^2 values (**Figure 3.10** and **3.11**). The number of inner-sphere water molecules present in complex **3C** and **3D** were found to be q ~ **3.0 ± 0.1** and **2.8 ± 0.1** respectively.

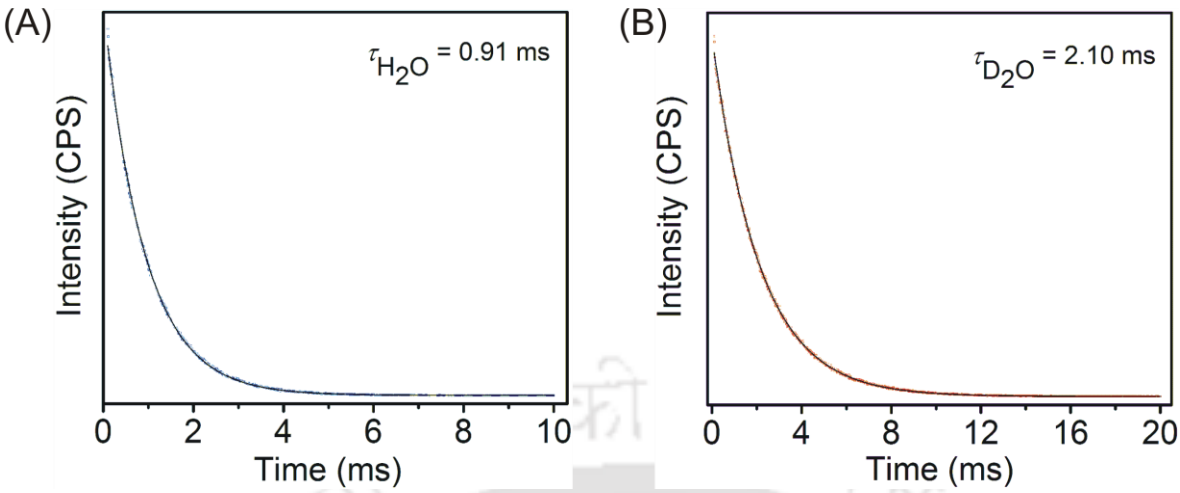

Figure 3.11. *Luminescence lifetime decay curves of complex* ***3D*** *in (A) H_2O, and (B) D_2O.*

Table 3.1. *Excited and emission wavelengths, lifetimes in H_2O and D_2O, and number of coordinated-water molecules.*

Complex	λ_{exc} (nm)	λ_{emis} (nm)	τ_{H2O} (ms)	τ_{D2O} (ms)	Q
3C	270	549	0.92	2.42	3.0 ± 0.1
3D	272	548	0.91	2.10	2.8 ± 0.1

3.5 Thermodynamic Stability:

Toxicity of free Gd(III) ion is directly related to the thermodynamic stability of the complex. The stepwise protonation constants of ligands (**Li_3cbda** and **H_2hbda**), as well as thermodynamic stability constant of its corresponding Gd(III) complexes (complex **3A** and **3B**) were determined by pH-potentiometric titrations. The protonation constants of ligands are defined by the equation:

$$K_i^H = [H_iL]/[H_{i-1}L][H^+] \qquad i = 1, 2, 3, 4, \ldots.$$

In 0.15 M NaCl and at 25 °C, the protonation constants of ligand **Li_3cbda** were found to be log K_1^H = 8.10, log K_2^H = 2.97, and log K_3^H = 2.35. The highest value of protonation constants (log K_1^H = 8.10) has been assigned to the protonation of amine nitrogen atom. Compared to similar systems, H_3tpaa[12] and H_3dpaaa,[13] the amine N-atom present in the ligand was more basic. It could be due to the presence of one methyl group in acetate arm, which imparted higher

electron density to the amine N-atom. The protonation constants; log K_2^H = 2.97, and log K_3^H = 2.35 corroborated to the reported protonation constants of carboxylates groups of picolinate moieties of analogous ligand H_3dpaaa.[13] Thus, both protonation constants were assigned to the protonation of two carboxylates groups of picolinate moiety present in ligand **Li_3cbda**. The protonation of acetate group might occur at lower pH and hence, could not be determined.

Using the same experimental conditions, the obtained stepwise protonation constants for ligand **H_2hbda**; log K_1^H = 7.68, log K_2^H = 4.63, and log K_3^H = 2.88. Considering already reported analogous systems, the protonation constant at log K_1^H = 7.68 and log K_2^H = 4.63 have been assigned to the protonation of amine nitrogen atom, and pyridine nitrogen atom respectively. While the protonation constant at log K_3^H = 2.88 was due to protonation of one of the carboxylate groups of picolinate moieties present in the ligand framework.

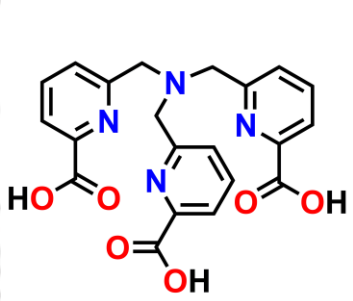

H_3tpaa

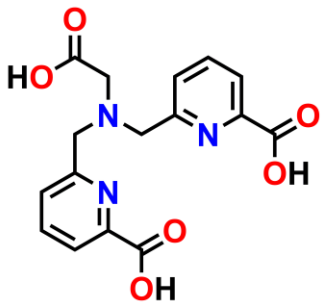

H_3dpaaa

Table 3.2. *Protonation constants, stability constants, and pGd value of its analogues.*

Ligand	log K_i^H	log K_{GdL}	pGd
H_3tpaa[12]	6.78, 4.11, 3.30, 2.50	10.2	11.20
H_3dpaaa[13]	7.33, 3.80, 2.90	10.6	12.30
Li_3cbda	**8.10, 2.97, 2.35**	**12.72**	**12.90**
H_2hbda	**7.68, 4.63, 2.88**	**16.12**	**16.61**

The stability constant of complex **3A** was determined by direct potentiometric titration of 1:1 metal-ligand mixture under the same experimental condition used for the determination of protonation constants of ligand **Li_3cbda**. The stability constant of the complex can be defined by the equation:

$$K_{GdL} = [GdL]/[Gd][L]$$

The stability constant of complex **3A** was found to be $\log K_{GdL}$ = 12.72, in 0.15 M NaCl solution, and at 25 °C. Under physiological condition, the best way to describe the stability of any complex is in terms of pM value, which is defined by $-\log[M]_{free}$ at pH ~ 7.4, and 25 °C; where [M] = 1 μM, and $[L]_{total}$ = 10 μM.[14] The calculated pGd value for ligand **Li_3cbda** was found to be 12.90, which was better than similar ligand systems (**Table 3.2**). Herein, complex **3A** was stable due to the presence of chiral methyl group in the ligand backbone, which provided some amount of rigidity to the complex. Furthermore, two picolinate units also stabilized the complex.

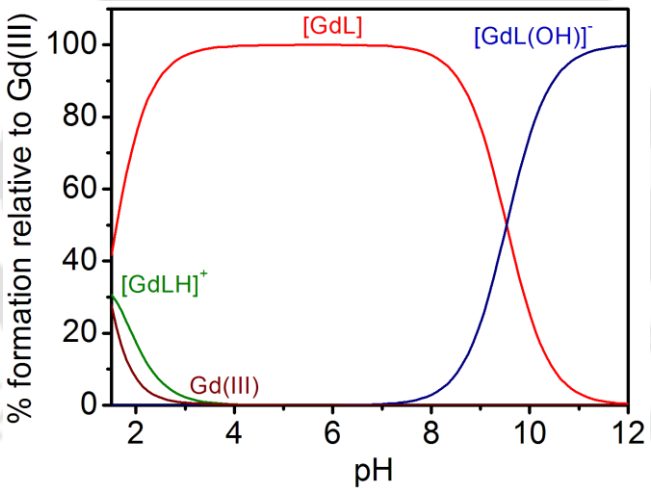

Figure 3.12. *Species distribution diagram of* ***Li_3cbda****:Gd(III) (1:1) solution, whrere [****Li_3cbda****] = [Gd(III)] = 1 mM (L in the figure represents* ***$cbda^{3-}$****).*

The species distribution diagram obtained for complex **3A** is presented in **Figure 3.12**. Complex **3A** was observed to be the most prominent species in the pH range ~ 4-9. Above pH ~

9, either deprotonation of the coordinated water molecules or addition of hydroxyl anion took place as indicated by the appearance of $[GdL(OH)]^-$ species.

The stability constant of complex **3B** was found to be $\log K_{GdL}$ = 16.12 in 0.15 M NaCl, and at 25 °C. Under physiological condition, the calculated pGd value for ligand **H_2hbda** was found to be 16.61, which was much higher compared to the similar ligand systems given (**Table 3.2**). According to previous reports, the presence of alcoholic donor group can stabilize its corresponding Ln(III) complexes.[1(a),15] Herein, the alcoholic group present in ligand **H_2hbda** stabilized its corresponding Gd(III) complex, **3B**.

Notably, stability constants and pGd values of both of the complexes suggested that complex **3B** was more stable than complex **3A**. Thus, it was conclusive that the effect of alcoholic group towards the thermodynamic stability of the corresponding tris(aquated) Gd(III) complex predominates over the chiral acetate group. It is also notable that the chirality of the coordinating-acetate group imparts more stability compared to achiral acetate-coordinating unit.

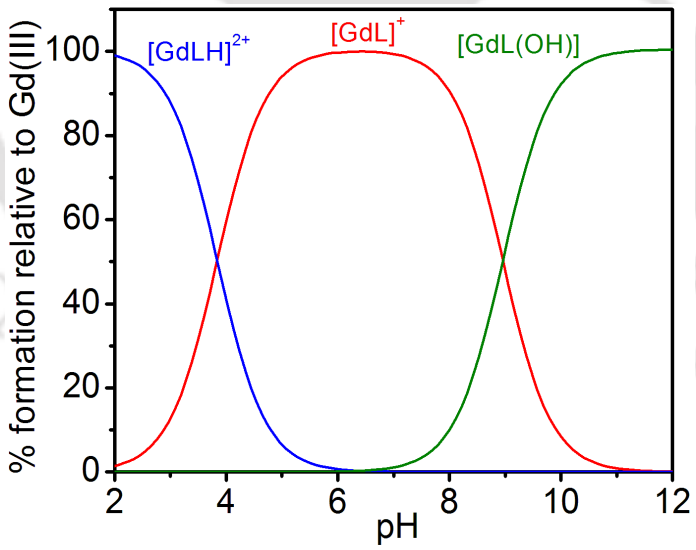

Figure 3.13. *Species distribution diagram of* ***H_2hbda****:Gd(III) (1:1) solution, whrere* ***[H_2hbda]*** *= [Gd(III)] = 1 mM (L in the figure represensts* ***hbda^{2-}****).*

The species distribution diagram of complex **3B** is given in **Figure 3.13**. Complex **3B** was most predominantly present in the pH range ~ 4-8. Below pH ~ 3, protonated species were observed as dominant species. Above pH ~ 8, $[GdL(OH)]^-$ species appeared either due to deprotonation of the coordinated water molecule or addition of hydroxyl anion.

3.6 Longitudinal Relaxivity:

The efficiency of any complex as T_1-contrast agent was gauged by their ability to enhance water protons longitudinal relaxation rates by 1 mM concentration at particular temperature and magnetic field strength. Using inversion recovery technique, T_1 relaxation times were measured for four different concentrations of the complexes in HEPES buffer, at pH ~ 7.4, and temperature 25 °C.

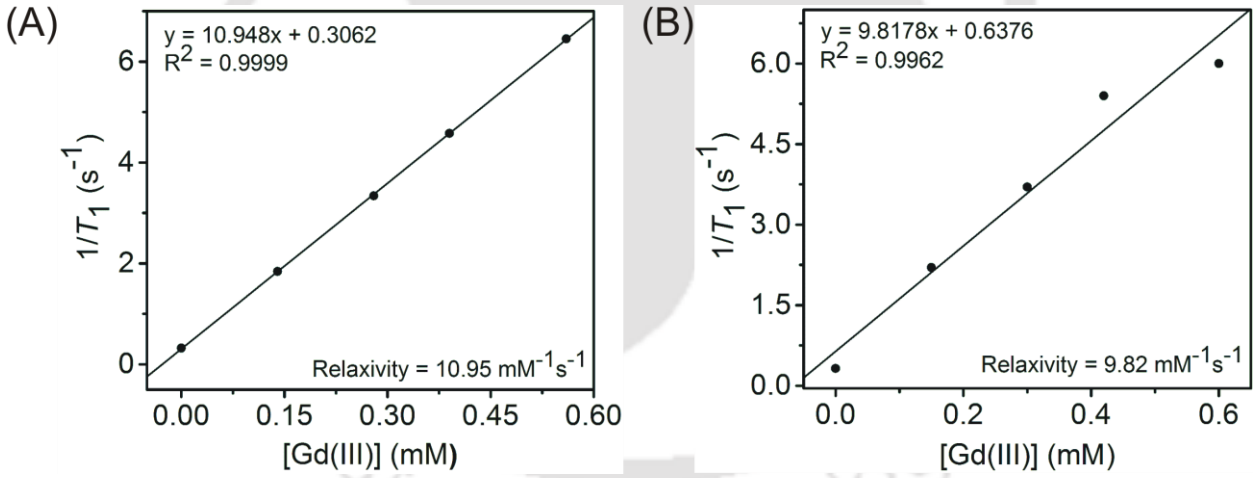

Figure 3.14. *$1/T_1$ vs [Gd(III)] plot for; (A) complex **3A**, and (B) complex **3B**; at 1.41 T, 25 °C, and pH ~7.4.*

The slope of linear plot of longitudinal relaxation rates, R_1 ($1/T_1$) *vs* [Gd(III)] ion provided longitudinal relaxivity value. The obtained longitudinal relaxivity values were 10.95 $mM^{-1}s^{-1}$ (for complex **3A**), and 9.82 $mM^{-1}s^{-1}$ (for complex **3B**) at 1.41 T, pH ~ 7.4, and 25 °C

(**Figure 3.14**). The exact concentration of Gd(III) ion present in the samples were estimated by ICP-AES technique. The high relaxivity value of complexes (**3A** and **3B**) was allied to the presence of three inner-sphere water molecules. The observed relaxivity value was higher than clinically approved mono(aquated) Gd(III) complexes. The values were comparable to some of tris(aquo) Gd(III) complexes: [Gd(dpaaa)(H_2O)$_3$] (9.4 $mM^{-1}s^{-1}$ at 1.06 T, 25 °C),[16(a)] [Gd(TACN-3,2-HOPO)(H_2O)$_3$] (13.1 $mM^{-1}s^{-1}$),[16(b)] [Gd(TACN-1,2-HOPO)(H_2O)$_3$] (12.5 $mM^{-1}s^{-1}$);[16(b)] and [Gd(edta)(H_2O)$_3$]$^-$ (7.15 $mM^{-1}s^{-1}$)[16(c)] at 0.47 T, 25 °C.

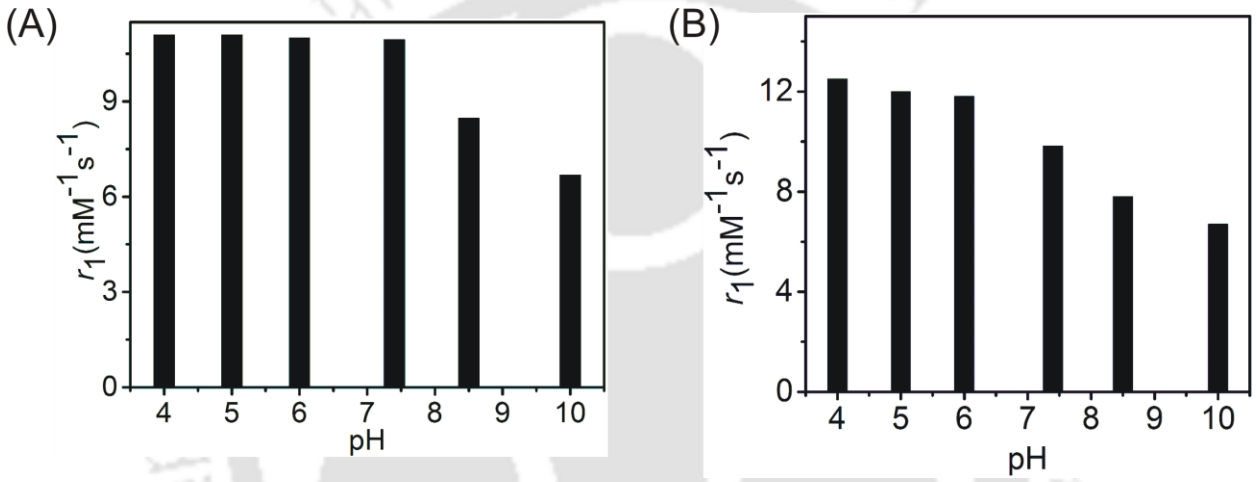

Figure 3.15. *r_1 relaxivity changes in the pH range 4-10 for; (A) complex **3A**, and (B) complex **3B**; at 1.41 T, and 25 °C.*

In solution state, the presence of variable equilibrium states of the complexes were investigated by measuring relaxivity values in a pH range of 4-10, at 1.41 T, and 25 °C. The obtained relaxivity values were plotted as bar diagram in **Figure 3.15**. The existence of complex **3A** in the pH range 4-7.4, was justified by constant relaxivity value (r_1 = 10.95 $mM^{-1}s^{-1}$ at 25 °C, 1.41 T) in that particular pH range. Above pH ~ 8, formation of hydroxyl species by the replacement of coordinated water molecule was indicated by diminishing of relaxivity value to r_1 = 6.68 $mM^{-1}s^{-1}$ at pH ~ 10. The presence of these species was in accordance to species mentioned in species distribution diagram (**Figure 3.12**).

However, complex **3B** possessed higher relaxivity value of r_1 = 12.50 $mM^{-1}s^{-1}$ at pH ~ 4. Which reduced to r_1 = 6.70 $mM^{-1}s^{-1}$ at pH ~ 10. Complex **3B** showed pH-dependent relaxivity variation. In most of the cases, the variation of relaxivity is due to the change in hydration state of the complex.[17]

Table 3.3. *Lifetimes of complex **3D**, in H_2O and D_2O, number of coordinated-water molecules.*

pH	τ_{H2O} (ms)	τ_{D2O} (ms)	***q***
4	0.86	1.98	3.0 ± 0.1
10	0.53	0.68	2.0 ± 0.1

To investigate this, luminescence lifetime measurements of excited Tb(III) congener, complex **3D** was carried out in H_2O and D_2O at pH ~ 4, and 10 (**Table 3.3**). At pH ~ 4, *q* value was found to be 3.0; which implied constant *q* value in the pH range of 4-7.4. While, at pH ~ 10; *q* value was observed to be 2.0. Thus, it was confirmed that the increase in relaxivity value at pH ~ 4 was not due to change in hydration state.

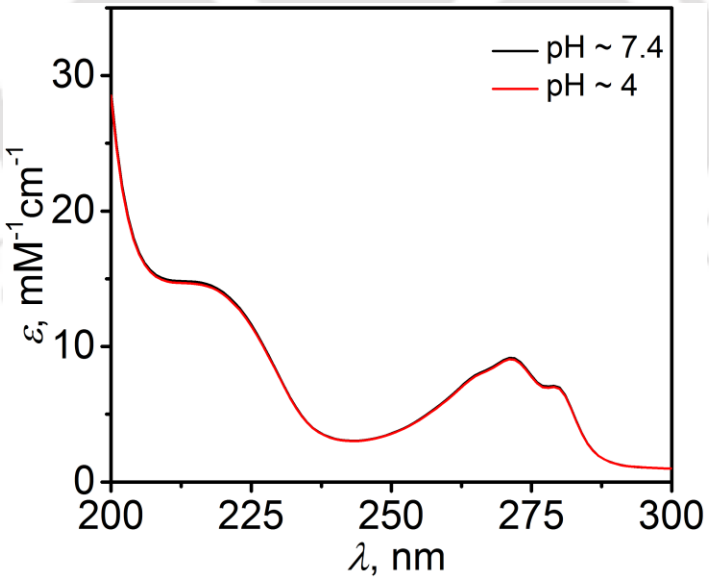

Figure 3.16. *UV-Vis spectra of complex **4B** at pH ~ 7.4, and 4.*

UV-Vis spectra of the complex were recorded at pH ~ 4, and 7.4 to investigate any possible structural changes. However, no noticeable changes were observed in the spectra given in **Figure 3.16**. Thus, luminescence lifetime, and UV-Vis measurements, clearly discarded the dissociation probability of complex **4B** at pH ~ 4.

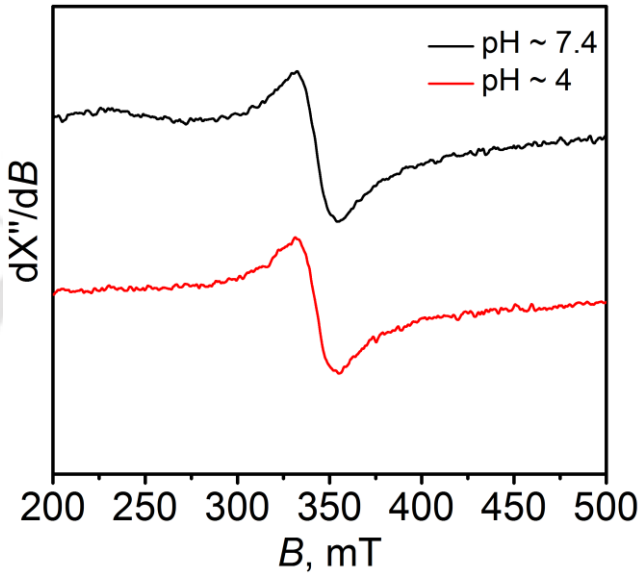

Figure 3.17. *X-band EPR spectra of complex* ***4B*** *at pH ~ 4, and 7.4; measured at room temperature, power = 0.995 mW, modulation frequency = 100 kHz, and amplitude = 200 G.*

The rotational correlational time of a contrast agent can be affected by pH of the medium. The overall tumbling rate can vary with pH of the medium.[18] Higher relaxivity value of complex **3B** at pH ~ 4 could be due to increase in rotational correlational time. To investigate, the slower rotational rate at acidic pH, X-band EPR measurements were carried out at pH ~ 4, and 7.4. The experimental X-band EPR spectrum is given in **Figure 3.17**. It was found that peak-to-peak line width, ΔHpp, was larger at pH ~ 4 than at pH ~ 7.4. There was about 9.72% of increase in ΔHpp value, which was not so much large as normally observed for slowly rotating macromolecular species.[18] However, it can be concluded that increase in relaxivity value might be due to formation of slowly rotating aggregation. The observed peak-to-peak EPR line widths of complex **3B** at both pH ~ 4, and 7.4 is given in **Table 3.4**.

Table 3.4. *Variable pH, peak-to-peak EPR line width, ΔHpp at X-band EPR measurement.*

pH	*ΔH*pp (Gauss)
4	238.50
7.4	217.36

Relaxivity value of complex **3B** was found to be decreased in basic pH range 8-10, which might be due to formation of hydroxyl species. It was supported by the species distribution diagram (**Figure 3.13**) of complex **3B**, and also from luminescence lifetime measurements at pH ~ 10 (q ~ 2.0).

3.7 Affinity for Physiological Anions:

One major criterion to be considered in designing MRI contrast agents is *in vivo* stability of these complexes in the presence of physiological anions. The anions such as biphosphate (HPO_4^{2-}), bicarbonate (HCO_3^-), fluoride (F^-), are present in non-negligible amounts (0.38 mM to 24.50 mM) in blood plasma.[14(g)] If the complex did not possess sufficient stability, then these anions might compete with the ligands for Gd(III) ion and could form insoluble adducts forming precipitations.[19] The endogenous anions could also displace inner-sphere water molecules forming ternary adduct.[19] In consequence, Gd(III) complexes would no longer efficiently relax bulk water molecules, and sharp reduction in relaxivity value takes place.

To investigate the binding affinities of these anions for complex **3A**, ([complex **3A**] = 0.5 mM) relaxivity values were monitored in the presence of 100 fold excess of these physiological anions ([HCO_3^-] = [HPO_4^{2-}] = [F^-] = 50 mM) at 25 °C, 1.41T, and pH ~ 7.4. The observed relaxivity values were, r_1 = 9.48 $mM^{-1}s^{-1}$ (Δr ~ -13.42%) for HPO_4^{2-}; r_1 = 7.31 $mM^{-1}s^{-1}$ (Δr ~ -33.24%) for HCO_3^-, and r_1 = 7.04 $mM^{-1}s^{-1}$ (Δr ~ - 35.70%) for F^- ion respectively (**Figure 3.18**). The reduction in relaxivity values might be due to the substitution of one of its inner-sphere water molecules by these anions. It might be due to the overall neutral charge of complex **3A**, only one of its coordinated-water molecules was substituted even in the presence of 100

equivalents of these physiological anions.[13] The observed interactions with the complex were found to be in decreasing order with increase in size of the anions.

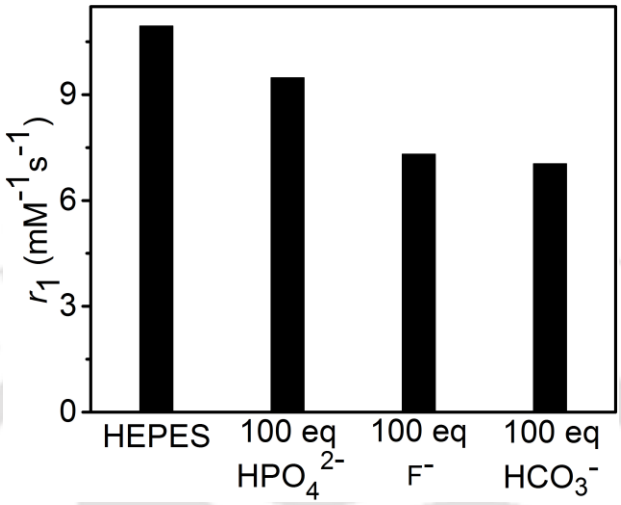

Figure 3.18. *Variation of relaxivity in the presence of 100 equivalents of physiological anions at 1.41 T, 25 °C, pH ~7.4; [complex **3A**] = 0.5 mM, and [physiological anions] = 50 mM.*

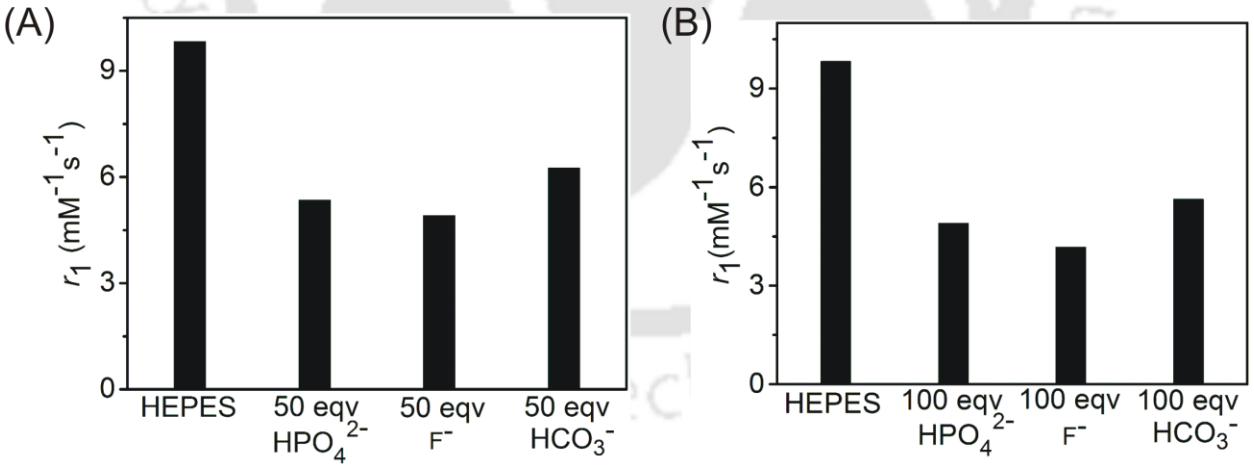

Figure 3.19. *Variation of relaxivity in the presence of physiological anions at 1.41 T, 25 °C, pH ~ 7.4; where [complex **3B**] = 0.5 mM, (A) [physiological anions] = 25 mM, and (B) [physiological anions] = 50 mM.*

In respect to complex **3A**, complex **3B** showed more affinity towards these physiologically available anions. In the presence of 100 equivalents of these anions, there was decrease in relaxivity value. The observed relaxivity values were, r_1 = 4.90 $mM^{-1}s^{-1}$ (Δr ~ - 49.90%) for HPO_4^{2-}, r_1 = 4.17 $mM^{-1}s^{-1}$ (Δr ~ - 57.54%) for F^- , and r_1 = 5.63 $mM^{-1}s^{-1}$ (Δr ~ - 42.67%) for HCO_3^- ion respectively [**Figure 3.19 (A)**]. Thus, two of the coordinated-water molecules of complex **3B** were replaced by these anions. Whereas, in the presence of 50 equivalents of these anions, the observed relaxivity values were, r_1 = 5.35 $mM^{-1}s^{-1}$ (Δr ~ - 45.52%) for HPO_4^{2-}, r_1 = 4.91 $mM^{-1}s^{-1}$ (Δr ~ -50.00%) for F^- , and r_1 = 6.25 $mM^{-1}s^{-1}$ (Δr ~ - 36.35%) for HCO_3^- ion respectively [**Figure 3.19 (B)**]. The observed relaxivity values implied that with increase in anions concentration from 50 equivalents to 100 equivalents number of substituted coordinated-water molecules increased from one to two. Due to overall positive charge of the complex, it was more affected by these physiological anions.[14(g)]

3.8 Phantom MR Imaging:

The potential of the complexes to enhance the NMR signal intensity were further investigated by acquiring T_1-weighted MR phantom images under MAGNETOM Avanto 1.5 T clinical MRI scanner. Aqueous solutions of both of the complexes in four different concentrations (0.25 mM, 0.50 mM, 0.70 mM, and 1.00 mM) were prepared in HEPES buffer maintaining pH at ~ 7.4. Micro centrifuge tubes containing different concentrations of the complexes were considered as phantoms under the clinical scanner. At 1.5 T, pH ~ 7.4, and 25 °C; the images were acquired at TR = 468 ms, and TE = 8.2 ms.

The obtained images showed enhancement in brightness with increase in concentration of complexes (**3A**, and **3B**). To compare the contrast efficiency of the complexes under the clinical scanner, commercially used contrast agent MultiHance® was used as reference at the same concentration of complexes (diluted to 1 mM concentration in HEPES buffer). The obtained images for complex **3A** under clinical imager are presented in **Figure 3.20(A)**.

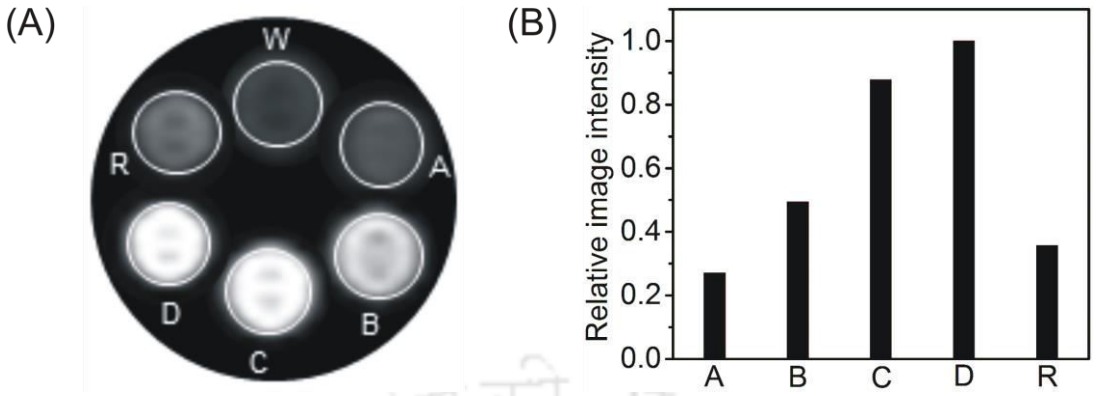

Figure 3.20. *T_1-weighted phantom images; (A) of micro-centrifuge tubes with different concentrations of complex* ***3A*** *(W = water, A = 0.25 mM, B = 0.50 mM, C = 0.70 mM, and D = 1.00 mM) at 1.5 T, 25 °C, pH ~ 7.4, TR = 468 ms, and TE = 8.2 ms; R stands for the reference MultiHance® in 1 mM concentration, and (B) relative image intensity plot using ImageJ Software.*

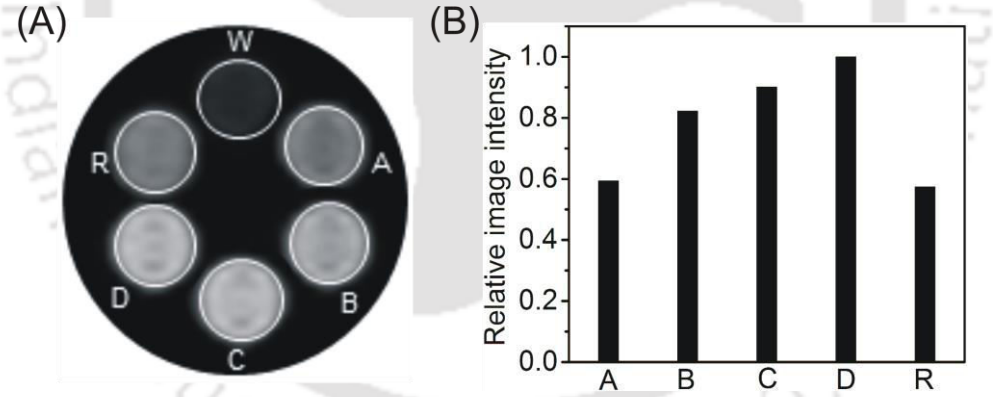

Figure 3.21. *T_1-weighted phantom images; (A) of micro-centrifuge tubes with different concentrations of complex* ***3B*** *(W = water, A = 0.25 mM, B = 0.50 mM, C = 0.70 mM, and D = 1.00 mM) at 1.5 T, 25 °C, pH ~ 7.4, TR = 468 ms, and TE = 8.2 ms; R stands for the reference MultiHance® in 1 mM concentration, and (B) relative image intensity plot using ImageJ Software.*

A comparative study was also performed to determine image intensities at different concentrations of the complexes by using ImageJ software. By considering same area for all the images, relative image intensity for complex **3A** is plotted as bar diagram in **Figure 3.20(B)**. The image intensity plot also revealed the increase in image intensity with increase in concentration of complex **3A**.

The obtained phantom images of complex **3B** under clinical imager is shown in **Figure 3.21(A)**. The acquired images showed enhancement in brightness of the images with increase in concentration of complex **3B**. The relative image intensity plot is given **Figure 3.21(B)**, which also implied increase in image intensity with increase in concentration of the complex solution. Thus, the obtained images clearly justified its contrast efficiency as T_1-weigted contrast agent.

3.9 Conclusion:

- In this chapter, tris(aquated) Gd(III) complexes [Gd(cbda)(H_2O)$_3$], **3A** and [Gd(hbda)(H_2O)$_3$]Cl, **3B** were synthesized using picolinate-based hexadentate ligands **Li_3cbda** and **H_2hbda** respectively.

- Complex **3A** afforded longitudinal relaxivity value of 10.95 $mM^{-1}s^{-1}$, and complex **3B** offered 9.82 $mM^{-1}s^{-1}$ at 1.41 T, pH ~ 7.4, and 25 °C. The observed relaxivity values were higher than commercially available mono(aquated) Gd(III) complexes, and comparable to similar tris(aquated) Gd(III) complexes.

- The complexes showed impressive thermodynamic stability. Complex **3A** (pGd = 12.90) was found to be more stable than analogous Gd(III) complexes due to presence of chiral L-alanine backbone. While, complex **3B** (pGd = 16.61) with one alcoholic group was found to be more stable than complex **3A**.

- In the presence of 100 equivalents of physiological anions, one of inner-sphere water molecules of complex **3A** was found to be substituted. While, cationic complex **3B** showed more affinity towards physiological anions than neutral complex **3A**. In case of complex **3B**, number of substituted water molecules in the presence of 100 equivalents of physiological anions increased to two.

- Phantom MR Imaging under clinical scanner at 1.5 T inferred the contrast efficiency of both of the complexes.

References

1. (*a*) P. Caravan, J. J. Ellision, T. J. McMurry and R. B. Lauffer, *Chem. Rev*., 1999, **99**, 2293; (*b*) S. Aime, L. Calabi, C. Cavallotti, E. Gianolio, G. B. Giovenzana, P. Losi, A. Maiocchi, G. Palmisano and M. Sisti, *Inorg. Chem*., 2004, **43**, 7588; (*c*) A. Datta and K. N. Raymond, *Acc. Chem. Res.*, 2009, **42**, 938; (*d*) D. Messeri, M. P. Lowe, D. Parker and M. Botta, *Chem. Commun*., 2001, 2742; (*e*) S. Aime, M. Botta, S. G. Crich, G. Giovenzana, R. Pagliarin, M. Sisti and E. Terreno, *Magn. Reson. Chem*., 1998, **36**, S200; (*f*) Z. Baranyai, L. Tei, G. B. Giovenzana, F. K. Kálmán and M. Botta, *Inorg. Chem*., 2012, **51**, 2597; (*g*) S. Aime, S. Baroni, D. D. Castelli, E. Brücher, I. Fábián, S. C. Serra, A. F. Mingo, R. Napolitano, L. Lattuada. F. Tedoldi and Z. Baranyai, *Inorg. Chem*., 2018, **57**, 5567; (*h*) B. Phukan, C. Mukherjee and R. Varshney, *Dalton Trans*., 2018, **47**, 135.

2. (*a*) A. M. Nonat, C. Gateau, P. H. Fries, L. Helm and M. Mazzanti, *Eur. J. Inorg. Chem*., 2012, 2049; (*b*) Y. Bretonnère, M. Mazzanti, J. Pécaut, F. Dunand and A. E. Merbach, *Chem. Commun*., 2001, 621; (c) A. Vágner, E. Gianolio, S. Aime, A. Maiocchi, I. Tóth, Z. Baranyai and L. Tei, *Chem. Commun*., 2016, **52**, 11235.

3. (*a*) E. M. gale, N. Kenton and P. Caravan, *Chem. Commun*., 2013, **49**, 8060; (*b*) T. J. McMurry, C. G. Pippin, C. Wu, K. A. Deal, M. W. Brechbiel, S. Mirzadeh and O. A. Gansow, *J. Med. Chem*., 1998, **41**, 3546; (*c*) P. Thakur, J. L. Conca, L. J. Van de Burgt and G. R. Choppin, *J. Coord. Chem*., 2009, **62**, 3719.

4. (*a*) J. Wang, G. R. Gao, Z. H. Zhang, X. D. Zhang, X. Z. Liu, Y. M. Kong and Y. Li, *Russ. J. Coord. Chem*., 2007, **33**, 258; (*b*) B. C. Smith, *Infrared Spectral Interpretation: A Systematic Approach*, CRC press, 1998.

5. (*a*) D. E Ray, J. B Cavanagh, C.C. Nolan and S.C. Williams, *Am. J. Neuroradiol*., 1996, **17**, 365; (*b*) D. E. Ray, J. L. Holton, C. C. Nolan, J. B. Cavanagh and E. S. Harpur, *Am. J. Neuroradiol*., 1998, **19**, 1455; (*c*) S. M. Roman-Goldstein, P. A. Barnett, C. I. McCormick, J. Szumowski, E. M. Shannon, F. L. Ramsey, M. Mass and E. A. Neuwelt, *J. Comput. Assist. Tomogr*., 1994, **18**, 731.

6. (*a*) X. Feng, Q. Xia, L. Yuan, X. Yang and K. Wang, *Neurotoxicology*, 2010, **31**, 391; (*b*) Q. Xia, X. Feng, H. Huang, L. Du, X. Yang and K. Wang, *J. Neurochem*., 2011, **117**, 38.

7. C. Cabella, S. G. Crich, D. Corpillo, A. Barge, C. Ghirelli, E. Bruno ,V. Lorusso, F. Uggeri and S. Aime, *Contrast Med. Mol. Imaging*, 2006, **1**, 23.

8. (*a*) A. Berge, G. Cravotto, E. Gianolio and F. Fedeli, *Contrast Media Mol. Imaging*, 2006, **1**, 184; (*b*) S. W. Kang, C. M. Park, K. H. Chao and H. S. Han, *Bull. Korean Chem. Soc*., 1993, **14**, 59; (*c*) S. Zhang, Z. Jiang, X. H. Liu, L. Zhou and W. Peng, *Nanoscale*, 2013, **5**, 8146.

9. K. V. Yatsimirsky, N. A. Kostromina, Z. A. Seka, N. K. Davidenko, E. E. Kriss and V. J. Ermolenko., *Khimya komplexnikh redkozemel' nikh ele-mentov*. Naukova Dumka: Kiev, 1966.

10. (*a*) G. R. Choppin and D. R. Peterman, *Coord. Chem. Rev*., 1998, **174**, 283; (*b*) J. G. Bünzli and C. Piguet, *Chem. Soc. Rev*., 2005, **34**, 1048; (*c*) W. D. Horrocks Jr. and D. R. Sudnick, *Acc. Chem. Res*., 1981, **14**, 384; (*d*) L. M. Manus, R. C. Strauch, A. H. Hung, A. L. Eckermann and T. J. Meade, *Anal. Chem*., 2012, **84**, 6278; (*e*) S. Faulkner, S. J. A. Pope and B. P. Burton-Pye, *Appl. Spectrosc*. *Rev*., 2005, **40**, 1; (*f*) L. G. Nielsen, A. K. R. Junker and T. J. Sørensen, *Dalton. Trans*., 2018 (DOI: 10.1039/c8dt01501e).

11. A. Beeby, I. M. Clarkson, R. S. Dickins, S. Faulkner, D. Parker, L. Royle, A. S. de Sousa, J. A. G. Williams and M. Woods, *J. Chem. Soc. Perk. T. 2*, 1999, 493.

12. Y. Bretonnière, M. Mazzanti, J. Pécaut, F. A. Dunand and A. E. Merbach, *Chem. Commun*., 2001, 621.

13. A. Nonant, P. H. Fries, J. Pécaut and M. Mazzanti, *Chem. -Eur. J*., 2007, **13**, 8489.

14. (*a*) D. M. J. Doble, M. Melchior, B. O'Sullivian, C. Siering, J. Xu, V. C. Pierre and K. N. Raymond, *Inorg. Chem*., 2003, **42**, 4930; (*b*) C. J. Jocher, M. Botta, S. Avedano, E. G. Moore, J. Xu, S. Aime and K. N. Raymond, *Inorg. Chem*., 2007, **46**, 4796; (*c*) C. J. Jocher, E. G. Moore, J. Xu, S. Avedano, M. Botta, S, Aime and K. N. Raymond, *Inorg. Chem*., 2007, **46**, 9182; (*d*) E. J. Warner, J. Kozhukh, M. Botta, E. G. Moore, S.

Avedano, S. Aime and K. N. Raymond, *Inorg. Chem*., 2009, **48**, 277; (*e*) D. T. Puerta, M. Botta, C. J. Jocher, E. J. Werner, S. Avedano, K. N. Raymond and S. M. Cohen, *J. Am. Chem. Soc*., 2006, **128**, 2222; (*f*) K. N. Raymond and V. C. Pierre, *Bioconjugate Chem*., 2005, **16**, 3; (*g*) V. C. Pierre, M. Botta, S. Aime and K. N. Raymond, *Inorg. Chem*., 2006, **45**, 8355.

15. L. Thompson, B. Shafer, J. Edgar and K. Mannila*, Adv. Chem. Ser*., 1967, **71**, 169.

16. (*a*) A. M. Nonat, C. Gateau. P. H. Fries, L. Helm and M. Mazzanti, *Eur. J. Inorg. Chem*., 2012, 2049; (*b*) E. J. Werner, S. Avedano, M. Botta, B. P. Hay, E. G. Moore, S. Aime and K. N. Raymond, *J. Am. Chem. Soc*., 2007, **129**, 1870; (*c*) A. C. Chang, H. G. Brittain, J. Telser and M. W. Tweedle, *Inorg. Chem*., 1990, **29**, 4468.

17. (*a*) S. Aime, S. G. Crich, E. Gianolio, G. B. Giovenzana, L. Tei and E. Terreno, *Coord. Chem. Rev*., 2006, 1562; (*b*) A. Wacker, F. Carniato, C. Platas-Iglesias, D. Esteban-Gomez, H. Wester, L. Tei and J. Notni, *Dalton Trans*., 2017, **46**, 16828; (*c*) M. Woods, G. E. Kiefer, S. Bott, A. Castillo-Muzquiz, C. Eshelbrenner, L. Michaudet, K. McMillan, S. D. K. Mudigunda, D. Ogrin, G. Tircsó, S. Zhang, P. Zhao and A. D. Sherry, *J. Am. Chem. Soc*., 2004, **126**, 9248.

18. S. Laus, A. Sour, R. Ruloff, É. Tóth and A. E. Merbach, *Chem.- Eur. J*., 2005, **11**, 3064.

19. (*a*) W. P. Cacheris, S. C. Quay and S. M. Rocklage, *Magn. Reson. Imaging*, 1990, **8**, 467; (*b*) A. Ranga, Y. Agarwal and K. J. Garg, *Indian J. Radiol. Imaging*, 2017, **27**,141; (*c*) A. Tartaro and M. T. Maccarone, *Reports in Medical Imaging*, 2015, **8**, 25.

20. (*a*) R. S. Dickins, S. Aime, A. S. Batsanov, A. Beeby, M. Botta, J. Bruce, J. A. K. Howard, C. S. Love, D. Parker, R. D. Peacock and H. Puschmann, *J. Am. Chem. Soc*., 2002, **124**, 12697; (*b*) S. Aime, M. Botta, J. I. Bruce, V. Mainero, D. Parker and E. Terreno, *Chem. Commun.*, 2001, 115; (*c*) J. I. Bruce, R. S. Dickins, L. J. Govenlock, T. Gunnlaugsson, S. Lopinski, M. P. Lowe, D. Parker, R. D. Peacock, J. J. B. Perry, S. Aime and M. Botta, *J. Am. Chem. Soc*., 2000, **122**, 9674.

भारतीय प्रौद्योगिकी संस्थान गुवाहाटी
Indian Institute of Technology Guwahati

Chapter IV

A Mono(aquated) Mn(II) Complex with Lipophilic Piperidine Ligand Backbone as T_1-weighted MRI Contrast Agent

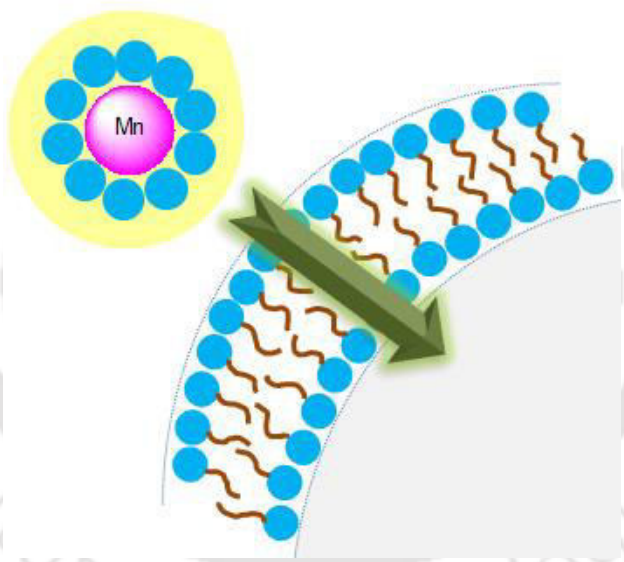

*Some results have been submitted for patent; with application no. **201831020333**.

4.1 Introduction:

Most of MRI contrast agents (CAs) are hydrophilic in nature. Therefore, they are mostly membrane impermeable and distributed in the extracellular matrix.[1] Due to hydrophilicity, these CAs are usually excreted out *via* renal filtration.[2] The elimination rate is quite slower in patients with chronic renal failure as compared to normal persons.[3] However, CAs can be made membrane permeable by the introduction of lipophilicity. The excretion route of these CAs can be altered to hepatobiliary system by increasing lipophiliciy of the agents.[4] Lipophilic character can be incorporated by designing suitable ligand frameworks with hydrophilic metal binding sites along with some parts which are lipophilic in nature.

Piperidine and its derivatives are common building blocks in several pharmaceuticals.[5] It is also lipophilic in nature.[6] In this context, ligand **H_3cpmda** was designed with piperidine moiety in the ligand backbone. Piperidine ring is observed in the most stable chair conformation.[7] Therefore; the presence of piperidine ring would provide structural rigidity to the complex.[6] Rigid ligand frameworks can provide thermodynamic stability to its corresponding metal-complexes.[8] The incorporation of three acetate arms would provide suitable hydrophilic binding cavity for Mn(II) ion.

Herein, Mn(II) complex was synthesized using pentadentate ligand **H_3cpmda**. Mn(II) complexes are generally six- or seven-coordinate. Hence, the corresponding Mn(II) complex of ligand **H_3cpmda** would have minimum one coordinated-water molecule. The ligand framework consisted of two amine N-atoms, and three acetate arms; which could provide high thermodynamic stability to the complex *via* five strong σ-bonds. With lipophilic rigid pentadentate ligand framework, **H_3cpmda** would form thermodynamically stable, Mn(II) complex with coordinated-water molecule.

4.2 Syntheses and Characterizations of Mn(II) Complexes of Ligand H_3cpmda:

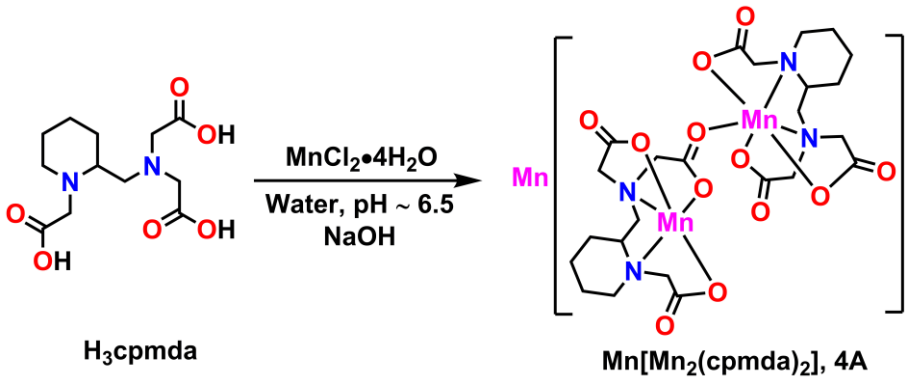

Scheme 4.1. *Synthesis of Mn(II) complex of ligand* ***H_3cpmda*** *using NaOH as base.*

1:1 molar equivalent of ligand **H_3cpmda** and $MnCl_2$•$4H_2O$ were reacted in water at pH ~ 6.5 by adding aqueous NaOH solution (**Scheme 4.1**). After 24 h of continuous stirring at room temperature, complex **4A** was isolated as colourless crystals in 41% yield from the filtrate by slow solvent evaporation technique.

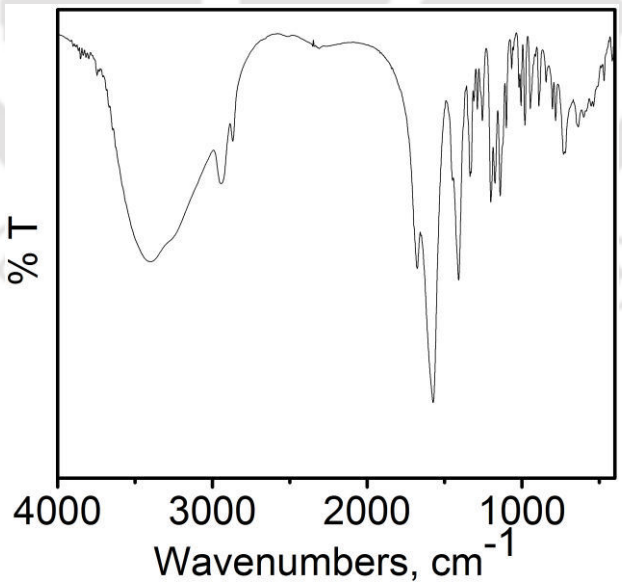

Figure 4.1. *FTIR spectrum of complex* ***4A***.

The FTIR spectrum of complex **4A** is given in **Figure 4.1**. The band appeared at 3403 cm^{-1} was due to ν(O–H) stretching of water molecule.[9(a)] The ν(C=O) stretching frequency for the complex was observed as a sharp band at 1676 cm^{-1}, whereas that of ligand was observed at 1729 cm^{-1}.[9(b)]

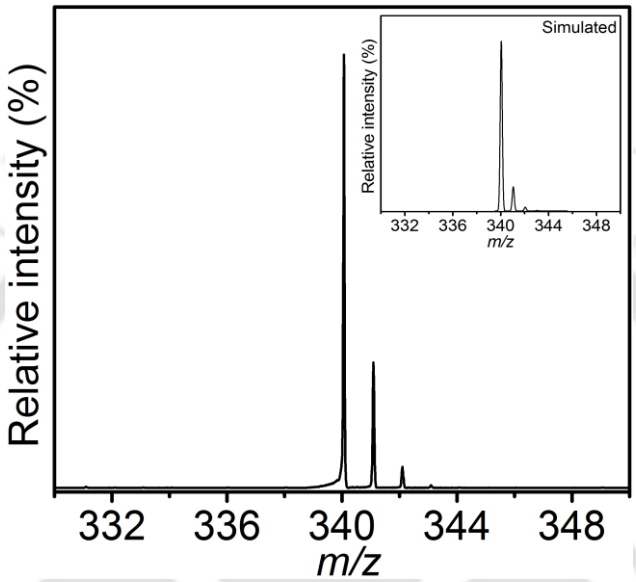

Figure 4.2. *ESI-MS (–ve) mass spectrum of aqueous solution of complex* ***4A****. Simulated spectrum has been given as inset.*

The electrospray ionization mass spectrum of complex **4A** in negative mode in Mili Q water provided a 100% molecular ion peak at *m/z* value 340.06 (**Figure 4.2**). This peak corresponded to $[C_{12}H_{17}N_2O_6Mn]^-$ (*m/z* = 340.05) and it was evident from the isotropic distribution pattern.

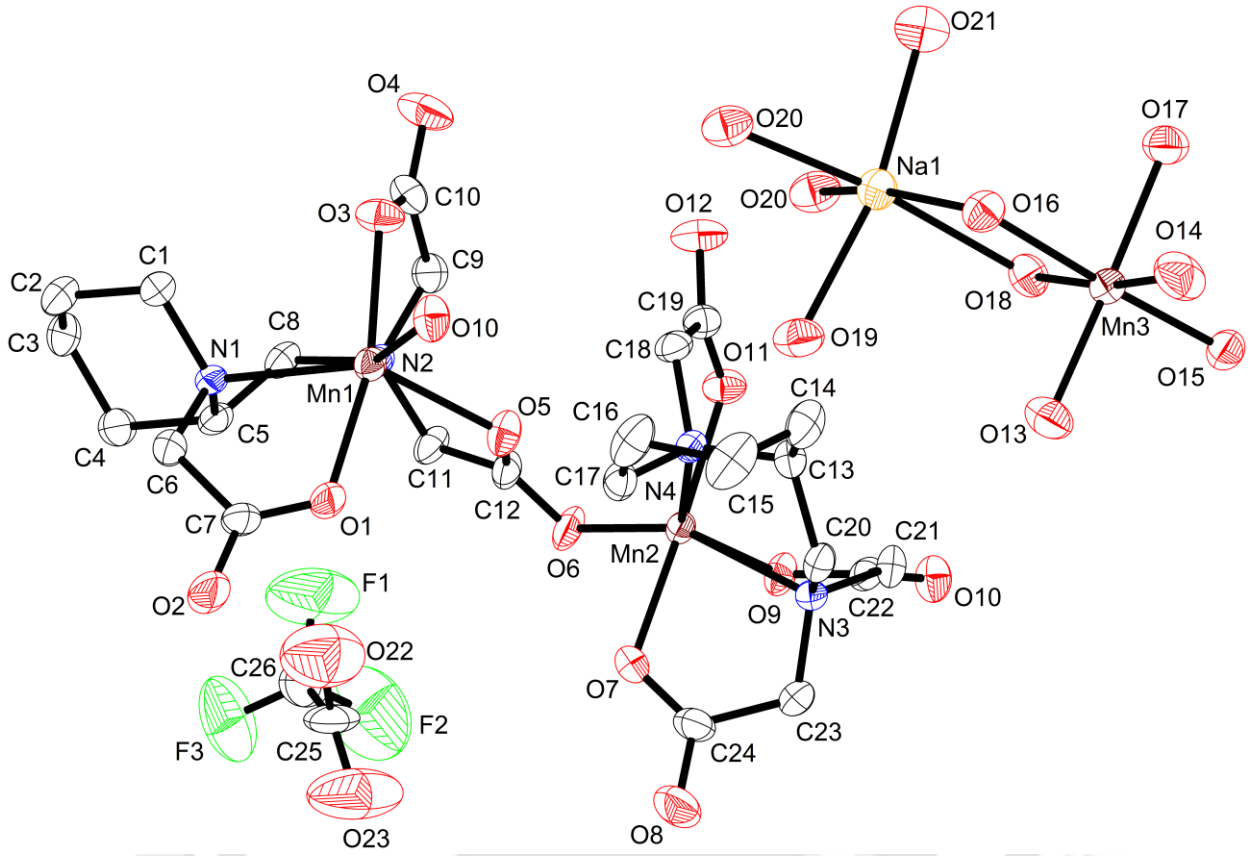

Figure 4.3. *ORTEP diagram of complex* ***4A*** *•* CF_3COONa *•*$10H_2O$ *Hydrogen atoms were omitted for clarity and thermal ellipsoids were drawn with 40% probability.*

Single crystal X-ray diffraction measurement was performed for complex **4A** at 293(2) K. It was found that complex **4A** crystallized in the monoclinic space group *P* 21/c. The molecular structure of complex **4A** is shown in **Figure 4.3**, and selected bond lengths and bond angles are tabulated in **Table 4.1**. In the dianionic form of complex **4A**, two six-coordinate Mn(II) units were present, which were connected by carbonyl-oxygen atom O6. The basal plane of each Mn(II) unit, was consisted of amine N-atom of 2-aminomethylpiperidine, N-atom from the piperidine ring, one carboxylate O-atom, and O-atom of bridging carbonyl-oxygen atom. The axial positions were occupied by two carboxylate O-atoms with an average angle of ~ 169°. In each mononegative unit, Mn1–N1(piperidine) = 2.349, Mn1–N2(amine) = 2.331, Mn1–O1(carboxylate) = 2.151, Mn1–O3(carboxylate) = 2.173, Mn1–O5(carboxylate) = 2.218, Mn1–O10(carbonyl-oxygen) = 2.186 Å; N2–Mn1–N1 = 76.99°, O5–Mn1–N2 = 72.36°,

O10–Mn1–O5 = 91.32°, O10–Mn1–N1 = 130.43°, and O1–Mn1–O3 = 165.86°; which implied an asymmetric environment of Mn(II) center which was in distorted octahedral geometry. In the asymmetric unit of complex **4A**, one CF_3COO^- ion was present. One Mn(II) ion, and one Na(I) ion were present as counter cations in the complex.

Table 4.1. *Selected bond lengths (Å) and bond angles (°) for complex* ***4A***.

Mn1–O1	2.151(4)	Mn2–O6	2.121(4)
Mn1–O3	2.173(4)	Mn2–O7	2.211(4)
Mn1–O5	2.218(4)	Mn2–O9	2.271(4)
Mn1–O10	2.186(4)	Mn2–O11	2.157(4)
Mn1–N1	2.349(4)	Mn2–N3	2.297(4)
Mn1–N2	2.331(4)	Mn2–N4	2.334(4)
O1–Mn1–O3	165.86(15)	O11–Mn2–O7	171.88(16)
O5–Mn1–N2	72.36(14)	O9–Mn2–N3	71.62(14)
O10–Mn1–N1	130.43(15)	O6–Mn2–N4	128.59(14)
N2–Mn1–N1	76.99(15)	N3–Mn2–N4	77.76(14)
O1–Mn1–N1	74.98(14)	O11–Mn2–N4	74.45(14)
O10–Mn1–O5	91.32(14)	O6–Mn2–O9	89.11(14)

In aqueous state, complex **4A** would release the external Mn(II) ion in free aqua form. The presence of free Mn(II) ion in higher concentration is toxic for living systems.[10] To substitute the Mn(II) ion present outside the coordination sphere, the complexation of ligand **H_3cpmda** with $MnCl_2 \bullet 4H_2O$ was further carried out using aqueous LiOH solution as base.

Table 4.2. *Crystallographic parameters and refinement data for complex* ***4A****.*

Empirical formula	C26 H54 F3 Mn3 N4 Na O26
Formula weight	1083.54
Crystal habit, colour	Block, colourless
Crystal size, mm^3	0.30 × 0.27 × 0.20
Temperature, T(K)	293(2)
Wavelength, λ (Å)	0.71073
Crystal system	monoclinic
Space group	P 21/c
Unit cell dimensions	a = 9.3034(5) Å b = 21.4897(11) Å c = 22.3628(16) Å α = 90.00° β = 93.331(5)° γ = 90.00°
Volume, V ($Å^3$)	4463.4(5)
Z	4
Calculated density, $g \cdot cm^{-3}$	1.612
Absorption coefficient, $\mu(mm^{-1})$	0.949
F(000)	2236
θ range for data collection	2.90° to 25.00°
Limiting indices	$-11 \le h \le 11$, $-22 \le k \le 25$, $-26 \le l \le 15$
Reflection collected/unique	7781/5846[R(int)= 0.0481]
Completeness to θ	99.2% (θ = 25.00°)
Max. and min. transmission	0.760/0.827
Refinement method	'SHELXL–97(Sheldrick, 1997)'
Data/restraints/parameters	7781/0/607
Goodness–of–fit on F^2	1.064
Final R indices [I>2σ(I)]	$R1$ = 0.0667, $wR2$ = 0.1615
R indices (all data)	$R1$ = 0.0913, $wR2$ = 0.1757
Largest diff. peak and hole	1.13 and –0.59 $e \cdot Å^{-3}$

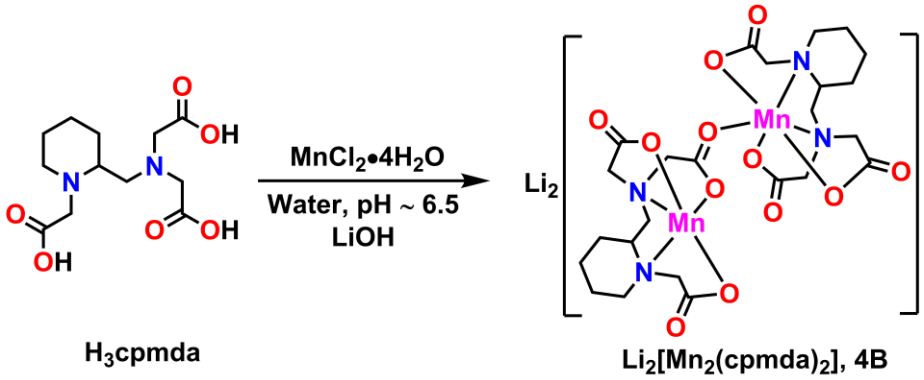

Scheme 4.2. *Synthesis of Mn(II) complex of ligand* ***H₃cpmda*** *using LiOH as base.*

1:1 molar equivalent of ligand **H₃cpmda** and $MnCl_2 \bullet 4H_2O$ were allowed to react in water at pH ~ 6.5 by adding aqueous LiOH solution dropwise, and stirred for a period of 24 h (**Scheme 4.2**). Complex **4B** was isolated as colourless crystals in 40% yield from methanol/water mixture of the filtrate by slow solvent evaporation technique.

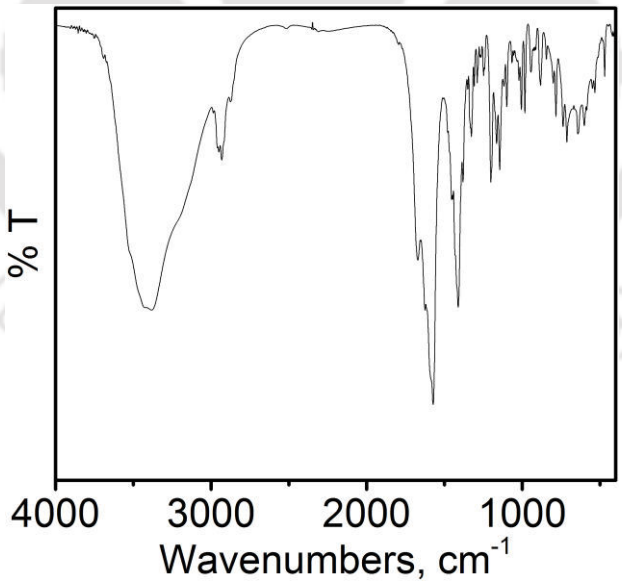

Figure 4.4. *FTIR spectrum of complex* ***4B****.*

The FTIR spectrum of complex **4B** is shown in **Figure 4.4**. In the spectrum, the band observed at 3405 cm^{-1} was due to ν(O–H) stretching.[9(a)] A sharp band was observed for ν(C=O) stretching at 1671 cm^{-1} in the complex, while it appeared at 1729 cm^{-1} for the ligand.[9(b)]

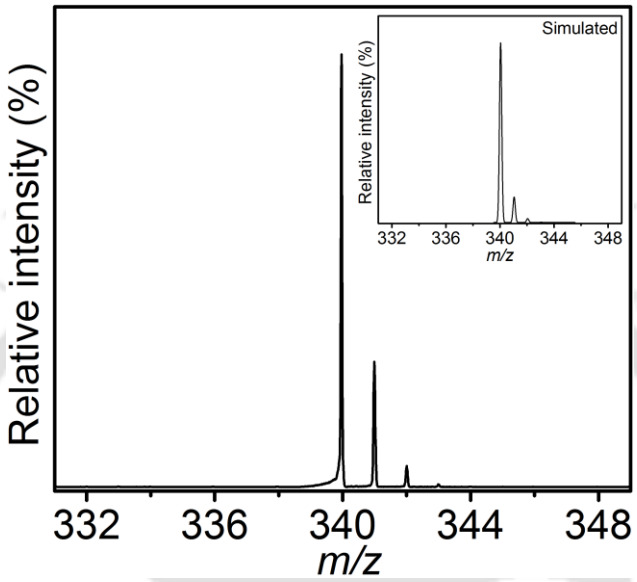

Figure 4.5. *ESI-MS (–ve) mass spectrum of aqueous solution of complex* ***4B****. Simulated spectrum has been given as inset.*

The electrospray ionization mass spectrum of aqueous solution of complex **4B** in negative mode provided a 100% molecular ion peak at *m/z* value 339.96. Examination of isotropic distribution pattern revealed that the observed peak corresponded to $C_{12}H_{17}N_2O_6Mn$ composition. Thus, mass spectrometric analysis supported the formation of the mononegative complex core.

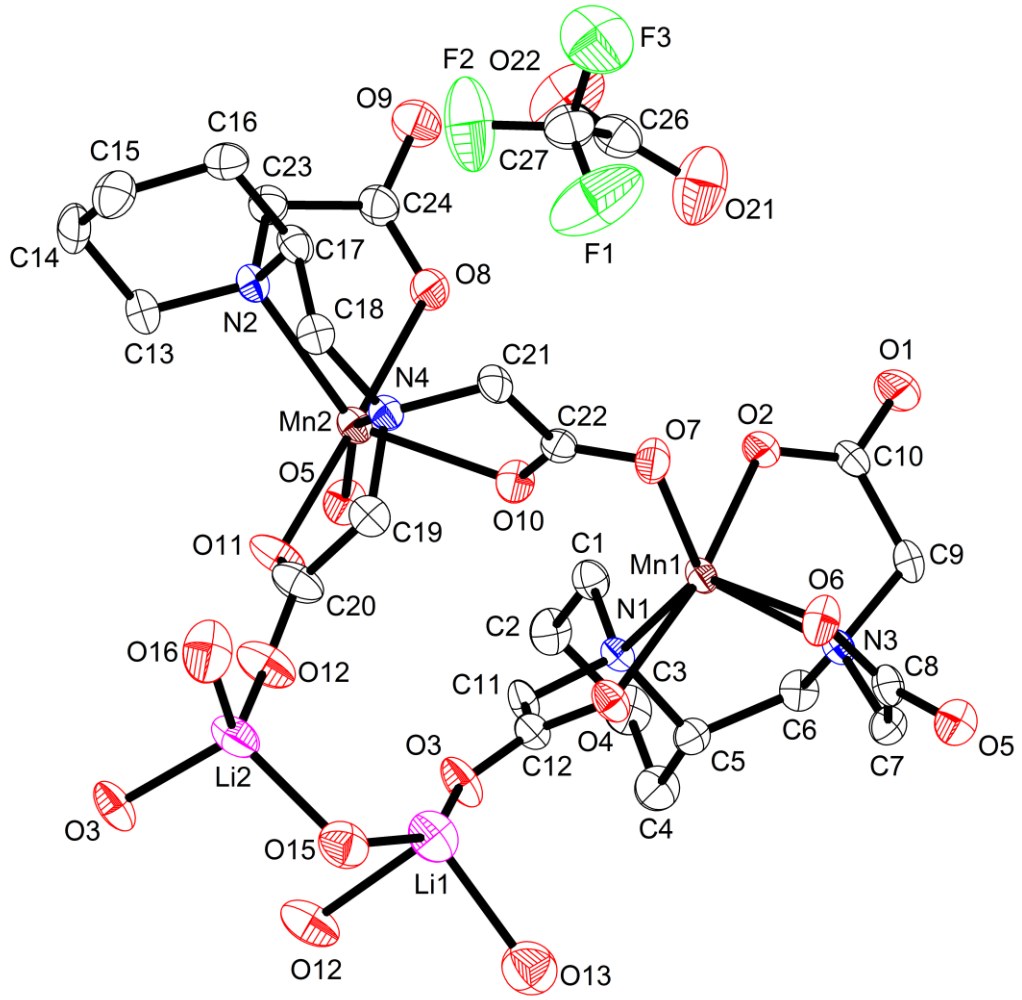

Figure 4.6. *ORTEP diagram of complex* ***4B•CF$_3$COOH•5H$_2$O****. Hydrogen atoms were omitted for clarity and thermal ellipsoids were drawn with 40% probability.*

Single crystal X-ray diffraction measurement on complex **4B** was performed. The complex crystallized in the monoclinic space group *P* 21/n. The molecular structure of complex **4B** is presented in **Figure 4.6**, and selected bond lengths and bond angles are given in **Table 4.3**. Complex **4B** was consisted of two six-coordinate Mn(II) units, which were connected by carbonyl-oxygen atom O7 (Mn2 center) and O5 (Mn1 center). However, in solution both units were separated from each other forming two mononuclear, mononegative, Mn(II) coorodination units. The fact was confirmed by the experimentally found molar conductivity (H_2O): 114.34 S cm^2 mol^{-1}.[11] The coordination environment of Mn(II) unit in complex **4B** was similar to complex

4A. In each mononuclear unit, Mn1–N1(piperidine) = 2.325, Mn1–N3(amine) = 2.317, Mn1–O2(carboxylate) = 2.181, Mn1–O4(carboxylate) = 2.190, Mn1–O6(carboxylate) = 2.226, and Mn1–O7(bridging carbonyl-oxygen) = 2.169 Å; N1–Mn1–N3 = 78.33°, N3–Mn1–O6 = 72.17°, O6–Mn1–O7 = 86.50°, O7–Mn1–N1 = 132.63°, and O2–Mn1–O4 = 166.33°; which implied the distorted octahedral geometry of the unit. Each asymmetric unit of complex **4B**, consisted of two Li(I) ions as counter cations.

Table 4.3. *Selected bond lengths (Å) and bond angles (°) for complex* ***4B***.

Mn1–O2	2.181(4)	Mn2–O5	2.134(4)
Mn1–O4	2.190(4)	Mn2–O8	2.167(4)
Mn1–O6	2.226(4)	Mn2–O10	2.234(4)
Mn1–O7	2.169(4)	Mn2–O11	2.173(4)
Mn1–N1	2.325(4)	Mn2–N2	2.348(4)
Mn1–N3	2.317(4)	Mn2–N4	2.324(4)
O2–Mn1–O4	166.33(14)	O8–Mn2–O11	176.60(16)
N3–Mn1–O6	72.17(14)	O10–Mn2–O5	92.51(14)
O6–Mn1–O7	86.50(14)	O8–Mn2–N4	103.50(15)
O7–Mn1–N1	132.63(14)	N2–Mn2–N4	77.50(14)
N1–Mn1–N3	78.33(14)	O5–Mn2–N2	124.44(15)
O2–Mn1–N3	75.30(14)	N4–Mn2–O10	72.78(14)

In the molecular structure of complex **4B**, two Li(I) ions were present outside the coordination sphere instead of Mn(II) ion. The obtained unit cell parameters of complex **4B** showed that $a \neq b \neq c$, and $\alpha = \beta = \gamma = 90°$; and the space group was monoclinic. Since, the space group was monoclinic; one of the bond angles should not be equal to 90°. But, after several measurements, the bond angles remained the same. Although, the crystallographic data of complex **4B** was compelling; it confirmed the absence of Mn(II) ion outside the coordination sphere.

Table 4.4. *Crystallographic parameters and refinement data for complex* ***4B****.*

Empirical formula	C27 H40 F3 Li2 Mn2 N4 O24
Formula weight	985.39
Crystal habit, colour	Block, colourless
Crystal size, mm^3	0.25 × 0.20 × 0.15
Temperature, T(K)	293(2)
Wavelength, λ (Å)	0.71073
Crystal system	Monoclinic
Space group	P 21/n
Unit cell dimensions	a = 9.3071(12) Å b = 20.419(3) Å c = 22.024(3) Å α = 90.00° β = 90.00° γ = 90.00°
Volume, V ($Å^3$)	4185.4(11)
Z	4
Calculated density, $g \cdot cm^{-3}$	1.564
Absorption coefficient, μ(mm^{-1})	0.707
F(000)	2020
θ range for data collection	2.95° to 25.00°
Limiting indices	$-6 \le h \le 11$, $-15 \le k \le 24$, $-26 \le l \le 22$
Reflection collected/unique	7171/ 5479[R(int)= 0.0434]
Completeness to θ	97.3% (θ = 25.00°)
Max. and min. transmission	0.844/ 0.899
Refinement method	'SHELXL–97(Sheldrick, 1997)'
Data/restraints/parameters	7781/0/607
Goodness–of–fit on F^2	1.064
Final R indices [I>2σ(I)]	R1 = 0.0717, wR2 = 0.1911
R indices (all data)	R1 = 0.0928, wR2 = 0.1755
Largest diff. peak and hole	1.02 and –0.59 $e \cdot Å^{-3}$

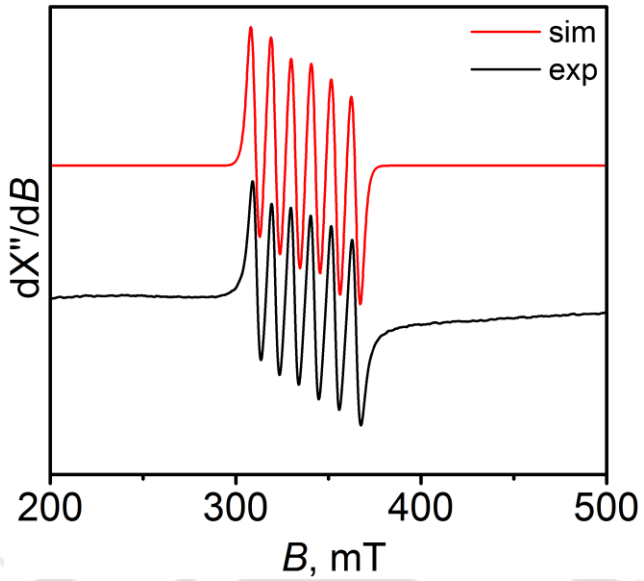

Figure 4.7. *X-band EPR spectrum (9.44 G) of complex* ***4B*** *at room temperature, power = 0.995 mW, modulation frequency = 100 kHz, and amplitude = 50 G.*

The oxidation state of the central Mn ion was investigated by X-band EPR measurement of an aqueous solution of complex **4B**, at room temperature. The experimental and simulated spectra are given in **Figure 4.7**. The appearance of six-line spectra implied the presence of hyperfine coupling with nucleus of I = 5/2. The experimental data was satisfactorily simulated using the following parameters: g_1 = 1.997, g_2 = 1.998, g_3 = 1.999, g_{av} = 1.998; ^{55}Mn (A_1, A_2, A_3) = (95, 53, 90) × 10^{-4} cm^{-1}, and A_{av} = 79 cm^{-1}. The resultant A_{av} and g_{av} values confirmed that the unpaired electrons reside on Mn ion, which was in +II oxidation state.

4.3 Thermodynamic Stability:

The accumulation of free Mn(II) ion inside living system is related to the overall thermodynamic stability of Mn(II) complexes. A disease "manganism" occurs due to damage of basal ganglia due to excess level of Mn(II) ion.[10] Therefore, high thermodynamic stability of Mn(II) complexes should be assured for *in vivo* applications.

Potentiometric titrations were carried out to determine the protonation constants of ligand **H_3cpmda**, as well as stability constant of its corresponding Mn(II) complex in 0.15 M NaCl

solution in 25 °C. The obtained protonation constants were; log K_1^H = 9.70, log K_2^H = 6.04, log K_3^H = 2.88, and log K_4^H = 1.18 respectively. The protonation constants indicated the stepwise protonation of the amine nitrogen atom, piperidine ring nitrogen atom, and carboxylate groups of the ligand. Considering the previously reported ligand framework of aazta, and its derivatives, first two protonation constants could be assigned to protonation of the amine nitrogen atom (log K_1^H= 9.70), and nitrogen atom of the piperidine ring (logK_2^H = 6.04).[12] The other two protonation constants were due to protonation of two of the acetate groups present in the ligand framework.

The stability constant of Mn(II) complex with ligand **H_3cpmda** was found to be 12.72 under the same experimental conditions used for determining the ligand protonation constants (0.15 M NaCl, and 25 °C). The most appropriate way to compare the thermodynamic stabilities of the complexes with different ligand systems is by calculating pMn values. pMn value is defined by –log$[Mn(II)]_{free}$ considering [Mn(II)] = [L] = 10^{-5} M at pH ~ 7.4. The calculated pMn value for $[Mn(cpmda)]^-$ was found to be 7.70 which was better than already reported five-coordinate ligand systems.[13] The piperidine ring present in the ligand framework imposed rigidity that was responsible for increasing stability of the complex. Three acetate arms and two N-atoms also contributed by forming five strong σ-bonding. The protonation constants, stability constants, and pMn values of some of reported pentadentate ligands are tabulated in **Table 4.5**.

Table 4.5. *Protonation constants, stability constants and pMn value of some five-coordinated ligands.*

Ligand	**log K_i^H**	**log K_{MnL}**	**pMn**
H_2no2a[13(a)]	11.82 6.70 2.87 1.02	11.56	6.23
H_2ono2a[13(a)]	10.59, 3.99, 1.83	7.43	4.62
H_4ono2p[13(a)]	12.32, 7.89, 5.44, 1.88	10.61	5.04
Hnompa[13(b)]	11.33, 7.30, 2.49	10.28	5.54
H_2nodahep[13(c)]	12.0, 5.81, 2.71	10.98	5.68
15-aneN_5[13(d)]	10.31, 9.29, 5.93	10.85	5.58
Hpydo1a[13(e)]	10.47, 8.71, 2.79	11.54	6.07
H_2pydo1p[13(e)]	11.84, 9.64, 6.23, 0.99	14.06	6.18
H_3cpmda	**9.70, 6.04, 2.88, 1.18**	**12.72**	**7.70**

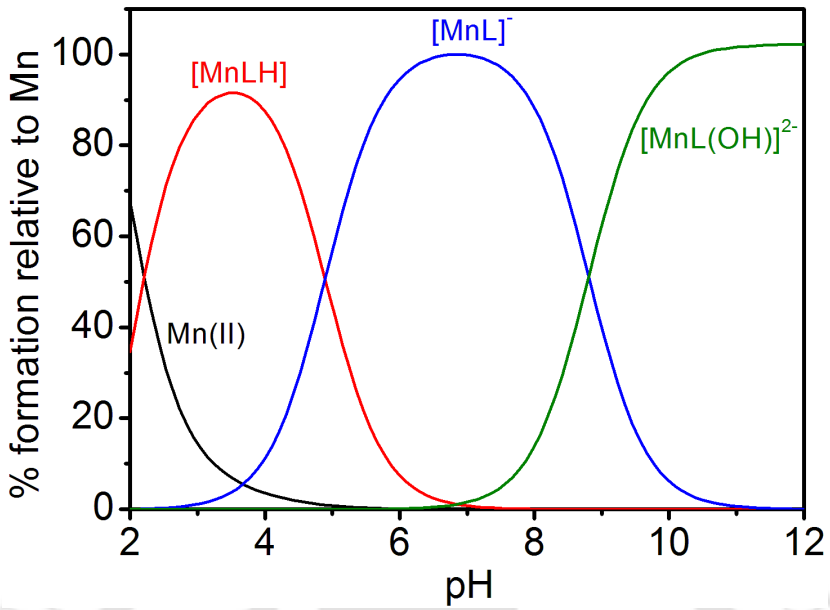

Figure 4.8. *Species distribution diagram of* ***H_3cpmda****:Mn(II) (1:1) solution, where [****H_3cpmda****] = [Mn(II)] = 1 mM (L in the figure represents* ***$cpmda^{3-}$****).*

The species distribution diagram is given in **Figure 4.8**. It was observed that complex **4B** was present as the most abundant species in the pH range ~ 5-9. Below pH ~ 5, protonated species was appearing; which was due to the protonation of one of the carboxylate groups present in the ligand framework. Above pH ~ 9, appearance of hydroxyl species indicated that either addition of hydroxyl anion or deprotonation of the coordinated water molecule took place under basic condition.

4.4 Longitudinal Relaxivity:

The efficiency of complex **4B** as a positive contrast agent was estimated from its ability to enhance the T_1-relaxation rate. Using inversion recovery method, T_1-relaxation times were measured for four different concentrations of complex **4B** in HEPES buffer at pH ~ 7.4 at 1.41 T, and 25 °C.

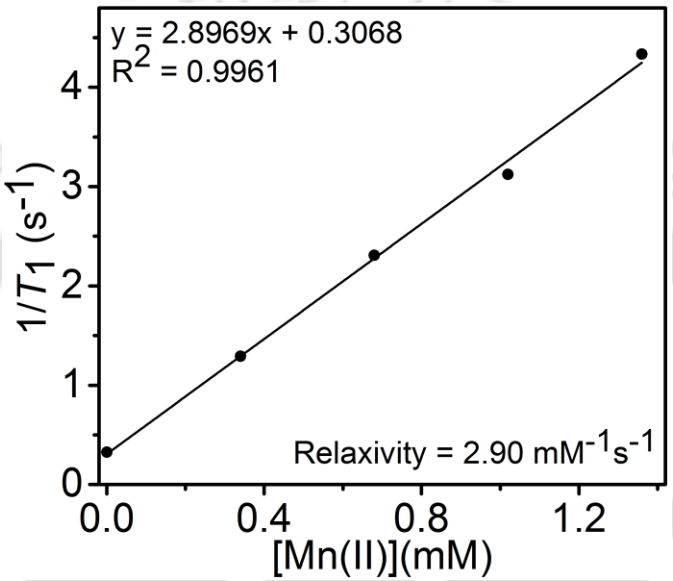

Figure 4.9. *$1/T_1$ vs [Mn(II)] plot at 1.41 T, 25 °C, and pH ~ 7.4.*

The inverse of T_1-relaxation times were plotted as the function of exact Mn(II) ion concentration (obtained from ICP-AES analysis) present in the samples. From the slope of the linear plot, the longitudinal relaxivity value obtained for complex **4B**, was 2.90 $mM^{-1}s^{-1}$ at 1.41 T, 25 °C, and pH ~ 7.4 (**Figure 4.9**). The obtained relaxivity value was found to be better than commercially used Mn(II)-based contrast agent, Teslascan® (2.8 $mM^{-1}s^{-1}$ at 0.47 T;[15(a)] 2.1 $mM^{-1}s^{-1}$ at 1.5 T).[15(b)] The longitudinal relaxivity value of complex **4B** was even better than some of mono(aquated) Mn(II) complexes; $[Mn(pyc3a)(H_2O)]^-$ (2.1 $mM^{-1}s^{-1}$ at 1.4 T, 37 °C),[4(b)] $[Mn(tmdta)(H_2O)]^-$ (2.2 $mM^{-1}s^{-1}$),[16(a)] $(aaz3a)(H_2O)]^-$ (2.49 $mM^{-1}s^{-1}$), $[Mn(meaaz3a)(H_2O)]^-$ (2.01

$mM^{-1}s^{-1}$), and $[Mn(aaz3ma)(H_2O)]^-$ (1.90 $mM^{-1}s^{-1}$) at 0.47 T, 25 °C;[12] and comparable to $[Mn(edta)(H_2O)]^-$ (3.3 $mM^{-1}s^{-1}$ at 0.47 T, 25 °C).[16(b)]

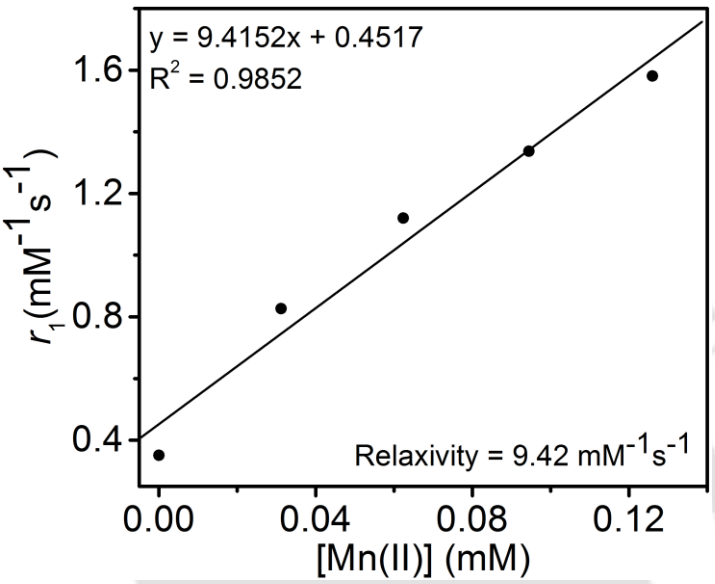

Figure 4.10. *$1/T_1$ vs [Mn(II)] plot in the presence of BSA solution at 1.41 T, 37 °C, and pH ~ 7.4.*

The binding of plasma proteins can increase the lifetime of contrast agents in vascular system. It is also accompanied by enhancement in relaxivity value due to increase in rotational correlation time because of binding with slow rotating plasma proteins.[17] The interaction with plasma protein was investigated by measuring the longitudinal relaxation times of complex **4B** in the presence of Bovine serum albumin (BSA) at physiological concentration (4.5% w/v, 0.66 mM). At 1.41 T, pH ~ 7.4, and 37 °C, longitudinal relaxation times of four different concentrations of complex **4B** were measured in the presence of 0.66 mM BSA solution. The slope of $1/T_1$ *vs* exact Mn(II) ion concentration (obtained from ICP-AES analysis) provided relaxivity value of 9.42 $mM^{-1}s^{-1}$ (**Figure 4.10**). A significant enhancement in relaxivity value was observed in the presence of BSA solution with respect to r_1 = 2.90 $mM^{-1}s^{-1}$ in HEPES buffer. The percentage of complex **4B** bound to BSA was determined by ultrafiltration technique using 5 kDa cut off membrane followed by quantification of Mn(II) ion by ICP-AES analysis. It

was found that 75% of complex **4B** bound to BSA. The enhancement in relaxivity value in the presence of BSA solution for complex **4B** was due to macromolecular association.

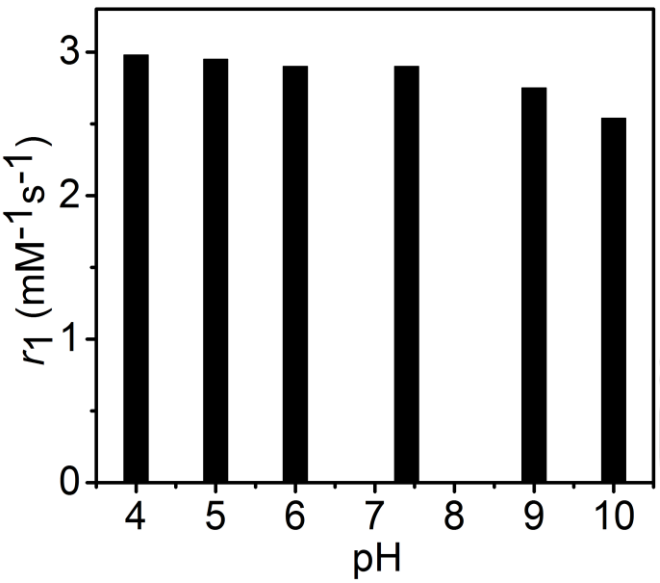

Figure 4.11. *r_1 relaxivity changes in the pH range 4-10; at 1.41 T and 25 °C.*

In order to verify the presence of variable equilibrium states of complex **4B** in solution, longitudinal relaxivity value of the complex was measured in a pH range of 4-10 at 1.41 T, and 25 °C. The observed relaxivity values are plotted as bar diagram in **Figure 4.11**. The r_1 values remained consistent in the pH range of 5-9; implying the presence of complex **4B** most abundantly in this pH range. However, above pH ~ 9, r_1 value seemed to be dropping slightly, and attained r_1 value of 2.54 $mM^{-1}s^{-1}$ (Δr_1 ~ -12.4%). This reduction in r_1 value could be related to the formation of hydroxyl species, which were also observed in species distribution diagram (**Figure 4.9**).

4.5 Affinity for Physiological Anions:

Physiological anions, including bicarbonate (HCO_3^-), biphosphate (HPO_4^{2-}), fluoride (F^-), are present in non-negligible concentrations (from 25 mM to 0.38 mM) in human blood plasma.[18] These anions might interact with the complex, and could lower relaxivity value by permanently replacing the coordinated water molecule.[19] To investigate the affinity of complex **4B** towards these anions, longitudinal relaxivity value of complex **4B** (0.50 mM) were measured in the presence of 200 equivalents of these anions ([HCO_3^-] = [HPO_4^{2-}] = [F^-] = 100 mM) at 1.41 T, pH ~ 7.4, and 25 °C.

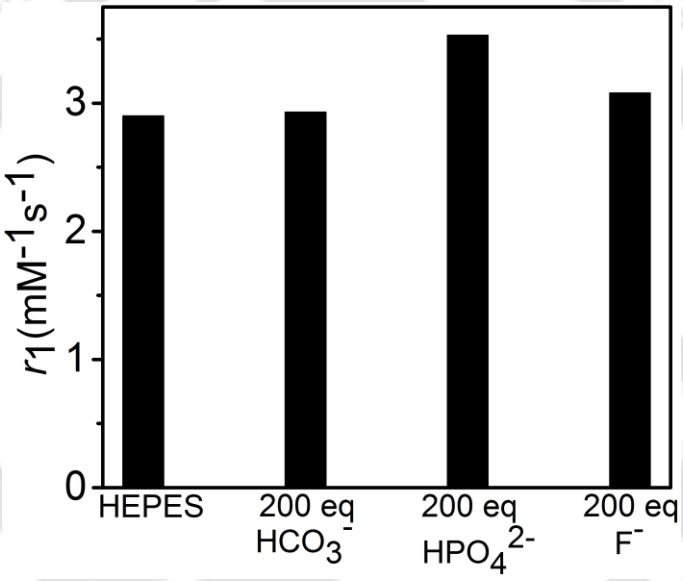

Figure 4.12. *Variation of relaxivity in the presence of 200 equivalents of physiological anions at 1.41 T, 25 °C, pH ~7.4; [complex **4B**] = 0.5 mM and [physiological anions] = 100 mM.*

The results obtained were shown as bar diagram in **Figure 4.12**. No appreciable changes were noticeable for HCO_3^- and F^- anions; which was due to low positive charge on Mn ion (+II), and overall negative charge of complex **4B**, which exerted some repelling force for these anions.[18,19(c)]

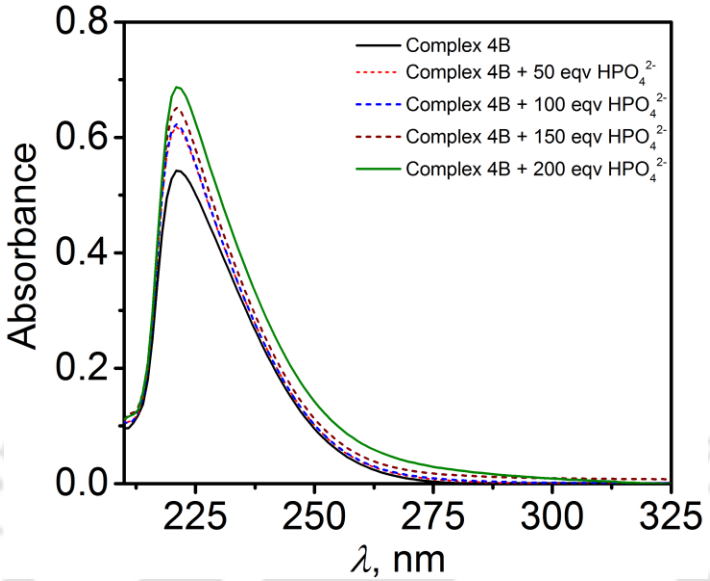

Figure 4.13. *Changes in UV-Vis spectra of complex **4B** in the presence of various equivalents of HPO_4^{2-} anion at 25 °C and pH ~ 7.4.*

However, slight rise in r_1 value (3.53 $mM^{-1}s^{-1}$, 17.8%) was observed for HPO_4^{2-} anion. The most evident reasons could be either release of free Mn(II) ion from the complex or due to formation of aggregation.[20] The dissociation of complex **4B** could take place forming Mn(II) aqua ion due to interaction of ligand and HPO_4^{2-} anion.[21] To investigate this probability, UV-Vis spectra of complex **4B** were recorded in the presence of various equivalents of HPO_4^{2} anion. No appreciable changes were noticeable in UV-Vis spectra even in the presence of 200 equivalents of HPO_4^{2-} anion (**Figure 4.13**). Hence, dissociation of complex **4B** forming free aqua Mn(II) ion was discarded. Thus, increase in relaxivity value might be due to formation of slowly rotating aggregation. The possibility of formation of anion-bridged dimers or small oligomers with second sphere relaxivity contribution also cannot be ignored.[20]

4.6 Phantom MR Imaging:

The potential of complex **4B** as brightening contrast agent was evaluated by acquiring T_1-weighted MR phantom images at 1.5 T, under a clinical MAGNETOM Avanto MRI scanner. The phantoms considered were micro-centrifuge tubes containing different concentrations of complex **4B** in HEPES buffer maintaining pH ~ 7.4.

The aqueous solutions of complex **4B** in four different concentrations (0.25 mM, 0.50 mM, 0.70 mM, and 1.00 mM) were prepared in HEPES buffer maintaining pH at ~ 7.4. The images were acquired at TR = 468 ms, TE = 8.2 ms, pH ~ 7.4, and 25 °C at 1.5 T. The brightness of images was observed to be increased with increase in concentration of complex **4B**. The contrast efficiency of complex **4B** was further compared with clinically used contrast agent MultiHance®. For that clinically used MultiHance® was diluted to 1 mM concentration in HEPES buffer and measured under same experimental conditions. The observed images under the clinical imager are presented in **Figure 4.14**.

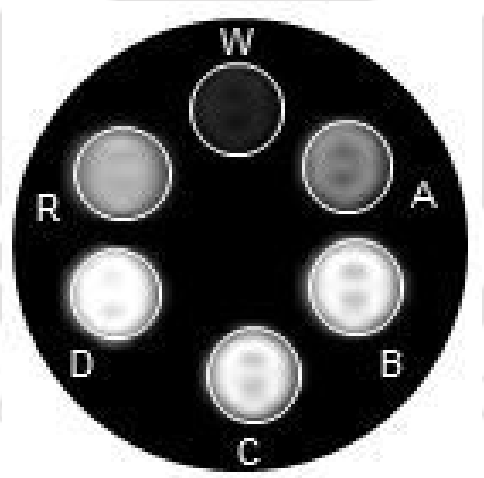

Figure 4.14. *T_1-weighted phantom images of micro-centrifuge tubes with different concentrations of complex **4B**(considering molecular weight of the whole complex) in HEPES buffer (W = water, A = 0.25 mM, B = 0.50 mM, C = 0.70 mM, and D = 1.00 mM) at 1.5 T, 25 °C, pH ~ 7.4, TR = 468 ms, and TE = 8.2 ms; R stands for the reference MultiHance® in 1 mM concentration.*

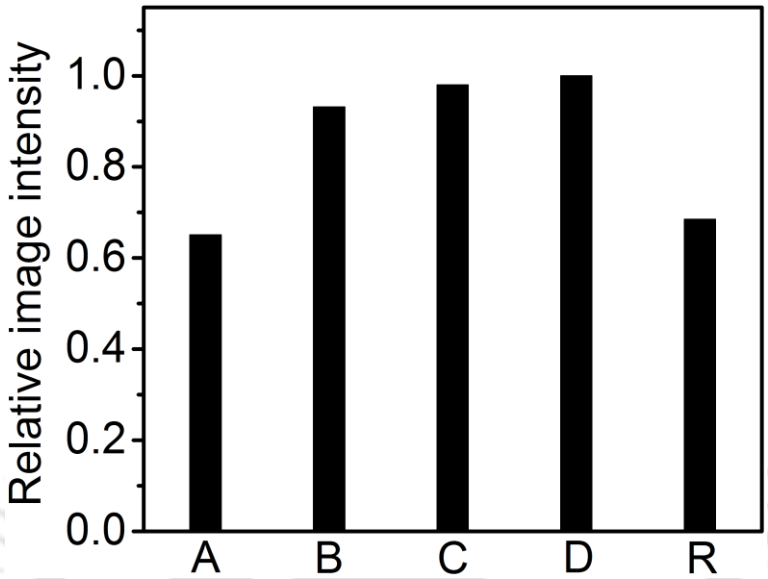

Figure 4.15. *Relative image intensity plot using ImageJ Software.*

The image intensity of acquired images was further compared by using ImageJ software considering same area for all of the images. The relative image intensity is plotted as bar diagram in **Figure 4.15**. From the image intensity plot, it was confirmed that brightness of images were getting increased with increase in concentration of complex **4B**.

4.7 Conclusion:

- Mono(aquated) Mn(II) complexes **4A** and **4B**, have been synthesized with lipophilic pentadentate ligand **H_3cpmda** using aqueous solutions of NaOH and LiOH as base respectively. The coordination environment of both of the complexes were similar, except complex **4A** possessed Mn(II) and Na(I) ions as counter cations, while complex **4B** possessed two Li(I) ions. To overcome the release of free Mn(II) ion by complex **4A** in solution state, complex **4B** was synthesized. In this chapter, complex **4B** was studied as T_1-weighted contrast agent.

- The complex offered impressive thermodynamic stability (pMn = 7.70) under physiological condition which was found to be better than already reported Mn(II) complexes with five coordinate ligand frameworks with one coordinated-water molecule.

- Complex **4B** showed longitudinal relaxivity value of 2.90 $mM^{-1}s^{-1}$ at 1.41 T, pH ~ 7.4, and 25 °C. The value increased to 9.42 $mM^{-1}s^{-1}$ at 1.41 T, pH ~ 7.4, and 37 °C in the presence of BSA solution. The relaxivity value was found to be consistent in a wide pH range.

- The complex stability remained unaffected in the presence of physiologically available anions.

- Under clinical imager at 1.5 T, phantom MR imaging assured the contrast efficiency of complex **4B**, established it as a potential brightening agent.

References

1. (*a*) T. Yamane, K. Hanaoka, Y. Muramatsu, K. Tamura and Y. Adachi, *Bioconjugate Chem*., 2011, **22**, 2227; (*b*) M. J. Allen and T. J. Meade, *J. Biol. Inorg. Chem.,* 2003, **8**, 746; (*c*) M. J. Allen, K. W. MacRenaris, P.N. Venkatasubramanian and T. J. Meade, *Chem. Biol*., 2004, **11**, 301.

2. (*a*) S. Aime and P. Caravan, *J. Mag. Reson. Imaging*, 2009, **30**, 1259; (*b*) H. J. Weimann, M. Laniado and W. Mutzel, *Physiol. Chem. Phys. Med. NMR*, 1984, **16**, 167; (*c*) M. F. Tweedle, S. M. Eaton, W. C. Eckelman, W. C. *et al*., *Invest. Radiol*., 1988, **23**, S236.

3. (*a*) B. Tombach, C. Bremer and P. Reimer, *et al*., *Invest. Radiol.,* 2000, **35**, 35; (*b*) G. Schuhmann-Giampieri and G. Krestin, *Invest. Radiol*., 1991, **26**, 975; (*c*) P. Joffe, H. S. Thomsen and M. Meusel, *Acad. Radiol.,* 1998, **5**, 491.

4. (*a*) G. Sechuhmsnn-Giampierri, H. Schitt-Willich and T. Frenzel, *J. Pharm. Sci*., 1993, **82**, 799; (*b*) E. M. Gale, I. P. Atanasova, F. Blasi, I. Ay and P. Caravan, *J. Am. Chem. Soc*., 2015, **137**, 15548.

5. (*a*) P. Martins, J. Jesus, S. Santos, L. R. Raposo, C. Roma-Rodrigues, P. V. Baptista and A. R. Fernandes, *Molecules*, 2015, **20**, 16852; (*b*) E. Vitaku, D. T. Smith and J. T. Njardarson, *J. Med. Chem*., 2014, **57**, 10257.

6. (*a*) H. Chong, K. Garmestani, L. H. Bryant, Jr., D. E. Milenic, T. Overstreet, N. Birch, T. Le, E. D. Brady and M. W. Brechbiel, *J. Med. Chem*., 2006, **49**, 2055; (*b*) H. Chong, K. Garmestani, L. H. Bryant, Jr. and M. W. Brechbiel, *J. Org. Chem*., 2001, **66**, 7745.

7. (*a*) M. N. Ponnuswamy, M. M. Gromiha, S. M. M. Sony and K. Saraboj, *Top Heterocycl. Chem*., 2006, **3**, 81; (*b*) J. B. Lambert, *J. Am. Chem. Soc*., 1967, **89**, 1836.

8. (*a*) H. Su, C. Wu, J. Zhu, T. Miao, D. Wang, C. Xia, X. Zhao, Q. Gong, B. Song and H. Ai, *Dalton Trans*., 2012, **41**, 14480; (*b*) R. S. Ranganathan, N. Raju, H. Fan, X. Zhang, M. F. Tweedle, J. F. Desreux and V. Jacques, *Inorg. Chem*., 2002, **41**, 6856; (*c*) M. Port, I. Raynal, L. V. Elst, R. N. Muller, F. Dioury, C. Ferroud and A. Guy, *Contrast Media*

Mol. Imaging, 2006, **1**, 121; (*d*) P. Caravan, *Chem. Soc. Rev*., 2006, **35**, 512; (*e*) F. Dioury, C. Ferroud, A. Guy and M. Port, *Tetrahedron*, 2009, **65**, 7573.

9. (*a*) J. Wang, G. R. Gao, Z. H. Zhang, X. D. Zhang, X. Z. Liu, Y. M. Kong and Y. Li, *Russ. J. Coord. Chem*., 2007, **33**, 258; (*b*) B. C. Smith, *Infrared Spectral Interpretation: A Systematic Approach*, CRC press, 1998.

10. (*a*) R. G. Lucchini, C. J. Martin and B. C. Doney, *Neuromol. Med*., 2009, **11**, 311; (*b*) J. Crossgrove and W. Zheng, *NMR Biomed*., 2004, **17**, 544.

11. W. J. Greay, *Coord. Chem. Rev*., 1971, **7**, 81.

12. L. Tei, G. Gugliotta, M. Fekete, F. K. Kálmán and M. Botta, *Dalton Trans*., 2011, **40**, 2025.

13. (*a*) B. Drahŏs, M. Pniok, J. Havĺickov´a, J. Kotek, I. C´ısaˇrov´a, P. Hermann, I. Lukeš and É Tóth, *Dalton Trans*., 2011, **40**, 10131; (*b*) E. Molnár, N. Camus, V. Patinec, G. A. Rolla, M. Botta, G. Tircsó, F. K. Kálmán, T. Fodor, R. Tripier and C. Platas-Iglesias, *Inorg. Chem*., 2014, **53**, 5136; (*c*) A. de Sá, C. S. Bonnet, C. F. G. C. Geraldes, É. Tóth, P. M. T. Ferreira and J. P. André, *Dalton Trans*., 2013, **42**, 4522; (*d*) B. Drahoš, J. Kotek, P. Hermann, I. Lukeš and É. Tóth, *Inorg. Chem*., 2010, **49**, 3224; (e) B. Drahoš, J. Kotek, I. Císařová, P. Hermann, L. Helm, I. Lukeš and É. Tóth, *Inorg. Chem*., 2011, **50**, 12785.

14. (*a*) N. Nestle, S. Pauls and A. Wunderlich, *Magn. Reson. Med*., 2006, **55**, 923; (*b*) M. Zarrini, F. S. Toosi, B. Davachi and S. Nekooei, *Rev. Clin. Med.*, 2015, **2**, 200.

15. (*a*) S. Gallo, N. Vasimalai, M. T. Fernandez-Arguelles and M. Bañbore-López, *Dalton Trans*., 2016, **45**, 17672; (*b*) H. Su, C. Wu, J. Zhu, T. Miao, D. Wang, C. Xia, X. Zhao, Q. Gong, B. Song and H. Ai, *Dalton Trans*., 2012, **41**, 14480.

16. (*a*) F. K. Kálmán and G. Tircsó, *Inorg. Chem*., 2012, **51**, 10065; (*b*) A. Forgács, R. Pujales-Paradela, M. Regueiro-Figueroa, L. Valencia, D. Esteban-Gómez, M. Botta and C. Platas-Iglesias, *Dalton Trans*., 2017, **46**, 1546.

17. (*a*) J. S. Troughton, M. T. Greenfield, J. M. Greenwood, S. Dumas, A. J. Wiethoff, J. Wang, M. Spiller, T. J. McMurry and P. Caravan, *Inorg. Chem*., 2004, **43**, 6313; (*b*) S. Aime, L. Anelli, M. Botta, M. Brocchetta, S. Canton, F. Fedeli, E. Gianolio and E. Terreno, *J. Biol. Inorg Chem.,* 2002, **7**, 58.

18. V. C. Pierre, M. Botta, S. Aime and K. N. Raymond, *Inorg. Chem*., 2006, **45**, 8355.

19. (*a*) R. S. Dickins, S. Aime, A. S. Batsanov, A. Beeby, M. Botta, J. Bruce, J. A. K. Howard, C. S. Love, D. Parker, R. D. Peacock and H. Puschmann, *J. Am. Chem. Soc*., 2002, **124**, 12697; (*b*) S. Aime, M. Botta, J. I. Bruce, V. Mainero, D. Parker and E. Terreno, *Chem. Commun.*, **2001**, 115; (*c*) J. I. Bruce, R. S. Dickins, L. J. Govenlock, T. Gunnlaugsson, S. Lopinski, M. P. Lowe, D. Parker, R. D. Peacock, J. J. B. Perry, S. Aime and M. Botta, *J. Am. Chem. Soc*., 2000, **122**, 9674.

20. B. Drahŏs, J. Kotek, P. Hermann, I. Lukeš and É. Tóth, *Inorg. Chem*., 2010, **49**, 3224.

21. S. Develay, R. Tripier, M. Le Baccon, V. Patinec, G. Serratrice and H. Handel, *Dalton Trans*., 2005, 3016.

Chapter V

A Stable Mono(aquated) Mn(II) Complex as T_1-weighted MRI Contrast Agent

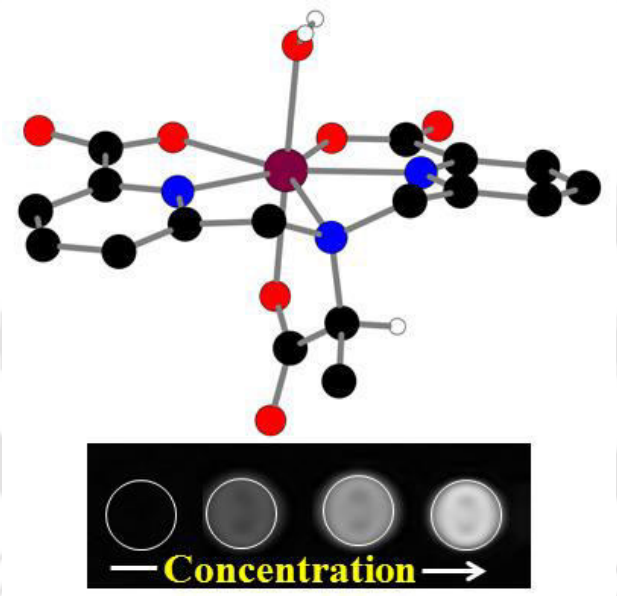

*Some results have been published in *Dalton Trans*., 2017, **46**, 10426–10432.

5.1 Introduction:

In search of less toxic and bio-friendly MRI contrast agents, Mn(II) ion has attained special attention for the development of a new class of potent contrast agents.[1] In order to ensure *in vivo* stability, and high contrast efficiency, Mn(II) ion is needed to be encapsulated with suitable ligand framework leaving at least one site available for binding with one water molecule. Recent experimental results suggest that rigid ligand frameworks can increase the thermodynamic stability of its corresponding metal-complexes.[2]

L-alanine is one of naturally available amino acids. A composition of $MnCl_2 \bullet 4H_2O$, L-alanine, and vitamin-D_3; known as CMC-001 is undergoing clinical trial as brightening agent.[3] It is tried for increasing the contrast between liver parenchyma, and focal liver lesions. In this context, ligand **Li_3cbda** was designed with L-alanine backbone, such that less toxic contrast agent could be obtained with this ligand framework. In this chapter, complexation of ligand **Li_3cbda** was carried out with Mn(II) ion. In the ligand framework, two picolinate moieties substituted two amine N-atoms of L-alanine. The incorporation of pyridine ring would increase the stability of the complex *via* metal-to-ligand back donation. In addition to that, three carboxylate O-atoms, one amine N-atom, two pyridine N-atoms would form six strong σ-bonds with Mn(II) ion, and also contributed to stability of the Mn(II) complex. The presence of chiral methyl group of L-alanine backbone, and two pyridine moieties would introduce some amount of structural rigidity, which could also stabilize the complex. Due to hexadentate nature of ligand framework, there would be possibility of binding one water molecule directly to Mn(II) ion.

5.2 Synthesis and Characterization of Mn(II) Complex of Ligand Li_3cbda:

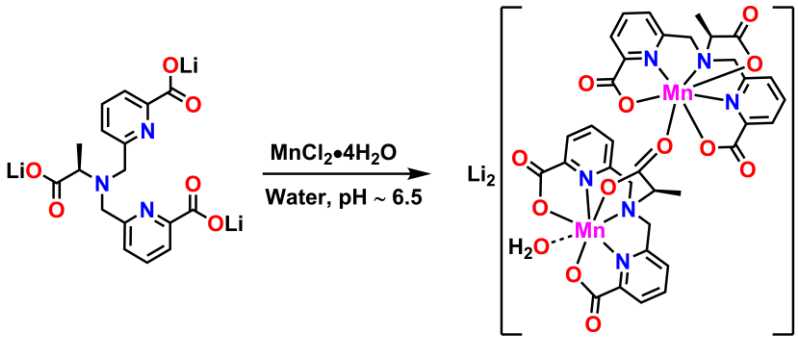

Scheme 5.1. *Synthesis of Mn(II) complex of ligand* ***Li_3cbda****.*

Complex **5A** was synthesized by reacting equivalent amount of ligand **Li_3cbda** and $MnCl_2 \bullet 4H_2O$ in water, followed by the adjustment of pH at ~ 6.5 by adding aqueous NaOH (**Scheme 5.1**). Using slow solvent evaporation technique, complex **5A** was isolated as yellow crystals in 34% yield.

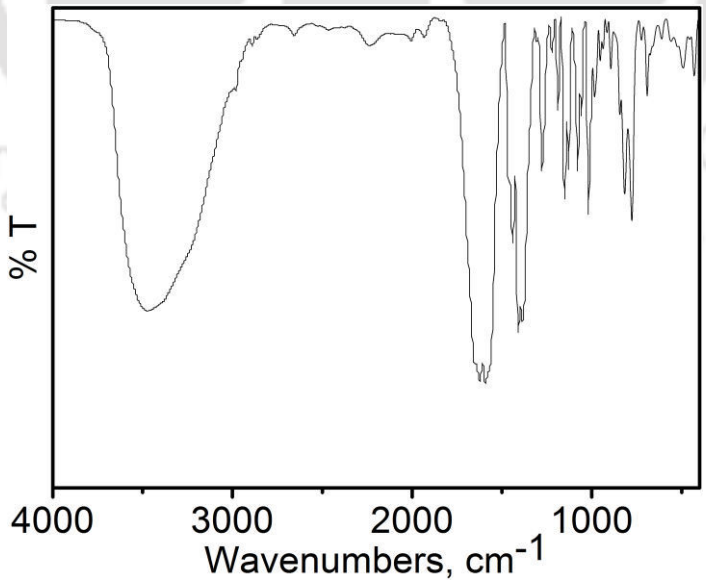

Figure 5.1. *FTIR spectrum of complex* ***5A****.*

The FTIR spectrum of complex **5A** is given in **Figure 5.1**. The broad band appeared at 3476 cm^{-1} was due to ν(O–H) stretching of coordinated-water molecule.[4] The band appeared at 1622 cm^{-1} was due to ν(C=O) stretching; which was found to be shifted from 1618 cm^{-1} in the ligand.

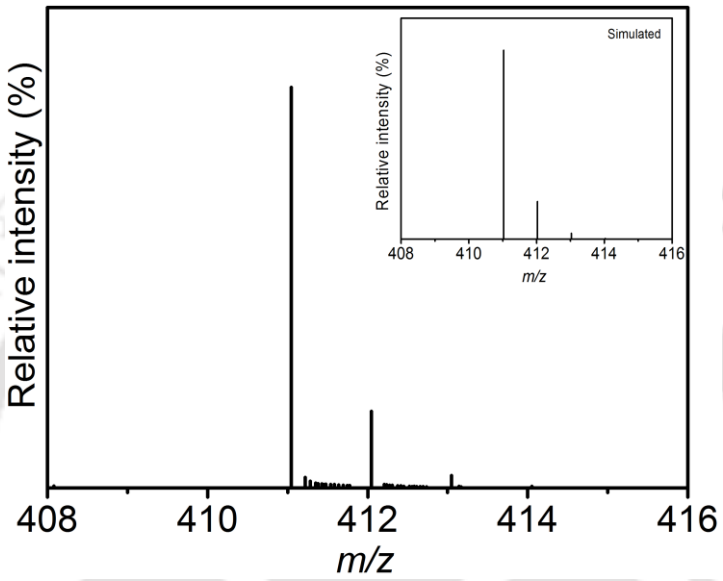

Figure 5.2. *ESI-MS (–ve) mass spectrum of aqueous solution of complex **5A**. Simulated spectrum has been given as inset.*

The electrospray ionization mass spectrum of complex **5A** in water provided a 100% molecular ion peak at *m/z* value of 411.04 in negative mode. This peak was appearing due to formation of $[C_{17}H_{14}N_3O_6Mn]^-$ (*m/z* = 411.02); and it was also confirmed by the isotropic distribution pattern (**Figure 5.2**). The simulated spectrum is also presented in the inset. It implied that complex **5A** dissociated to two monomeric units in aqueous solution forming two seven coordinate Mn(II) units with one coordinated-water molecule.

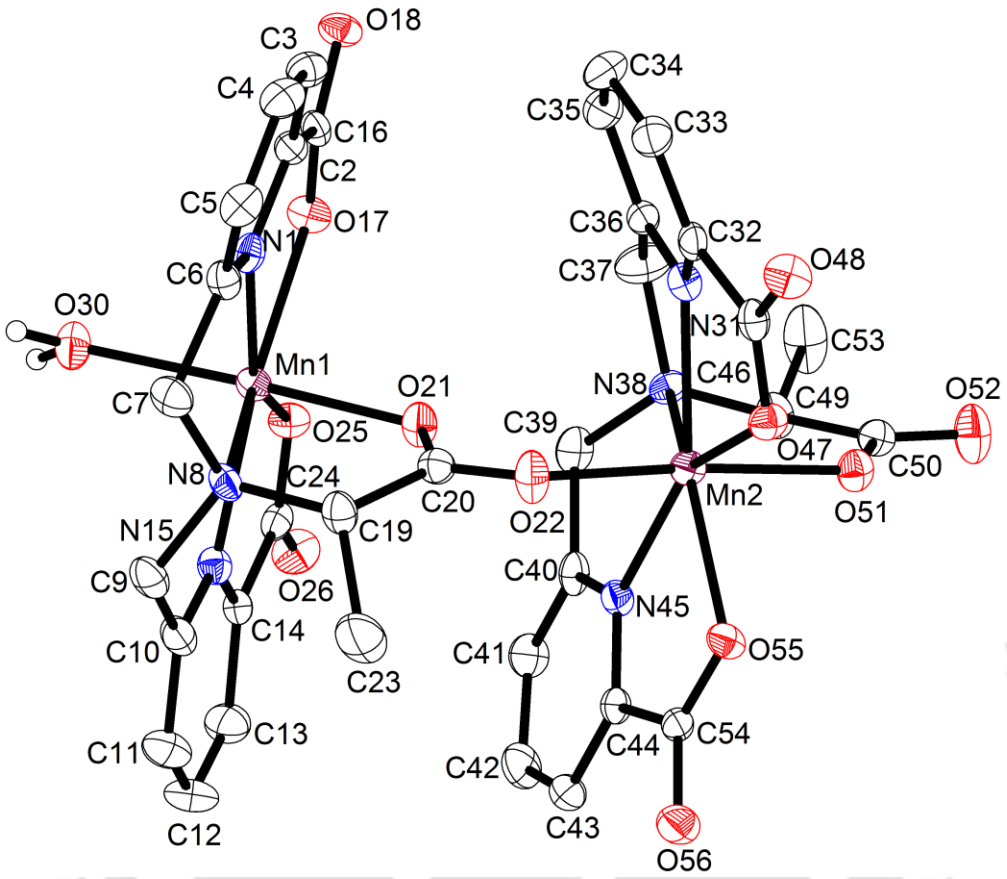

Figure 5.3. *ORTEP diagram of dianionic form of complex **5A**. Hydrogen atoms were omitted for clarity and thermal ellipsoids were drawn with 40% probability.*

Single-crystal X-ray diffraction measurements were carried out at 293(2) K to determine the molecular structure of complex **5A**. The complex crystallized in the triclinic space group *P*1. The structure of the dianionic unit of the complex is given in Figure **5.3**, and the selected bond lengths and bond angles are given in **Table 5.1**.

The dianionic unit of complex **5A** consisted of two seven-coordinate Mn(II)-coordination units, which were connected by carbonyl-oxygen atom O22. In each pentagonal bipyramidal Mn(II)-coordination unit, the basal plane was consisted of one alanine N-atom, two pyridine N-atoms, and two picolinic carboxylate O-atoms. The axial positions were occupied by an alanine-carboxylate O-atom, and an O atom either of the coordinated water molecule O30 (Mn1 center)

or the bridging O22 (Mn2 center). The axial O21–Mn1–O30 and O22–Mn2–O51 units were almost along the straight lines with an average angle of ~ 171° in each unit (**Table 5.1**). The Mn–N(pyridine) = 2.200–2.243, Mn–N(alanine) = 2.506–2.520, Mn–O(alanine-carboxylate) = 2.154–2.173, and Mn–O(picolinic-carboxylate) = 2.231–2.296 Å; bond lengths were in accordance with those of the previously reported similar Mn(II) complexes.[5] In complex **5A**, two Li(I) ions were present as counter cations. Both the ions were coordinated to picolinic-carboxylate O-atoms and because of the coordination, a considerable difference was observed in the Mn–O (picolinic-carboxylate) bond length (**Table 5.1**).

Table 5.1. *Selected bond distances (Å) and bond angles (°) for complex* ***5A.***

Mn1–O17	2.281(5)	Mn2–O22	2.192(5)
Mn1–O25	2.231(5)	Mn2–O51	2.173(5)
Mn1–O21	2.154(4)	Mn2–O47	2.296(4)
Mn1–O30	2.232(5)	Mn2–O55	2.278(4)
Mn1–N1	2.243(5)	Mn2–N38	2.520(5)
Mn1–N15	2.226(6)	Mn2–N31	2.200(6)
Mn1–N8	2.506(6)	Mn2–N45	2.215(5)
N15–Mn1–O25	72.09(18)	O51–Mn2–O22	171.06(2)
O21–Mn1–O30	170.8(2)	N45–Mn2–O55	72.60(17)
O25–Mn1–O17	75.13(17)	N31–Mn2–O47	73.08(17)
N1–Mn1–O17	71.58(18)	O55–Mn2–O47	77.31(16)

Although the solid-state structure of the complex **5A** comprised two mononuclear units; in solution the two units separated from each other and resulted in two mononuclear, mononegative, Mn(II)-coordination units. The formation of the mononegative, mononuclear unit was confirmed by ESI-MS (−ve) analysis, and conductivity measurements; Molar conductivity (H_2O): 148.95 S cm^2 mol^{-1}.[6]

Table 5.2. *Crystallographic data of complex* ***5A***.

Empirical formula	C34 H42 Li2 Mn2 N6 O19
Formula weight	962.49
Crystal habit, colour	Block, yellow
Crystal size, mm^3	0.30 × 0.25 × 0.15
Temperature, T	293(2)
Wavelength, λ (Å)	0.71073
Space group	$P1$
Unit cell dimensions	a = 10.8880(6) Å
	b = 13.0650(12) Å
	C = 15.9220(12) Å
	α = 71.613(7)°
	β = 73.658(6)°
	γ = 79.514(6)°
Volume, V ($Å^3$)	2051.6(3)
Z	2
Calculated density, $g \cdot cm^{-3}$	1.558
Absorption coefficient, μ (mm^{-1})	0.702
F(000)	992
θ range for data collection	3.023 to 27.498°
Limiting indices	$-14 \le h \le 13$, $-16 \le k \le 16$,
	$-20 \le l \le 14$
Reflection collected/unique	16557/11501[R(int)= 0.0381]
Completeness to θ	99.8% (θ = 25.00°)
Max. and min. transmission	0.900/0.810
Refinement method	Full-matrix least-squares on F^2
Data/restraints/parameters	11501/27/1211
Goodness–of–fit on F^2	1.027
Final R indices [$I>2\sigma(I)$]	$R1$ = 0.0381, $wR2$ = 0.0815
R indices (all data)	$R1$ = 0.0487, $wR2$ = 0.0900
Largest diff. peak and hole	0.267 and -0.293 e.$Å^{-3}$

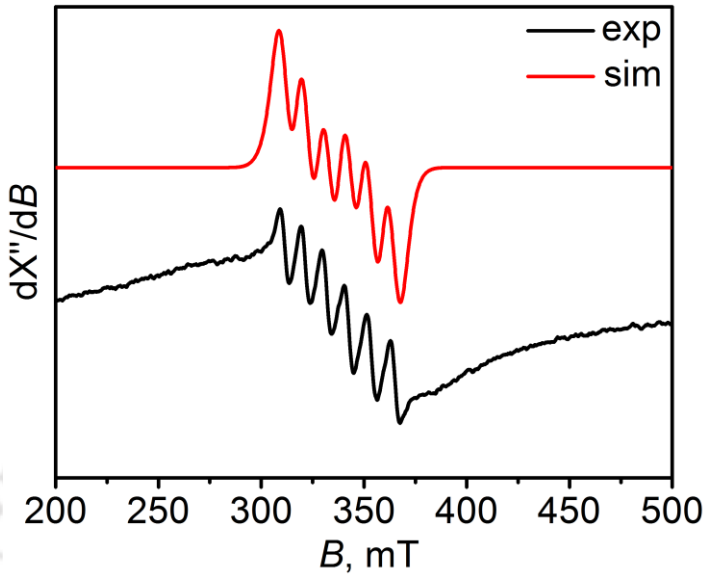

Figure 5.4. *X-band EPR spectrum (9.44 GHz) of complex* ***5A*** *measured at room temperature, power = 0.995 mW, modulation frequency = 100 kHz, and amplitude = 200 G.*

The oxidation state of central Mn ion was determined from X-band EPR measurement of the aqueous solution of complex **5A** at room temperature. The experimental as well as simulated spectra are shown in **Figure 5.4**. A six-line spectrum appeared as anticipated for the nucleus with I = 5/2 (Mn). The experimental spectrum was further simulated using the following parameters: g_1 = 1.994, g_2 = 1.997, g_3 = 2.000, g_{av} = 1.997; ^{55}Mn(A_x, A_y, A_z) = (90, 54, 93) × 10^{-4} cm^{-1}, and A_{av} = 79. The A_{av} and g_{av} values clearly indicated that the unpaired electrons resided at the Mn center, which was in +II oxidation state.

5.3 Thermodynamic Stability:

Before *in vivo* application, high thermodynamic stability of the complex is needed to be ensured. At first, stepwise protonation constant of ligand **Li_3cbda** and stability of complex **5A** was assessed by pH-potentiometric titration in a constant ionic strength of 0.15 M NaCl, 25 °C. The calculated protonation constant values obtained from the titration were; log K_1^H = 8.10, log K_2^H = 2.97, and log K_3^H = 2.35. Among them first protonation constant; log K_1^H = 8.10, has been assigned to the protonation of nitrogen atom present in amine group of the ligand; and the value

was in accordance with the previously reported similar ligand systems.[7] The other two protonation constants were attributed to the protonation of two picolinate carboxylate groups.

By pH-potentiometric titration of ligand **Li_3cbda** with Mn(II) ion in 1:1 molar equivalent under same experimental condition provided stability constant for complex **5A** as 11.90. To obtain a better comparison of stability of any complex formed with various ligands, pMn value was calculated for the ligand. The pMn value was given by $-\log[Mn(II)]_{free}$, at a particular condition of constant pH ~ 7.4, 25 °C, with [Mn(II)] = [L] = 10^{-5} M.[8] The calculated pMn value for $[Mn(cbda)]^-$ was found to be 8.06. The observed value for complex **5A** was comparable to already reported analogous mono(aquated) Mn(II) complexes. The protonation constants, stability constants and pMn values of some of reported hexadentate ligands were tabulated in **Table 5.3**.

Table 5.3. *Protonation constants, stability constants and pMn value of some six-coordinated ligands.*

Ligand	**log K_i^H**	**log K_{MnL}**	**pMn**
H_4edta[7(b)]	10.17, 6.11, 2.68	13.88	7.95
H_3dpaaa[7(b)]	7.26, 3.90, 3.29, 1.77	13.19	8.98
H_4cdta[9(a)]	9.36, 5.95, 3.62, 2.57	14.32	8.67
H_3pyc3a[9(a)]	10.16, 6.39, 3.13	14.14	8.17
H_3aaz3a[9(b)]	10.24, 5.78, 3.67, 2.18	11.00	6.57
Li_3cbda	**8.10, 2.97, 2.35**	**11.90**	**8.06**

The species distribution diagram is presented in **Figure 5.5**. It depicted that complex $[Mn(cbda)]^-$ was present as the most prominent species in a wide pH range of 4-8. Below, pH ~ 4, protonated species were started appearing. Hydroxyl species were appeared at pH > 8; which was forming either due to the addition of hydroxyl anion or due to deprotonation of the coordinated water molecule.

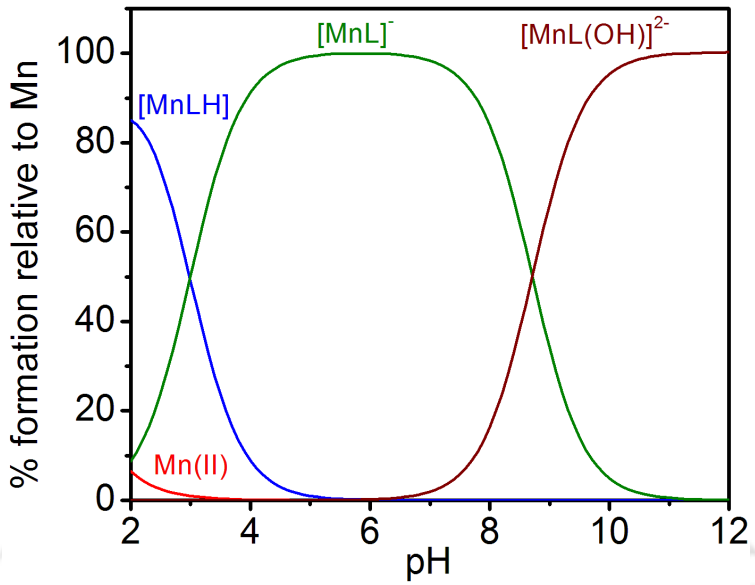

Figure 5.5. *Species distribution diagram of* ***Li_3cbda****:Mn(II) (1:1) solution, whrere* ***[Li_3cbda]*** *= [Mn(II)] = 1 mM (L in the figure represents* ***$cbda^{3-}$****).*

5.4 Longitudinal Relaxivity:

The efficiency of the complex as a positive contrast agent was assessed by longitudinal relaxivity (r_1) measurement. The r_1 relaxivity was determined at 1.41 T, in HEPES buffer, at pH ~7.4, and temperature 25 °C.

Using inversion recovery technique, T_1 relaxation times were measured for four different concentrations of the complex. The slope of the linear plot of relaxation rate R_1 ($1/T_1$) *versus* Mn(II) concentration provided the longitudinal relaxivity r_1 = 3.02 $mM^{-1}s^{-1}$ at 1.41 T, pH ~7.4, and 25 °C (**Figure 5.6**). The exact concentration of Mn(II) ion in the solution was determined by ICP-AES technique. The value was closely comparable to r_1 value exhibited at 0.47 T by mono(aquated) $[Mn(edta])^{2-}$ (3.3 $mM^{-1}s^{-1}$), $[Mn_2(enota)]$ (3.4 $mM^{-1}s^{-1}$), $[Mn(edta\text{-}bom)]^{2-}$ (3.6 $mM^{-1}s^{-1}$),[9(b)] and $[Mn(dpaaa)]^{2-}$ (3.6 $mM^{-1}s^{-1}$)[7(b)] complexes, and greater than those of Teslascan® (2.8 $mM^{-1}s^{-1}$ at 0.47 T; 2.1 $mM^{-1}s^{-1}$ at 1.5 T)[2(a),11] and $[Mn(pyc3a)]^{2-}$ (2.1 $mM^{-1}s^{-1}$,1.4 T).[9(a)]

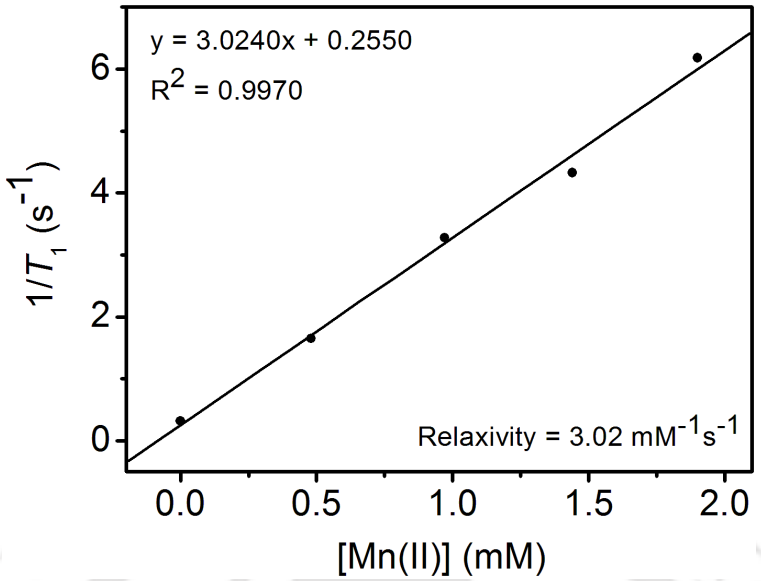

Figure 5.6. *$1/T_1$ vs [Mn(II)] plot at 1.41 T, 25 °C, and pH ~ 7.4.*

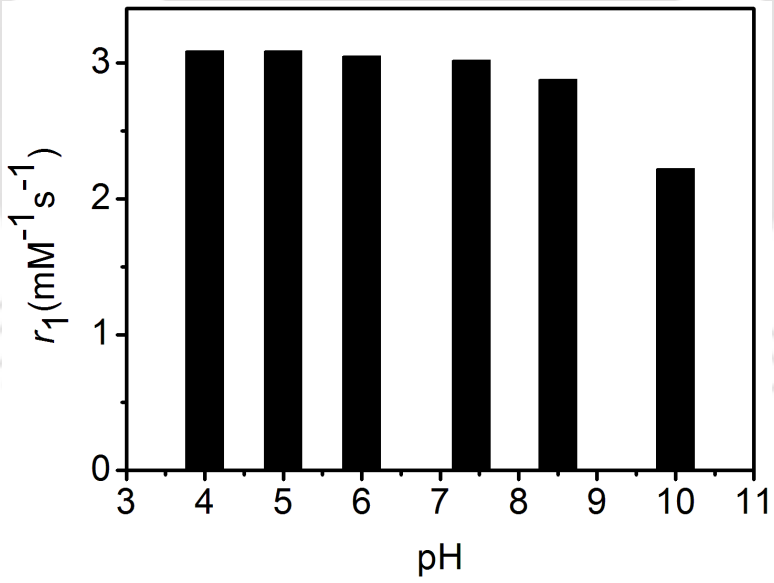

Figure 5.7. *r_1 relaxivity changes in the pH range 4-10; at 1.41 T, and 25 °C.*

To understand the coordination equilibrium of complex **5A** in solution, a pH-dependent relaxivity study was performed in the pH range 4-10 at 1.41 T, and 25 °C (**Figure 5.7**). The

relaxivity of the complex remained fairly constant in a range of pH from 4 to 7.4. However, at pH ~ 10, the relaxivity value diminished to 2.22 $mM^{-1}s^{-1}$ (26%). This was possibly due to the replacement of the coordinated water molecule by a hydroxyl group.

5.5 Affinity for Physiological Anions:

Physiological anions, including bicarbonate (HCO_3^-), biphosphate (HPO_4^{2-}), and fluoride (F^-), are present in non-negligible concentrations (from 25 mM to 0.38 mM) in human blood plasma.[12] The anions might considerably interact with the complex, and could lower the stability as well as relaxivity value by permanently replacing the coordinated water molecule *in vivo*.[13]

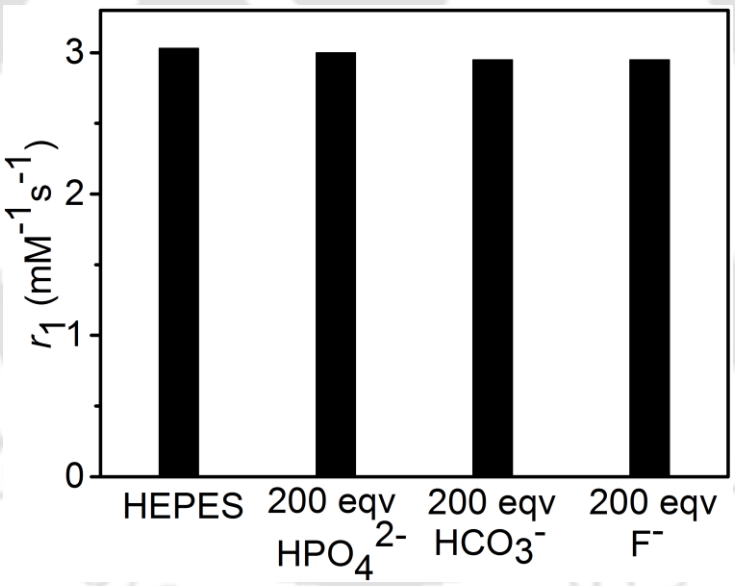

Figure 5.8. *Variation of relaxivity in the presence of 200 equivalents of physiological anions at 1.41 T, 25 °C, pH ~7.4; [complex* ***5A****] = 0.5 mM, and [physiological anions] = 100 mM.*

In this context, the interactions of the complex with the anions were investigated by measuring the change in the relaxivity value of the complex ([complex **5A**] = 0.5 mM) in the presence of 200 equivalents of the anions ([HCO_3^-] = [HPO_4^{2-}] = [F^-] = 100 mM) at 1.41 T, pH ~ 7.4, and 25 °C (**Figure 5.8**). Gratifyingly, no appreciable change in the relaxivity value was

found. This implied neither the stability of the complex was being challenged nor the coordinated water molecule was being substituted by the anions. A low positive charge on Mn ion (+II) and an overall negative charge of the complex possibly promoted a repelling effect between the complex and the anions. Thus, complex **5A** remained inert to the anions.

5.6 Phantom MR Imaging:

The positive contrast efficiency of complex **5A** was investigated by obtaining the T_1-weighted phantom images at 1.5 T, pH ~ 7.4, and 25 °C using a clinical MRI BRIVO MR355 system.

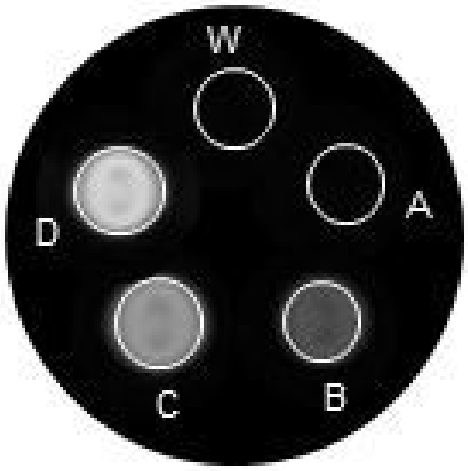

Figure 5.9. *T_1-weighted MR images of the micro-centrifuge tubes (phantom images) containing aqueous solution of complex **5A** at differentconcentrations (W = water, A = 0.25 mM, B = 0.50 mM, C = 0.70 mM, D = 1.00 mM) at 1.5 T, 25 °C, and pH ~7.4.*

Phantoms used were micro-centrifuge tubes containing four different concentrations (0.25 mM, 0.50 mM, 0.70, and 1.00 mM) of the aqueous solutions of complex **5A** (**Figure 5.9**) in HEPES buffer, pH ~ 7.4, 25 °C. The acquired images showed increase in brightness with increase in concentration.

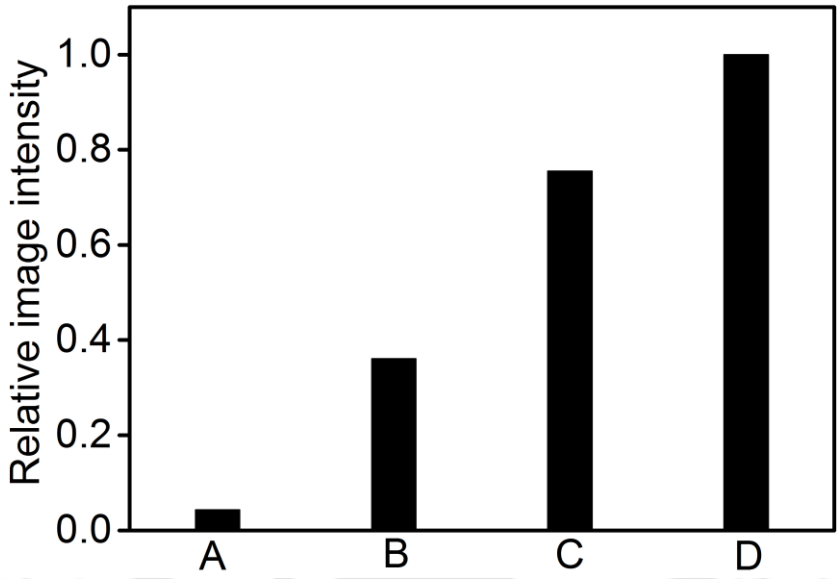

Figure 5.10. *Relative image intensity plot using ImageJ Software.*

A comparison of image intensities was conducted by using ImageJ software considering the same image area. The relative image intensity is plotted as bar diagram in **Figure 5.10**. The image intensity plot justified the fact that images became brighter with increase in concentration of complex **5A**.

5.7 Conclusion:

- A water-soluble, mono(aquated), seven-coordinate Mn(II) complex, **5A** with chiral ligand **Li_3cbda** has been synthesized. The X-ray crystal structure analysis revealed the presence of two mononuclear Mn(II) units connected by carbonyl atom, which in aqueous solution existed in monomeric form with one coordinated water molecule.

- Complex **5A** showed very high thermodynamic stability (pMn = 8.06) compared to Mn(II)-edta complex as well as similar Mn(II)-based mono(aquated) complexes. The stability of the complex remained consistent in the presence of physiological anions.

- At 1.41 T, pH ~ 7.4, and 25 °C, complex **5A** offered r_1 relaxivity of 3.02 $mM^{-1}s^{-1}$, which was about 1.4 times higher as compared to that of Teslascan® (r_1 = 2.1 $mM^{-1}s^{-1}$, at 1.5 T), and close to that of the clinically approved mono(aquated) Gd(III)-based MRI CAs, which shows r_1 = 3-5 $mM^{-1}s^{-1}$ at 1.5 T.

- T_1-weighted phantom MR imaging at 1.5 T confirmed the candidature of the complex in the category of Mn(II)-based T_1-weighted positive contrast agent.

References

1. (*a*) B. Drahoš, I. Lukeš and É. Tóth, *Eur. J. Inorg. Chem*., 2012, **2012**, 1975; (*b*) S. M. Rocklage, W. P. Cacheris, S. C. Quay, F. E. Hahn and K. N. Raymond, *Inorg. Chem*., 1989, **28**, 477; (*c*) V. Kubíc˘ek and É. Tóth, *Adv. Inorg. Chem*., 2009, **61**, 63; (*d*) P. Hermann, J. Kotek, V. Kubíc˘ek and I. Lukeš, *Dalton Trans*., 2008, 3027; (*e*) S. Aime, S. G. Crich, E. Gianolio, G. Giovenzana, L. Tei and E. Terreno, *Coord. Chem. Rev*., 2006, **250**, 1562; (*f*) E. Boros, E. M. Gale and P. Caravan, *Dalton Trans*., 2015, **44**, 4804.

2. (*a*) H. Su, C. Wu, J. Zhu, T. Miao, D. Wang, C. Xia, X. Zhao, Q. Gong, B. Song and H. Ai, *Dalton Trans*., 2012, **41**, 14480; (*b*) R. S. Ranganathan, N. Raju, H. Fan, X. Zhang, M. F. Tweedle, J. F. Desreux and V. Jacques, *Inorg. Chem*., 2002, **41**, 6856; (*c*) M. Port, I. Raynal, L. V. Elst, R. N. Muller, F. Dioury, C. Ferroud and A. Guy, *Contrast Media Mol. Imaging*, 2006, **1**, 121; (*d*) P. Caravan, *Chem. Soc. Rev*., 2006, **35**, 512; (*d*) F. Dioury, C. Ferroud, A. Guy and M. Port, *Tetrahedron*, 2009, **65**, 7573; (*e*) B. Drahoš, M. Pniok, J. Havĺickov´a, J. Kotek, I. C´ısa˘rov´a, P. Hermann, I. Lukeš and É. Tóth, *Dalton Trans.,* 2011, **40**, 10131.

3. J. T. Jørgensen, M. Rief, T. B. Brismar, M. Wagner and N. Albiin, *Acta Radiol*., 2012, **53**, 707.

4. (*a*) J. Wang, G. R. Gao, Z. H. Zhang, X. D. Zhang, X. Z. Liu, Y. M. Kong and Y. Li, *Russ. J. Coord. Chem*., 2007, **33**, 258; (*b*) B. C. Smith, *Infrared Spectral Interpretation: A Systematic Approach*, CRC press, 1998.

5. (*a*) A. Forgács, M. Regueiro-Figueroa, J. L. Barriada, D. Esteban-Gómez, A. de Blas, T. Rodríguez-Blas, M. Botta and C. Platas-Iglesias, *Inorg. Chem*., 2015, **54**, 9576; (*b*) Q. Zhang, J. D. Gorden, R. J. Beyers and C. R. Goldsmith, *Inorg. Chem*., 2011, **50**, 9365; (*c*) E. Molnar, N. Camus, V. Patinec, G. A. Rolla, M. Botta, G. Tircso, F. K. Kálmán, T. Fodor, R. Tripier and C. Platas-Iglesias, *Inorg. Chem*., 2014, **53**, 5136; (d) B. Phukan, A. B. Patel and C. Mukherjee, *Dalton Trans*., 2015, **44**, 12990; (e) B. Drahoš, J. Kotek, I. Císařová, P. Hermann, L. Helm, I. Lukeš and É. Tóth, *Inorg. Chem*., 2011, **50**, 12785.

6. W. J. Greay, *Coord. Chem. Rev*., 1971, **7**, 81.

7. (*a*) A. Nonant, P. H. Fries, J. Pécaut and M. Mazzanti, *Chem. - Eur. J*., 2007, **13**, 8489; (*b*) A. Forgács, R. Pujales-Pardela, M. Regueiro-Figueroa, L. Valencia, D. Esteban-Gómez, M. Botta and C. Platas-Igesias, *Dalton Trans*., 2017, **46**, 1546.

8. (*a*) B. Drahoš, J. Kotek, P. Hermann, I. Lukeš and É. Tóth, *Inorg. Chem*., 2010, **49**, 3224; (*b*) D. M. J. Doble, M. Melchior, B. O'Sullivan, C. Siering, J. Xu, V. C. Pierre and K. N. Raymond, *Inorg. Chem*., 2003, **42**, 4930; (c) C. J. Jocher, M. Botta, S. Avedano, E. G. Moore, J. G. Moore, J. Xu, S. Aime and K. N. Raymond, *Inorg. Chem*., 2007, **46**, 4796.

9. (*a*)) E. M. Gale, I. P. Atanasova, F. Blasi, I. Ay and P. Caravan, *J. Am. Chem. Soc*., 2015, **137**, 15548; (*b*) L. Tei, G. Gugliotta, M. Fekete, F. K. Kálmán and M. Botta, *Dalton Trans*., 2011, **40**, 2025.

10. (*a*) M. Zarrini, F. S. Toosi, B. Davachi and S. Nekooei, *Rev. Clin. Med.*, 2015, **2**, 200; (*b*) N. Nestle, S. Pauls and A. Wunderlich, *Magn. Reson. Med*., 2006, **55**, 923.

11. S. Gallo, N. Vasimalai, M. T. Fernandez-Arguelles and M. Bañbore-López, *Dalton Trans*., 2016, **45**, 17672.

12. V. C. Pierre, M. Botta, S. Aime and K. N. Raymond, *Inorg. Chem*., 2006, **45**, 8355.

13. (*a*) R. S. Dickins, S. Aime, A. S. Batsanov, A. Beeby, M. Botta, J. Bruce, J. A. K. Howard, C. S. Love, D. Parker, R. D. Peacock and H. Puschmann, *J. Am. Chem. Soc*., 2002, **124**, 12697; (*b*) S. Aime, M. Botta, J. I. Bruce, V. Mainero, D. Parker and E. Terreno, *Chem. Commun.*, 2001, 115; (*c*) J. I. Bruce, R. S. Dickins, L. J. Govenlock, T. Gunnlaugsson, S. Lopinski, M. P. Lowe, D. Parker, R. D. Peacock, J. J. B. Perry, S. Aime and M. Botta, *J. Am. Chem. Soc*., 2000, **122**, 9674.

Chapter VI

A High Relaxivity, Stable Mn(II) Complex of Picolinate-Based Ligand as MRI Contrast Agent

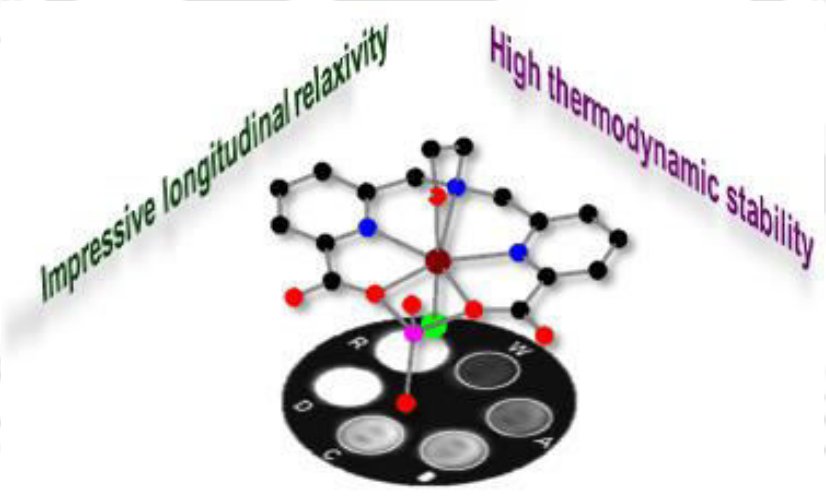

*Some results have been submitted for patent; with application no. **201831020332**.

6.1 Introduction:

In recent years, high spin, thermodynamically stable Mn(II) complexes have been special attractions, due to their applications as potential MRI contrast agents.[1] Mn(II) ions form stable coordination complexes with negatively charged oxygen and nitrogen donor atoms.[2] Based on it, different classes of ligands have been designed; linear, macrocyclic, and other types of ligands. Linear ligands mainly consist of edta or dtpa derivatives;[3] while macrocyclic ligand frameworks are derivatives of nota or dota.[4] Another class of ligand frameworks which are structurally different from these two systems; are derivatives of aazta.[5] Most of Mn(II) complexes with these ligands have maximum of one coordinated-water molecule. These small Mn(II) complexes afford maximum relaxivity value of 2.4-3.7 $mM^{-1}s^{-1}$ at 0.47 T, 25 °C.[1(a)] Pyridine based 15-18 membered macrocycles were studied in late 1992.[6] Tóth *et al.* reported a series of ligands with pyridine moiety in macrocyclic systems (12-pydo1r, 15-pyN_5, 15-pyN_3O_2). The corresponding Mn(II) complexes are showing moderate thermodynamic stability. All these illustrations are evidences of pyridine moiety favoring Mn(II) ion encapsulation by rigidifying the macrocyclic cavity, that assists enhancement in thermodynamic stability.[7]

In this chapter, Mn(II) complex was synthesized with picolinate-based ligand **H_2hbda**. The six-coordinate ligand framework would allow at least one directly coordinated-water molecule in its corresponding Mn(II) complex. Incorporation of two pyridine moieties in the ligand framework, would provide a thermodynamically stable Mn(II) complex by metal-to-ligand π-back donation. Additionally, two carboxylate O-atoms, one amine N-atom, two pyridine N-atoms would also contribute to stability by strong σ-bonding to Mn(II) center.

6.2 Synthesis and Characterization of Mn(II) Complex of Ligand H_2hbda:

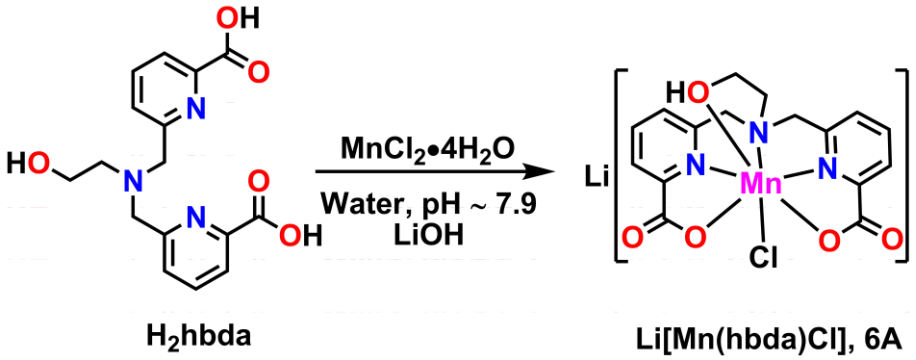

Scheme 6.1. *Synthesis of Mn(II) complex of ligand* ***H_2hbda*** .

Ligand **H_2hbda** and $MnCl_2$•$4H_2O$ were reacted in 1:1 molar equivalent in water, at pH ~ 7.9 by adding aqueous LiOH solution (**Scheme 6.1**). After continuous stirring for 24 h, the filtrate of the reaction mixture on slow evaporation provided crystals of complex **6A** in 42% yield.

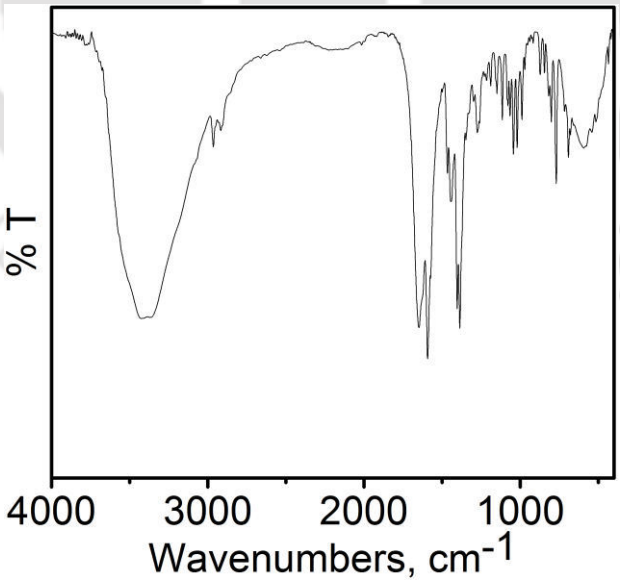

Figure 6.1. *FTIR spectrum of complex* ***6A***.

The FTIR spectrum of complex **6A** is presented in **Figure 6.1**. A broad band appeared at 3426 cm^{-1} was assigned to ν(O–H) stretching of water molecule, and the –OH group present in the ligand backbone.[8] In the spectrum, band for ν(C=O) stretching was observed at 1648 cm^{-1}, which was found to be shifted from its position at 1616 cm^{-1} with respect to the ligand.

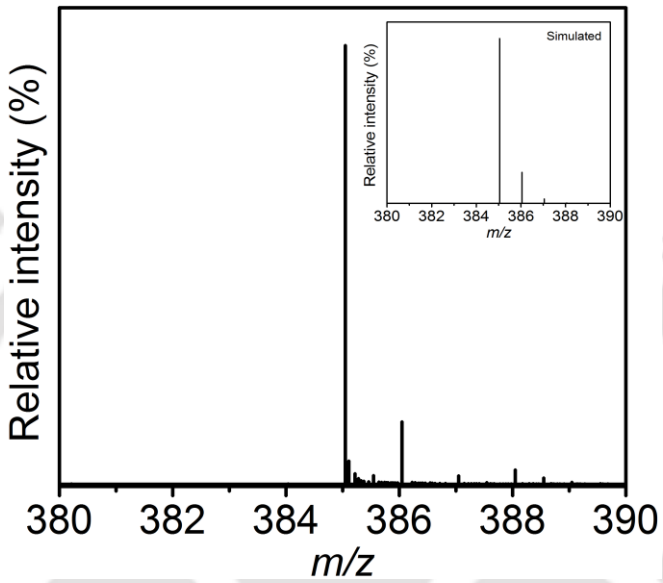

Figure 6.2. *ESI-MS (+ve) mass spectrum of aqueous solution of complex* ***6A****. Simulated spectrum has been given as inset.*

The electrospray ionization mass spectrum of an aqueous solution of complex **6A** in positive mode provided a 100% molecular ion peak at *m*/*z* = 385.0468 ($[M+H]^+$; where M = $C_{16}H_{15}N_3O_5Mn$). This peak corresponded to $C_{16}H_{16}N_3O_5Mn$ composition as evident by isotropic distribution pattern examination. Thus, mass spectrometric analysis indicated the formation of a neutral species, [Mn(hbda)(H_2O)].

Single crystal X-ray diffraction measurement was performed at 293(2) K for determining the molecular structure of complex **6A**. The complex crystallized in the triclinic space group *P*-1. The molecular structure of complex **6A** is given in **Figure 6.3**, and the selected bond lengths and bond angles are tabulated in **Table 6.1**.

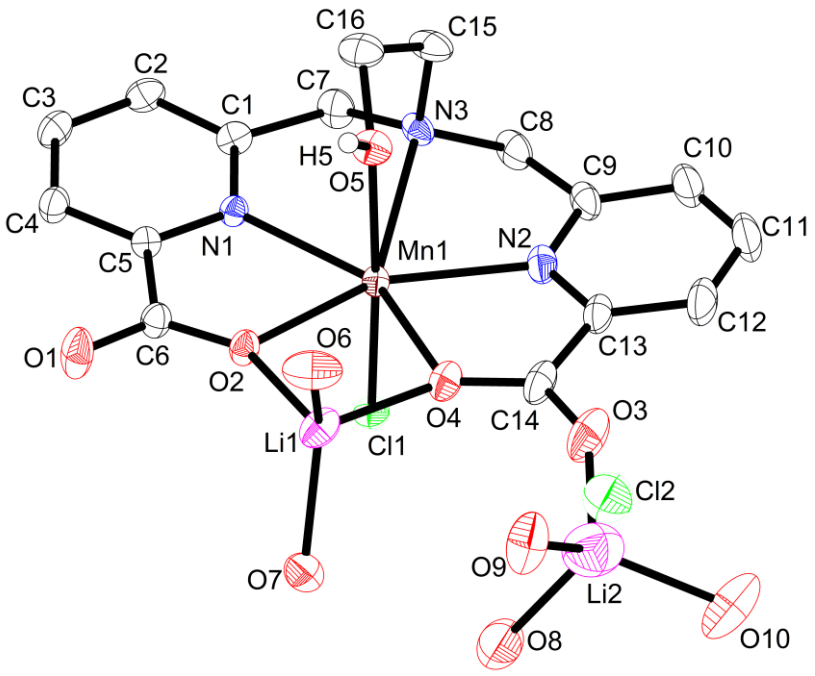

Figure 6.3. *ORTEP diagram of complex* ***6A•LiCl•5H$_2$O****. Hydrogen atoms were omitted for clarity and thermal ellipsoids were drawn with 40% probability.*

Complex **6A** was consisted of a seven coordinate Mn(II) unit in pentagonal bipyramidal geometry. The basal plane was consisted of amine N-atom of 2-aminoethan-1-ol, two picolinic carboxylate O-atoms, and two pyridine N-atoms. The axial positions were occupied by OH group of 2-aminoethan-1-ol, and one Cl-atom, where O5–Mn1–Cl1 bond angle was ~ 172°. The Mn1–N1(pyridine) = 2.245, Mn1–N3(amine) = 2.463, Mn1–O2(picolinic-carboxylate) = 2.242, Mn1–N2(pyridine) = 2.220, Mn1–O4(picolinic-carboxylate) = 2.242, Mn1–O5(2-aminoethan-1-ol) = 2.297, and Mn–Cl1 = 2.5791 Å, which were in accordance with previously reported Mn(II) complexes of similar coordination environment.[9] In the molecular structure of complex **6A**, two Cl^- ions were observed, one directly coordinated to Mn(II) center, and one was found free outside the coordination unit. To balance two negatively charged Cl^- anions, two Li(I) ions were observed as counter cations. Although, solid state structure of complex **6A**, showed one directly coordinated Cl-atom, it was substituted by one H_2O molecule in aqueous state. Thus a neutral, mono(aquated) Mn(II) complex, [Mn(hbda)(H_2O)] was generated in aqueous solution.

Table 6.1. *Selected bond distances (Å) and bond angles (°) for complex* ***6A****.*

Mn1–O2	2.242(3)	Mn1–N2	2.220(4)
Mn1–O4	2.242(3)	Mn1–N3	2.463(4)
Mn1–O5	2.297(3)	Mn1–Cl1	2.5791(12)
Mn1–N1	2.245(3)		
O5–Mn1–Cl1	171.67(9)	N1–Mn1–N3	70.42(13)
N2–Mn1–O4	72.15(15)	O2–Mn1–N1	71.72(12)
N2–Mn1–N3	70.07(15)	O2–Mn1–O4	75.30(12)

Table 6.2. *Crystallographic parameters and refinement data for complex* ***6A****.*

Empirical formula	C16 H23 Cl2 Li2 Mn N3 O10
Formula weight	557.09
Crystal habit, colour	Block, colourless
Crystal size, mm^3	0.30 × 0.28 × 0.25
Temperature, T	293(2)
Wavelength, λ (Å)	0.71073
Crystal system	triclinic
Space group	P -1
Unit cell dimensions	a = 7.3941(4) Å b = 12.3924(6) Å c = 13.2656(8) Å α = 78.457(5)° β = 81.206(5)° γ = 87.364(4)°
Volume, V ($Å^3$)	1176.80(11)
Z	2
Calculated density, $g \cdot cm^{-3}$	1.572
Absorption coefficient, μ (mm^{-1})	0.843
F(000)	570.0
θ range for data collection	3.00° to 25.00°
Limiting indices	$-8 \le h \le 8$, $-14 \le k \le 14$, $-13 \le l \le 15$
Reflection collected/unique	7582/4147[R(int)= 0.0248]
Completeness to θ	99.8% (θ = 25.00°)
Max. and min. transmission	0.777/0.810
Refinement method	'SHELXL–97(Sheldrick, 1997)'
Data/restraints/parameters	4147/3/314
Goodness–of–fit on F^2	1.100
Final R indices [I>2σ(I)]	$R1$ = 0.0618, $wR2$ = 0.1642
R indices (all data)	$R1$ = 0.0711, $wR2$ = 0.1734
Largest diff. peak and hole	0.48 and −1.16 $e \cdot Å^{-3}$

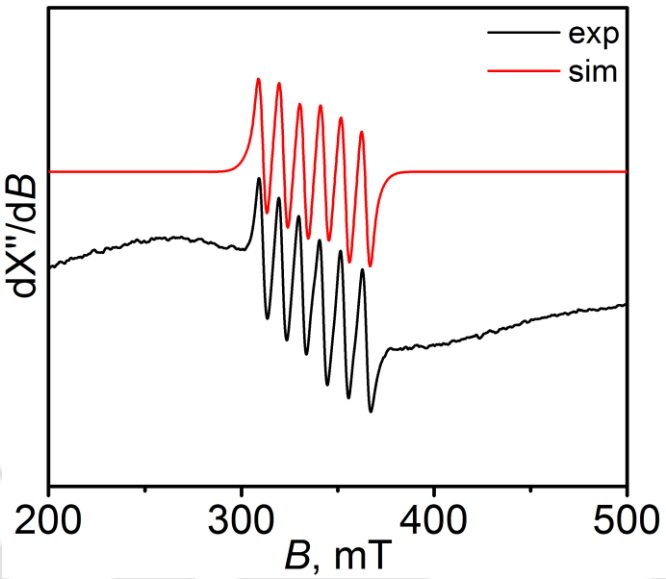

Figure 6.4. *X-band EPR spectrum (9.44 GHz) of complex* ***6A*** *measured at room temperature, power = 0.995 mW, modulation frequency = 100 kHz, and amplitude = 100 G.*

To investigate the oxidation state of central Mn ion in complex **6A**, X-band EPR measurement was performed at room temperature. The aqueous solution of complex **6A** showed a six-line spectrum, which is given in **Figure 6.4**. For hyperfine coupling with a nucleus with I = 5/2 (Mn), six-line spectrum is usually anticipated, and it was appeared as such. The experimental data was simulated using following parameters; g_1 = 1.996, g_2 = 1.997, g_3 = 2.000, g_{av} = 1.998; ^{55}Mn(A_1, A_2, A_3) = (93, 53, 95) × 10^{-4} cm^{-1}, and A_{av} = 80. From the resultant A_{av} and g_{av} values it can be concluded that the unpaired electrons were present on Mn center, which was in +II oxidation state.

6.3 Thermodynamic Stability:

In order to confirm *in vivo* safety, high thermodynamic stability has to be ensured. The stepwise protonation constants of the ligand were determined by performing pH-potentiometric titration in 0.15 M NaCl solution at 25 °C. The protonation constant values obtained from the titration were; log K_1^H = 7.68, log K_2^H = 4.63, and log K_3^H = 2.88. The first two protonation constants value

corresponded to the protonation of amine nitrogen atom ($\log K_1^H$ = 7.68) and pyridine nitrogen atom ($\log K_2^H$ = 4.63).[10] The latter one was due to protonation of one of the carboxylate groups of the picolinate moieties ($\log K_3^H$ = 2.88) present in the ligand backbone.

The stability constant of corresponding Mn(II) complex with ligand **H_2hbda** was determined by direct pH-potentiometric titration. The metal-ligand concentration ratio was considered to be 1:1 and the titration was carried out at the same experimental conditions used for determining the protonation constants of ligand **H_2hbda**.

Table 6.3. *Protonation constants, stability constants, and pMn value of its analogues.*

Ligand	**log K_i^H**	**log K_{MnL}**	**pMn**
H_3pyc3a[1(c)]	10.16, 6.39, 3.13	14.14	8.17
H_3dpaaa[11(a)]	7.26, 3.90, 3.29, 1.77	13.19	8.98
H_4edta[11(a)]	10.17, 6.11, 2.68	13.88	7.95
H_4cdta[1(c)]	9.36, 5.95, 3.62, 2.57	14.32	8.67
1,4-H_2do2a[11(b)]	11.40, 9.58, 3.74, 1.65	15.22	7.03
H_3nota[11(c)]	13.17, 5.74, 3.22, 1.96	16.30[11(d)]	7.94
H_3aaz3a[5]	10.24, 5.78, 3.67, 2.18	11.00	6.57
H_2hbda	**7.68, 4.63, 2.88**	**13.46**	**9.00**

The stability constant of complex **6A** was found to be $\log K_{MnL}$ = 13.46, in 0.15 M NaCl solution at 25 °C. Under physiological condition, the stability constant of any complex is more precisely described in terms of pM value; which is given by $-\log[M]_{free}$ at pH ~ 7.4, and 25 °C, where $[M] = [L]_{total} = 10\ \mu M$.[12] The calculated pMn value for ligand **H_2hbda** was found to be 9.00, which was substantially higher compared to the previously reported hexadentate ligands, examples are given in **Table 6.3**.[7(a)] Alcoholic group stabilizes corresponding Ln(III) complexes ($\Delta \log K = 2.9$; where $\Delta \log K$ refers free energy change after binding).[12] Herein, it was observed that due to presence of alcoholic group, the stability of complex **6A** was also found to be increased. Furthermore, the presence of two pyridine moieties also contributed to stability *via* metal-to-ligand back donation. Additionally, two pyridine N-atoms, two carboxylate O-atoms, and one amine N-atom stabilized the complex by five strong σ-bonding.

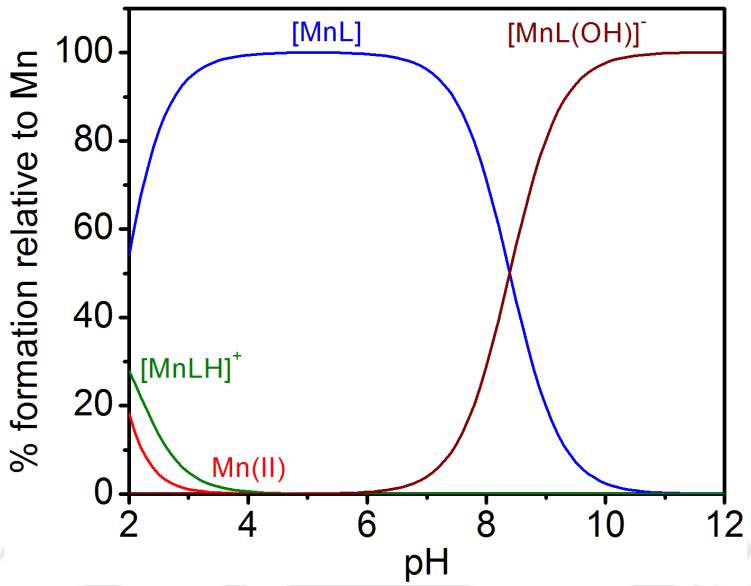

Figure 6.5. *Species distribution diagram of* ***H_2hbda****:Mn(II) (1:1) solution, whrere* ***[H_2hbda]*** *= [Mn(II)] = 1 mM (L in the figure represents* ***$hbda^{2-}$****).*

The species distribution diagram of complex **6A** is given in **Figure 6.5**. It was found that complex **6A** was present most abundantly within pH range ~ 4-9. Above pH ~ 9, $[MnL(OH)]^-$ species was strated appeareing, which possibly formed either due to deprotonation of coordinated water molecule, or substitution of water molecule by hydroxyl anion.

6.4 Longitudinal Relaxivity:

The efficiency of complex **6A** as T_1-contrast agent was evaluated by measuring T_1-relaxation times of the complex in HEPES buffer maintaining pH ~ 7.4, at 1.41 T, and 25 °C. Utilizing inversion recovery method, T_1 relaxation times of four different concentrations of complex **6A** were determined, and longitudinal relaxation rates ($R_1 = 1/T_1$) were plotted as the function of exact Mn(II) concentration (determined from ICP-AES analysis). The obtained linear plot is given in **Figure 6.6.**

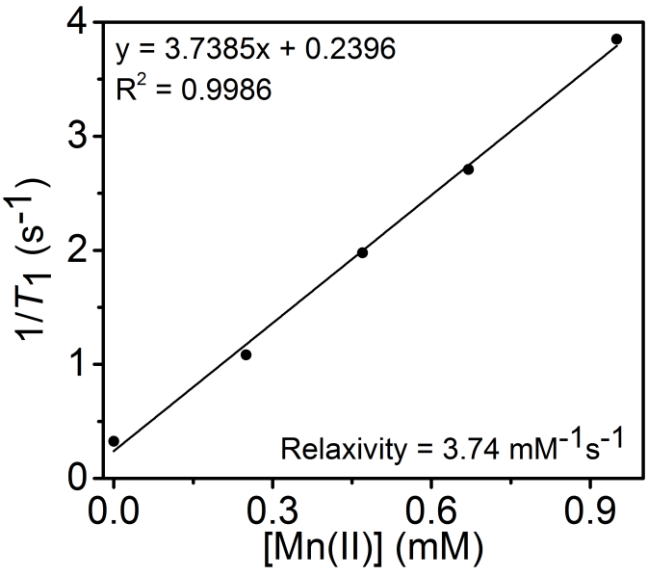

Figure 6.6. *$1/T_1$ vs [Mn(II)] plot 1.41 T, 25 °C, and pH ~ 7.4.*

The longitudinal relaxivity value for complex **6A** obtained from the slope of the linear plot was found to be 3.74 $mM^{-1}s^{-1}$ at 1.41 T, pH ~ 7.4, and 25 °C. Complex **6A** afforded impressive relaxivity value compared to similar mono(aquated) Mn(II) complexes $[Mn(edta)]^{2-}$ (3.3 $mM^{-1}s^{-1}$),[14(a)] $[Mn(edta)(bom)]^{2-}$ (3.6 $mM^{-1}s^{-1}$),[3(c)] $[Mn(dpaaa)]^{-}$ (3.6 $mM^{-1}s^{-1}$),[11(a)] $[Mn(cdta)]^{2-}$ (3.6 $mM^{-1}s^{-1}$)[11(d)] at 0.47 T, 25 °C; $[Mn(pyc3a)]^{-}$ (2.1 $mM^{-1}s^{-1}$ at 1.41 T, 37 °C).[1(c)] The relaxivity value of complex **6A** was also higher than commercially available Mn(II)-based contrast agent Teslascan® (2.8 mM^{-1} s^{-1} at 0.47 T;[14(b)] 2.1 mM^{-1} s^{-1} at 1.5 T).[1(b)]

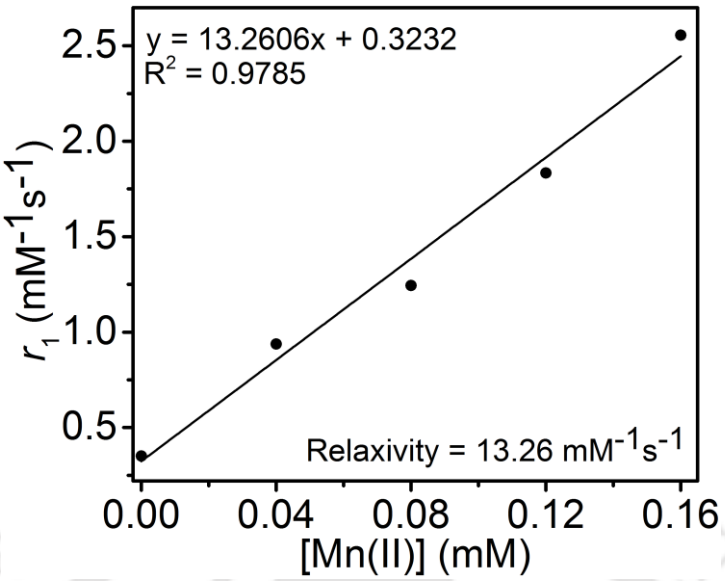

Figure 6.7. *$1/T_1$ vs [Mn(II)] plot in the presence of BSA solution at 1.41 T, 37 °C, and pH ~ 7.4.*

The relaxivity value of complex **6A** was further studied in the presence of BSA. The complex relaxivity can be increased by binding with slowly rotating plasma proteins.[3(a),(c)] It also increases the lifetime of contrast agents in the vascular system. To investigate the interaction of complex **6A** with plasma protein, the longitudinal relaxation times of complex **6A** was measured in the presence of 4.5% BSA (~ 0.66 mM, physiological concentration). At 1.41 T, pH ~ 7.4, and 37 °C, relaxation times were measured for four different concentrations of complex **6A** in the presence of BSA. The obtained linear plot for $1/T_1$ *vs* exact Mn(II) ion concentration (obtained from ICP-AES analysis) is given in **Figure 6.7**. The slope of the linear plot provided relaxivity value of 13.26 $mM^{-1}s^{-1}$, at 1.41 T, 37 °C. A significant increment in relaxivity value was achieved in the presence of BSA solution compared to relaxivity value of 3.74 $mM^{-1}s^{-1}$ in HEPES buffer. The percentage of complex **6A** bound to BSA was calculated by ultrafiltration technique using 5 KDa cut off membrane, and Mn(II) ion was quantified by ICP-AES analysis. It was found that 71% of complex **6A** bound to BSA. The enhancement in relaxivity value of complex **6A** in the presence of BSA solution was expected to be due to macromolecular association.

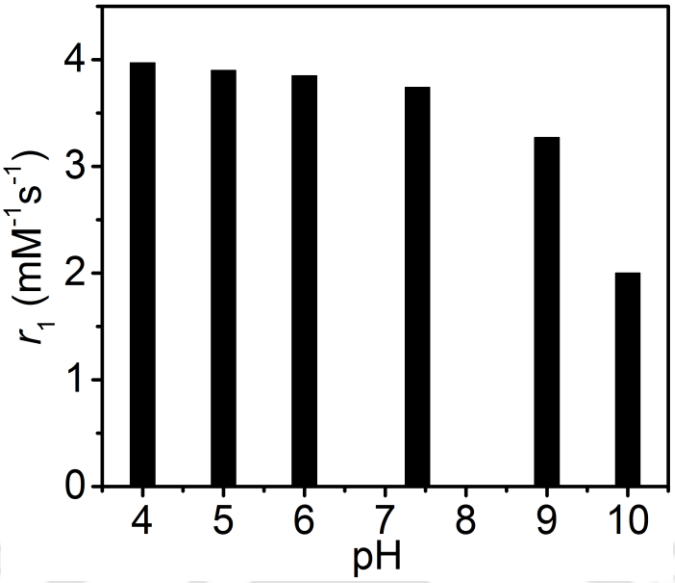

Figure 6.8. *r_1 relaxivity changes in the pH range 4-10; at 1.41 T and 25 °C.*

In order to verify the presence of variable coordination equilibrium states of complex **6A** in solution, relaxivity of complex **6A** was investigated as a function of pH at 1.41 T, and 25 °C. The pH dependant-relaxivity plot is shown in **Figure 6.8**. The plot distinctly indicated the existence of complex **6A** in the pH range of 4 ~ 8. However, from pH ~ 9, relaxivity value was found to be diminished attainig value of 2.00 $mM^{-1}s^{-1}$ (Δr_1 = 1.74, 46%) at pH ~ 10. It was anticipated due to formation of hydroxyl species, which was also justified from the species distribution diagram (**Figure 6.5**).

6.5 Affinity for Physiological Anions:

The physiologically available small endogenous anions like bicarbonate (HCO_3^-), biphosphate (HPO_4^{2-}), fluoride (F^-); are playing an essential role during *in vivo* application of a complex as MRI contrast agent. These anions could substitute inner-sphere water molecules, and significantly lessen *in vivo* relaxivity of the complex.[15] To investigate the interaction with these anions, longitudinal relaxivity value of complex **6A** ([Complex **6A**] = 0.5 mM) were recorded in

the presence of 200 equivalents of various anions ([HPO_4^{2-}] = [HCO_3^-] = [F^-] = 100 mM) at 1.41 T, pH ~ 7.4, and 25 °C.

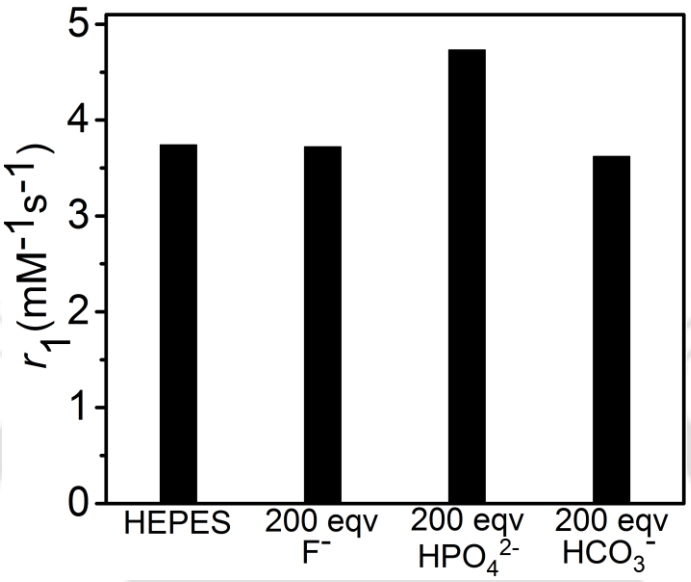

Figure 6.9. *Variation of longitudinal relaxivity in the presence of 200 equivalents of physiological anions at 1.41 T, 25 °C, pH ~ 7.4; [complex **6A**] = 0.5 mM, and [physiological anions] = 100 mM.*

The obtaind relaxivity values are presented as a bar diagram in **Figure 6.9**. No change in relaxivity value in the presence of HCO_3^- and F^- anion, suggested that the complex was inert towards these physiological anions. It could be explained by overall neutral charge of the complex in aqueous state.[15(c),16] However, relaxivity value was found to be increased in the presence of HPO_4^{2-} (4.73 $mM^{-1}s^{-1}$, 26%) anion. The main reason behind this increment was anticipated to be either dissociation of the complex releaseing free Mn(II) ion or formation of aggregation.[7(a)]

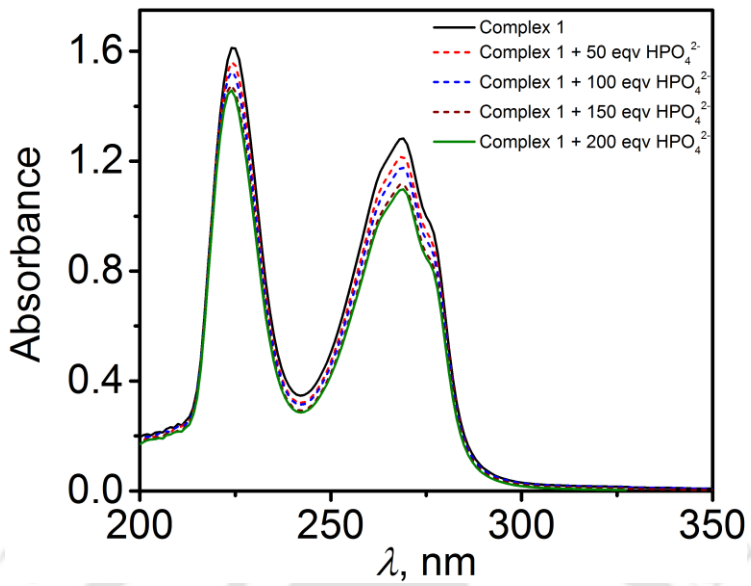

Figure 6.10. *Changes in UV-Vis spectra of complex* ***6A*** *in the presence of* HPO_4^{2-} *anion at 25 °C, and pH ~ 7.4.*

To understand the probable reason, the absorption spectra of complex **6A** were recorded in the presence of various equivalents of HPO_4^{2-} anion (**Figure 6.10**). No significant abrupt changes were noticed in the UV-Vis spectra. It implimented no such (26%) dissociation probability of complex **6A** in the presence of HPO_4^{2-} anion. Thus, increase in the relaxivity value was possibly due to formation of slowly rotating aggregation.[7(a)]

6.6 Phantom MR Imaging:

The efficiency of complex **6A** as a positive contrast agent was evaluated by acquiring T_1-weighted phantom images under clinical imager at 1.5 T. Phantoms used were micro-centrifuge tubes containing different concentrations of aqueous solution of complex **6A** in HEPES buffer at pH ~ 7.4, and 25 °C. The images were measured in MAGNETOM Avanto 1.5 T MRI scanner.

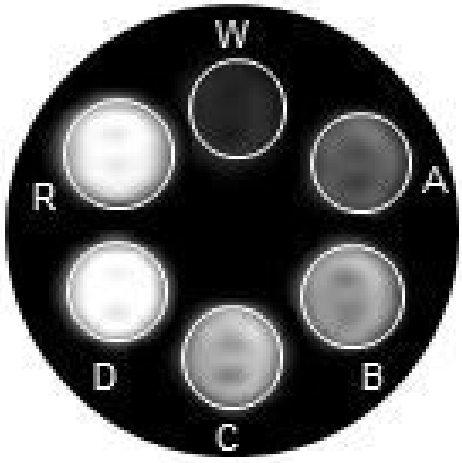

Figure 6.11. *T_1-weighted phantom images of micro-centrifuge tubes with different concentrations of complex **6A** in HEPES buffer (W = water, A = 0.25 mM, B = 0.50 mM, C = 0.70 mM, and D = 1.00 mM) at 1.5 T, 25 °C, pH ~ 7.4, TR = 468 ms, and TE = 8.2 ms; R stands for the reference MultiHance® in 1 mM concentration.*

The acquired images showed intensification of brightness with increase in concentration of complex **6A** (**Figure 6.11**). It justified the concentration dependant signal enhancement by complex **6A**. ImageJ Software was used to determine the intensity of obtained images considering constant image area. The calculated relative image intensity is shown in **Figure 6.12**. It confirmed the enhancement in brightness with increase in concentration of complex **6A**. The efficiency of the complex as a contrast agent, and as the alternative to Gd(III)-based contrast agent was reflected by almost equal image intensity of 1 mM complex **6A** to that of 1 mM MultiHance®, the commercially used contrast agent.

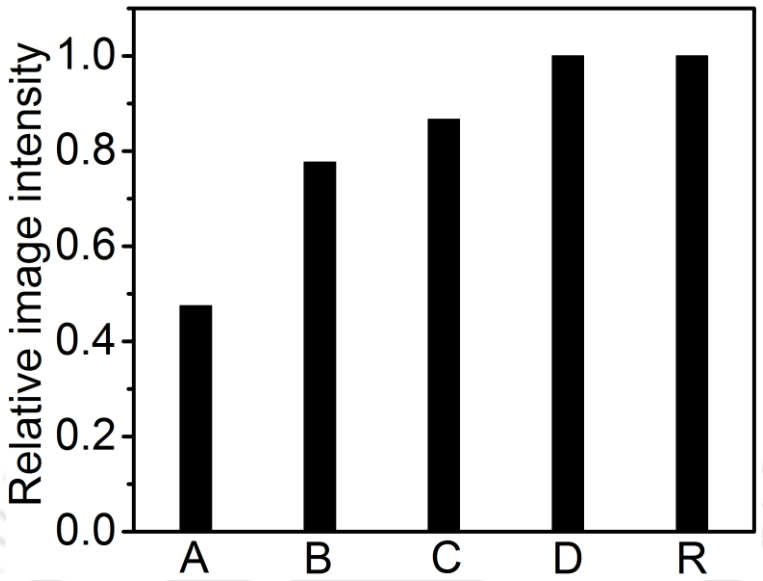

Figure 6.12. *Relative image intensity plot using ImageJ Software.*

6.7 Conclusion:

- A water soluble, seven-coordinate Mn(II) complex was synthesized using hexadentate picolinate-based ligand **H_2hbda**. The structural analysis confirmed the pentagonal bipyramidal geometry of complex **6A**, with one directly coordinated Cl-atom to Mn(II) center. However, in aqueous solution water molecule substituted Cl-atom, forming mono(aquated), neutral Mn(II) complex.

- Complex **6A** showed significantly high thermodynamic stability (pMn = 9.00) compared to analogous Mn(II)-based mono(aquated) complexes. The complex stability was not even challenged by 200 equivalents of physiological anions.

- It showed impressive longitudinal relaxivity value of 3.74 $mM^{-1}s^{-1}$ at 1.41 T, pH ~ 7.4, and 25 °C, which was higher than commercially available Mn(II) based contrast agents (Teaslascan®); and comparable to some of commercially available mono(aquated) Gd(III)-based MRI contrast agents. Relaxivity value was further improved by interacting with BSA (r_1 = 13.26 $mM^{-1}s^{-1}$ at 1.41 T, 37 °C).

- T_1-weighted phantom MR imaging under clinical imager at 1.5 T consolidated complex **6A** as potential Mn(II)-based positive contrast agent.

References

1. (*a*) B. Drahoš, I. Lukeš and É. Tóth, *Eur. J. Inorg. Chem*., 2012, 1975; (*b*) H. Su, C. Wu, J. Zhu, T. Miao, D. Wang, C. Xia, X. Zhao, Q. Gong, B. Song and H. Ai, *Dalton Trans*., 2012, **41**, 14480; (*c*) E. M. Gale, I. P. Atanasova, F. Blasi, I. Ay and P. Caravan, *J. Am. Chem. Soc*., 2015, **137**, 15548; (*d*) E. Boros, E. M. Gale and P Caravan, *Dalton Trans*., 2015, **44**, 4804.

2. *The Chemistry of Contrast Agents in Medical Magnetic Resonance Imaging*, ed. A. E. Merbach and E´. Tóth, John Wiley & Sons, Chichester (England), 2013.

3. (*a*) S. H. Koenig, C. Baglin and R. D. Brown III, *Magn. Reson. Med*., 1984, **1**, 496; (*b*) J. S. Troughton, M. T. Greenfield, J. M. Greenwood, S. Dumas, A. J. Wiethoff, J. Wang, M. Spiller, T. J. McMurry and P. Caravan, *Inorg. Chem*., 2004, **43**, 6313; (*c*) S. Aime, P. L. Anelli, M. Botta, M. Brocchetta, S. Canton, F. Fedeli, E. Gianolio and E. Terreno, *J. Biol. Inorg. Chem*., 2002, **7**, 58; (*d*) J. Maigut, R. Meier, A. Zahl and R. v. Eldik, *Inorg. Chem.*, 2008, **47**, 5702; (*e*) A. Bertin, J. Steibel, A.-I. Michou-Gallani, J.-L. Gallani and D. Felder-Flesch, *Bioconjugate Chem*., 2009, **20**, 760.

4. (*a*) C. F. G. C. Geraldes, A. D. Sherry, R. D. Brown III and S. H. Koenig, *Magn. Reson. Med*., 1986, **3**, 242; (*b*) E. Balogh, Z. He, W. Hsieh, S. Liu and É. Tóth, *Inorg. Chem.*, 2007, **46**, 238; (*c*) A. Bianchi, L. Calabi, C. Giorgi, P. Losi, P. Mariani, D. Palano, P. Paoli, P. Rossi and B. Valtancoli, *J. Chem. Soc*., *Dalton Trans*., 2001, 917; (*d*) S. Wang and T. D. Westmoreland, *Inorg. Chem*., 2009, **48**, 719.

5. L. Tei, G. Gugliotta, M. Fekete, F. K. Kálmán and M. Botta, *Dalton Trans*., 2011, **40**, 2025.

6. S. C. Jackels, M. M. Durham, J. E. Newton and T. C. Henninger, *Inorg. Chem*., 1992, **31**, 234.

7. (*a*) B. Drahoš, J. Kotek, P. Hermann, I. Lukeš and É. Tóth, *Inorg. Chem*., 2010, **49**, 3224; (*b*) B. Drahoš, M. Pniok, J. Havĺickov´a, J. Kotek, I. C´ısaˇrov´a, P. Hermann, I. Lukeš

and É. Tóth, *Dalton Trans.,* 2011, **40**, 10131; (*c*) B. Drahoš, J. Kotek, I. C´ısaˇrov´a, P. Hermann, L. Helm, I. Lukeš and É. Tóth, *Inorg. Chem.,* 2011, **50**, 12785.

8. (*a*) J. Wang, G. R. Gao, Z. H. Zhang, X. D. Zhang, X. Z. Liu, Y. M. Kong and Y. Li, *Russ. J. Coord. Chem*., 2007, **33**, 258; (*b*) B. C. Smith, *Infrared Spectral Interpretation: A Systematic Approach*, CRC press, 1998.

9. (*a*) A. Forgács, M. Regueiro-Figueroa, J. L. Barriada, D. Esteban-Gómez, A. de Blas, T. Rodríguez-Blas, M. Botta and C. Platas-Iglesias, *Inorg. Chem*., 2015, **54**, 9576; (*b*) Q. Zhang, J. D. Gorden, R. J. Beyers and C. R. Goldsmith, *Inorg. Chem*., 2011, **50**, 9365; (*c*) E. Molnar, N. Camus, V. Patinec, G. A. Rolla, M. Botta, G. Tircso, F. K. Kálmán, T. Fodor, R. Tripier and C. Platas-Iglesias, *Inorg. Chem*., 2014, **53**, 5136; (*d*) B. Phukan, A. B. Patel and C. Mukherjee, *Dalton Trans*., 2015, **44**, 12990; (*e*) B. Drahoš, J. Kotek, I. Císařová, P. Hermann, L. Helm, I. Lukeš and É. Tóth, *Inorg. Chem*., 2011, **50**, 12785.

10. A. Nonant, P. H. Fries, J. Pécaut and M. Mazzanti, *Chem. – Eur. J*., 2007, **13**, 8489.

11. (*a*) A. Forgács, R. Pujales-Paradela, M. Regueiro-Figueroa, L. Valencia, D. Esteban-Gómez, M. Botta and C. Platas-Iglesias, *Dalton Trans*., 2017, **46**, 1546-1558; (*b*) A. Forgács, L. Tei, Z. Baranyai, D. Esteban-Gómez, C. Platas-Iglesias and M. Botta, *Dalton Trans*., 2017, **46**, 8494; (*c*) B. Drahoš, V. Kub´ıˇcek, C´. S. Bonnet, P. Hermann, I. Lukeš and É. Tóth, *Dalton Trans.*, 2011, **40**, 1945; (*d*) F. K. Kálmán and G. Tircsó, *Inorg*. *Chem*., 2012, **51**, 10065.

12. (*a*) P. Caravan, J. J. Ellision, T. J. McMurry and R. B. Lauffer, *Chem. Rev*., 1999, **99**, 2293; (*b*) L. Thompson, B. Shafer, J. Edgar and K. Mannila, *Adv. Chem. Ser*., 1967, **71**, 169.

13. (*a*) M. Zarrini, F. S. Toosi, B. Davachi and S. Nekooei, *Rev. Clin. Med.*, 2015, **2**, 200; (*b*) N. Nestle, S. Pauls and A. Wunderlich, *Magn. Reson. Med*., 2006, **55**, 923.

14. (*a*) G. A. Rolla, C. Platas-Iglesias, M. Botta, L. Tei and L. Helm, *Inorg. Chem*., 2013, **52**, 3268; (*b*) S. Gallo, N. Vasimalai, M. T. Fernandez-Arguelles and M. Bañbore-López, *Dalton Trans*., 2016, **45**, 17672.

15. (*a*) R. S. Dickins, S. Aime, A. S. Batsanov, A. Beeby, M. Botta, J. Bruce, J. A. K. Howard, C. S. Love, D. Parker, R. D. Peacock and H. Puschmann, *J. Am. Chem. Soc*., 2002, **124**, 12697; (*b*) S. Aime, M. Botta, J. I. Bruce, V. Mainero, D. Parker and E. Terreno, *Chem. Commun.*, 2001, 115; (*c*) J. I. Bruce, R. S. Dickins, L. J. Govenlock, T. Gunnlaugsson, S. Lopinski, M. P. Lowe, D. Parker, R. D. Peacock, J. J. B. Perry, S. Aime and M. Botta, *J. Am. Chem. Soc*., 2000, **122**, 9674.

16. V. C. Pierre, M. Botta, S. Aime and K. N. Raymond, *Inorg. Chem*., 2006, **45**, 8355.

Thesis Conclusions and Perspectives

The main objective of this thesis has been the development of new thermodynamically stable, water-soluble, Gd(III), and Mn(II) complexes with better relaxivity value compared to current commercially available Gd(III)-based MRI contrast agents.

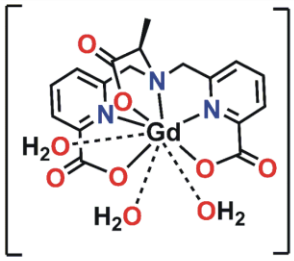

[Gd(cbda)(H$_2$O)$_3$], 3A

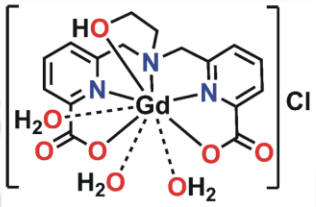

[Gd(hbda)(H$_2$O)$_3$]Cl, 3B

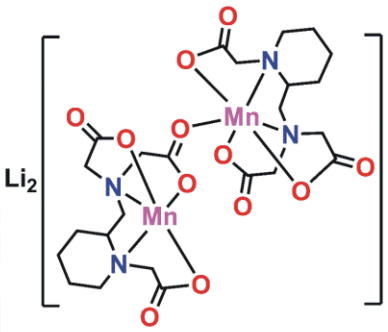

Li$_2$[Mn$_2$(cpmda)$_2$], 4B

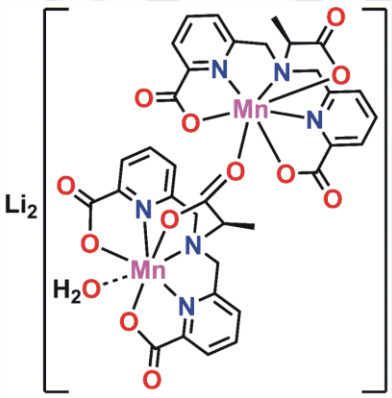

Li$_2$[Mn$_2$(cbda)$_2$(H$_2$O)], 5A

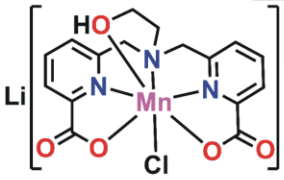

Li[Mn(hbda)Cl], 6A

In contrast to relatively low relaxivity value of current clinically used Gd(III)-based MRI contrast agents, tris(aquated) picolinate-based Gd(III) complexes, **3A** and **3B** showed better relaxivity value of 10.95 $mM^{-1}s^{-1}$, and 9.82 $mM^{-1}s^{-1}$ at 1.41 T, 25 °C, and pH ~ 7.4. With three coordinated-water molecules both of the complexes showed sufficient thermodynamic stability, and could be used as future T_1-weighted contrast agents. Due to lower value of osmolality and viscosity of neutral MRI contrast agents; complex **3A** has advantages over ionic contrast agents. They can be injected in large dosages in less time. While, cationic complex **3B** could be used to detect the variation of negatively charged glycosaminoglycans (GAGs) present in cartilage; to diagnose the earlier stages of Osteoarthritis (OA).

In search of safer alternative to Gd(III)-based contrast agents, complex **4B** offered longitudinal relaxivity value of 2.90 $mM^{-1}s^{-1}$ at 1.41 T, 25 °C, and pH ~ 7.4; and showed impressive thermodynamic stability (pMn = 7.70). With lipophilic piperidine ligand backbone this complex holds promise as a suitable alternative in case of patients having severe renal problems.

Looking forward to bio-friendly efficient T_1-weighted contrast agents, L-alanine based complex **5A** offered impressive longitudinal relaxivity value of 3.02 $mM^{-1}s^{-1}$ at 1.41 T, 25 °C, and pH ~ 7.4. With one coordinated-water molecule, complex **5A** possessed impressive thermodynamic stability (pMn = 8.06). Thus, complex **5A** can be used as positive contrast agent with better contrast efficiency.

Seven-coordinate Mn(II) complex, **6A** offered significant thermodynamic stability (pMn = 9.00) compared to already reported analogous Mn(II)-based contrast agents with one inner-sphere water molecule. In aqueous solution, the neutral complex showed high efficiency with longitudinal relaxivity value of 3.74 $mM^{-1}s^{-1}$ at 1.41 T, 25 °C, and pH ~ 7.4; which is almost equivalent to clinically used Gd(III)-based contrast agents.

The results included in this thesis recommended these new Gd(III) and Mn(II) complexes as possible candidature for T_1-weighted MRI contrast agents. In addition to described complexes, the following ligand frameworks could be also synthesized and studied as positive MRI contrast agents.

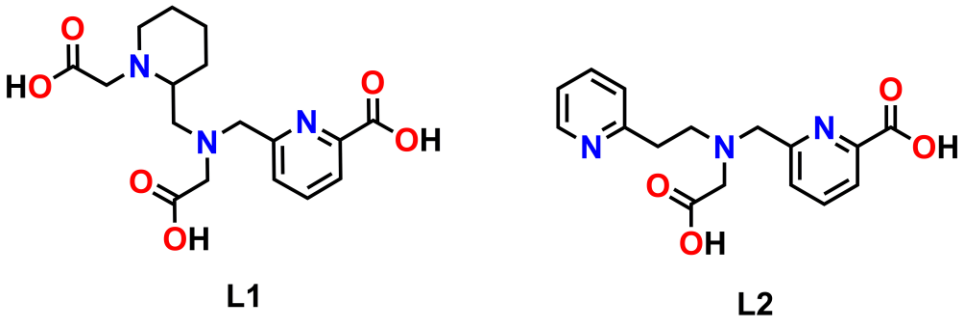

Scheme. *Proposed ligands for the synthesis of new MRI contrast agents.*

Chapter VII

Equipment and Experimental Section

7.1 Methods and Equipments:

Chemicals and Solvents

All the chemicals and solvents were obtained from commercial sources and were used as supplied, unless noted otherwise.

Infrared Spectroscopy

Solid state FTIR spectra were recorded (4000-400 cm^{-1}) on 'Perkin Elmer Instrument' at room temperature. The pellet has been made by grinding the sample with IR grade KBR powder.

NMR Spectroscopy

^{1}H and ^{13}C-NMR spectra were recorded by using 'Varian Mercury plus 400 MHz' and 'Bruker AscendTm 600 MHz' nuclear magnetic resonance (NMR) spectrometer 298 K. Chemical shifts, δ (in ppm), were reported relative to TMS [δ (^{1}H) 0.0 ppm, δ (^{13}C) 0.0 ppm] which was used as internal standard. Otherwise, the solvent residual proton and carbon resonance were taken as references [For $CDCl_3$, δ (^{1}H) 7.26 ppm, and δ (^{13}C) 77.2 ppm; for CD_3OD δ (^{1}H) 3.31, 4.87 ppm, and δ (^{13}C) 49.0 ppm; for D_2O δ (^{1}H) 4.79 ppm]. The resultant spectra were drawn by using 'MestReNova' NMR data processing software.

Mass Spectrometry

Mass spectra were recorded on QTOF-MS Spectrometer ('Waters, Model: Q-Tof Premier') or 'Agilent Accurate-Mass Q-TOF LC/MS 6520' spectrometer and peaks were given in *m/z* (% of basis peak). HPLC grade CH_3CN, CH_3OH and Milli Q water were used as solvents for taking the mass spectra.

Single Crystal X-ray Crystallography

Single crystal suitable for X-ray diffraction study was obtained from evaporation of water at room temperature (25 °C). X-ray crystallographic data were collected by using a 'Super Nova, Single source at offset, Eos diffractometer'. Structures were solved by direct methods using either SHELXS-97 or Siemens ShelXTL software packages and refined with full-matrix least squares on F^2 using these softwares. All the non-hydrogen atoms were refined anisotropically.

UV-Vis Spectroscopy

The electronic absorption spectrum of the sample(s) was recorded on a 'Perkin Elmer, Lamda 25, UV/Vis spectrometer' in Mili Q water using cuvette of 1 cm width.

X-band EPR Spectroscopy

First derivative X-band EPR spectra of powdered or solution samples were measured with 'JEOL JES-FA200 Spectrometer'. The resulting data was simulated by using W95EPR-program written by Frank Neese (MPI for Bioinorganic Chemistry, Mülheim, and University of Bonn).

Potentiometric Titration

Potentiometric measurements were carried out in 'Metrhom 888 Titrando' workstation combined with 'Metrhom 6.0259.100 glass electrode'. **T**he number the protonation constants of the ligands, and the stability constant of the metal complexes were determined by potentiometric titrations at a constant ionic strength by using 0.1 M KCl at 25 °C, against standardised 0.1 M NaOH as the titrant. The protonation and stability constants were evaluated using base mL-pH data pairs obtained in the pH range 2-12, using Hyperquad2008.

Luminescence Lifetime Measurements

Lanthanide luminescence lifetime measurements were accomplished on 'FluoroMax-4 spectrofluorimeter (Horiba)'. The solutions were excited with a pulsed Xenon lamp having pulse width of ~ 3 μs, and time per pulse of 61 ms. Luminescence decay curves were generated by 'decay by delay' method with an initial delay of 0.1 ms and maximum delay up to 20 ms.

Relaxivity Measurements

The longitudinal relaxation times at 1.41 T, were measured using 'BRUKER minispec mq60NMR Analyzer' at 25 °C, and 37 °C.

Inversion Recovery Method

In this method, the spin at equilibrium position is first exposed to a 180° pulse which inverts the magnetization M_0 to its opposite direction and becomes antiparallel to the direction of applied

magnetic field. After a delay time, known as inversion recovery time (TI), the system is exposed to another 90° pulse. During this delay time, the magnetization starts to recover to its original position, which becomes observable in xy-plane upon application of another 90° pulse. A schematic representation of the method is shown **Figure 7.1**.

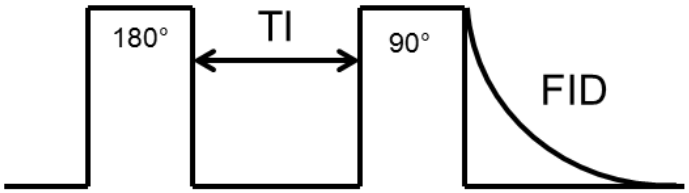

Figure 7.1. *Pulse sequence in inversion recovery method.*

Saturation Recovery Method

In this method, the spin system in the equilibrium position is first exposed to a 90° pulse which tips down the magnetization in xy-plane. After a delay time known as repetition time (TR), the system is exposed to another 90° pulse which again pushes the magnetization to xy-plane where FID is monitored. During this delay time (TR), the magnetization starts to recover to its original position, which is detected in xy-plane upon application of another 90° pulse. A schematic representation of the method is shown in **Figure 7.2**.

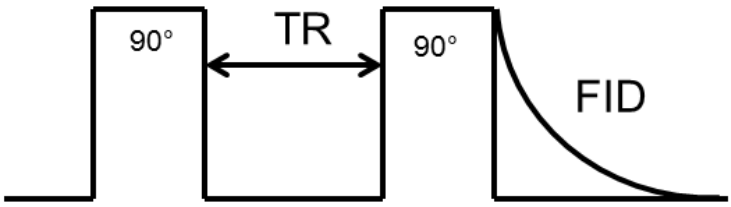

Figure 7.2. *Pulse sequence in saturation recovery method.*

7.2 Experimental Section:

7.2.1 Synthesis of Ligand Li_3cbda:

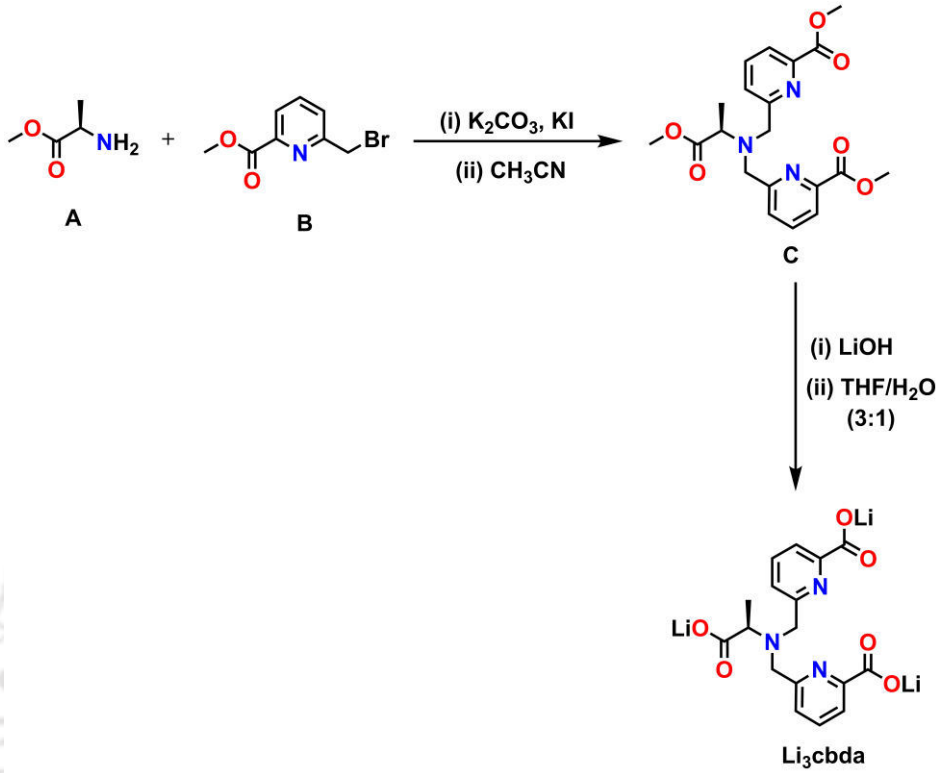

Scheme 7.1. *Synthetic route of ligand* ***Li_3cbda****.*

Synthesis of [$C_4H_9NO_2$], (A): To a stirred solution of L-alanine (0.490 g, 5.50 mmol) in 15 mL of dry MeOH under nitrogen atmosphere, $SOCl_2$ (0.60 mL, 8.25 mmol) was added dropwise under cooled condition. Then, the reaction mixture was allowed to stir at room temperature for 24 h. The solvent was completely evaporated *in vacuo*, providing white solid compound as product after washing several times with diethyl ether.

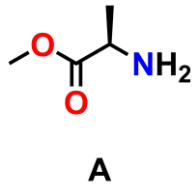

Yield = 0.495 g, 87%.

FTIR (KBR, cm^{-1}): 3548, 2958, 1745, 1630, 1517, 1462, 1441, 1391, 1374, 1331, 1255, 1214, 1118, 1011, 975, 905, 843, 756.

^{1}H-NMR ($CDCl_3$, 600.17 MHz): δ 8.69 (s, 2H), 4.26 (q, J = 6.0 Hz, 1H), 3.82 (s, 3H), 1.72 (d, J = 6.0 Hz, 3H) ppm.

ESI-MS (+) *m/z* for $[C_4H_9NO_2 + H]^+$: clacd, 104.0706; found 104.0706.

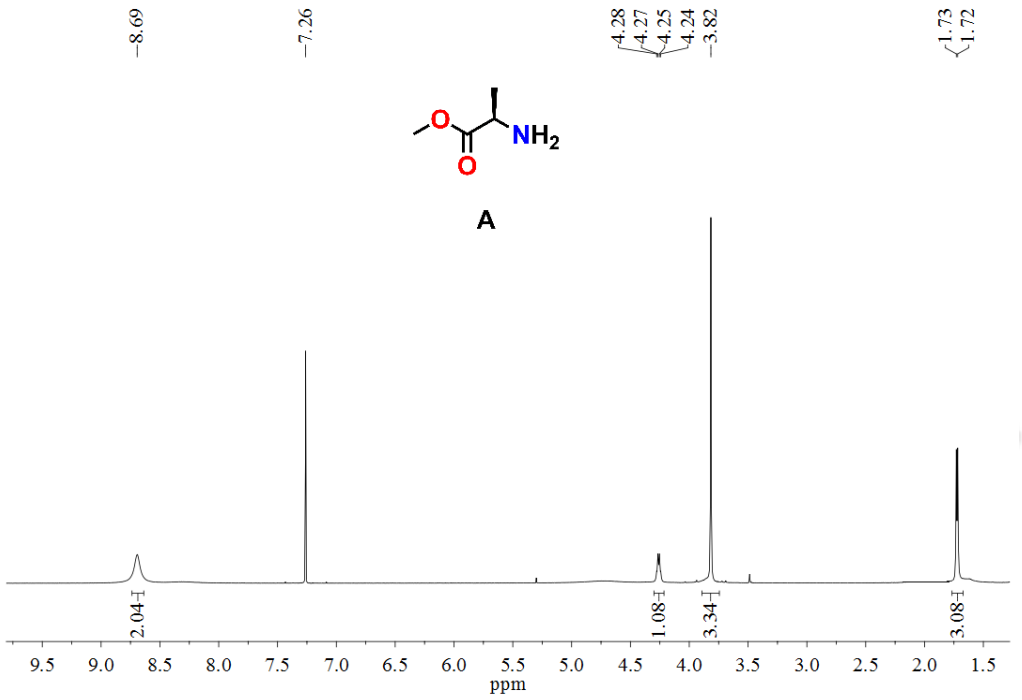

Figure 7.3. *^{1}H-NMR spectrum of $[C_4H_9NO_2]$, (**A**).*

Synthesis of [$C_8H_8BrNO_2$], (B): Synthesis of methyl 6-(bromomethyl)picolinate, **B** involved the following steps,

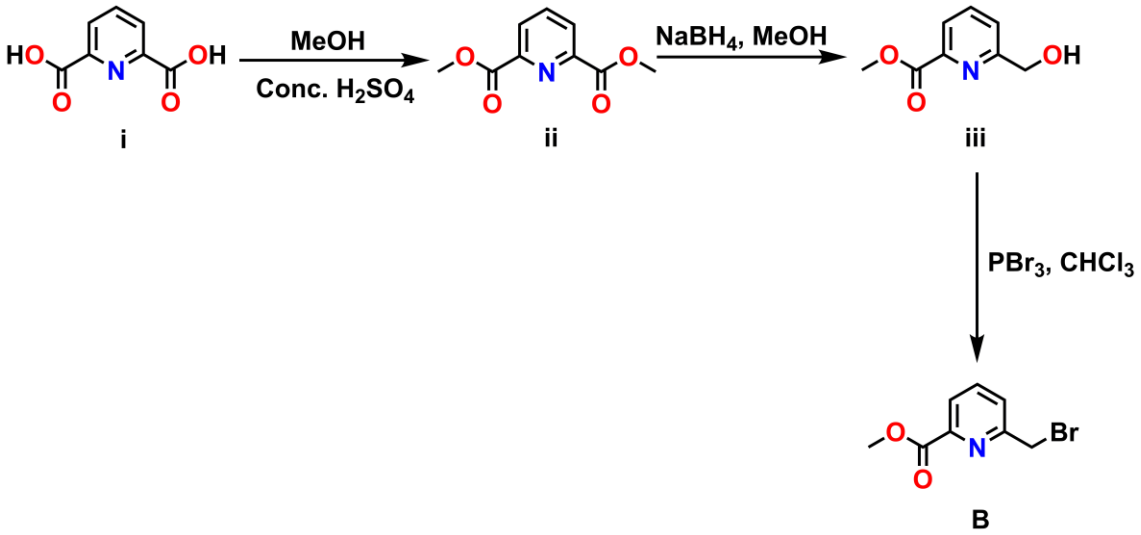

Scheme 7.2. *Synthetic route of 6-(bromomethyl)picolinate, (**B**).*

Synthesis of [$C_9H_9NO_4$], (ii): To a stirred solution of pyridine-2,6-dicarboxylic acid, (**i**) (3.342 g, 20.00 mmol) in 45 mL of methanol under inert atmosphere, conc. H_2SO_4 (4.5 mL) was added dropwise at 0 °C. Then, the reaction mixture was refluxed for 48 h. After that, the reaction mixture was allowed to cool down to room temperature, and kept as such for 1.5 h. White crystalline compounds appeared from the reaction mixture, which was filtered, washed thoroughly with water.

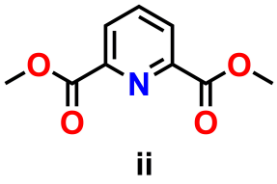

ii

Yield = 3.24 g, 83%.

FTIR (KBR, cm^{-1}): 3451, 3063, 2968, 2925, 2854, 1742, 1572, 1450, 1438, 1290, 1246, 1197, 1165, 1145, 1081, 997, 952, 813, 758, 723.

^{1}H-NMR ($CDCl_3$, 600.17 MHz): δ 8.32 (d, J = 12.0 Hz, 2H), 8.03 (t, J = 6.0 Hz, 1H), 4.03 (s, 6H) ppm.

ESI-MS (+) *m/z* for $[C_9H_9NO_4 + H]^+$: calcd, 196.0604; found, 196.0619.

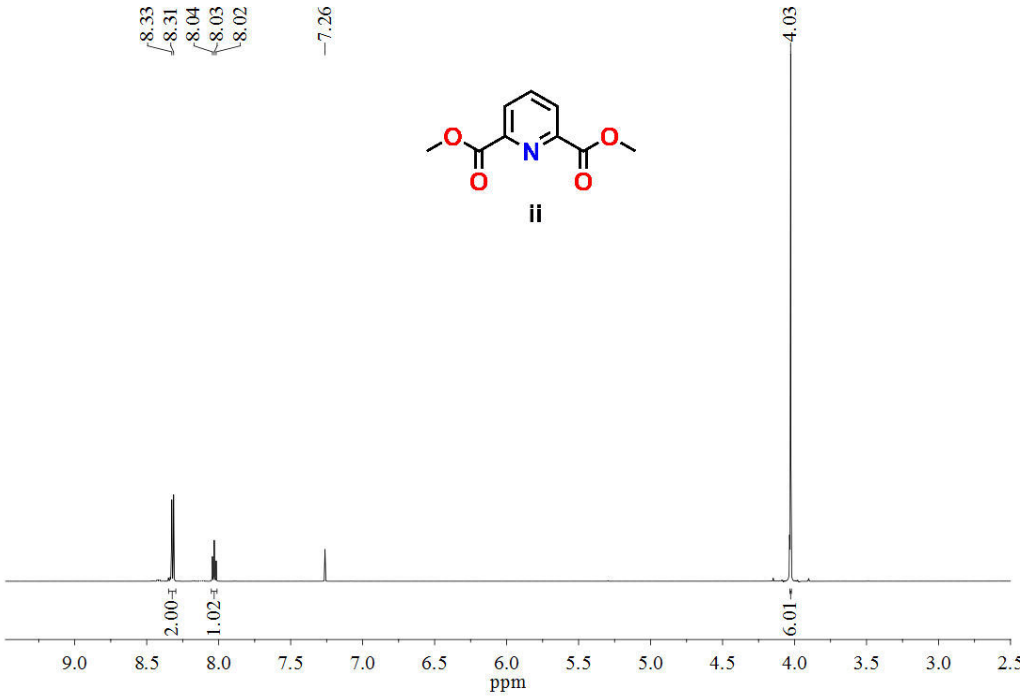

Figure 7.4. *^{1}H-NMR spectrum of $[C_9H_9NO_4]$,* ***(ii)****.*

Synthesis of $[C_8H_9NO_3]$, (iii): To a stirred solution of dimethyl pyridine-2,6-dicarboxylate, (**ii**) (1.307 g, 6.70 mmol) in 10 mL of methanol under inert atmosphere at 0 °C, $NaBH_4$ (0.385 g, 10.05 mmol) was added in small portions. The reaction mixture was then stirred at room temperature for 5 h. After complete evaporation of solvent, saturated aqueous $NaHCO_3$ (15 mL) solution was added to the residue. The aqueous solution was then extracted with $CHCl_3$ (3 × 15 mL), organic layer was dried over Na_2SO_4, and filtered. The filtrate was concentrated to dryness to obtain white solid compound, which was further purified by column chromatography on silica gel by using ethyl acetate/hexane (1:1) as the eluent.

iii

Yield = 0.685 g, 61.20%.

FTIR (KBR, cm^{-1}): 3926, 2955, 2909, 1746, 1592, 1469, 1449, 1294, 1217, 1196, 1148, 1163, 1093, 1072, 1000, 984, 870, 826, 762, 714, 673.

^{1}H-NMR ($CDCl_3$, 600.17 MHz): δ 8.04 (d, J = 6.0 Hz, 1H), 7.85 (t, J = 6.0 Hz, 1H), 7.54(d, J = 6.0 Hz, 1H), 4.87 (s, 2H), 4.00 (s, 3H) ppm.

ESI-MS (+) *m/z* for $[C_8H_9NO_3 + H]^+$: calcd, 168.0655; found, 168.0657.

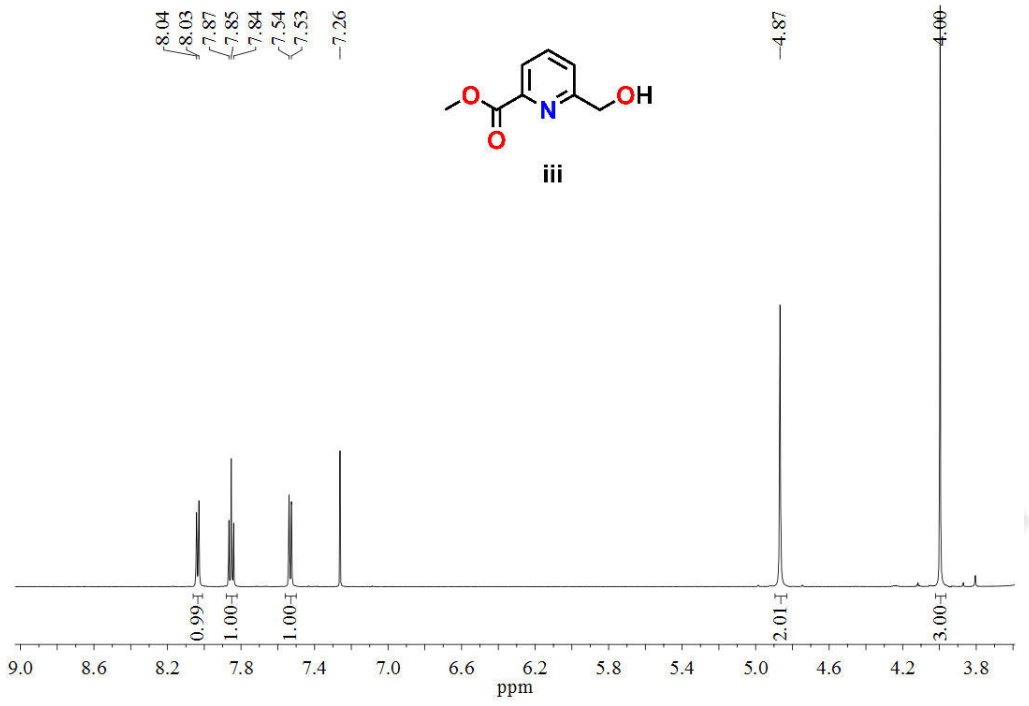

Figure 7.5. *^{1}H-NMR spectrum of $[C_8H_9NO_3]$,* ***(iii).***

Synthesis of $[C_8H_8BrNO_2]$, (B): To a stirred solution of 6-(methoxycarbonyl)picolinic acid, **(iii)** (0.870 g, 5.20 mmol) in 15 mL of $CHCl_3$, under nitrogen atmosphere at 0 °C, PBr_3 (0.50 mL, 5.20 mmol) was added dropwise. The stirring was continued at room temperature for 12 h. The reaction mixture was quenched by using aqueous $NaHCO_3$ solution (15 mL), and extracted with CH_2Cl_2 (3 × 15 mL). The organic part was dried over Na_2SO_4, and filtered. The filtrate was concentrated to complete dryness to obtain off-white solid compound, which was purified by column chromatography on silica gel using ethyl acetate/hexane (1:3) as the eluent.

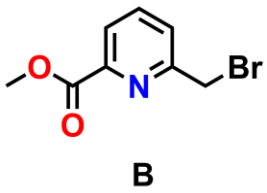

B

Yield = 0.718 g, 60%.

FTIR (KBR, cm^{-1}): 3458, 3062, 3040, 2981, 2951, 1739, 1587, 1441, 1424, 1300, 1238, 1238, 1221, 1198, 1172, 1149, 1086, 993, 895, 838, 796, 770, 744, 670, 627, 582.

^{1}H-NMR ($CDCl_3$, 600.17 MHz): δ 8.06 (d, J = 6.0 Hz, 1H), 7.87 (t, J = 6.0 Hz, 1H), 7.70 (d, J = 6.0 Hz, 1H), 4.65 (s, 2H), 4.02 (s, 3H) ppm.

ESI-MS (+) m/z for $[C_8H_9BrNO_2 + H]^+$: calcd, 229.9811; found, 229.9815.

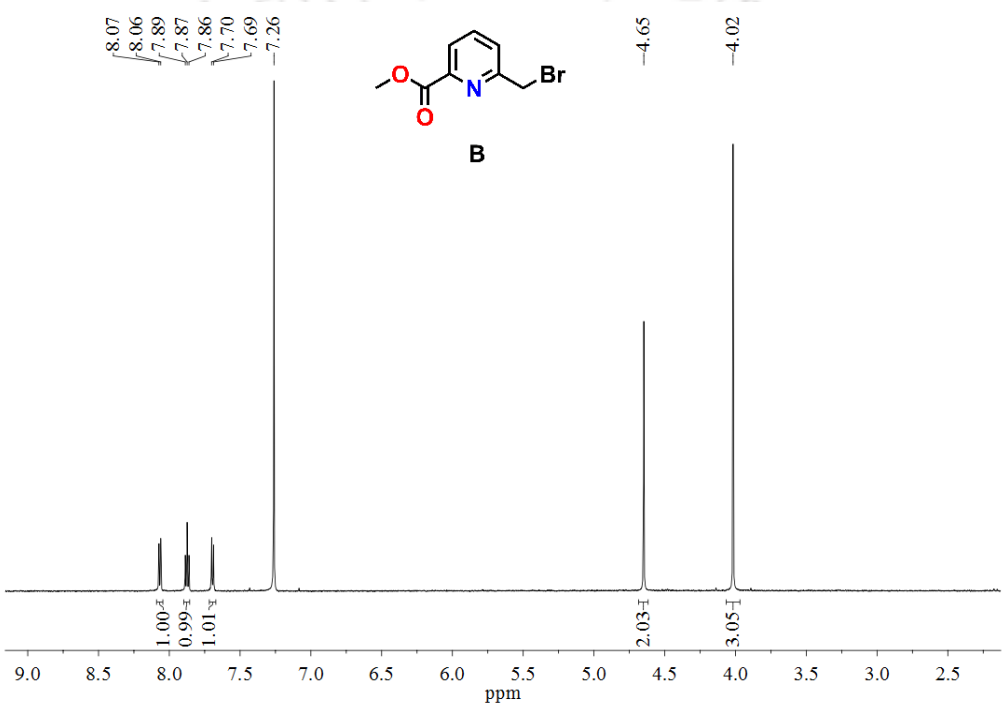

Figure 7.6. *^{1}H-NMR spectrum of $[C_8H_9BrNO_2]$,* ***(B).***

Synthesis of [$C_{20}H_{23}N_3O_6$], (C): Methyl 6-(bromomethyl)picolinate, **B** (1.520 g, 6.60 mmol), K_2CO_3 (1.660 g, 12.00 mmol), and KI (1.106 g, 6.60 mmol) were added to a stirred solution of compound **A** (0.309 g, 3.00 mmol) in dry acetonitrile (20 mL), under nitrogen atmosphere. The resulting solution was stirred at room temperature for 1 h, and then at 50 °C for 4 days. Then, the reaction mixture was filtered, and the filtrate was concentrated to dryness. Water (15 mL) was added to it, and extracted with $CHCl_3$ (3 × 20 mL). The organic phase was dried over Na_2SO_4, and concentrated *in vacuo* to obtain the crude product as brownish liquid. The pure compound was obtained as light-yellow solid by column chromatography on silica gel using ethyl acetate/hexane (3:2) as the eluent.

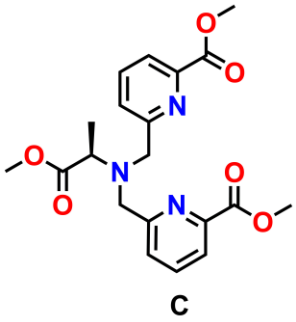

C

Yield = 0.633, 52%.

FTIR (KBR, cm^{-1}): 3439, 2956, 1734, 1632, 1591, 1516, 1460, 1442, 1356, 1313, 1255, 1224, 1141, 1113, 1084, 1056, 978, 894, 812, 766.

^{1}H-NMR ($CDCl_3$, 600.17 MHz): δ 7.96 (d, J = 6.0 Hz, 2H), 7.84 (d, J = 6.0 Hz, 4H), 7.78 (t, J = 18.0 Hz, 4H), 4.10 (t, J = 18.0 Hz, 4H), 3.98 (s, 6H), 3.73 (s, 3H), 3.60 (q, J = 6.0 Hz, 1H), 1.40 (d, J = 6.0 Hz, 3H) ppm.

^{13}C-NMR ($CDCl_3$, 150.93 MHz): δ 176.04, 166.25, 159.58, 147.73, 137.71, 125.60, 125.53, 56.63, 53.26, 53.07, 52.12, 19.19 ppm.

ESI-MS (+) *m/z* for $[C_{20}H_{23}N_3O_6 + H]^+$: calcd, 402.1660; found, 402.1690.

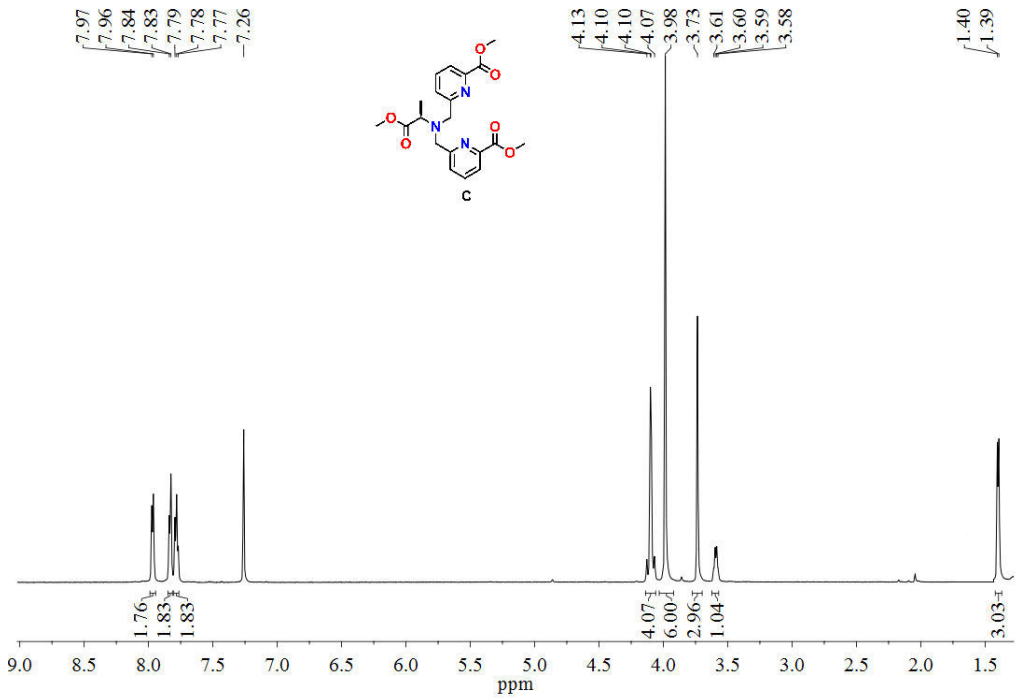

Figure 7.7. *^{1}H-NMR spectrum of [$C_{20}H_{23}N_3O_6$], (**C**).*

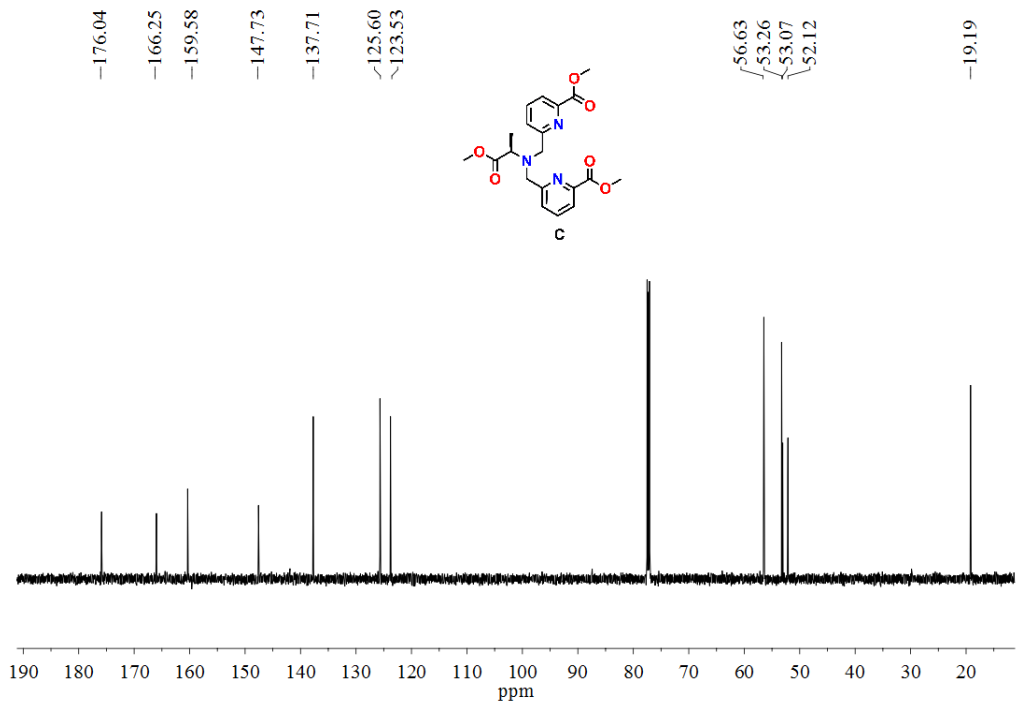

Figure 7.8. *^{13}C-NMR spectrum of [$C_{20}H_{23}N_3O_6$], (**C**).*

Synthesis of $[C_{17}H_{14}N_3O_6Li_3]$, (Li_3cbda): To a solution of compound **C** (0.288 g, 0.70 mmol) in 6 mL of THF, LiOH (0.051 g, 2.10 mmol in 2 mL H_2O) was added, and stirred at room temperature for 24 h. The reaction mixture was neutralized by adding 1 N HCl solution. The ligand was obtained as a yellowish solid by complete removal of the solvent.

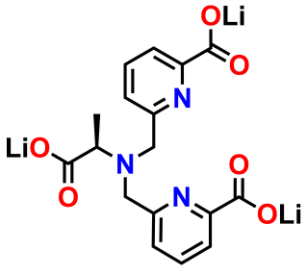

Li_3cbda

Yield = 0.232 g, 88%.

FTIR (KBR, cm^{-1}): 3472, 2978, 1618, 1588, 1465, 1443, 1404, 1280, 1265, 1188, 1164, 1083, 1008, 938, 776, 725, 682, 440.

^{1}H-NMR (CD_3OD, 600.17 MHz): δ 7.96 (d, J = 6.0 Hz, 2H), 7.86 (t, J = 6.0 Hz, 2H), 7.58 (d, J = 12.0 Hz, 2H), 4.36 (s, 4H), 3.74 (q, J = 6.0 Hz, 1H), 1.52 (d, J = 6.0 Hz, 3H) ppm.

^{13}C-NMR (CD_3OD, 150.93 MHz): δ 178.54, 170.62, 157.15, 153.35, 138.28, 125.08, 123.01, 61.24, 55.44, 11.75 ppm.

ESI-MS (+) *m/z* for $[C_{17}H_{14}N_3O_6Li_3 + H]^+$: calcd, 378.16; found, 378.16.

7.2.2 Synthesis of Ligand H_2hbda:

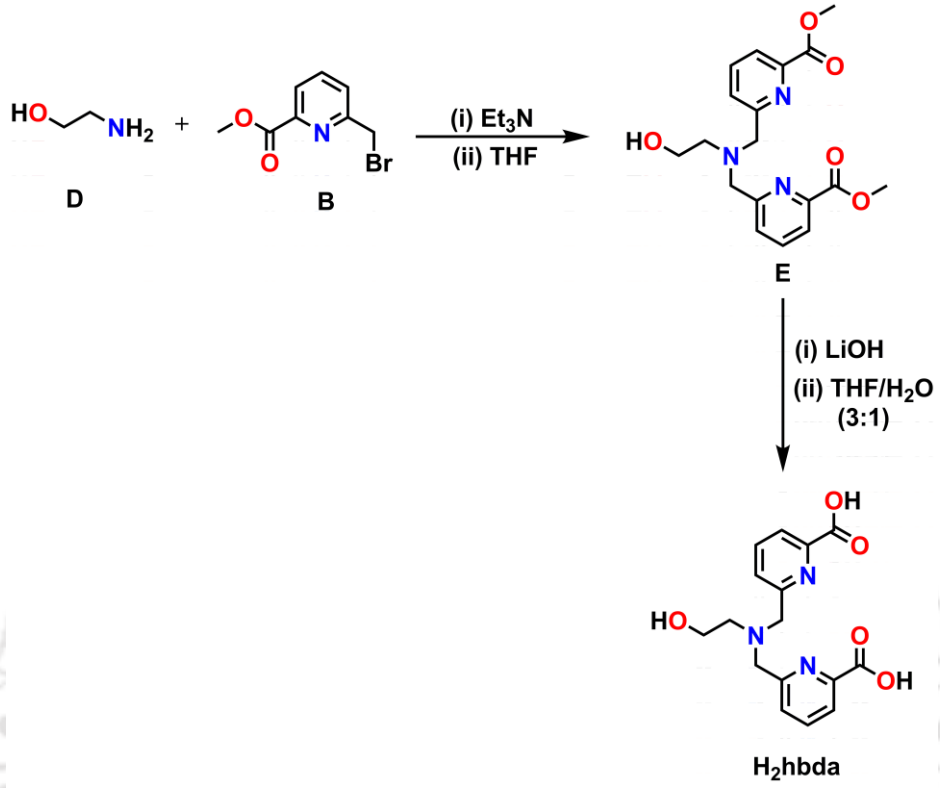

Scheme 7.3. *Synthetic route of ligand* ***H_2hbda****.*

Synthesis of [$C_{18}H_{21}N_3O_5$], (E): 2-aminoethan-1-ol, **D** (0.275 g, 4.50 mmol), and Et_3N (1.37 mL, 9.90 mmol) were added to a solution of methyl-6-(bromomethyl)picolinate, **B** (2.27 g, 9.90 mmol) in THF (20 mL). The mixture was allowed to stir for a period of 24 h at room temperature. Resultant solution was concentrated to dryness; the oily residue was extracted with H_2O/CH_2Cl_2 (1:3) mixture. The organic phase was evaporated to dryness to give a yellowish liquid, which was purified by column chromatography on silica with methanol/ethylacetate (gradient = 1%) mixture as the eluent to give compound **E** as white solid.

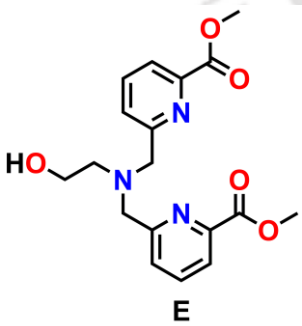

Yield = 0.725 g, 45%.

FTIR (KBr pellet cm^{-1}): 3358, 3088, 2988, 2948, 2869, 2809, 1738, 1722, 1591, 1440, 1370, 1346, 1324, 1305, 1287, 1269, 1226, 1202, 1191, 1163, 1140, 1082, 1066, 1039, 978, 962, 909, 888, 829, 791, 767, 719, 679, 627, 534.

^{1}H-NMR ($CDCl_3$, 600.17 MHz): δ 7.98 (d, J = 6 Hz, 2H), 7.73 (t, J = 6 Hz, 2H), 7.58 (d, J = 6 Hz, 2H), 4.04 (s, 4H), 4.01 (s, 6H), 3.70 (t, J = 6 Hz, 2H), 2.90 (t, J = 6 Hz, 2H) ppm.

^{13}CNMR ($CDCl_3$, 101 MHz): δ 165.11, 159.73, 146.75, 137.03, 125.85, 123.15, 59.74, 59.30, 56.92, 52.44 ppm.

ESI-MS (+) *m/z* for $[C_{18}H_{21}N_3O_5 + H]^+$: calcd, 360.1554; found, 360.1558.

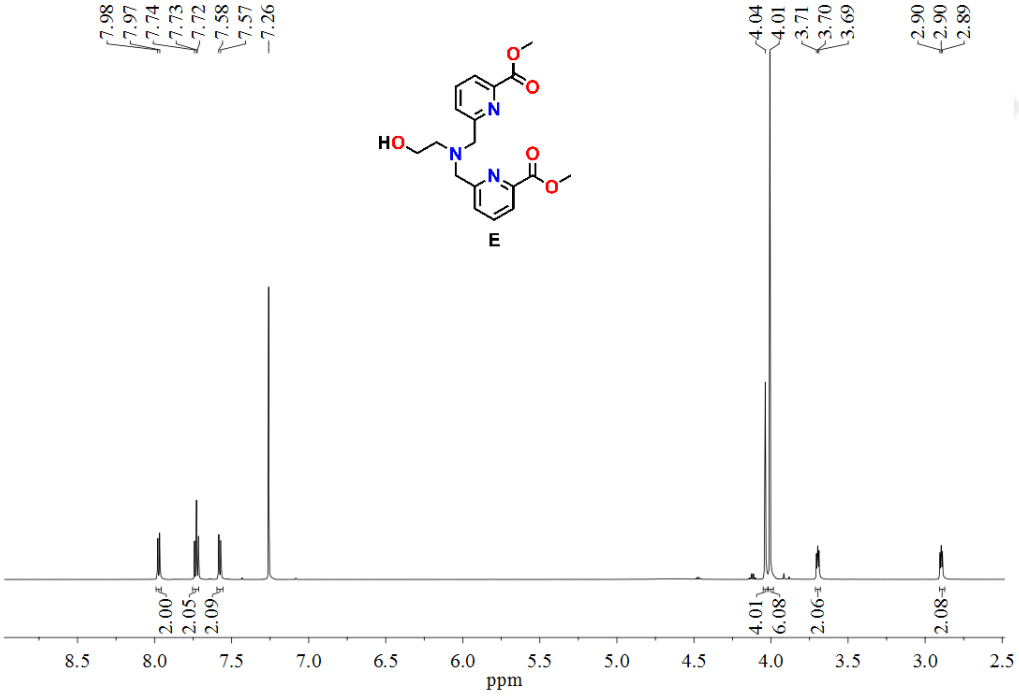

Figure 7.9. *^{1}H-NMR spectrum of $[C_{18}H_{21}N_3O_5]$, (**E**).*

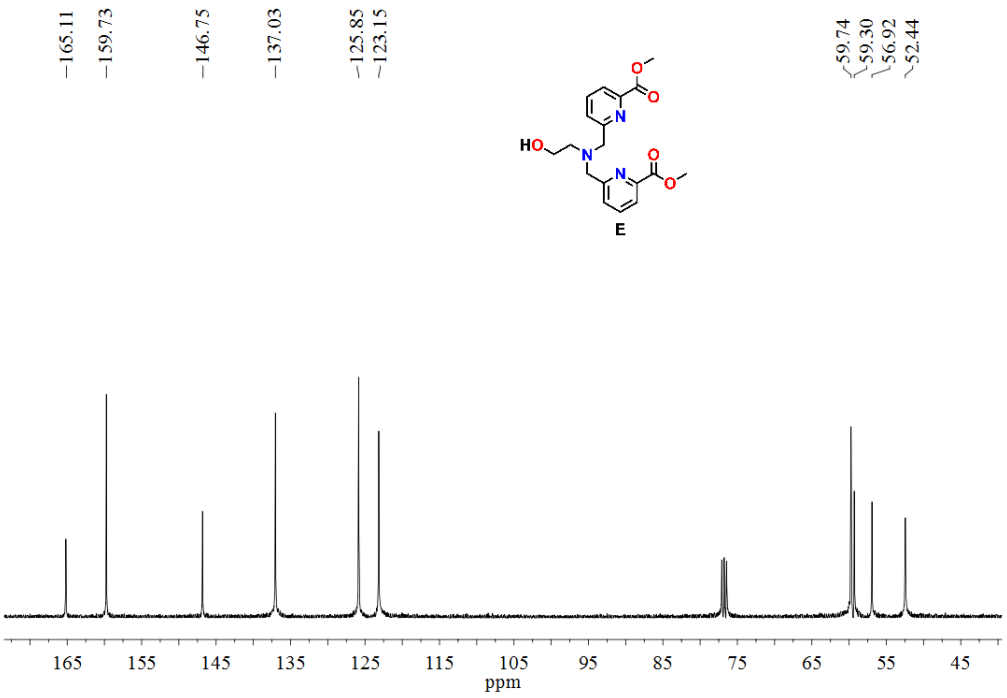

Figure 7.10. *^{13}C-NMR spectrum of [$C_{18}H_{21}N_3O_5$], (**E**).*

Synthesis of [$C_{16}H_{17}N_3O_5$], (H_2hbda): To a solution of compound **E** (0.359 g, 1.00 mmol) in THF (6 mL), LiOH (0.051 g, 2.10 mmol in 2 mL H_2O) was added, and stirred at room temperature for 24 h under dark. The reaction mixture was then neutralized by adding 1 N HCl solution. The ligand was obtained as dilithium salt after complete evaporation of solvents followed by washing with diethyl ether.

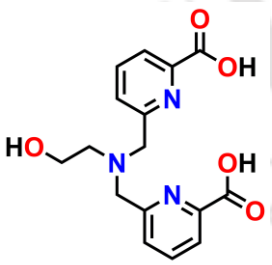

H_2hbda

Yield = 0.275 g, 83%.

FTIR (KBr pellet cm^{-1}): 3405, 3182, 2965, 2922, 2852, 2809, 1651, 1616, 1589, 1461, 1438, 1402, 1378, 1307, 1291, 1267, 1183, 1158, 1149, 1086, 1070, 1060, 1005, 805, 779, 770, 727, 680, 514.

^{1}H-NMR (D_2O, 600.17 MHz): δ 7.76 (t, J = 6 Hz, 2H), 7.71 (d, J = 6 Hz, 2H), 7.46 (d, J = 6 Hz, 2H), 3.92 (s, 4 H), 3.74 (t, J = 6 Hz, 2H), 2.86 (d, J = 6 Hz, 2H) ppm.

^{13}C-NMR (D_2O, 150.93 MHz): δ 173.03, 157.36, 152.36, 138.20, 126.16, 122.12, 59.10, 58.68, 56.29 ppm.

ESI-MS (+) *m/z* for $[C_{16}H_{17}N_3O_5 + H]^+$: calcd, 332.1241; found, 332.1245.

7.2.3 Synthesis of Ligand H_3cpmda:

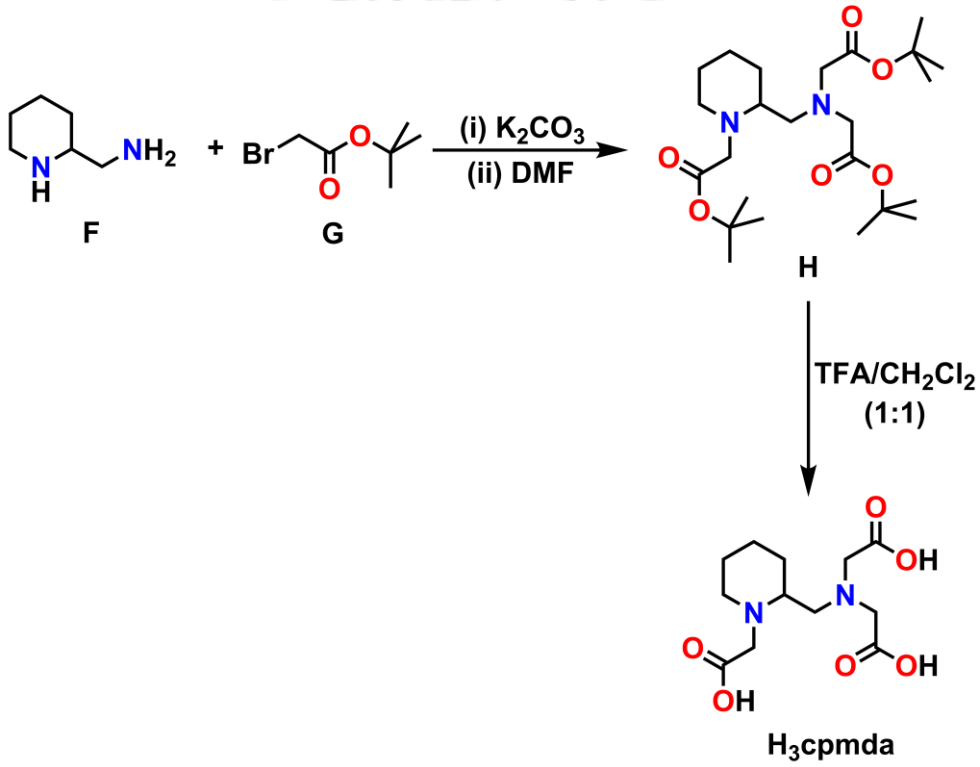

Scheme 7.4. *Synthetic route of ligand* ***H_3cpmda****.*

Synthesis of [$C_{24}H_{44}N_2O_6$], (H): K_2CO_3 (2.489 g, 18.00 mmol) was added to a stirred solution *tert*-butyl bromoacetate, **G** (2.927 g, 15.00 mmol) in DMF (10 mL). The reaction mixture was cooled to 0 °C, and a solution of piperidin-2-ylmethanamine, **F** (0.343 g, 3.00 mmol) in DMF (1.0 mL) was added drop wise over 10 min. The suspension was then stirred at room temperature for 24 h. After adding saturated $NaHCO_3$ solution brownish residue was extracted with diethyl ether. The organic phase was evaporated to dryness to give an oily residue, which was further purified by column chromatography on silica with hexane/ethyl acetate (5:1) mixture as the eluent to get the compound as light brownish oil.

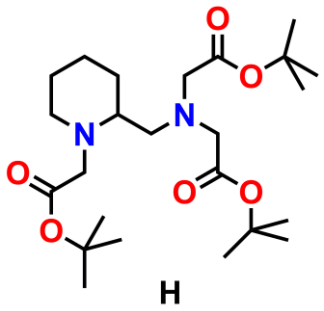

H

Yield = 0.684 g, 50%.

FTIR (KBr pellet cm^{-1}): 3436, 3003, 2978, 2933, 2856, 1732, 1633, 1456, 1393, 1368, 1255, 1218, 1154, 990, 852, 754.

^{1}H-NMR ($CDCl_3$, 600.17 MHz): δ 3.52 (d, J = 18 Hz, 1H), 3.41 (s, 6H), 2.96 (dd, J = 12, 6 Hz, 2H), 2.80 (d, J = 12 Hz, 2H), 2.64-2.67 (m, 2H), 2.58-2.62 (m, 2H), 2.48-2.51 (m, 2H), 1.45 (s, 27H) ppm.

^{13}C-NMR ($CDCl_3$, 150.93 MHz): δ 170.97, 170.65, 80.79, 80.46, 57.73, 57.61, 56.47, 56.26, 53.49, 30.63, 28.18, 28.16, 25.67, 23.66 ppm.

ESI-MS (+) *m/z* for $[C_{24}H_{44}N_2O_6 + H]^+$: calcd, 457.3270; found, 457.3272.

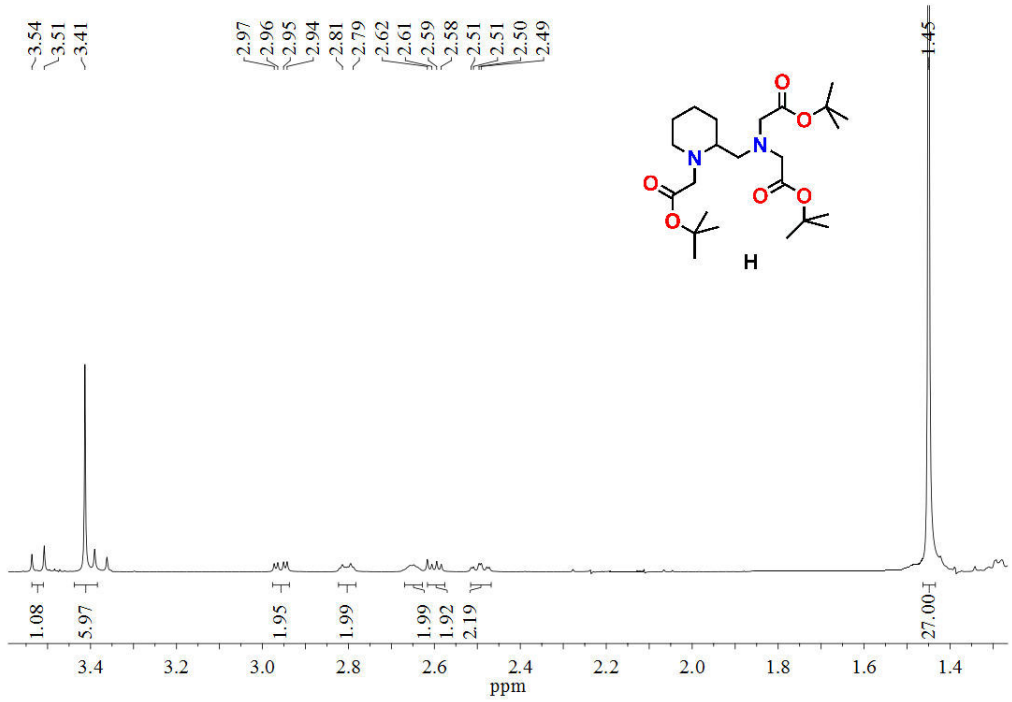

Figure 7.11. *^{1}H-NMR spectrum of [$C_{24}H_{44}N_2O_6$], (**H**).*

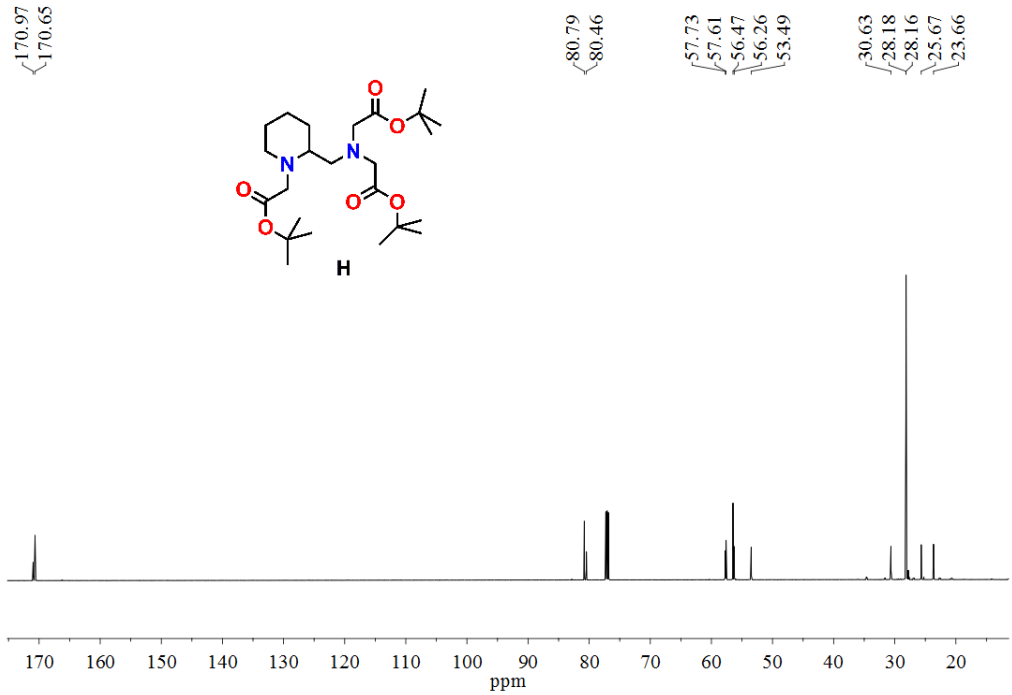

Figure 7.12. *^{13}C-NMR spectrum of [$C_{24}H_{44}N_2O_6$], (**H**).*

Synthesis of [$C_{12}H_{20}N_2O_6$•CF_3COOH], (H_3cpmda): Compound **H** (0.200g, 0.44 mmol) was stirred with 1:1 mixture of TFA/CH_2Cl_2 (4 mL) at room temperature for 72 h. Addition of diethyl ether after complete removal of all the solvents gave the ligand as yellowish hygroscopic solid.

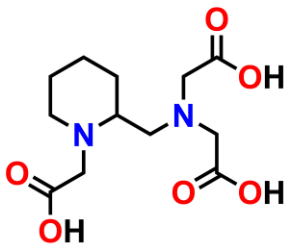

H_3cpmda

Yield = 0.164 g, 93%.

FTIR (KBr pellet cm^{-1}): 3433, 3020, 2960, 2879, 2548, 1729, 1666, 1466, 1421, 1327, 1255, 1196, 1141, 1022, 985, 896, 874, 837, 798, 721, 668.

^{1}H-NMR (C_2D_6SO, 400.17 MHz): 3.50 (s, 6H), 3.09-3.06 (m, 2H), 2.86 (d, J = 12 Hz, 1H), 1.71-1.63 (m, 6H), 1.52-1.41 (m, 2H) ppm.

^{13}C-NMR (CD_3OD, 150.93 MHz): 169.20, 49.85, 49.57, 28.34, 28.21, 23.65, 23.57 (two coincidental signals), 162.84 (q, J_{C-F} = 35 Hz, CF_3COO), 118.15 (q, J_{C-F} = 293 Hz, CF_3COO) ppm.

ESI-MS (+) *m/z* for $[C_{12}H_{20}N_2O_6 + H]^+$: calcd, 289.1394; found, 289.1395.

7.2.4 Synthesis of Complex 3A:

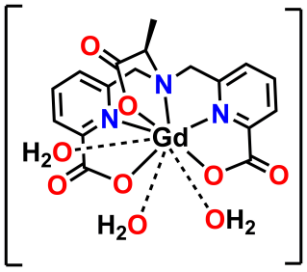

[Gd(cbda)(H_2O)$_3$], 3A

To an aqueous solution of ligand **Li_3cbda** (0.189 g, 0.50 mmol), $GdCl_3$•xH_2O (0.126 g, 0.48 mmol) was added and stirred for 15 minutes till the solution became clear. The pH of the reaction mixture was adjusted to ~ 6.5 by adding aqueous NaOH solution dropwise; followed by continuous stirring at room temperature for 24 h. Resultant solution was filtered and white solid product was obtained after complete evaporation of the filtrate.

Yield = 0.092 g, 34 %.

FTIR (KBr pellet cm^{-1}): 3421, 2928, 1650, 1626, 1596, 1470, 1439, 1408, 1377, 1273, 1160, 1134, 1118, 1085, 1017, 775, 689.

ESI-MS (+) *m/z* for $[C_{17}H_{14}N_3O_6Gd + H]^+$: calcd, 515.0153; found, 515.005.

7.2.5 Synthesis of Complex 3B:

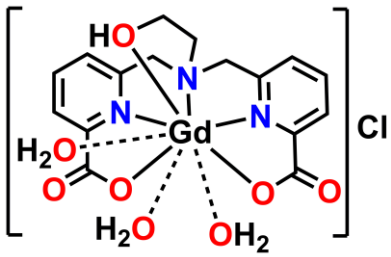

$[Gd(hbda)(H_2O)_3]Cl$, 3B

To an aqueous solution of ligand **H_2hbda** (0.127 g, 0.38 mmol), $GdCl_3 \bullet xH_2O$ (0.090 g, 0.34 mmol) was added, and kept on stirring until the solution became transparent. Then, pH of the reaction medium was adjusted to ~ 6.5 by adding aqueous NaOH solution dropwise; followed by continuous stirring at room temperature for 24 h. Resultant solution was filtered, and white solid product was obtained after complete evaporation of the filtrate.

Yield = 0.070 g, 38 %.

FTIR (KBr pellet cm^{-1}): 3436, 2851, 2829, 1624, 1591, 1468, 1444, 1406, 1378, 1279, 1226, 1188, 1156, 1116, 1093, 1046, 1012, 974, 955, 942, 812, 775, 690.

ESI-MS (+) *m/z* for $[C_{16}H_{15}N_3O_5Gd]^+$: calcd, 487.0209; found, 487.0291.

7.2.6 Synthesis of Complex 3C:

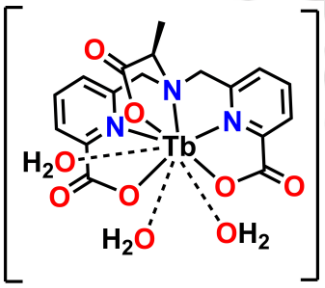

$[Tb(cbda)(H_2O)_3]$, 3C

To an aqueous solution of ligand **Li_3cbda** (0.192 g, 0.51 mmol), $TbCl_3 \bullet 6H_2O$ (0.182 g, 0.49 mmol) was added and kept on stirring till it became transparent. The pH of the solution was adjusted to ~ 6.5 by adding aqueous NaOH solution dropwise, and continued to stir at room temperature for 24 h. Reaction mixture was filtered, and white crystalline product was obtained on complete evaporation of solvent. The obtained complex was washed thoroughly with MeOH to remove excess ligand and Tb(III) salt.

Yield = 0.145 g, 52 %.

FTIR (KBr pellet cm^{-1}): 3425, 1626, 1592, 1470, 1441, 1407, 1385, 1263, 1190, 1159, 1138, 1086, 1017, 876, 774, 686.

ESI-MS (+) *m/z* for $[C_{17}H_{14}N_3O_6Tb + H]^+$: calcd, 516.0209; found, 516.0248.

7.2.7 Synthesis of Complex 3D:

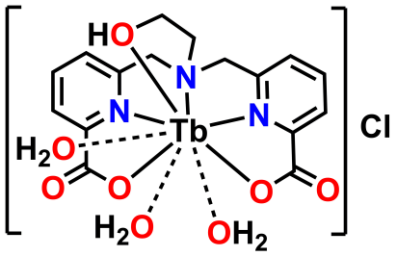

[Tb(hbda)(H$_2$O)$_3$]Cl, 3D

To an aqueous solution of ligand **H$_2$hbda** (0.120 g, 0.36 mmol), $TbCl_3 \bullet 6H_2O$ (0.125 g, 0.35 mmol) was added, and kept on stirring till it became transparent. The pH of the solution was adjusted to ~ 6.5 by adding aqueous NaOH solution dropwise, and continued to stir at room temperature for 24 h. Reaction mixture was filtered, and white crystalline product was obtained on complete evaporation of solvent. The obtained complex was washed thoroughly with MeOH to remove excess ligand and Tb(III) salt.

Yield = 0.085 g, 45 %.

FTIR (KBr pellet cm^{-1}): 3413, 1623, 1591, 1472, 1447, 1409, 1280, 1224, 1191, 1158, 1116, 1085, 1017, 812, 774, 689.

ESI-MS (+) *m/z* for $[C_{16}H_{15}N_3O_5Tb]^+$: calcd, 488.0265; found, 488.0313.

7.2.8 Synthesis of Complex 4A:

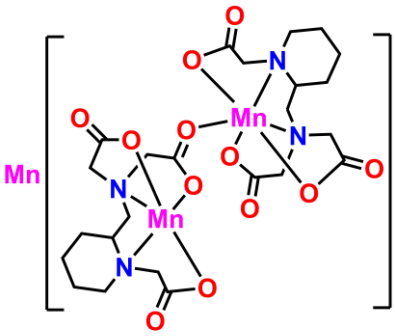

Mn[Mn$_2$(cpmda)$_2$], 4A

To an aqueous solution of ligand **H$_3$cpmda** (0.244 g, 0.60 mmol), $MnCl_2 \bullet 4H_2O$ (0.114 g, 0.58 mmol) was added, and allowed to stir for 15 min until it became transparent. The pH of the reaction medium was adjusted to ~ 6.5 by adding aqueous NaOH solution, and stirring was continued for 24 h at room temperature. Then, the reaction mixture was filtered off, and

filtrate gave colourless crystals of complex **4A** on slow solvent evaporation method.

Yield = 0.129 g, 42%.

FTIR (KBr pellet cm^{-1}): 3403, 2944, 2869, 1676, 1574, 1409, 1335, 1311, 1288, 1202, 1174, 1141, 1101, 1066, 1006, 980, 946, 844, 803, 783, 731.

ESI-MS (–) *m/z* for $[C_{12}H_{17}N_2O_6Mn]^-$: calcd 340.05; found, 340.06.

7.2.9 Synthesis of Complex 4B:

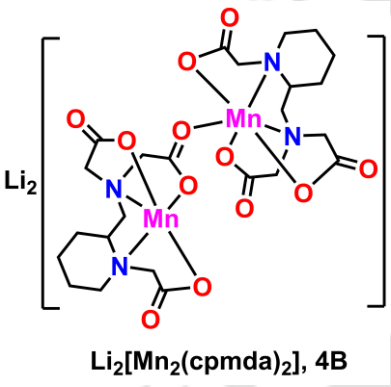

$Li_2[Mn_2(cpmda)_2]$, **4B**

A solution of ligand **H_3cpmda** (0.152 g, 0.38 mmol), and $MnCl_2 \bullet 4H_2O$ (0.071 g, 0.36 mmol) in H_2O (5 mL) was stirred for 15 min until it became transparent. The pH of the solution was adjusted to ~ 6.5 by adding aqueous LiOH solution. At the end of continuous stirring for 24 h at room temperature, the reaction mixture was filtered off. Filtrate gave colourless crystals of complex **4B** on slow solvent evaporation of the filtrate.

Yield = 0.070 g, 40%.

FTIR (KBr pellet cm^{-1}): 3383, 2950, 2932, 2876, 1671, 1624, 1595, 1572, 1452, 1446, 1412, 1327, 1202, 1165, 1145, 1100, 1006, 983, 882, 783, 713, 601.

ESI-MS (–) *m/z* for $[C_{12}H_{17}N_2O_6]^-$: calcd 340.05; found, 339.96.

7.2.10 Synthesis of Complex 5A:

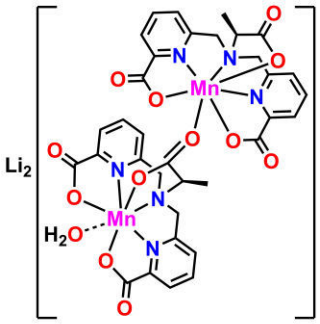

$Li_2[Mn_2(cbda)_2(H_2O)]$, 5A

To an aqueous solution (5 mL) of ligand **Li_3cbda** (0.188 g, 0.50 mmol), $MnCl_2 \bullet 4H_2O$ (0.097 g, 0.49 mmol) was added. The resulting mixture was stirred for 15 min to obtain a transparent solution. The pH of the solution was then adjusted to ~ 6.5 by adding aqueous NaOH solution dropwise. Stirring was continued at room temperature (25 °C) for 24 h. After this, the reaction mixture was filtered, and the filtrate was subjected to slow evaporation. The appeared yellow crystals of complex **5A** were washed thoroughly with MeOH.

Yield = 0.072 g, 34%.

FTIR (KBr pellet cm^{-1}): 3476, 1657, 1622, 1593, 1441, 1409, 1387, 1278, 1222, 1188, 1150, 1130, 1079, 1059, 1019, 985, 953, 894, 844, 817, 778, 692, 491, 431.

ESI-MS (–) *m/z* for $[C_{17}H_{14}N_3O_6\ Mn]^-$: calcd, 411.02; found, 411.04.

7.2.11 Synthesis of Complex 6A:

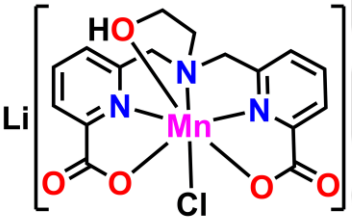

Li[Mn(hbda)Cl], 6A

A solution of ligand **H_2hbda** (0.127 g, 0.38 mmol), and $MnCl_2 \bullet 4H_2O$ (0.069 g, 0.35 mmol) was allowed to stir until it completely dissolved. pH of the medium was adjusted to ~ 7.9 by adding aqueous LiOH solution dropwise, and stirring continued for 24 h at room temperature. The filtrate part of the reaction mixture on slow solvent evaporation method provided colourless crystals of complex **6A**.

Yield = 0.082 g, 42 %.

FTIR (KBr pellet cm^{-1}): 3426, 2965, 2917, 1648, 1593, 1574, 1466, 1444, 1404, 1387, 1348, 1275, 1215, 1188, 1149, 1115, 1079, 1066, 1044, 1020, 989, 873, 845, 801, 769, 692.

ESI-MS (+) *m/z* for $[C_{16}H_{15}N_3O_5Mn + H]^+$: calcd, 385.0465; found, 385.0468.


भारतीय प्रौद्योगिकी संस्थान गुवाहाटी
Indian Institute of Technology Guwahati

Addendum

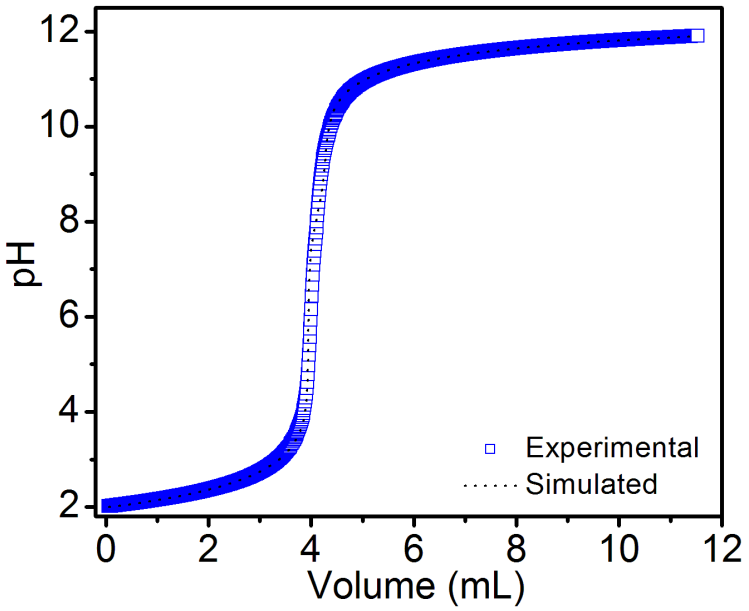

Figure 1. *Experimental and simulated curves representing pH-potentiometric titration of ligand Li_3cbda against standard NaOH solution in 0.15 M NaCl.*

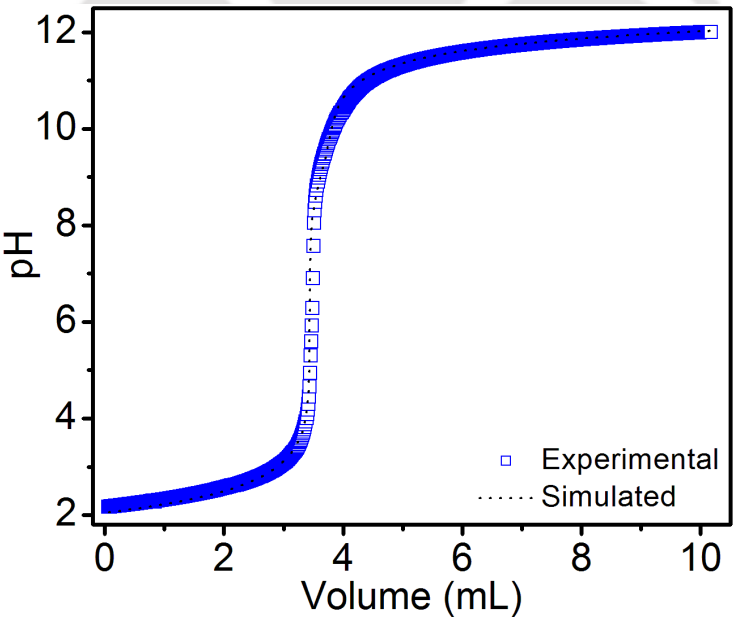

Figure 2. *Experimental and simulated curves representing pH-potentiometric titration of ligand Li_3cbda:Mn(II) solution against standard NaOH solution in 0.15 M NaCl.*

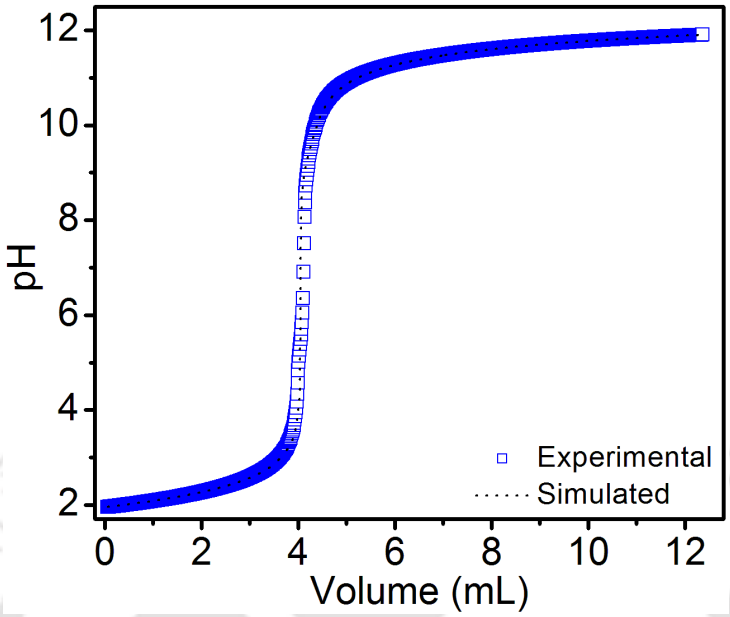

Figure 3. *Experimental and simulated curves representing pH-potentiometric titration of ligand Li_3cbda:Gd(III) solution against standard NaOH solution in 0.15 M NaCl.*

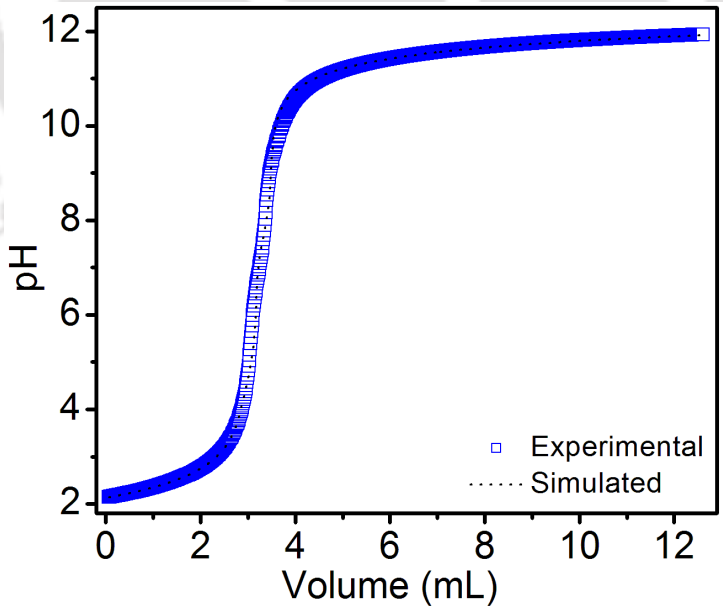

Figure 4. *Experimental and simulated curves representing pH-potentiometric titration of ligand H_2hbda against standard NaOH solution in 0.15 M NaCl.*

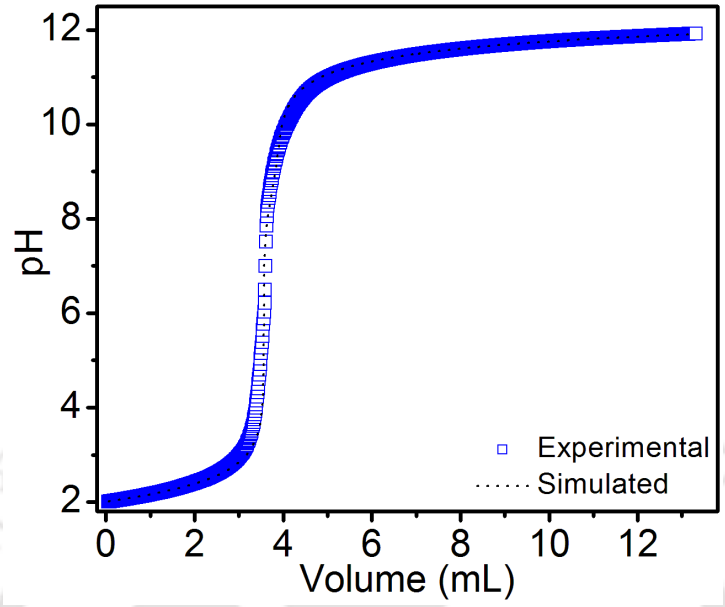

Figure 5. *Experimental and simulated curves representing pH-potentiometric titration of ligand H_2hbda:Mn(II) solution against standard NaOH solution in 0.15 M NaCl.*

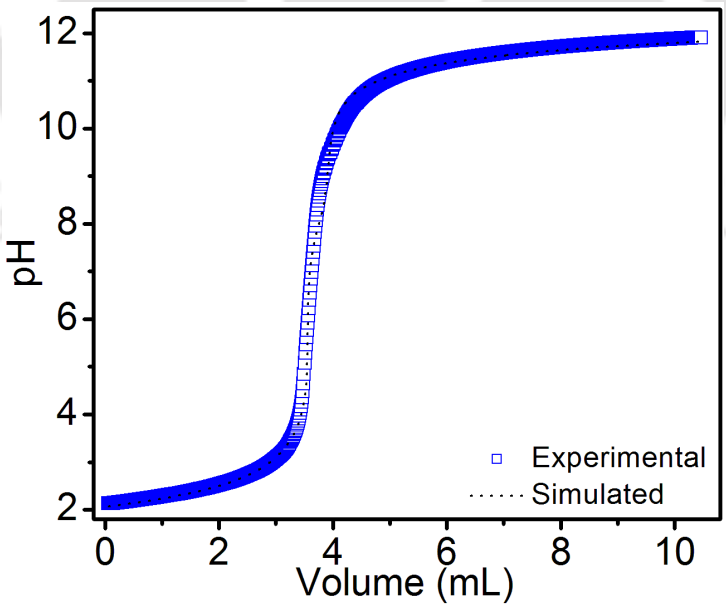

Figure 6. *Experimental and simulated curves representing pH-potentiometric titration of ligand H_2hbda:Gd(III) solution against standard NaOH solution in 0.15 M NaCl.*

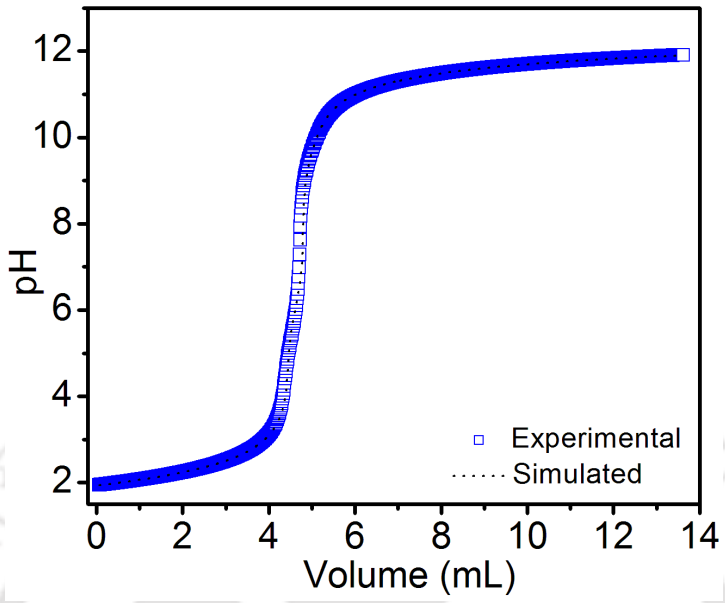

Figure 7. *Experimental and simulated curves representing pH-potentiometric titration of ligand H_3cpmda against standard NaOH solution in 0.15 M NaCl.*

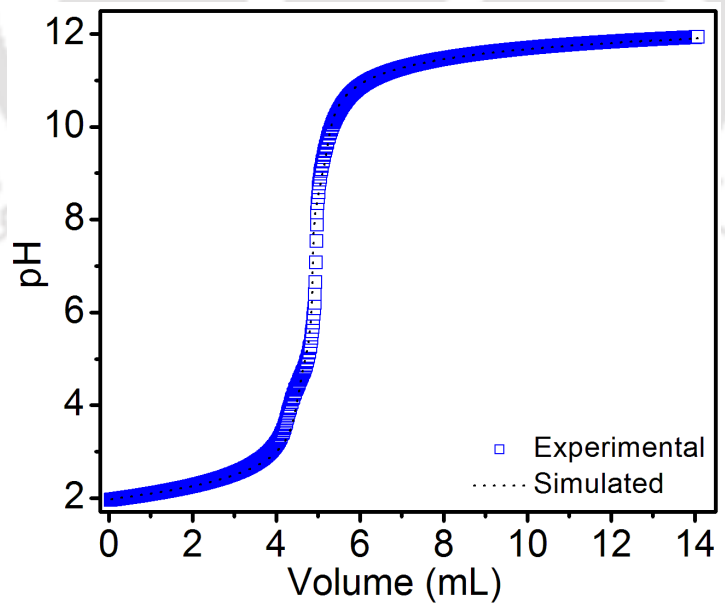

Figure 8. *Experimental and simulated curves representing pH-potentiometric titration of ligand H_3cpmda:Mn(II) against standard NaOH solution in 0.15 M NaCl.*

Table 1. Stability constants[a] of H_3cpmda complexes with selected metal ions[b]

Constant[a]	Ca(II)	Mn(II)	Zn(II)	Cu(II)
logK_{ML}	9.76	12.72	13.82	14.08
logK_{MLH}	4.94	5.00	3.29	5.64
log$K_{ML(OH)}$	9.49	8.8	10.02	10.07
pM	6.22	7.70	8.25	8.38

[a]Defined as $K_{ML} = [ML]/[M][L]$; $K_{MLHi} = [MLH_i]/[MLH_{i-1}][H^+]$; $K_{ML(OH)} = [ML]/[ML(OH)][H^+]$; pM defined as $-\log[M_{free}]$ when [M] = [L] = 10 μM, pH = 7.4; [b] 25 °C, I = 0.15 M NaCl.

Table 2. Stability constants[a] of Li_3cbda complexes with selected metal ions[b]

Constant[a]	Ca(II)	Mn(II)	Zn(II)	Cu(II)
logK_{ML}	9.39	11.90	12.54	13.88
logK_{MLH}	2.76	2.99	3.69	4.42
log$K_{ML(OH)}$		8.99	6.67	6.9
pM	6.80	8.06	8.38	9.05

[a]Defined as $K_{ML} = [ML]/[M][L]$; $K_{MLHi} = [MLH_i]/[MLH_{i-1}][H^+]$; $K_{ML(OH)} = [ML]/[ML(OH)][H^+]$; pM defined as $-\log[M_{free}]$ when [M] = [L] = 10 μM, pH = 7.4; [b] 25 °C, I = 0.15 M NaCl.

Table 3. Stability constants[a] of H_2hbda complexes with selected metal ions[b]

Constant[a]	Ca(II)	Mn(II)	Zn(II)	Cu(II)
logK_{ML}	9.44	13.46	14.22	15.18
logK_{MLH}	2.44	1.71	3.32	3.24
log$K_{ML(OH)}$	4.28	8.39	8.88	8.14
pM	6.98	9.00	9.37	9.85

[a]Defined as $K_{ML} = [ML]/[M][L]$; $K_{MLHi} = [MLH_i]/[MLH_{i-1}][H^+]$; $K_{ML(OH)} = [ML]/[ML(OH)][H^+]$; pM defined as $-\log[M_{free}]$ when [M] = [L] = 10 μM, pH = 7.4; [b] 25 °C, I = 0.15 M NaCl.